

A MODULAR MULTILEVEL CONVERTER  
WITH SELF VOLTAGE BALANCING

By

Yunting Liu

A DISSERTATION

Submitted to  
Michigan State University  
in partial fulfillment of the requirements  
for the degree of

Electrical Engineering—Doctor of Philosophy

2019

## **ABSTRACT**

### **A MODULAR MULTILEVEL CONVERTER WITH SELF VOLTAGE BALANCING**

By

Yunting Liu

Modular multilevel converter (MMC) was proposed in 2003 to extend power electronic converters to high voltage applications. Each MMC contains several identical submodules in series. MMC allows redundant submodules since its operation would not be disturbed by redundant submodules. This is a unique feature compared to other types of multilevel converters. In addition, the installation and uninstallation of submodules is easy. This modular feature makes MMC stand out for medium/high-voltage high-power applications. However, as the number of modules increases, the control complexity of voltage balance of each submodule sharply increases. Conventionally, the MMC submodule voltage cannot be balanced by open-loop modulation methods without voltage monitoring and control. This dissertation proposes a  $\Gamma$ -matrix modulation ( $\Gamma$ MM) that completely eliminates the voltage monitoring and control. In another word, the submodule voltage is self balanced.

The MMC submodule voltage balancing nature with respect to each switching pattern is comprehensively analyzed in Chapter 2. The mathematical analysis reveals that the MMC is self balanced by nature if considering all possible switching patterns. Based on the enlightenment of Chapter 2, the  $\Gamma$ MM is proposed in Chapter 3 to bridge the gap between mathematical analysis and MMC switching operations. With this novel modulation, the MMC achieves self voltage balancing. The two-, three-, four-, and eleven-level MMCs are studied to verify the effectiveness of  $\Gamma$ MM. Also, compared to the conventional MMC, the  $\Gamma$ MM based MMC has smaller submodule capacitance and smaller

arm inductance. This small capacitance and inductance feature extremely reduces the volume and weight of MMC.

To understand the mechanisms of the self balance phenomena of MMC, a state-space model of MMC is proposed in Chapter 4. The existing MMC modeling are developed on different degrees of assumptions and simplifications. This makes them unsuitable for understanding the nature of this circuit from its physical basement. Compared to existing MMC modeling, the proposed state-space model well captured the MMC dynamics. With this state-space model, the MMC capacitor voltage convergence and divergence can be well observed. Four-level MMC with both full-rank  $\Gamma$  and non-full-rank  $\Gamma$  are studied to demonstrate that this model could explain both convergence and divergence of the capacitor voltage. In addition, a generalized MMC model is derived. The generalized model can be applied to higher level MMC. An eleven-level MMC case study is provided to verify the proposed model when extended to higher level. The arm inductor voltage assumption is discussed in Chapter 5.

To Dr. K. P. Liu, Dr. June Li, Ms. F. Li, Prince Ding, and Mumu.  
You are and will always be the love of my life.

## ACKNOWLEDGMENTS

First of all, I would like to express my sincere thanks to my guidance committee, Dr. Fang Zheng Peng, Dr. Bingsen Wang, Dr. Joydeep Mitra, and Dr. Ranjan Mukherjee. I am so grateful for your mentoring in the discipline of power electronics and helping me grow from a beginner to a professional researcher. I would not have known that I enjoyed doing research so much if I were not assigned with the modular multilevel converter research. Thank you so much for enlightening me to this great topic in my PhD journey.

My gratitude also goes to my teaching assistant advisor Dr. Dean M. Aslam, whose help and encouragement always cheered me up. He convinced me that I could possibly become an educator, probably as good as he is.

Special thanks go to the Department of Electrical and Computer Engineering and the Office of Institutional Equity at Michigan State University. I could not get my degree without their support.

My PhD is partly supported by II-VI foundation and Ford-MSU alliance grant. It is my great honor to work with the research group from Ford.

I would like to thank all my colleagues from MSU power group for their valuable inputs towards my research. I would also like to thank all my friends out of the area of power electronics for their caring and friendships in all these years.

The last but not the least, I would like to proudly give my special thanks to my family. I have a family of six. Each of them, regardless of their age, gender or species, has set a role model for me in all aspects. There is no word can express my appreciation to them. Their love to me and my love to them are the greatest motivation in my life.

## TABLE OF CONTENTS

LIST OF TABLES .....	ix
LIST OF FIGURES .....	x
<b>1 INTRODUCTION .....</b>	<b>1</b>
1.1 BACKGROUND.....	1
1.2 PROBLEM DEFINITION .....	3
1.3 MOTIVATION BEHIND THE RESEARCH.....	4
1.4 CONTRIBUTION OF THE RESEARCH.....	5
1.5 DISSERTATION OUTLINE.....	5
<b>2 THE SELF-BALANCING NATURE OF MMC CAPACITOR VOLTAGE.....</b>	<b>7</b>
2.1 INTRODUCTION.....	7
2.2 TWO-LEVEL MMC CAPACITOR VOLTAGE .....	8
2.3 THREE-LEVEL MMC CAPACITOR VOLTAGE.....	10
2.4 <i>N</i> -LEVEL MMC CAPACITOR VOLTAGE.....	14
2.4.1 MASSIVE DATA DILEMMA.....	17
2.4.2 SUBMATRIX EXTRACTION .....	18
2.4.3 <i>N</i> -LEVEL MMC CONJECTURE.....	27
2.4.4 COMPUTER-AID PROOF .....	28
2.5 CONCLUSION .....	30
<b>3 <math>\Gamma</math>-MATRIX MODULATION (<math>\Gamma</math>MM).....</b>	<b>31</b>
3.1 INTRODUCTION.....	31
3.2 $\Gamma$ MM BASED TWO-LEVEL MMC .....	31
3.3 $\Gamma$ MM BASED THREE-LEVEL MMC.....	40
3.4 $\Gamma$ MM BASED <i>N</i> -LEVEL MMC.....	49
3.4.1 CASE STUDY: $\Gamma$ MM BASED FOUR-LEVEL MMC.....	52
3.4.2 CASE STUDY: $\Gamma$ MM BASED FOUR-LEVEL MMC WITH NON-FULL-RANK $\Gamma$ MATRIX.....	61
3.4.3 CASE STUDY: $\Gamma$ MM BASED FOUR-LEVEL MMC WITH CAPACITANCE DEVIATION .....	67
3.4.4 CASE STUDY: $\Gamma$ MM BASED ELEVEN-LEVEL MMC.....	68
3.5 DISCUSSIONS .....	76
3.6 CONCLUSION .....	77
<b>4 THE STATE-SPACE MODEL OF MODULAR MULTILEVEL CONVERTER ..</b>	<b>78</b>
4.1 MOTIVATIONS .....	78
4.2 INTRODUCTION.....	80
4.3 PRIOR-ART MMC MODEL.....	82
4.4 CONTRIBUTION.....	88
4.5 REVIEW OF $\Gamma$ -MATRIX MODULATION.....	89

4.5.1	LEVEL POINTER PREPARATION .....	90
4.5.2	$\Gamma$ -MATRIX ADAPTATION .....	93
4.6	STATE-SPACE MODEL OF TWO-LEVEL MMC .....	95
4.6.1	STATE-SPACE MODEL .....	96
4.6.2	STATE-SPACE MODEL WITH STRAY RESISTANCE .....	106
4.6.3	MODEL ANALYSIS AND SIMULATION .....	117
4.6.4	STATE-SPACE MODEL WITH LOAD AS STATE VARIABLE.....	126
4.7	STATE-SPACE MODEL OF THREE-LEVEL MMC.....	136
4.7.1	STATE-SPACE MODEL .....	138
4.7.2	STATE SPACE MODEL WITH STRAY RESISTANCE.....	145
4.7.3	MODEL ANALYSIS AND SIMULATION .....	153
4.8	STATE-SPACE MODEL OF $N$ -LEVEL MMC.....	164
4.8.1	STATE-SPACE MODEL .....	165
4.8.2	MODEL ANALYSIS AND SIMULATION .....	170
4.8.2.1	CASE STUDY: $\Gamma$ MM BASED FOUR-LEVEL MMC.....	170
4.8.2.2	CASE STUDY: $\Gamma$ MM BASED FOUR-LEVEL MMC WITH NON-FULL-RANK MATRIX .....	179
4.8.2.3	CASE STUDY: $\Gamma$ MM BASED ELEVEN-LEVEL MMC.....	187
4.9	CONCLUSION .....	197
5	THE ARM INDUCTORS VOLTAGE DROP ASSUMPTION .....	198
5.1	INTRODUCTION.....	198
5.2	DYNAMIC RESPONSE OF MMC IN SWITCHING CYCLES.....	198
5.2.1	STATE I.....	198
5.2.2	STATE II .....	205
5.3	ZERO VOLTAGE DROP ASSUMPTION .....	207
5.4	SIMULATION .....	208
5.4.1	$\tau / T_{sw} = 0.02$ .....	209
5.4.2	$\tau / T_{sw} = 0.25$ .....	213
5.4.3	$\tau / T_{sw} = 1$ .....	218
5.4.4	$\tau / T_{sw} = 2$ .....	223
5.4.5	$\tau / T_{sw} = 10$ .....	228
5.5	CONCLUSION .....	233
6	CONCLUSIONS AND RECOMMENDATIONS FOR FUTURE WORK .....	234
6.1	CONCLUSIONS.....	234
6.2	RECOMMENDATIONS FOR FUTURE WORK.....	235
6.2.1	STATE-SPACE MODEL OF TWO-LEVEL MMC .....	236
6.2.2	MECHANISMS OF VOLTAGE CONVERGENCE OF TWO-LEVEL MMC .....	239
6.2.2.1	THE SENSE OF SMELL OF A STATE MACHINE.....	239
6.2.2.2	UNDERSTAND TWO-LEVEL MMC BEHAVIORS .....	241
6.2.3	DISCUSSIONS ON HIGH LEVEL MMC.....	245
APPENDICES	.....	248
APPENDIX A: PROOF BY INDUCTION AND CONTRADICTION.....		249
APPENDIX B: MATLAB SCRIPT .....		254

BIBLIOGRAPHY..... 258

## LIST OF TABLES

Table 1 Two-level mmc simulation key parameters. ....	33
Table 2 Three-level MMC simulation key parameters. ....	43
Table 3 Four-level MMC simulation key parameters. ....	54
Table 4 Eleven-level MMC simulation key parameters. ....	69
Table 5 Initial values of state space at four time instants. ....	118
Table 6 Two-level MMC simulation key parameters. ....	120
Table 7 Initial values of state space at four time instants. ....	154
Table 8 Three-level MMC simulation key parameters. ....	156
Table 9 Initial values of state space at four time instants. ....	171
Table 10 Four-level MMC simulation key parameters. ....	173
Table 11 Initial values of state space at four time instants. ....	180
Table 12 Initial values of state variables at four time instants. ....	188
Table 13 Eleven-level MMC simulation key parameters. ....	191
Table 14 Three-level MMC simulation key parameters. ....	209
Table 15 Three-level MMC simulation key parameters. ....	214
Table 16 Three-level MMC simulation key parameters. ....	219
Table 17 Three-level MMC simulation key parameters. ....	224
Table 18 Three-level MMC simulation key parameters. ....	229
Table 19 Two-level MMC simulation key parameters for state machine study. ....	243

## LIST OF FIGURES

Figure 1.1 The topology of a three-phase MMC. ....	2
Figure 1.2 The multilevel ac waveform at the MMC ac terminals. ....	3
Figure 2.1 Two-level MMC with pole connected to (a) positive dc rail (Level 1); and (b) negative dc rail (Level 2). ....	10
Figure 2.2 Three-level MMC with pole voltage of (a) $V_{dc}$ (Level 1); (b)(c)(d)(e) zero volt (Level 2); and (f) $-V_{dc}$ (Level 3). ....	11
Figure 2.3 $N$ -level MMC with pole voltage of (a) $(N-1)V_{dc}$ (Level 1); (b) $(N-2)V_{dc}$ (Level 2); and (c) $-(N-1)V_{dc}$ (Level $N$ ). ....	16
Figure 2.4 Numbering of levels in an $N$ -level MMC, when (a) $N$ is an odd number; and (b) $N$ is an even number. ....	17
Figure 2.5 The flowchart of checking the rank of $\Gamma$ matrix. ....	29
Figure 3.1 Relationship of ac-side voltage $v_s^*$ and pole voltage $v_a$ . ....	31
Figure 3.2 Two-level MMC simulation topology. ....	32
Figure 3.3 Two-level MMC (a) load voltage and (b) load current. ....	36
Figure 3.4 Two-level MMC mid-point voltage (a) $v_{ab}$ ; (b) $v_{bc}$ ; and (c) $v_{ca}$ . ....	37
Figure 3.5 Submodule capacitor (a)/(c) voltage; and (b)/(d) current. ....	38
Figure 3.6 (a) Line current of phase-A and its corresponding (b) upper arm current, (c) lower arm current. ....	39
Figure 3.7 Dc input voltage and current. ....	39
Figure 3.8 Relationship of ac-side voltage $v_s^*$ and pole voltage $v_a$ . ....	40
Figure 3.9 $\Gamma$ -matrix modulation strategy for three-level MMC. ....	41
Figure 3.10 Three-level MMC simulation topology. ....	42

Figure 3.11 Three-level MMC (a) load voltage and (b) load current. ....	45
Figure 3.12 Three-level MMC mid-point voltage (a) $v_{ab}$ ; (b) $v_{bc}$ ; and (c) $v_{ca}$ . ....	46
Figure 3.13 Submodule capacitor (a)/(c) voltage; and (b)/(d) current. ....	47
Figure 3.14 (a) Line current of phase-A and its corresponding (b) upper arm current, (c) lower arm current. ....	48
Figure 3.15 Dc input voltage and current. ....	48
Figure 3.16 Ac-side voltage $v_s^*$ and carriers, when (a) $N$ is an odd number; and (b) $N$ is an even number. ....	49
Figure 3.17 Ac-side voltage $v_s^*$ and pole voltage $v_a$ , when (a) $N$ is an odd number; and (b) $N$ is an even number. ....	50
Figure 3.18 $\Gamma$ -matrix modulation strategy for $N$ -level MMC. ....	52
Figure 3.19 Four-level MMC simulation topology. ....	53
Figure 3.20 $\Gamma$ -matrix modulation strategy for four-level MMC. ....	55
Figure 3.21 Four-level MMC (a) load voltage and (b) load current. ....	57
Figure 3.22 Four-level MMC mid-point voltage (a) $v_{ab}$ ; (b) $v_{bc}$ ; and (c) $v_{ca}$ . ....	58
Figure 3.23 Submodule capacitor (a)/(c) voltage; and (b)/(d) current. ....	59
Figure 3.24 (a) Line current in phase-A and its corresponding (b) upper arm current, (c) lower arm current. ....	60
Figure 3.25 Dc input voltage and current. ....	60
Figure 3.26 All submodule capacitor voltages in phase-A. ....	61
Figure 3.27 Four-level MMC (a) load voltage and (b) load current. ....	63
Figure 3.28 Four-level MMC mid-point voltage (a) $v_{ab}$ ; (b) $v_{bc}$ ; and (c) $v_{ca}$ . ....	64
Figure 3.29 Submodule capacitor (a)/(c) voltage; and (b)/(d) current. ....	65

Figure 3.30 (a) Line current and its corresponding (b) upper arm current, (c) lower arm current. ....	66
Figure 3.31 Dc input voltage and current. ....	66
Figure 3.32 All submodule capacitor voltages in phase-A. ....	67
Figure 3.33 Submodule capacitor $C_3$ voltage. ....	67
Figure 3.34 All submodule capacitor voltages in phase-A. ....	68
Figure 3.35 Eleven-level MMC simulation topology. ....	68
Figure 3.36 Eleven-level MMC (a) load voltage and (b) load current. ....	72
Figure 3.37 Eleven-level MMC mid-point voltage (a) $v_{ab}$ ; (b) $v_{bc}$ ; and (c) $v_{ca}$ . ....	73
Figure 3.38 Submodule capacitor (a)/(c) voltage; and (b)/(d) current. ....	74
Figure 3.39 (a) Line current in phase-A and its corresponding (b) upper arm current, (c) lower arm current. ....	75
Figure 3.40 Dc input voltage and current. ....	75
Figure 3.41 All submodule capacitor voltages in phase-A. ....	76
Figure 4.1 The VSC model of MMC. ....	82
Figure 4.2 Five independent loop currents and six independent node voltages in topology. ....	84
Figure 4.3 Loop current selection (a) single-phase oriented [47]-[48] (b) inductor current oriented [49]-[50] and (c) circulating current oriented [45],[51]-[52]. ....	84
Figure 4.4 Common-mode and differential-mode voltage as state variables [46]. ....	86
Figure 4.5 State variable selections (a) dc current + common/differential-mode voltage oriented (b) inductor current + common/differential-mode voltage oriented and (c) circulating current + common/differential-mode voltage oriented. ....	86
Figure 4.6 The selection of MMC internal state variables. ....	88

Figure 4.7 The state variable selection of [51]. .....	89
Figure 4.8 The state variable selection of this dissertation. ....	89
Figure 4.9 $N$ -level MMC circuit. ....	90
Figure 4.10 Numbering of levels in an $N$ -level MMC, when (a) $N$ is an odd number; and (b) $N$ is an even number. ....	91
Figure 4.11 ac-side voltage $v_s^*$ and carriers, when (a) $N$ is an odd number; and (b) $N$ is an even number. ....	92
Figure 4.12 ac-side voltage $v_s^*$ and pole voltage $v_a$ , when (a) $N$ is an odd number; and (b) $N$ is an even number. ....	92
Figure 4.13 $\Gamma$ -matrix modulation for $N$ -level MMC. ....	95
Figure 4.14 two-level MMC with pole connected to (a) positive dc rail (Level 1); and (b) negative dc rail (Level 2). ....	95
Figure 4.15 two-level MMC model with pole connected to (a) positive dc rail; and (b) negative dc rail. ....	96
Figure 4.16 Load inductor voltage modeling. ....	101
Figure 4.17 Two-level MMC with pole connected to (a) positive dc rail (Level 1); and (b) negative dc rail (Level 2). ....	107
Figure 4.18 Two-level MMC model with pole connected to (a) positive dc rail; and (b) negative dc rail. ....	107
Figure 4.19 Two-level single-phase MMC circuit for simulation study. ....	119
Figure 4.20 Upper arm current ( $x_1$ ) simulation and state-space model comparison. ....	121
Figure 4.21 Lower arm current ( $x_2$ ) simulation and state-space model comparison. ....	122
Figure 4.22 Capacitor voltage ( $x_3$ ) simulation and state-space model comparison. ....	123
Figure 4.23 Capacitor voltage ( $x_4$ ) simulation and state-space model comparison. ....	124

Figure 4.24 Comparison of simulation and state-space model in a long run. (a) upper arm current; (b) lower arm current; (c) capacitor voltage $V_{C1}$ ; (d) capacitor voltage $V_{C2}$ . ....	125
Figure 4.25 Two-level MMC with pole connected to (a) positive dc rail (Level 1); and (b) negative dc rail (Level 2). .....	127
Figure 4.26 Two-level MMC model with pole connected to (a) positive dc rail; and (b) negative dc rail. ....	127
Figure 4.27 Three-level MMC with pole voltage of (a) $V_{dc}$ (Level I); (b)(c)(d)(e) zero volt (Level II); and (f) $-V_{dc}$ (Level III). .....	137
Figure 4.28 Load inductor voltage modeling. ....	144
Figure 4.29 Three-level MMC with pole connected to positive dc rail (Level 1). ....	146
Figure 4.30 Three-level single-phase MMC circuit for simulation study. ....	155
Figure 4.31 Upper arm current ( $x_1$ ) simulation and state-space model comparison. ....	157
Figure 4.32 Lower arm current ( $x_2$ ) simulation and state-space model comparison. ....	158
Figure 4.33 Capacitor voltage ( $x_3$ ) simulation and state-space model comparison. ....	159
Figure 4.34 Capacitor voltage ( $x_4$ ) simulation and state-space model comparison. ....	160
Figure 4.35 Capacitor voltage ( $x_5$ ) simulation and state-space model comparison. ....	161
Figure 4.36 Capacitor voltage ( $x_6$ ) simulation and state-space model comparison. ....	162
Figure 4.37 Comparison of simulation and state-space model in a long run. (a) upper arm current; (b) lower arm current; (c) capacitor voltage $V_{C1}$ ; (d) capacitor voltage $V_{C2}$ ; (e) capacitor voltage $V_{C3}$ ; (f) capacitor voltage $V_{C4}$ . ....	163
Figure 4.38 Accumulated error on load current. ....	164
Figure 4.39 A single-phase $N$ -level MMC. ....	165
Figure 4.40 Load inductor voltage modeling. ....	169
Figure 4.41 Four-level single-phase MMC circuit for simulation study. ....	172

Figure 4.42 Upper arm current ( $x_1$ ) simulation and state-space model comparison. ....	174
Figure 4.43 Lower arm current ( $x_2$ ) simulation and state-space model comparison. ....	175
Figure 4.44 Capacitor voltage ( $x_5$ ) simulation and state-space model comparison. ....	176
Figure 4.45 Capacitor voltage ( $x_6$ ) simulation and state-space model comparison. ....	177
Figure 4.46 Comparison of simulation and state-space model in a long run. (a) upper arm current; (b) lower arm current; (c) capacitor voltage $V_{C3}$ ; (d) capacitor voltage $V_{C4}$ . ....	178
Figure 4.47 Load current $i_s = x_1 - x_2$ . ....	179
Figure 4.48 Upper arm current ( $x_1$ ) simulation and state-space model comparison. ....	182
Figure 4.49 Lower arm current ( $x_2$ ) simulation and state-space model comparison. ....	183
Figure 4.50 Capacitor voltage ( $x_5$ ) simulation and state-space model comparison. ....	184
Figure 4.51 Capacitor voltage ( $x_6$ ) simulation and state-space model comparison. ....	185
Figure 4.52 Comparison of simulation and state-space model in a long run. (a) upper arm current; (b) lower arm current; (c) capacitor voltage $V_{C3}$ ; (d) capacitor voltage $V_{C4}$ . ....	186
Figure 4.53 Load current $i_s = x_1 - x_2$ . ....	187
Figure 4.54 Eleven-level single-phase MMC circuit for state-space model study. ....	190
Figure 4.55 Upper arm current ( $x_1$ ) simulation and state-space model comparison. ....	192
Figure 4.56 Lower arm current ( $x_2$ ) simulation and state-space model comparison. ....	193
Figure 4.57 Capacitor voltage ( $x_{12}$ ) simulation and state-space model comparison. ....	194
Figure 4.58 Capacitor voltage ( $x_{13}$ ) simulation and state-space model comparison. ....	195
Figure 4.59 Comparison of simulation and state-space model in a long run. (a) Upper arm current; (b) lower arm current; (c) capacitor voltage $V_{C10}$ ; (d) capacitor voltage $V_{C11}$ ...	196
Figure 4.60 Load current $i_s = x_1 - x_2$ . ....	197

Figure 5.1 Two-level MMC model with pole connected to (a) positive dc rail; and (b) negative dc rail.....	199
Figure 5.2 Phase inductor voltage modeling.....	200
Figure 5.3 Three-level MMC simulation topology.....	208
Figure 5.4 Three-level MMC (a) load voltage and (b) load current. ....	210
Figure 5.5 Three-level MMC mid-point voltage (a) $v_{ab}$ ; (b) $v_{bc}$ ; and (c) $v_{ca}$ .....	211
Figure 5.6 Sub-module capacitor (a)/(c) voltage; and (b)/(d) current. ....	212
Figure 5.7 (a) Line current and its corresponding (b) upper arm current, (c) lower arm current. ....	213
Figure 5.8 Three-level MMC (a) load voltage and (b) load current. ....	215
Figure 5.9 Three-level MMC mid-point voltage (a) $v_{ab}$ ; (b) $v_{bc}$ ; and (c) $v_{ca}$ .....	216
Figure 5.10 Sub-module capacitor (a)/(c) voltage; and (b)/(d) current. ....	217
Figure 5.11 (a) Line current and its corresponding (b) upper arm current, (c) lower arm current. ....	218
Figure 5.12 Three-level MMC (a) load voltage and (b) load current. ....	220
Figure 5.13 Three-level MMC mid-point voltage (a) $v_{ab}$ ; (b) $v_{bc}$ ; and (c) $v_{ca}$ .....	221
Figure 5.14 Sub-module capacitor (a)/(c) voltage; and (b)/(d) current. ....	222
Figure 5.15 (a) Line current and its corresponding (b) upper arm current, (c) lower arm current. ....	223
Figure 5.16 Three-level MMC (a) load voltage and (b) load current. ....	225
Figure 5.17 Three-level MMC mid-point voltage (a) $v_{ab}$ ; (b) $v_{bc}$ ; and (c) $v_{ca}$ .....	226
Figure 5.18 Sub-module capacitor (a)/(c) voltage; and (b)/(d) current. ....	227

Figure 5.19 (a) Line current and its corresponding (b) upper arm current, (c) lower arm current. ....	228
Figure 5.20 Three-level MMC (a) load voltage and (b) load current. ....	230
Figure 5.21 Three-level MMC mid-point voltage (a) $v_{ab}$ ; (b) $v_{bc}$ ; and (c) $v_{ca}$ .....	231
Figure 5.22 Sub-module capacitor (a)/(c) voltage; and (b)/(d) current. ....	232
Figure 5.23 (a) Line current and its corresponding (b) upper arm current, (c) lower arm current. ....	233
Figure 6.1 Recommendations for future work.....	236
Figure 6.2 Two-level single-phase MMC circuit for state machine study. ....	243
Figure 6.3 The $\langle d^0, f_i \rangle$ resulting from the state machine proposed in Chapter 3. ....	244
Figure 6.4 (a) Upper arm capacitor voltage; (b) lower arm capacitor voltage; and (c) the sense of smell $\langle d^0, f_i \rangle$ . ....	245

# 1 INTRODUCTION

## 1.1 BACKGROUND

The modular multilevel converter (MMC) is pioneeringly proposed by Lesnicar *et al.* [1] in 2003. The MMC has become the most attractive multilevel converter topology for medium/high-power applications, specifically for voltage-sourced converter high-voltage direct current (VSC-HVDC) transmission systems. Several identical submodules (SMs) with low-voltage ratings could be stacked up. Compared to other multilevel converter topologies, MMC features in modularity and scalability to meet any voltage level requirements.

The topology of a three-phase MMC is shown in Figure 1.1. The MMC converts the dc system, normally high dc voltage source, to ac system, normally three phases, and feeds an ac load. The dc system of an MMC is often referred to as dc-bus or dc-link, connected to the positive and negative rails of the converter legs. The three-phase ac system is connected to the mid-point of each leg ( $v_a, v_b, v_c$ ). Each leg of the MMC is divided into two arms. The arms connected to the positive rail are referred to as upper arms, and the arms connected to the negative rail are referred to as lower arms. Each arm has a group of submodules and an inductor ( $L$ ). The arm inductor is connected in series with each group of submodules to limit the current due to the instantaneous voltage difference between submodules and the dc system.

All submodules are identical, each corresponding to one voltage step in the resulting multilevel ac waveform at the MMC ac terminals. The multilevel ac waveform is shown in Figure 1.2. At each time instant, the controller determines how many submodules needed to create the voltage level that closest to the output sinusoidal voltage reference. The

topology is easy to adapt to any voltage level since the number of submodules can be adjusted. The resulting waveform has a very small total harmonic distortion (THD) as the number of submodules increases.

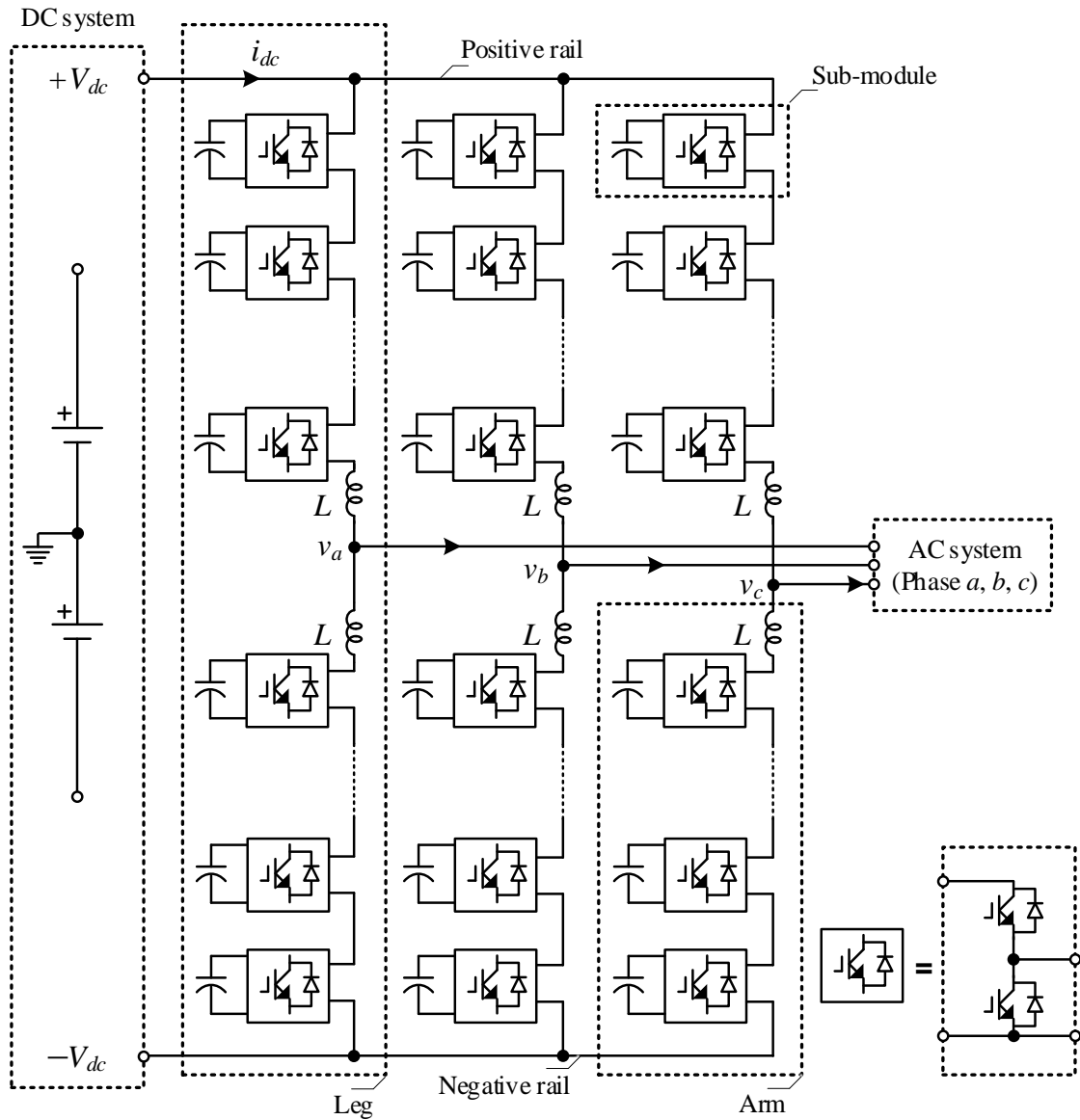


Figure 1.1 The topology of a three-phase MMC.

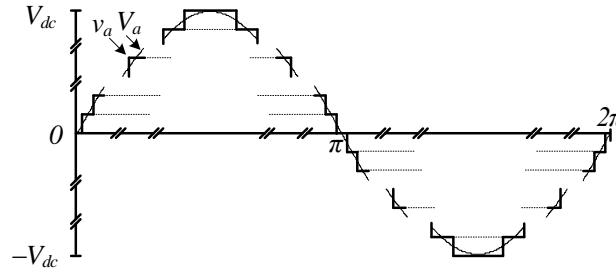


Figure 1.2 The multilevel ac waveform at the MMC ac terminals.

## 1.2 PROBLEM DEFINITION

MMCs have two inherent properties:

- 1) bulky dc capacitors are needed to absorb the fundamental-frequency ripple power from ac side;
- 2) numerous voltage sensors and feedback control are needed to coordinate the dc capacitor voltage of each submodule.

These two properties result in poor power density for MMC and computational inefficiency for control algorithm, especially in high-voltage/-power applications as the number of submodules increases.

Many existing literatures have attempted to resolve the capacitor voltage balancing problems [2]-[30]. They can be classified into the following categories,

- 1) each submodule has a fast local dc voltage controller to prevent the individual voltage from deviation, while a slower upper controller balances the over-all arm voltages [2]-[8];
- 2) the submodules are sorted, or compared, continuously in order of capacitor voltage value by controller, to determine which submodule(s) to be inserted, or by-passed, at each switching cycle [9]-[19];

- 3) the circuit topology is modified to have an inherent ability to self-balance without the need of control algorithms [20]-[27];
- 4) the switching patterns are swap among the submodules in an arm within a fundamental cycle to guarantee the submodules with an equalized exposure to the loading conditions [27]-[29].

### **1.3 MOTIVATION BEHIND THE RESEARCH**

As discussed in Chapter 1.2, the existing solution for capacitor voltage balancing can be classified into four categories. Among these four categories, 1) and 2) require submodule voltage measuring, normally together with arm current measuring, to have a sophisticated closed-loop control on capacitor voltage; whereas 3) achieves the sensorless voltage balance, or self-balancing, by modifying the MMC topology, which usually results in complex circuitry; 4) has the potential to combine the merits of 1), 2) and 3), which are maintaining the basic MMC circuitry and also no need for feedback control to balance the capacitor voltage. However, none of the literatures in category 4) mathematically proves it no need of feedback control for MMC voltage balancing.

Few literatures discussed the mitigation of voltage ripples on dc capacitors. Normally, the low-frequency voltage ripple on dc capacitor is deemed as unavoidable since each individual submodule is modeled as a single-phase inverter in existing literatures.

Adam *et al.* [31] discusses the basic operation principle of MMCs and the capacitors voltage balancing technique for three-level and five-level MMCs. More importantly, it leaves a hint that the two-level MMC has a self voltage balancing ability and the low-frequency ripples on submodule capacitors are eliminated by nature. Adam *et al.* conclude that three-level, and above, MMCs have no such merits.

## 1.4 CONTRIBUTION OF THE RESEARCH

The overall objective of this research is to prove and develop the algorithms for MMC to achieve the self voltage balancing. This overall research goal was achieved with the following major contributions:

- ❖ Mathematically proved that MMCs have the self voltage balancing capability;
- ❖ Developed a novel modulation that secures the self voltage balancing for MMC, which allows the MMCs to become sensorless.
- ❖ Reduced the low-frequency voltage ripple on submodule dc capacitors, which allowed a smaller dc capacitance.
- ❖ Derived the general state-space model for MMC to catch the dynamics of the voltage convergence/divergence.

## 1.5 DISSERTATION OUTLINE

This dissertation is organized as follows:

Chapter 2 of this dissertation mathematically proves that MMCs have the self voltage balancing capability, regardless of the number of levels.

Based on the mathematical proof in Chapter 2, a novel modulation is proposed in Chapter 3 to transform the mathematical analysis into engineering practice, which allows the MMCs to become sensorless. Since the proposed modulation guarantees less low-frequency ripple on dc capacitors, smaller capacitors can be utilized in MMC submodules. Simulation results are provided for verification purposes.

Chapter 4 derives the general state-space model of MMC to capture the dynamics of the voltage convergence/divergence.

Chapter 5 verifies the inductor voltage drop assumptions that proposed in Chapter 2.

Chapter 6 proposes the possible future works.

## 2 THE SELF-BALANCING NATURE OF MMC CAPACITOR VOLTAGE

### 2.1 INTRODUCTION

Modular multilevel converter (MMC) was proposed by Lesnicar *et al.* [1] in 2003. MMCs have an inherent property: numerous voltage sensors and feedback control are needed to coordinate the dc capacitor voltage of each submodule. This property results in computational inefficiency in control algorithms, especially for high-voltage applications where the MMC installations often consist of hundreds of submodules.

Many existing literatures have attempted to resolve the capacitor voltage balancing problems [2]-[30]. They can be classified into the following categories,

- 1) Each submodule has a local dc voltage controller to prevent the individual voltage from deviation, while a slower upper controller balances the over-all arm voltages [2]-[8];
- 2) The submodules are sorted, or compared, continuously in order of capacitor voltage value. A main controller determines which submodule(s) to be inserted, or bypassed, at each switching cycle [9]-[19];
- 3) The circuit topology is modified to have an inherent capability to self balance without the need of control algorithms [20]-[27];
- 4) The submodule patterns are swapped among the submodules in an arm to guarantee the submodules with an equalized exposure to the loading conditions [28]-[30].

Among the four categories, 1) and 2) require submodule voltage measuring, normally together with arm current measuring, to have a sophisticated closed-loop control on capacitor voltage; whereas 3) achieves the self voltage balancing by modifying the MMC topology, which usually results in complex circuitry; 4) has the potential to maintain the

basic MMC circuitry and also no need for feedback control to balance the capacitor voltage. However, this method is hard to extend to high level since it is impossible to identify all submodule patterns for high-level MMCs.

Few literatures discussed the mitigation of voltage ripples on dc capacitors. Normally, the low-frequency voltage ripple on dc capacitor is deemed as unavoidable since each individual submodule is modeled as a single-phase inverter in existing literatures.

Adam *et al.* [31] discusses the basic operation principle of MMCs and the capacitors voltage balancing technique for three-level and five-level MMCs. More importantly, it leaves a hint that the two-level MMC has a self voltage balancing ability and the low-frequency ripples on submodule capacitors are eliminated by nature. Adam *et al.* [31] conclude that three-level, and above, MMCs have no such merits.

This Chapter mathematically proves that MMCs have the self voltage balancing capability, regardless of the number of levels. This implies that MMC voltage balancing control is unnecessary. The mathematical proof starts from two- and three-level MMCs. Then, the general  $N$ -level MMC analysis is derived thereafter. Based on the mathematical proof, a novel modulation will be proposed to transform the mathematical analysis into engineering practice in Chapter 3 of this dissertation.

## 2.2 TWO-LEVEL MMC CAPACITOR VOLTAGE

The pole voltage  $v_a$  of a two-level MMC can either be  $1/2V_{dc}$  or  $-1/2V_{dc}$  as shown in Figure2.1. Assume that the voltage drop on arm inductors could be neglected. If the pole is attached to the positive dc rail, the lower arm capacitor  $C_2$  is clamped to the dc source voltage  $V_{dc}$  as shown in Figure2.1(a). If the pole is attached to the negative dc rail, the

upper arm capacitor  $C_1$  is clamped to the dc source voltage  $V_{dc}$  as shown in Figure 2.1(b).

$C_1$  and  $C_2$  voltage could be formulated as,

$$\begin{cases} V_{dc} = V_{C2} \\ V_{dc} = V_{C1} \end{cases}, \quad (2.1)$$

Re-write (2.1) into matrix form

$$\begin{bmatrix} V_{dc} \\ V_{dc} \end{bmatrix} = \begin{bmatrix} 0 & 1 \\ 1 & 0 \end{bmatrix} \cdot \begin{bmatrix} V_{C1} \\ V_{C2} \end{bmatrix} = \mathbf{\Gamma} \begin{bmatrix} V_{C1} \\ V_{C2} \end{bmatrix}, \quad (2.2)$$

, where  $\mathbf{\Gamma} = \begin{bmatrix} 0 & 1 \\ 1 & 0 \end{bmatrix}$ .

Since the rank of  $\mathbf{\Gamma}$  is two,  $[V_{C1} \ V_{C2}]^T$  has the only solution,

$$\begin{bmatrix} V_{C1} \\ V_{C2} \end{bmatrix} = \mathbf{\Gamma}^{-1} \begin{bmatrix} V_{dc} \\ V_{dc} \end{bmatrix} = \begin{bmatrix} V_{dc} \\ V_{dc} \end{bmatrix}. \quad (2.3)$$

The solution of (2.1) is  $V_{C1} = V_{C2} = V_{dc}$ . The two-level MMC has its capacitors' voltages balanced by nature.

Note that this capacitor voltage balance analysis assumes that the voltage drop of arm inductors could be neglected. It requires the inductor voltage to be stabilized to zero in every switching cycle. Normally, a smaller arm inductor results in faster convergence to zero. Here is the question. What is a reasonable value for the arm inductor to be regarded as neglectable in theoretical analysis without losing the practical sense? I would like to leave this topic in future. The arm inductance value needs to be determined based on the detailed model of a two-level MMC.

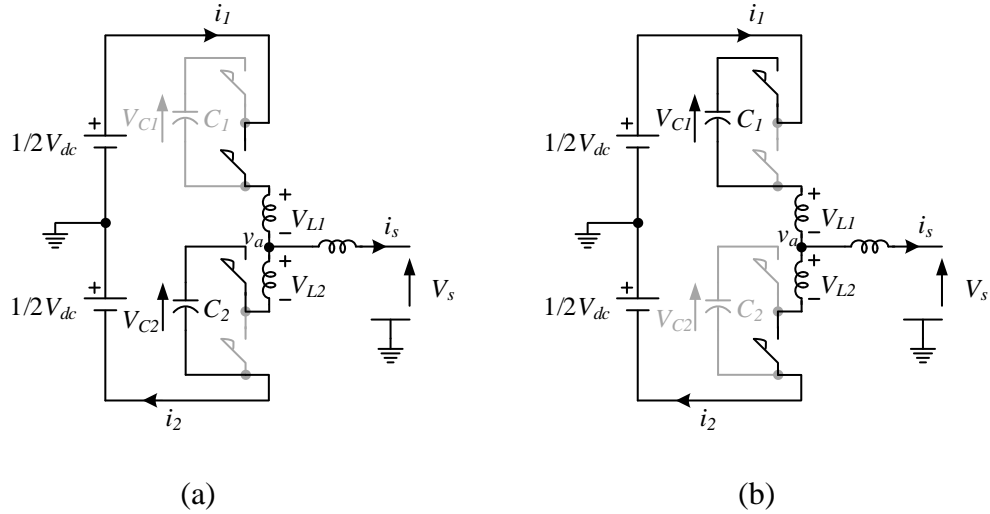


Figure 2.1 Two-level MMC with pole connected to (a) positive dc rail (Level 1); and (b) negative dc rail (Level 2).

### 2.3 THREE-LEVEL MMC CAPACITOR VOLTAGE

Figure 2.2 shows a three-level MMC. The pole voltage  $v_a$  of a three-level MMC can either be  $V_{dc}$ , zero, or  $-V_{dc}$  if all capacitor voltages are  $V_{dc}$ . For a three-level MMC, there are two, and only two, out of four submodules at inserting mode at any instant. The other two submodules are at by-pass mode meanwhile. If the voltage drop on arm inductors could be neglected, the sum of the voltages of the two inserting-mode submodules are clamped to the dc source voltage. For example, if the module three and four are at inserting mode, as shown in Figure 2.2(a), the sum of capacitor  $C_3$  voltage and  $C_4$  voltage is clamped to  $2V_{dc}$ . Figure 2.2 shows all the possible states of a three-level MMC. The capacitor voltage of Figure 2.2(a)-(f) could be formulated as,

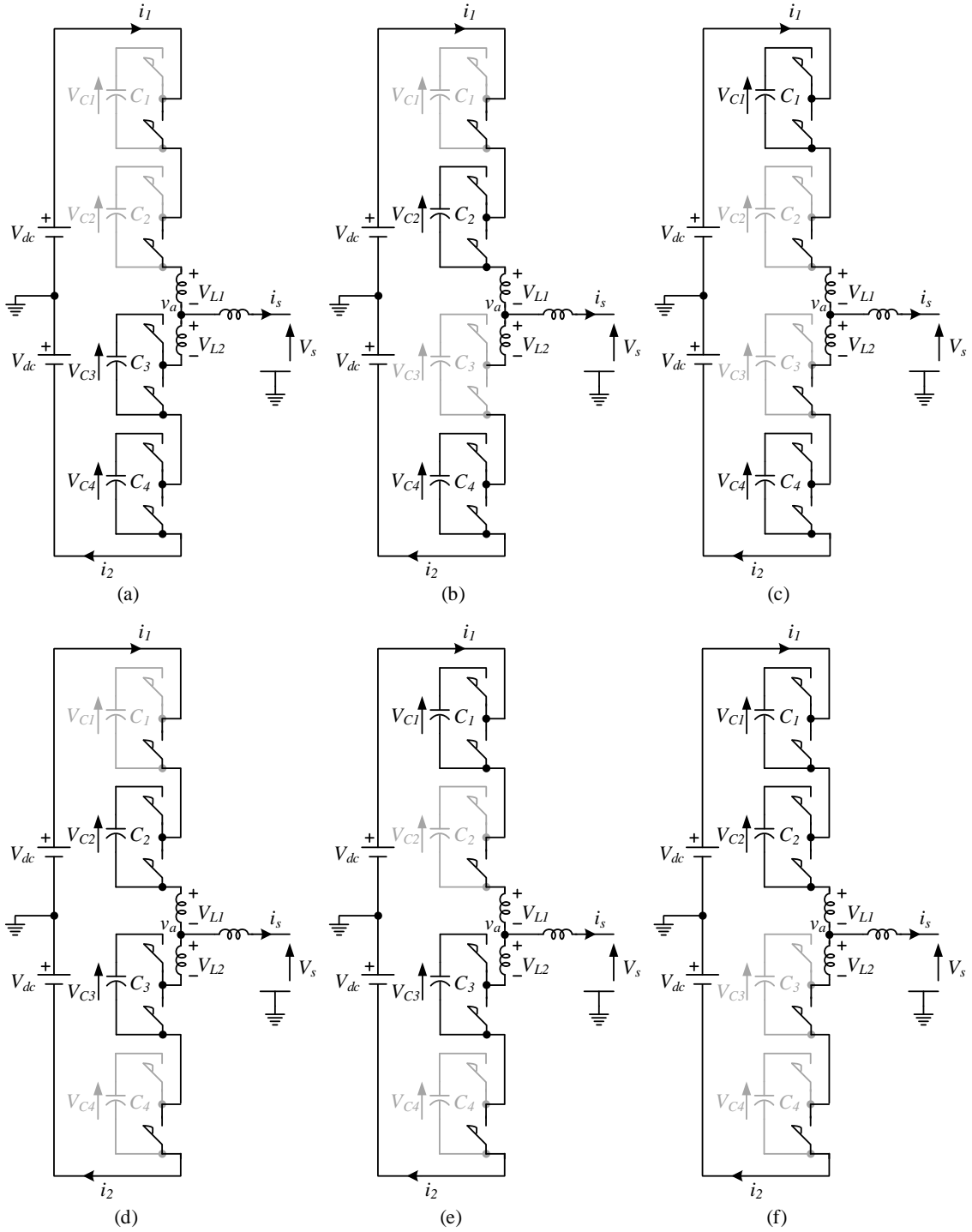


Figure 2.2 Three-level MMC with pole voltage of (a)  $V_{dc}$  (Level 1); (b)(c)(d)(e) zero volt (Level 2); and (f)  $-V_{dc}$  (Level 3).

$$\begin{cases} 2V_{dc} = V_{C3} + V_{C4} \\ 2V_{dc} = V_{C2} + V_{C4} \\ 2V_{dc} = V_{C1} + V_{C4} \\ 2V_{dc} = V_{C2} + V_{C3} \\ 2V_{dc} = V_{C1} + V_{C3} \\ 2V_{dc} = V_{C1} + V_{C2} \end{cases}. \quad (2.4)$$

Re-write (2.4) into matrix form

$$\begin{bmatrix} 2V_{dc} \\ 2V_{dc} \\ 2V_{dc} \\ 2V_{dc} \\ 2V_{dc} \\ 2V_{dc} \end{bmatrix} = \begin{bmatrix} 0 & 0 & 1 & 1 \\ 0 & 1 & 0 & 1 \\ 1 & 0 & 0 & 1 \\ 0 & 1 & 1 & 0 \\ 1 & 0 & 1 & 0 \\ 1 & 1 & 0 & 0 \end{bmatrix} \cdot \begin{bmatrix} V_{C1} \\ V_{C2} \\ V_{C3} \\ V_{C4} \end{bmatrix} = \begin{bmatrix} \Gamma_1 \\ \Gamma_2 \\ \Gamma_3 \end{bmatrix} \cdot \begin{bmatrix} V_{C1} \\ V_{C2} \\ V_{C3} \\ V_{C4} \end{bmatrix}, \quad (2.5)$$

$$\text{where } \Gamma_1 = [0 \ 0 \ 1 \ 1], \Gamma_2 = \begin{bmatrix} 0 & 1 & 0 & 1 \\ 1 & 0 & 0 & 1 \\ 0 & 1 & 1 & 0 \\ 1 & 0 & 1 & 0 \end{bmatrix}, \text{ and } \Gamma_3 = [1 \ 1 \ 0 \ 0].$$

Define the submodule state to be ‘1’ when at inserting mode; and the submodule to be ‘0’ when at by-pass mode.  $\Gamma_1$  contains all the possible combinations of submodule patterns when pole voltage  $v_a$  is at Level 1 [see Figure2.2(a)].  $\Gamma_2$  contains all the possible combinations of submodule patterns when pole voltage  $v_a$  is at Level 2 [see Figure2.2(b)-(e)].  $\Gamma_3$  contains all the possible combinations of submodule patterns when pole voltage  $v_a$  is at Level 3 [see Figure2.2(f)]. When MMC visits one of submodule patterns, one equation of equation set (2.4) is satisfied at a time. We can regard visiting a submodule combination as solving an equation of (2.4).

**Lemma 1** [32]: Consider the non-homogeneous system  $\Gamma V_C = V_{dc}$ .  $\Gamma$  is the coefficient matrix.  $V_C$  is unknown. The sizes of  $\Gamma$ ,  $V_{dc}$  and  $V_C$  are  $m \times n$ ,  $m \times 1$  and  $n \times 1$ , respectively.  $\Gamma V_C = V_{dc}$  has no more than one solution if  $\text{rank}[\Gamma] = n$ .

Now we need to check how many equations of (2.4) we need to solve to guarantee a solution for all capacitors' voltages. First check the rank of  $\Gamma_1$ ,  $\Gamma_2$ , and  $\Gamma_3$  respectively.

$$\text{rank}[\Gamma_1]=1, \text{rank}[\Gamma_2]=3, \text{rank}[\Gamma_3]=1, \quad (2.6)$$

which means  $\Gamma_1$  has one linearly independent row,  $\Gamma_2$  has three linearly independent rows, and  $\Gamma_3$  has one linearly independent row. In another word, we cannot find definite solutions for all capacitors' voltages by solving the equations within same level. For example, if considering the equations within Level 2 only,

$$\begin{cases} 2V_{dc} = V_{C1} + V_{C4} \\ 2V_{dc} = V_{C2} + V_{C4} \\ 2V_{dc} = V_{C2} + V_{C3} \\ 2V_{dc} = V_{C1} + V_{C3} \end{cases} \quad (2.7)$$

Simplify (2.7)

$$\begin{cases} V_{C1} = V_{C2} \\ V_{C3} = V_{C4} \\ 2V_{dc} = V_{C1} + V_{C4} \end{cases} \quad (2.8)$$

Eq.(2.7) and (2.8) have multiple solutions. There are no definite solutions for all capacitors' voltages by solving the equations within Level 2.

Then what about combining two levels together? For example  $[\Gamma_1 \Gamma_2]^T$  or  $[\Gamma_2 \Gamma_3]^T$ .

Due to THD considerations, MMC pole voltage jumps between two adjacent levels at a time. Hence, checking the rank of two adjacent levels complies with practical sense. We are going to check the rank of two adjacent levels, to see whether we could find the solutions for all capacitors' voltages.

The ranks of  $[\Gamma_1 \Gamma_2]^T$  and  $[\Gamma_2 \Gamma_3]^T$  are

$$\text{rank} \begin{bmatrix} \mathbf{\Gamma}_1 \\ \mathbf{\Gamma}_2 \end{bmatrix} = 4, \text{ and } \text{rank} \begin{bmatrix} \mathbf{\Gamma}_2 \\ \mathbf{\Gamma}_3 \end{bmatrix} = 4, \quad (2.9)$$

which guarantee that  $[\mathbf{\Gamma}_1 \ \mathbf{\Gamma}_2]^T$  and  $[\mathbf{\Gamma}_2 \ \mathbf{\Gamma}_3]^T$  have four linearly independent rows each. Hence, we could find no more than one set of solutions for all capacitors' voltages if combining any two adjacent levels. There is one possible set of solutions for (2.4),

$$\begin{bmatrix} V_{C1} \\ V_{C2} \\ V_{C3} \\ V_{C4} \end{bmatrix} = \begin{bmatrix} V_{dc} \\ V_{dc} \\ V_{dc} \\ V_{dc} \end{bmatrix}. \quad (2.10)$$

These solutions of capacitor voltages are quite intuitive. Since (2.4) have no more than one solution, (2.10) must be the unique solution. Hence, the three-level MMC has its capacitors' voltages balanced by nature.

## 2.4 N-LEVEL MMC CAPACITOR VOLTAGE

Figure 2.3 shows an  $N$ -level MMC. Assume that all capacitor voltages are  $V_{dc}$ . The pole voltage  $v_a$  of an  $N$ -level MMC is an element of  $\{ (N-1)V_{dc}/2, (N-3)V_{dc}/2, (N-5)V_{dc}/2, \dots, V_{dc}, 0, -V_{dc}, \dots, -(N-3)V_{dc}/2, -(N-1)V_{dc}/2 \}$ , if  $N$  is an odd number. The pole voltage  $v_a$  of an  $N$ -level MMC is an element of  $\{ (N-1)V_{dc}/2, (N-3)V_{dc}/2, (N-5)V_{dc}/2, \dots, V_{dc}/2, -V_{dc}/2, \dots, -(N-3)V_{dc}/2, -(N-1)V_{dc}/2 \}$ , if  $N$  is an even number. Figure 2.4 shows the numbering of levels in an  $N$ -level MMC, starting from the first level to the  $N$ -th level. For an  $N$ -level MMC, there are  $N-1$ , and only  $N-1$ , out of  $2N-2$  submodules at inserting mode at a time. The other  $N-1$  submodules are at by-pass mode meanwhile. If the voltage drop on arm inductors could be ignored, the sum of the voltages of the  $N-1$  inserting-mode submodules are clamped to the dc source voltage. For example, if the  $SM_N$  through  $SM_{2N-2}$  are at inserting mode, as shown in Figure 2.3(a), the sum of capacitor  $C_N$  voltage through  $C_{2N-2}$

voltage is clamped to  $(N-1)V_{dc}$ . Figure 2.3(b) shows the sum of capacitor  $C_1$  and capacitor  $C_{N-1}$  through  $C_{2N-2}$  voltages is clamped to  $(N-1)V_{dc}$ ; and Figure 2.3(c) shows the sum of capacitor  $C_1$  through  $C_{N-1}$  voltages is clamped to  $(N-1)V_{dc}$ . All capacitor voltage balancing could be formulated as,

$$\begin{bmatrix} (N-1)V_{dc} \\ \vdots \\ (N-1)V_{dc} \end{bmatrix}_{(m_1+m_2+\dots+m_N) \times 1} = \begin{bmatrix} (\mathbf{\Gamma}_1)_{m_1 \times (2N-2)} \\ (\mathbf{\Gamma}_2)_{m_2 \times (2N-2)} \\ \vdots \\ (\mathbf{\Gamma}_k)_{m_k \times (2N-2)} \\ \vdots \\ (\mathbf{\Gamma}_N)_{m_N \times (2N-2)} \end{bmatrix} \cdot \begin{bmatrix} V_{C1} \\ V_{C2} \\ \vdots \\ V_{C(2N-2)} \end{bmatrix}_{(2N-2) \times 1}, \quad (2.11)$$

where  $m_k = C_{N-1}^{k-1} C_{N-1}^{N-k} = (C_{N-1}^{k-1})^2$ ,  $1 < k < N$ .

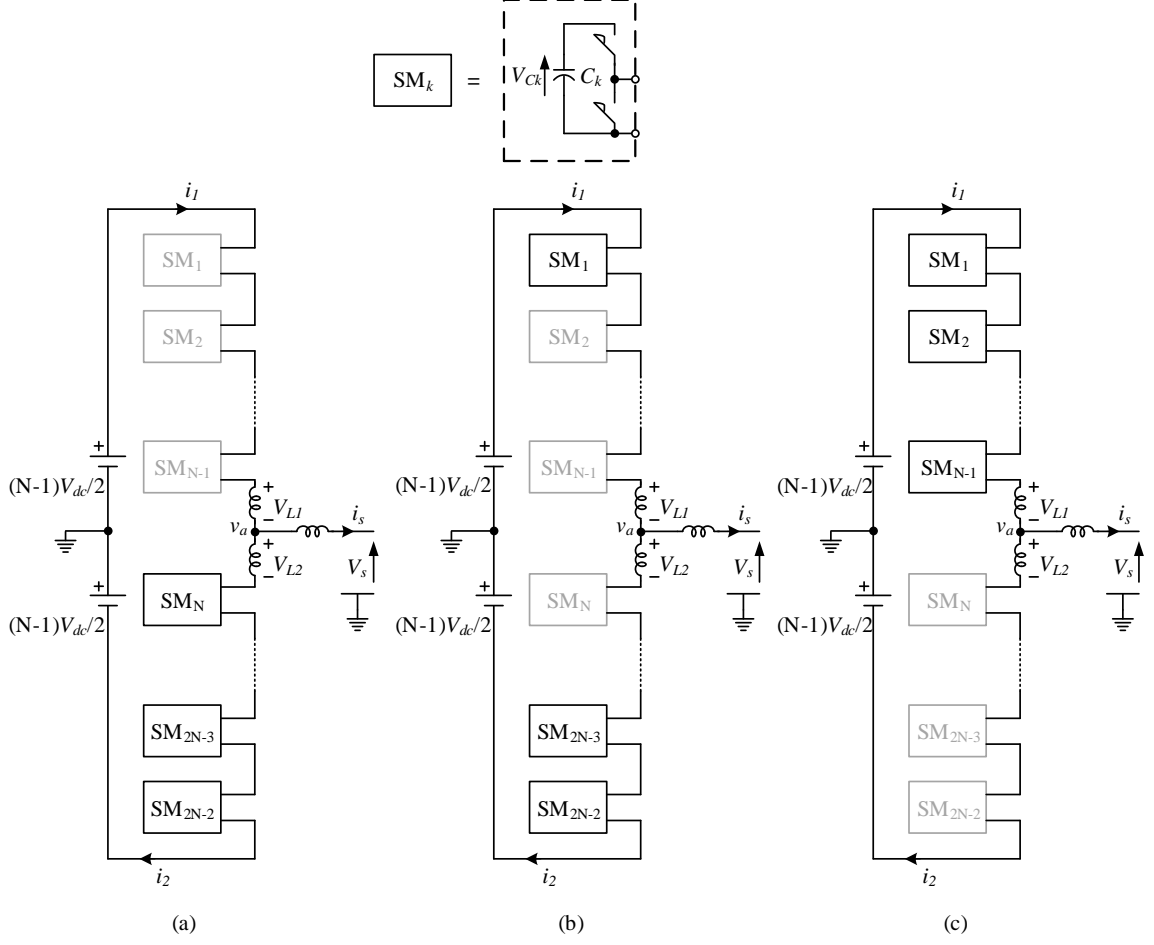


Figure 2.3  $N$ -level MMC with pole voltage of (a)  $(N-1)V_{dc}$  (Level 1); (b)  $(N-2)V_{dc}$  (Level 2); and (c)  $-(N-1)V_{dc}$  (Level  $N$ ).

Define the submodule state to be ‘1’ when at inserting mode; and the submodule to be ‘0’ when at by-pass mode.  $k$ -th level is an arbitrary level, except for the first level and  $N$ -th level. In another word,  $1 < k < N$ .  $\Gamma_k$  contains all the possible switching patterns when pole voltage  $v_a$  is at  $k$ -th level.  $\Gamma_k$  is an  $m_k$  by  $(2N-2)$  matrix. When MMC visits one switching pattern, one equation in (2.11) is satisfied at a time. We can regard visiting a switching pattern as solving an equation in (2.11).

From Chapter 2.3, we have already observed a unique feature of three-level MMC, which is the rank of any two adjacent levels is four. This guarantees the three-level MMC

has its capacitors' voltages balanced by nature. If we could extend this observation to  $N$ -level MMC, which means the rank of any two adjacent levels is  $2N-2$ , this will guarantee that the  $N$ -level MMC has its capacitors' voltages balanced by nature.

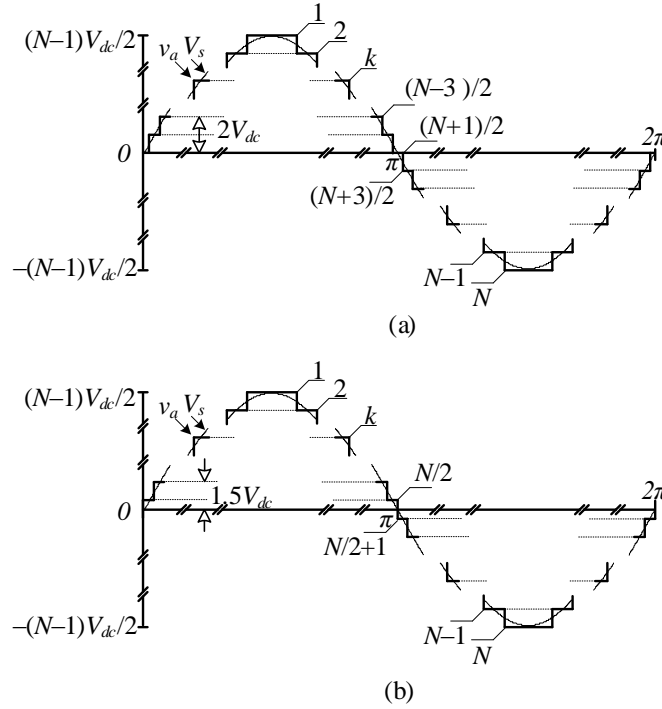


Figure 2.4 Numbering of levels in an  $N$ -level MMC, when (a)  $N$  is an odd number; and (b)  $N$  is an even number.

### 2.4.1 MASSIVE DATA DILEMMA

However, it is not always easy to obtain the  $\Gamma$  matrix. Notice that the  $\Gamma_k$  matrix of a  $N$ -level MMC is a  $m_k$ -by- $(2N-2)$  matrix, where  $m_k = C_{N-1}^{k-1} C_{N-1}^{N-k} = (C_{N-1}^{k-1})^2$ . For example, the  $\Gamma_5$  matrix of a 9-level MMC is a 4900-by-16 matrix; the  $\Gamma_{50}$  matrix of a 100-level MMC is a  $2.5 \times 10^{57}$ -by-198 matrix. In High-Voltage DC (HVDC) transmission applications, the MMC is built with 200 - 400 levels [33]. The  $\Gamma$  matrix expands rapidly as the MMC level increases, which becomes impossible for computers to process. However, it is not always

necessary to have a whole picture of  $\Gamma$  matrix. The only thing we care about  $\Gamma$  matrix is its rank.

**Lemma 2** [34]: The rank of an  $m \times n$  matrix cannot exceed  $m$  or  $n$ . The maximum value possible is the smaller of  $m$  and  $n$ .

Since  $\Gamma_k$  is an  $m_k$ -by- $(2N-2)$  matrix. The rank of  $\Gamma_k$  cannot exceed  $2N-2$ .  $\Gamma_k$  should be able to extract a  $(2N-2)$ -by- $(2N-2)$  submatrix, or even smaller than  $(2N-2)$ -by- $(2N-2)$ , while holding the same rank as the original  $\Gamma_k$ . In another word, if we could find a submatrix  $\hat{\Gamma}_k$  of  $\Gamma_k$  which guarantees that  $[\hat{\Gamma}_k \quad \hat{\Gamma}_{k+1}]^T$  has a rank of  $2N-2$ , we can conclude that  $[\Gamma_k \quad \Gamma_{k+1}]$  also has a rank of  $2N-2$  and the  $N$ -level MMC has its capacitors' voltages balanced by nature.

#### 2.4.2 SUBMATRIX EXTRACTION

$\Gamma$  matrix extraction is critical before we proceed to calculate the rank of  $\Gamma$  matrix. To simplify the problem, let us first investigate the  $\Gamma$  matrix of two-level MMC. The  $\Gamma$  matrix of two-level MMC is as follows,

$$\mathbf{\Gamma}^{(2)} = \begin{bmatrix} \mathbf{\Gamma}_1^{(2)} \\ \mathbf{\Gamma}_2^{(2)} \end{bmatrix} = \begin{bmatrix} 0 & 1 \\ 1 & 0 \end{bmatrix} \begin{matrix} \leftarrow 1^{\text{st}} \text{ level} \\ \leftarrow 2^{\text{nd}} \text{ level} \end{matrix} \quad (2.12)$$

Every specific column is always representing one certain submodule states (1 represents inserting mode and 0 represents by-pass mode). Since  $\mathbf{\Gamma}_1^{(2)}$  and  $\mathbf{\Gamma}_2^{(2)}$  are 1-by-2 matrix, there is no need to extract submatrices from these two.

The  $\Gamma$  matrix of three-level MMC is as follows,

$$\mathbf{\Gamma}^{(3)} = \begin{bmatrix} \mathbf{\Gamma}_1^{(3)} \\ \mathbf{\Gamma}_2^{(3)} \\ \mathbf{\Gamma}_3^{(3)} \end{bmatrix} = \begin{bmatrix} 0 & 0 & 1 & 1 \\ 0 & 1 & 0 & 1 \\ 1 & 0 & 0 & 1 \\ 0 & 1 & 1 & 0 \\ 1 & 0 & 1 & 0 \\ 1 & 1 & 0 & 0 \end{bmatrix} = \begin{bmatrix} 0 & \overline{0} & \overline{1} & 1 \\ 0 & \underline{1} & \underline{0} & 1 \\ 1 & 0 & 0 & 1 \\ 0 & 1 & 1 & 0 \\ 1 & \overline{0} & \overline{1} & 0 \\ 1 & \underline{1} & \underline{0} & 0 \end{bmatrix} = \begin{bmatrix} 0 & \mathbf{\Gamma}_1^{(2)} & 1 \\ 0 & \mathbf{\Gamma}_2^{(2)} & 1 \\ 1 & \mathbf{T}_{1(a)}^{(2)} & 1 \\ 0 & \mathbf{T}_{1(b)}^{(2)} & 0 \\ 1 & \mathbf{\Gamma}_1^{(2)} & 0 \\ 1 & \mathbf{\Gamma}_2^{(2)} & 0 \end{bmatrix} \begin{matrix} \leftarrow 1^{\text{st}} \text{ level} \\ \leftarrow 2^{\text{nd}} \text{ level} \\ \leftarrow 3^{\text{rd}} \text{ level} \end{matrix} \quad (2.13)$$

Eq.(2.13) could be interpreted as follows:

The  $\mathbf{\Gamma}^{(3)}$  could be derived from  $\mathbf{\Gamma}^{(2)}$ . For example, adding a “0” to the left of  $\mathbf{\Gamma}_1^{(2)}$  and a “1” to the right of  $\mathbf{\Gamma}_1^{(2)}$ , the matrix  $[0 \mathbf{\Gamma}_1^{(2)} 1]$  becomes the  $\mathbf{\Gamma}_1^{(3)}$ . Adding a “0” to the left of  $\mathbf{\Gamma}_2^{(2)}$  and a “1” to the right of  $\mathbf{\Gamma}_2^{(2)}$ , the matrix  $[0 \mathbf{\Gamma}_2^{(2)} 1]$  becomes part of  $\mathbf{\Gamma}_2^{(3)}$ . Adding a “1” to the left of  $\mathbf{\Gamma}_1^{(2)}$  and a “0” to the right of  $\mathbf{\Gamma}_1^{(2)}$ , the matrix  $[1 \mathbf{\Gamma}_1^{(2)} 0]$  becomes part of  $\mathbf{\Gamma}_2^{(3)}$ . Adding a “1” to the left of  $\mathbf{\Gamma}_2^{(2)}$  and a “0” to the right of  $\mathbf{\Gamma}_2^{(2)}$ , the matrix  $[0 \mathbf{\Gamma}_2^{(2)} 1]$  becomes part of  $\mathbf{\Gamma}_2^{(3)}$ . There are two submodule states that cannot be directly derived from  $\mathbf{\Gamma}^{(2)}$ , which are  $[1 \mathbf{T}_{1(a)}^{(2)} 1]$  and  $[0 \mathbf{T}_{1(b)}^{(2)} 0]$ .  $\mathbf{T}_{1(a)}^{(2)}$  is derived from  $\mathbf{\Gamma}_1^{(2)}$  by manipulating the right most “1” in  $\mathbf{\Gamma}_1^{(2)}$  to “0”.  $\mathbf{T}_{1(b)}^{(2)}$  is derived from  $\mathbf{\Gamma}_1^{(2)}$  by manipulating the left most “0” in  $\mathbf{\Gamma}_1^{(2)}$  to “1”.

$\mathbf{\Gamma}_1^{(3)}$  and  $\mathbf{\Gamma}_3^{(3)}$  are 1-by-4 matrices. There is no need to extract submatrices from these two.  $\mathbf{\Gamma}_2^{(3)}$  is a 4-by-4 matrix with a rank of three.  $\mathbf{\Gamma}_2^{(3)}$  should be able to find a 3-by-4 submatrix which holds the same rank.  $\mathbf{\Gamma}_2^{(3)}$  is as follows

$$\mathbf{\Gamma}_2^{(3)} = \begin{bmatrix} 0 & 1 & 0 & 1 \\ 1 & 0 & 0 & 1 \\ 0 & 1 & 1 & 0 \\ 1 & 0 & 1 & 0 \end{bmatrix} = \begin{bmatrix} 0 & \mathbf{\Gamma}_2^{(2)} & 1 \\ 1 & \mathbf{T}_{1(a)}^{(2)} & 1 \\ 0 & \mathbf{T}_{1(b)}^{(2)} & 0 \\ 1 & \mathbf{\Gamma}_1^{(2)} & 0 \end{bmatrix}. \quad (2.14)$$

There are four possible ways to extract a 3-by-4 submatrix from  $\mathbf{\Gamma}_2^{(3)}$ . Two of them are selected as examples.  $\mathbf{\Gamma}_2^{(3)}$  can be segmented to

$$\mathbf{\Gamma}_2^{(3)} = \begin{bmatrix} 0 & \mathbf{\Gamma}_2^{(2)} & 1 \\ 1 & \mathbf{T}_{1(a)}^{(2)} & 1 \\ 0 & \mathbf{T}_{1(b)}^{(2)} & 0 \\ \hline 1 & \mathbf{\Gamma}_1^{(2)} & 0 \end{bmatrix} = \begin{bmatrix} \hat{\mathbf{\Gamma}}_2^{(3)} \\ \mathbf{M}_2^{(3)} \end{bmatrix}, \quad (2.15)$$

or

$$\mathbf{\Gamma}_2^{(3)} = \begin{bmatrix} 0 & \mathbf{\Gamma}_2^{(2)} & 1 \\ \hline 1 & \mathbf{T}_{1(a)}^{(2)} & 1 \\ 0 & \mathbf{T}_{1(b)}^{(2)} & 0 \\ 1 & \mathbf{\Gamma}_1^{(2)} & 0 \end{bmatrix} = \begin{bmatrix} \mathbf{M}_2^{(3)} \\ \hat{\mathbf{\Gamma}}_2^{(3)} \end{bmatrix}, \quad (2.16)$$

where  $\hat{\mathbf{\Gamma}}_2^{(3)}$  is the core matrix extracted from  $\mathbf{\Gamma}_2^{(3)}$ .  $\mathbf{M}_2^{(3)}$  is the redundant submatrix to discard. Let us check the rank of  $\hat{\mathbf{\Gamma}}_2^{(3)}$

$$\text{rank}[\hat{\mathbf{\Gamma}}_2^{(3)}] = 3. \quad (2.17)$$

$\hat{\mathbf{\Gamma}}_3^{(3)}$  holds the same rank as  $\mathbf{\Gamma}_3^{(3)}$ . Instead of checking the rank of  $[\mathbf{\Gamma}_1^{(3)} \ \mathbf{\Gamma}_2^{(3)}]^T$  and  $[\mathbf{\Gamma}_2^{(3)} \ \mathbf{\Gamma}_3^{(3)}]^T$ , let us check the rank of  $[\mathbf{\Gamma}_1^{(3)} \ \hat{\mathbf{\Gamma}}_2^{(3)}]^T$  and  $[\hat{\mathbf{\Gamma}}_2^{(3)} \ \mathbf{\Gamma}_3^{(3)}]^T$ .

$$\text{rank} \begin{bmatrix} \mathbf{\Gamma}_1^{(3)} \\ \hat{\mathbf{\Gamma}}_2^{(3)} \end{bmatrix} = 4, \text{ and } \text{rank} \begin{bmatrix} \hat{\mathbf{\Gamma}}_2^{(3)} \\ \mathbf{\Gamma}_3^{(3)} \end{bmatrix} = 4. \quad (2.18)$$

Since  $[\mathbf{\Gamma}_1^{(3)} \ \hat{\mathbf{\Gamma}}_2^{(3)}]^T$  and  $[\hat{\mathbf{\Gamma}}_2^{(3)} \ \mathbf{\Gamma}_3^{(3)}]^T$  are submatrices of  $[\mathbf{\Gamma}_1^{(3)} \ \mathbf{\Gamma}_2^{(3)}]^T$  and  $[\mathbf{\Gamma}_2^{(3)} \ \mathbf{\Gamma}_3^{(3)}]^T$ , the rank of  $[\mathbf{\Gamma}_1^{(3)} \ \mathbf{\Gamma}_2^{(3)}]^T$  and  $[\mathbf{\Gamma}_2^{(3)} \ \mathbf{\Gamma}_3^{(3)}]^T$  should also be four.

Let's extend the similar matrix extraction procedure to the four-level MMC.

The  $\mathbf{\Gamma}$  matrix of four-level MMC is as follows,

$$\mathbf{\Gamma}^{(4)} = \begin{bmatrix} \mathbf{\Gamma}_1^{(4)} \\ \mathbf{\Gamma}_2^{(4)} \\ \mathbf{\Gamma}_3^{(4)} \\ \mathbf{\Gamma}_4^{(4)} \end{bmatrix} = \begin{bmatrix} 0 & 0 & 0 & 1 & 1 & 1 \\ 0 & 0 & 1 & 0 & 1 & 1 \\ 0 & 1 & 0 & 0 & 1 & 1 \\ 0 & 0 & 1 & 1 & 0 & 1 \\ 0 & 1 & 0 & 1 & 0 & 1 \\ 1 & 0 & 0 & 1 & 0 & 1 \\ 0 & 1 & 0 & 1 & 1 & 0 \\ 1 & 0 & 0 & 0 & 1 & 1 \\ 1 & 0 & 0 & 1 & 1 & 0 \\ 0 & 0 & 1 & 1 & 1 & 0 \\ 1 & 0 & 1 & 0 & 1 & 0 \\ 1 & 1 & 0 & 0 & 1 & 0 \\ 1 & 0 & 1 & 1 & 0 & 0 \\ 1 & 1 & 0 & 1 & 0 & 0 \\ 1 & 0 & 1 & 0 & 0 & 1 \\ 0 & 1 & 1 & 0 & 1 & 0 \\ 0 & 1 & 1 & 0 & 0 & 1 \\ 0 & 1 & 1 & 1 & 0 & 0 \\ 1 & 1 & 0 & 0 & 0 & 1 \\ 1 & 1 & 1 & 0 & 0 & 0 \end{bmatrix}. \quad (2.19)$$

$\mathbf{\Gamma}_1^{(4)}$  and  $\mathbf{\Gamma}_4^{(4)}$  are 1-by-6 matrices. There is no need to extract submatrices from these two.  $\mathbf{\Gamma}_2^{(4)}$  and  $\mathbf{\Gamma}_3^{(4)}$  are 9-by-6 matrices with a rank of 5.  $\mathbf{\Gamma}_2^{(4)}$  and  $\mathbf{\Gamma}_3^{(4)}$  should be able to find the 5-by-6 submatrices which hold the same rank.  $\mathbf{\Gamma}_2^{(4)}$  is as follows

$$\mathbf{\Gamma}_2^{(4)} = \begin{bmatrix} 0 & 0 & 1 & 0 & 1 & 1 \\ 0 & 1 & 0 & 0 & 1 & 1 \\ 0 & 0 & 1 & 1 & 0 & 1 \\ 0 & 1 & 0 & 1 & 0 & 1 \\ 1 & 0 & 0 & 1 & 0 & 1 \\ 0 & 1 & 0 & 1 & 1 & 0 \\ 1 & 0 & 0 & 0 & 1 & 1 \\ 1 & 0 & 0 & 1 & 1 & 0 \\ 0 & 0 & 1 & 1 & 1 & 0 \end{bmatrix} = \begin{bmatrix} 0 & 0 & 1 & 0 & 1 & 1 \\ 0 & 1 & 0 & 0 & 1 & 1 \\ 0 & 0 & 1 & 1 & 0 & 1 \\ 1 & 0 & 0 & 1 & 0 & 1 \\ 0 & 1 & 0 & 1 & 1 & 0 \\ 0 & 1 & 0 & 1 & 0 & 1 \\ 1 & 0 & 0 & 0 & 1 & 1 \\ 1 & 0 & 0 & 1 & 1 & 0 \\ 0 & 0 & 1 & 1 & 1 & 0 \end{bmatrix} = \begin{bmatrix} \mathbf{0} & \hat{\mathbf{Y}}_2^{(3)} & \mathbf{1} \\ 1 & \mathbf{T}_{1(a)}^{(3)} & 1 \\ 0 & \mathbf{T}_{1(b)}^{(3)} & 0 \\ \mathbf{M}_2^{(4)} \end{bmatrix}, \quad (2.20)$$

where  $\hat{\Gamma}_2^{(3)}$  follows (2.15).  $\mathbf{T}_{1(a)}^{(3)}$  is derived from  $\Gamma_1^{(3)}$  by manipulating the right most “1” in  $\Gamma_1^{(3)}$  to “0”.  $\mathbf{T}_{1(b)}^{(3)}$  is derived from  $\Gamma_1^{(3)}$  by manipulating the left most “0” in  $\Gamma_1^{(3)}$  to “1”. There are multiple ways to extract a submatrix from  $\Gamma_2^{(4)}$ . One of them is selected as example. This segmentation is similar to (2.15).  $\Gamma_2^{(4)}$  can be segmented to

$$\Gamma_2^{(4)} = \begin{bmatrix} \mathbf{0} & \hat{\Gamma}_2^{(3)} & \mathbf{1} \\ 1 & \mathbf{T}_{1(a)}^{(3)} & 1 \\ 0 & \mathbf{T}_{1(b)}^{(3)} & 0 \\ \hline & \mathbf{M}_2^{(4)} & \end{bmatrix} = \begin{bmatrix} \hat{\mathbf{Y}}_2^{(4)} \\ \mathbf{M}_2^{(4)} \end{bmatrix}, \quad (2.21)$$

where  $\hat{\Gamma}_2^{(4)}$  is the core submatrix extracted from  $\Gamma_2^{(4)}$ .  $\mathbf{M}_2^{(4)}$  is the redundant submatrix to discard. Let us check the rank of  $\hat{\Gamma}_2^{(4)}$

$$\text{rank}[\hat{\Gamma}_2^{(4)}] = 5. \quad (2.22)$$

$\hat{\Gamma}_2^{(4)}$  holds the same rank as  $\Gamma_2^{(4)}$ .

$\Gamma_3^{(4)}$  is as follows

$$\Gamma_3^{(4)} = \begin{bmatrix} 1 & 0 & 1 & 0 & 1 & 0 \\ 1 & 1 & 0 & 0 & 1 & 0 \\ 1 & 0 & 1 & 1 & 0 & 0 \\ 1 & 1 & 0 & 1 & 0 & 0 \\ 1 & 0 & 1 & 0 & 0 & 1 \\ 0 & 1 & 1 & 0 & 1 & 0 \\ 0 & 1 & 1 & 0 & 0 & 1 \\ 0 & 1 & 1 & 1 & 0 & 0 \\ 1 & 1 & 0 & 0 & 0 & 1 \end{bmatrix} = \begin{bmatrix} 1 & 0 & 1 & 0 & 1 & 0 \\ 1 & 1 & 0 & 0 & 1 & 0 \\ 1 & 0 & 1 & 1 & 0 & 0 \\ 1 & 0 & 1 & 0 & 0 & 1 \\ 0 & 1 & 1 & 0 & 1 & 0 \\ \hline 1 & 1 & 0 & 1 & 0 & 0 \\ 0 & 1 & 1 & 0 & 0 & 1 \\ 0 & 1 & 1 & 1 & 0 & 0 \\ 1 & 1 & 0 & 0 & 0 & 1 \end{bmatrix} = \begin{bmatrix} \mathbf{1} & \hat{\Gamma}_2^{(3)} & \mathbf{0} \\ 1 & \mathbf{T}_{2(a)}^{(3)} & 1 \\ 0 & \mathbf{T}_{2(b)}^{(3)} & 0 \\ \hline & \mathbf{M}_3^{(4)} & \end{bmatrix}, \quad (2.23)$$

where  $\hat{\Gamma}_2^{(3)}$  follows (2.15).  $\mathbf{T}_{2(a)}^{(3)}$  is derived from  $\hat{\Gamma}_2^{(3)}$  by manipulating the right most “1” in first row of  $\hat{\Gamma}_2^{(3)}$  to “0”.  $\mathbf{T}_{2(b)}^{(3)}$  is derived from  $\hat{\Gamma}_2^{(3)}$  by manipulating the left most “0” in first row of  $\hat{\Gamma}_2^{(3)}$  to “1”. There are multiple ways to extract a submatrix from  $\Gamma_3^{(4)}$ . One

of them is selected as example. This segmentation logic is similar to (2.16).  $\Gamma_3^{(4)}$  can be segmented to

$$\Gamma_3^{(4)} = \begin{bmatrix} \mathbf{M}_3^{(4)} \\ \hline \mathbf{1} & \mathbf{T}_{2(a)}^{(3)} & \mathbf{1} \\ \mathbf{0} & \mathbf{T}_{2(b)}^{(3)} & \mathbf{0} \\ \hline \mathbf{1} & \hat{\Gamma}_2^{(3)} & \mathbf{0} \end{bmatrix} = \begin{bmatrix} \mathbf{M}_3^{(4)} \\ \hat{\Gamma}_3^{(4)} \end{bmatrix}, \quad (2.24)$$

where  $\hat{\Gamma}_3^{(4)}$  is the core submatrix extracted from  $\Gamma_2^{(4)}$ .  $\mathbf{M}_2^{(4)}$  is the redundant submatrix to discard. Let us check the rank of  $\hat{\Gamma}_3^{(4)}$

$$\text{rank}[\hat{\Gamma}_3^{(4)}] = 5. \quad (2.25)$$

$\hat{\Gamma}_3^{(4)}$  holds the same rank as  $\Gamma_3^{(4)}$ .

Instead of checking the rank of  $[\Gamma_1^{(4)} \Gamma_2^{(4)}]^T$ ,  $[\Gamma_2^{(4)} \Gamma_3^{(4)}]^T$ , and  $[\Gamma_3^{(4)} \Gamma_4^{(4)}]^T$ , let us check the rank of  $[\Gamma_1^{(4)} \hat{\Gamma}_2^{(4)}]^T$ ,  $[\hat{\Gamma}_2^{(4)} \hat{\Gamma}_3^{(4)}]^T$  and  $[\hat{\Gamma}_3^{(3)} \Gamma_4^{(3)}]^T$ .

$$\text{rank} \begin{bmatrix} \Gamma_1^{(4)} \\ \hat{\Gamma}_2^{(4)} \end{bmatrix} = 6, \quad \text{rank} \begin{bmatrix} \hat{\Gamma}_2^{(4)} \\ \hat{\Gamma}_3^{(4)} \end{bmatrix} = 6, \quad \text{and} \quad \text{rank} \begin{bmatrix} \hat{\Gamma}_3^{(4)} \\ \Gamma_4^{(4)} \end{bmatrix} = 6. \quad (2.26)$$

Since  $[\Gamma_1^{(4)} \hat{\Gamma}_2^{(4)}]^T$ ,  $[\hat{\Gamma}_2^{(4)} \hat{\Gamma}_3^{(4)}]^T$  and  $[\hat{\Gamma}_3^{(3)} \Gamma_4^{(3)}]^T$  are submatrices of  $[\Gamma_1^{(4)} \Gamma_2^{(4)}]^T$ ,  $[\Gamma_2^{(4)} \Gamma_3^{(4)}]^T$ , and  $[\Gamma_3^{(4)} \Gamma_4^{(4)}]^T$ , the rank of  $[\Gamma_1^{(4)} \Gamma_2^{(4)}]^T$ ,  $[\Gamma_2^{(4)} \Gamma_3^{(4)}]^T$ , and  $[\Gamma_3^{(4)} \Gamma_4^{(4)}]^T$  should also be six.

Here are some observations from four-level MMC:

- a. The first and last level matrices,  $\Gamma_1^{(4)}$  and  $\Gamma_4^{(4)}$ , have no need to extract submatrices;
- b. The second level matrix,  $\Gamma_2^{(4)}$ , needs to extract a submatrix, and this core submatrix

$\hat{\Gamma}_2^{(4)}$  can be derived from  $\hat{\Gamma}_2^{(3)}$  and  $\Gamma_1^{(3)}$ ;

- c. The second to the last matrix,  $\Gamma_3^{(4)}$ , needs to extract a submatrix, and this core submatrix  $\hat{\Gamma}_3^{(4)}$  can be derived from  $\hat{\Gamma}_2^{(3)}$  only.

Let's extend this matrix extraction procedure to  $N$ -level MMC:

- a. The first and last level matrices,  $\Gamma_1^{(N)}$  and  $\Gamma_N^{(N)}$ , have no need to extract submatrices;
- b. The second to  $(N-2)$ th level matrices,  $\Gamma_2^{(N)}$  to  $\Gamma_{N-2}^{(N)}$ , need to extract submatrices, and these core submatrices,  $\hat{\Gamma}_2^{(N)}$  to  $\hat{\Gamma}_{N-2}^{(N)}$ , can be derived from  $\Gamma_1^{(N-1)}$  and  $\hat{\Gamma}_2^{(N-1)}$  to  $\hat{\Gamma}_{N-2}^{(N-1)}$ ;
- c. The second to the last matrix,  $\Gamma_{N-1}^{(N)}$ , needs to extract a submatrix, and this core submatrix  $\hat{\Gamma}_{N-1}^{(N)}$  can be derived from  $\hat{\Gamma}_{N-2}^{(N-1)}$  only.

Assume that the  $\Gamma$  matrix and its core submatrix  $\hat{\Gamma}$  of  $(N-1)$ -level MMC are as follows,

$$\Gamma^{(N-1)} = \begin{bmatrix} \Gamma_1^{(N-1)} \\ \Gamma_2^{(N-1)} \\ \vdots \\ \Gamma_k^{(N-1)} \\ \vdots \\ \Gamma_{N-1}^{(N-1)} \end{bmatrix}, \hat{\Gamma}^{(N-1)} = \begin{bmatrix} \Gamma_1^{(N-1)} \\ \hat{\Gamma}_2^{(N-1)} \\ \vdots \\ \hat{\Gamma}_k^{(N-1)} \\ \vdots \\ \hat{\Gamma}_{N-2}^{(N-1)} \\ \Gamma_{N-1}^{(N-1)} \end{bmatrix}, \quad (2.27)$$

$\Gamma_1^{(N-1)}$  and  $\Gamma_{N-1}^{(N-1)}$  are 1-by- $(2N-4)$  matrices. There is no need to extract submatrices from these two.  $\Gamma_2^{(N-1)}$  to  $\Gamma_{N-2}^{(N-1)}$  are  $m_k$ -by- $(2N-4)$  matrices, where  $m_k = C_{N-2}^{k-1} C_{N-2}^{N-k-1} = (C_{N-2}^{k-1})^2$  as described in (2.11).  $\hat{\Gamma}^{(N-1)}$  is extracted from  $\Gamma^{(N-1)}$  and holds the same rank as  $\Gamma^{(N-1)}$ .

Assume that the  $\Gamma$  matrix and its core submatrix  $\hat{\Gamma}$  of  $N$ -level MMC are as follows,

$$\mathbf{\Gamma}^{(N)} = \begin{bmatrix} \mathbf{\Gamma}_1^{(N)} \\ \mathbf{\Gamma}_2^{(N)} \\ \vdots \\ \mathbf{\Gamma}_k^{(N)} \\ \vdots \\ \mathbf{\Gamma}_N^{(N)} \end{bmatrix}, \hat{\mathbf{Y}}^{(N)} = \begin{bmatrix} \mathbf{\Gamma}_1^{(N)} \\ \hat{\mathbf{\Gamma}}_2^{(N)} \\ \vdots \\ \hat{\mathbf{\Gamma}}_k^{(N)} \\ \vdots \\ \hat{\mathbf{\Gamma}}_{N-1}^{(N)} \\ \mathbf{\Gamma}_N^{(N)} \end{bmatrix}, \quad (2.28)$$

$\mathbf{\Gamma}_1^{(N)}$  and  $\mathbf{\Gamma}_N^{(N)}$  are 1-by- $(2N-2)$  matrices. There is no need to extract submatrices from these two.  $\mathbf{\Gamma}_2^{(N)}$  to  $\mathbf{\Gamma}_{N-1}^{(N)}$  are  $m_k$ -by- $(2N-2)$  matrices, where  $m_k = C_{N-1}^{k-1} C_{N-1}^{N-k} = (C_{N-1}^{k-1})^2$  as described in (2.11).  $\hat{\mathbf{\Gamma}}^{(N)}$  is extracted from  $\mathbf{\Gamma}^{(N)}$  and holds the same rank as  $\mathbf{\Gamma}^{(N)}$ . Instead of extracting  $\hat{\mathbf{\Gamma}}^{(N)}$  directly from  $\mathbf{\Gamma}^{(N)}$ ,  $\hat{\mathbf{\Gamma}}^{(N)}$  could also be derived from  $\hat{\mathbf{\Gamma}}^{(N-1)}$ .

$$\mathbf{\Gamma}_1^{(N)} = [\underbrace{0 \cdots 0}_{N-1} \quad \underbrace{1 \cdots 1}_{N-1}], \quad (2.29)$$

$$\hat{\mathbf{\Gamma}}_k^{(N)} = \begin{bmatrix} \mathbf{0} & \hat{\mathbf{\Gamma}}_k^{(N-1)} & \mathbf{1} \\ 1 & \mathbf{T}_{k-1(a)}^{(N-1)} & 1 \\ 0 & \mathbf{T}_{k-1(b)}^{(N-1)} & 0 \end{bmatrix}, \quad (2.30)$$

where  $2 \leq k \leq N-2$ .

$$\hat{\mathbf{\Gamma}}_{N-1}^{(N)} = \begin{bmatrix} 1 & \mathbf{T}_{N-2(a)}^{(N-1)} & 1 \\ 0 & \mathbf{T}_{N-2(b)}^{(N-1)} & 0 \\ \mathbf{1} & \hat{\mathbf{\Gamma}}_{N-2}^{(N-1)} & \mathbf{0} \end{bmatrix}, \quad (2.31)$$

$$\mathbf{\Gamma}_N^{(N)} = [\underbrace{1 \cdots 1}_{N-1} \quad \underbrace{0 \cdots 0}_{N-1}]. \quad (2.32)$$

Eq.(2.31)-(2.32) demonstrate how to derive  $\hat{\mathbf{\Gamma}}^{(N)}$  from  $\hat{\mathbf{Y}}^{(N-1)}$ .  $\mathbf{\Gamma}_1^{(N)}$  is a 1-by- $(2N-2)$  matrix with the first  $N-1$  elements to be zero and the last  $N-1$  elements to be one.  $\hat{\mathbf{\Gamma}}_k^{(N)}$  consists of three parts. The first part is derived from  $\hat{\mathbf{\Gamma}}_k^{(N-1)}$  by adding a zero vector to the left

of  $\hat{\Gamma}_k^{(N-1)}$  and a one vector to the right of  $\hat{\Gamma}_k^{(N-1)}$ . The second part is derived from  $\mathbf{T}_{k-1(a)}^{(N-1)}$  by adding two “1”s to the left and right of  $\mathbf{T}_{k-1(a)}^{(N-1)}$ , where  $\mathbf{T}_{k-1(a)}^{(N-1)}$  is derived from  $\hat{\Gamma}_{k-1}^{(N-1)}$  by manipulating the right most “1” in first row of  $\hat{\Gamma}_{k-1}^{(N-1)}$  to “0”. The third part is derived from  $\mathbf{T}_{k-1(b)}^{(N-1)}$  by adding two “0”s to the left and right of  $\mathbf{T}_{k-1(b)}^{(N-1)}$ , where  $\mathbf{T}_{k-1(b)}^{(N-1)}$  is derived from  $\hat{\Gamma}_{k-1}^{(N-1)}$  by manipulating the left most “0” in first row of  $\hat{\Gamma}_{k-1}^{(N-1)}$  to “1”.  $\hat{\Gamma}_{N-1}^{(N)}$  consists of three parts. The first part is derived from  $\mathbf{T}_{N-2(a)}^{(N-1)}$  by adding two “1”s to the left and right of  $\mathbf{T}_{N-2(a)}^{(N-1)}$ , where  $\mathbf{T}_{N-2(a)}^{(N-1)}$  is derived from  $\hat{\Gamma}_{N-2}^{(N-1)}$  by manipulating the right most “1” in first row of  $\hat{\Gamma}_{N-2}^{(N-1)}$  to “0”. The second part is derived from  $\mathbf{T}_{N-2(b)}^{(N-1)}$  by adding two “0”s to the left and right of  $\mathbf{T}_{N-2(b)}^{(N-1)}$ , where  $\mathbf{T}_{N-2(b)}^{(N-1)}$  is derived from  $\hat{\Gamma}_{N-2}^{(N-1)}$  by manipulating the left most “0” in first row of  $\hat{\Gamma}_{N-2}^{(N-1)}$  to “1”. Both  $\hat{\Gamma}_k^{(N-1)}$  and  $\hat{\Gamma}_{N-1}^{(N)}$  are  $(2N-3)$ -by- $(2N-2)$  matrix. The third part is derived from  $\hat{\Gamma}_{N-2}^{(N-1)}$  by adding a zero vector to the left of  $\hat{\Gamma}_{N-2}^{(N-1)}$  and a one vector to the right of  $\hat{\Gamma}_{N-2}^{(N-1)}$ .  $\Gamma_N^{(N)}$  is a 1-by- $(N-1)$  matrix with the first  $N-1$  elements to be one and the last  $N-1$  elements to be zero.

$\hat{\Gamma}_k^{(N-1)}$  and  $\hat{\Gamma}_{N-2}^{(N-1)}$  are expected to be a  $(2N-5)$ -by- $(2N-4)$  matrix, with an expected rank of  $2N-5$ .  $\hat{\Gamma}_k^{(N)}$  and  $\hat{\Gamma}_{N-1}^{(N)}$  are expected to be a  $(2N-3)$ -by- $(2N-2)$  matrix, with an expected rank of  $2N-3$ . The reason why we cannot find a uniform formula for both  $\hat{\Gamma}_k^{(N)}$  and  $\hat{\Gamma}_{N-1}^{(N)}$  is that  $\hat{\Gamma}_{N-1}^{(N)}$  cannot be derived from  $\Gamma_{N-1}^{(N-1)}$ . Remember that  $\Gamma_{N-1}^{(N-1)}$  is a 1-by- $(2N-4)$  matrix. If  $\hat{\Gamma}_{N-1}^{(N)}$  is derived similar to (2.30) as follows,

$$\hat{\mathbf{\Gamma}}_{N-1}^{(N)} = \begin{bmatrix} \mathbf{0} & \mathbf{\Gamma}_{N-1}^{(N-1)} & \mathbf{1} \\ \mathbf{1} & \mathbf{T}_{k-1(a)}^{(N-1)} & \mathbf{1} \\ \mathbf{0} & \mathbf{T}_{k-1(b)}^{(N-1)} & \mathbf{0} \end{bmatrix}. \quad (2.33)$$

$\hat{\mathbf{\Gamma}}_{N-1}^{(N)}$  becomes a 3-by- $(2N-2)$  matrix. The rank of a 3-by- $(2N-2)$  matrix cannot exceed 3, which cannot satisfy the rank expectation.

### 2.4.3 N-LEVEL MMC CONJECTURE

The rank of any two adjacent levels is expected to be  $2N-2$ . To secure the self voltage balancing for  $N$ -level MMC, which is the same as the number of submodules. To check the rank of any two adjacent levels, one option is analytically proving that:

- a. The rank of  $\left[ \mathbf{\Gamma}_1^{(N)} \quad \hat{\mathbf{\Gamma}}_2^{(N)} \right]^T$  is  $2N-2$ ;
- b. The rank of  $\left[ \hat{\mathbf{\Gamma}}_k^{(N)} \quad \hat{\mathbf{\Gamma}}_{k+1}^{(N)} \right]^T$  is  $2N-2$ , where  $2 \leq k \leq N-3$ ;
- c. The rank of  $\left[ \hat{\mathbf{\Gamma}}_{N-2}^{(N)} \quad \hat{\mathbf{\Gamma}}_{N-1}^{(N)} \right]^T$  is  $2N-2$ ;
- d. The rank of  $\left[ \hat{\mathbf{\Gamma}}_{N-1}^{(N)} \quad \mathbf{\Gamma}_N^{(N)} \right]^T$  is  $2N-2$ .

Or alternatively prove that

- a. If the rank of  $\left[ \mathbf{\Gamma}_1^{(N-1)} \quad \hat{\mathbf{\Gamma}}_2^{(N-1)} \right]^T$  is  $m$  for an  $(N-1)$ -level MMC, then the rank of  $\left[ \mathbf{\Gamma}_1^{(N)} \quad \hat{\mathbf{\Gamma}}_2^{(N)} \right]^T$  is  $m+2$  for an  $N$ -level MMC;
- b. If the rank of  $\left[ \hat{\mathbf{\Gamma}}_k^{(N-1)} \quad \hat{\mathbf{\Gamma}}_{k+1}^{(N-1)} \right]^T$  is  $m$  for an  $(N-1)$ -level MMC, then the rank of  $\left[ \hat{\mathbf{\Gamma}}_k^{(N)} \quad \hat{\mathbf{\Gamma}}_{k+1}^{(N)} \right]^T$  is  $m+2$  for an  $N$ -level MMC, where  $2 \leq k \leq N-3$ ;
- c. If the rank of  $\left[ \hat{\mathbf{\Gamma}}_{N-2}^{(N-1)} \quad \mathbf{\Gamma}_{N-1}^{(N-1)} \right]^T$  is  $m$  for an  $(N-1)$ -level MMC, then the rank of  $\left[ \hat{\mathbf{\Gamma}}_{N-2}^{(N)} \quad \hat{\mathbf{\Gamma}}_{N-1}^{(N)} \right]^T$  is  $m+2$  for an  $N$ -level MMC;

d. If the rank of  $\begin{bmatrix} \hat{\mathbf{\Gamma}}_{N-2}^{(N-1)} & \mathbf{\Gamma}_{N-1}^{(N-1)} \end{bmatrix}^T$  is  $m$  for an  $(N - 1)$ -level MMC, then the rank of

$\begin{bmatrix} \hat{\mathbf{\Gamma}}_{N-1}^{(N)} & \mathbf{\Gamma}_N^{(N)} \end{bmatrix}^T$  is  $m + 2$  for an  $N$ -level MMC.

Since we have proved that two-, three-, and four-level MMCs have self voltage balancing feature, this feature can be extended to five-, six-, seven-level, and so on.

The proof of the conjectures above requires comprehensive knowledge of linear algebra and is out of the scope of this dissertation. Some trials are included in Appendix A. The author of this dissertation would like to leave this proof for the future work.

#### 2.4.4 COMPUTER-AID PROOF

As per power electronics engineering, it is not always necessary to consider the operation of an MMC with more than 500 levels. In High-Voltage DC (HVDC) transmission applications, the MMC is built with 200–400 submodules in each arm [33]. The first HVDC installation Trans Bay Cable project utilized an MMC structure with around 200 submodules per arm [35]. Normally there are hundreds of submodules per arm in HVDC applications [36]. Thanks to the powerful computation capability of modern computers, they make it possible to generate the  $\hat{\mathbf{\Gamma}}$  matrix of a hundreds-level MMC by giving the  $\hat{\mathbf{\Gamma}}$  matrix of a three-level MMC. A Matlab script is created to generate the  $\hat{\mathbf{\Gamma}}$  of 3-level MMC to 533-level MMC, and to justify the rank of any two adjacent levels. The flowchart of the Matlab script is shown in Figure 2.5. The Matlab script is attached in Appendix B.

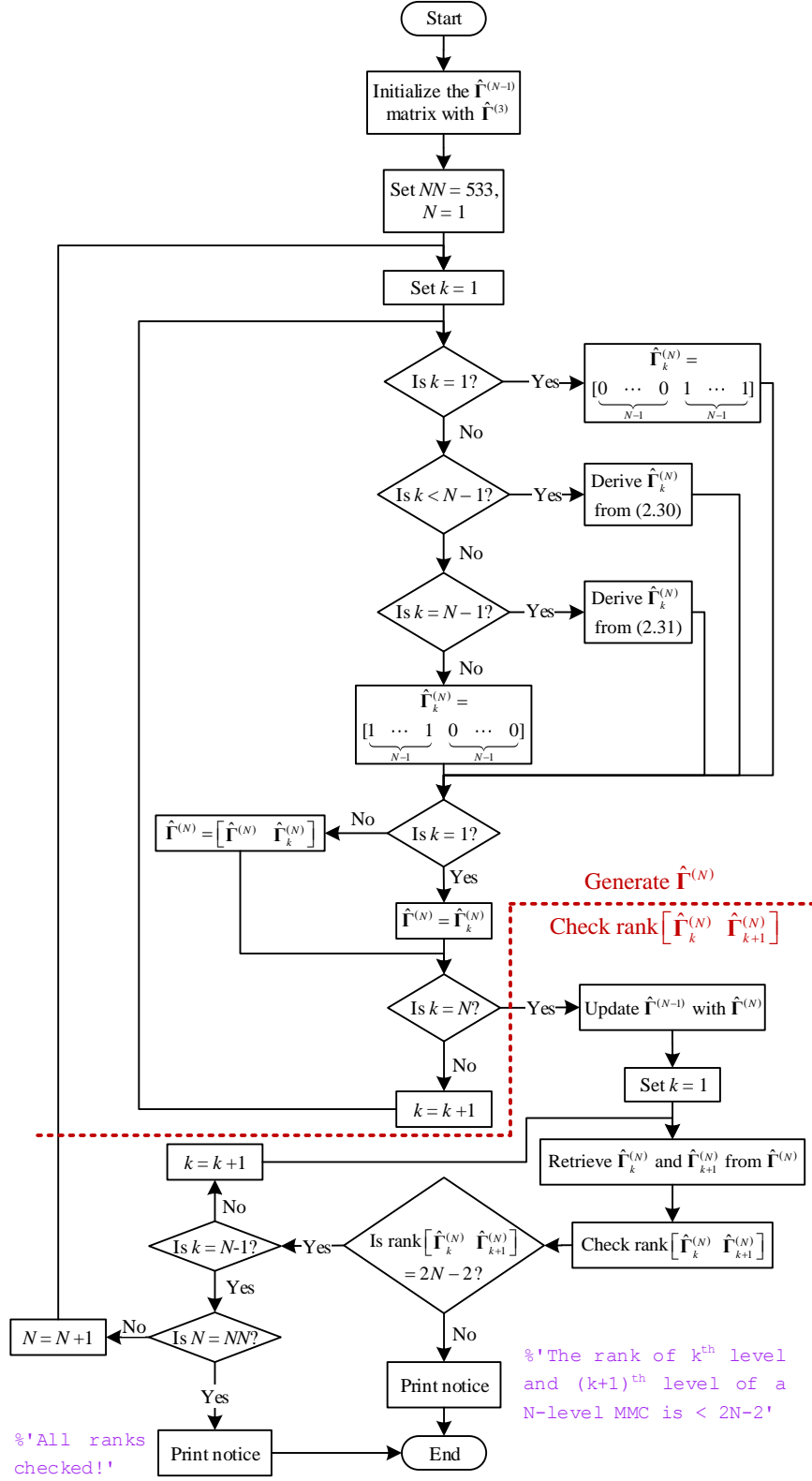


Figure 2.5 The flowchart of checking the rank of  $\Gamma$  matrix.

According to the MATLAB result, the rank of any two adjacent levels is  $2N - 2$ , up to 533-level MMC. A rank of  $2N - 2$  guarantees that  $\hat{\Gamma}$  matrix of any two adjacent levels, from 2-level MMC to 533-level MMC, has  $2N - 2$  linearly independent rows. Hence, we could find no more than one set of solutions for  $2N - 2$  capacitors' voltages if combining any two adjacent levels. There is one possible set of solutions for (2.11),

$$\begin{bmatrix} V_{C1} \\ V_{C2} \\ \vdots \\ V_{C(2N-2)} \end{bmatrix}_{(2N-2) \times 1} = \begin{bmatrix} V_{dc} \\ V_{dc} \\ \vdots \\ V_{dc} \end{bmatrix}_{(2N-2) \times 1}. \quad (2.34)$$

These solutions of capacitor voltages are quite intuitive. Since (2.11) has no more than one set of solutions, (2.34) must be the only set of solutions.

The author of this dissertation conjectures that this conclusion can be extended to any level MMC. If the conjecture is true, we can conclude that MMC has self voltage balancing by nature. If the conjecture is false, we can conclude that MMC has self voltage balancing by nature up to 533 levels at least.

## 2.5 CONCLUSION

This chapter explores the self voltage balancing nature of MMC. Mathematically, MMC submodule voltage can balance If utilizing certain submodule patterns. A computer-aid procedure is given to guarantee that  $N$ -level MMC, where  $N < 534$ , has this self voltage balancing by nature. This chapter conjectures that this conclusion can be extended to any level of MMC.

### 3 $\Gamma$ -MATRIX MODULATION ( $\Gamma$ MM)

#### 3.1 INTRODUCTION

As discussed in Chapter 2, the MMC structure has self voltage balancing feature in a mathematical sense. Here comes a question. How to realize this self voltage balancing feature over math to engineering? As mentioned in Chapter 2, when MMC visits one submodule pattern, one equation in (2.11) is satisfied at a time. When MMC visits all submodule patterns in the  $\Gamma$ , or the  $\hat{\Gamma}$ , it is said to have finished one iteration. MMC capacitor voltages are expected to converge to (2.34) after several iterations. This chapter focuses on developing an effective modulation, namely  $\Gamma$ -Matrix Modulation ( $\Gamma$ MM), to realize the self voltage balancing feature for MMC. With this novel  $\Gamma$ -Matrix Modulation, the low-frequency ripple on dc capacitors is highly reduced, which makes it possible to have an extremely small submodule capacitor to absorb only the switching-level ripples.

#### 3.2 $\Gamma$ MM BASED TWO-LEVEL MMC

As shown in Figure 2.1, the pole voltage  $v_a$  of a two-level MMC can either be  $1/2V_{dc}$  or  $-1/2V_{dc}$  if the  $V_{C1} = V_{C2} = V_{dc}$ . Assume the expected ac-side voltage to be  $v_s^*$ , and the pole voltage  $v_a$  to follow the PWM strategy. The relationship of  $v_s^*$  and  $v_a$  is plotted in Figure 3.1.

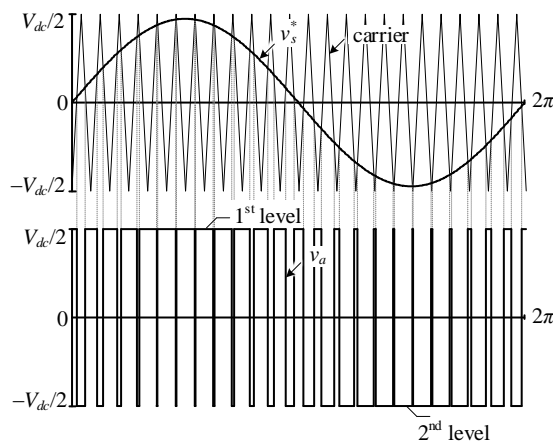


Figure 3.1 Relationship of ac-side voltage  $v_s^*$  and pole voltage  $v_a$ .

When the pole voltage  $v_a$  at first level, one of the rows in  $\Gamma_1^{(2)}$  will be assigned to the MMC as the chosen submodule pattern to realize this first-level pole-voltage. Recall that there is only one row in  $\Gamma_1^{(2)}$ , which is [0 1]. This row can be interpreted as this: the  $SM_1$  is at by-pass mode and the  $SM_2$  is at inserting mode. The switches of each submodule need to follow this piece of  $\Gamma$ -matrix command accordingly. Similarly, when the pole voltage  $v_a$  at second level, one of the rows in  $\Gamma_2^{(2)}$  will be assigned to MMC as the chosen submodule pattern to realize this second-level pole-voltage. Recall that there is only one row in  $\Gamma_2^{(2)}$ , which is [1 0]. This row can be interpreted as this: the  $SM_1$  is at inserting mode and the  $SM_2$  is at by-pass mode. The switches of each submodule need to follow this piece of  $\Gamma$ -matrix command accordingly. A MATLAB/Simulink simulation is conducted to demonstrate the  $\Gamma$ M based two-level MMC.

### ❖ Case Study 2.1 $\Gamma$ M Based Two-Level MMC

**Objective:** In this case study, the working principle and the performance of  $\Gamma$ M based 2-level MMC are studied through MATLAB/Simulink. The simulation topology is shown in Figure3.2.

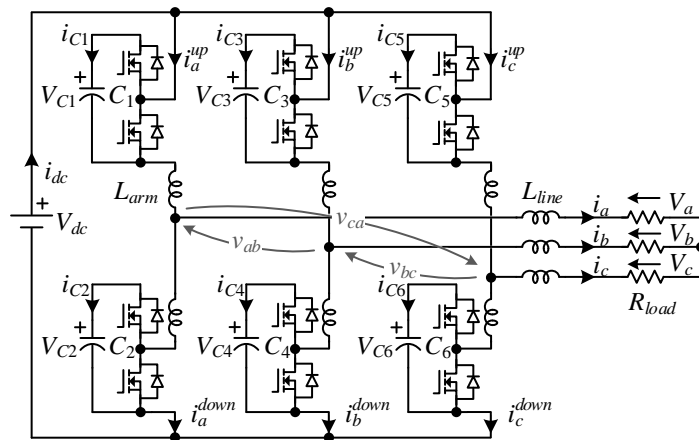


Figure 3.2 Two-level MMC simulation topology.

**Parameters:** The key parameters of the MMC are as follows: rated apparent power  $S = 50$  kVA, output phase voltage  $V_a = V_b = V_c = 320$  V, output line current  $I_a = I_b = I_c = 52$  A, rated output fundamental frequency  $f_0 = 60$  Hz, rated load resistance  $R_{load} = 6.2 \Omega$ , rated dc-bus voltage  $V_{dc} = 1$  kV, number of submodules per arm:  $N - 1 = 1$ , submodule capacitance  $C_i = 85 \mu\text{F}$  ( $i = 1, 2, \dots, 6$ ), line inductance  $L_{line} = 1$  mH, and arm inductance  $L_{arm} = 0.1 \mu\text{H}$ . The switching frequency is  $f_{sw} = 10$  kHz. The definition of switching frequency is the frequency of the MMC pole voltage jumping from one level to the other adjacent level. The key parameters are summarized in Table 1.

Table 1

Two-level mmc simulation key parameters.

Apparent Power, $S$	50 kVA
Fundamental Frequency, $f_0$	60 Hz
Switching Frequency, $f_{sw}$	10 kHz
DC-Bus Voltage, $V_{dc}$	1000 V
Phase Voltage, $V_a, V_b, V_c$	320 V
Line Current, $I_a, I_b, I_c$	52 A
Load Resistance, $R_{load}$	6.2 $\Omega$ (100% p.u.)
Line Inductance, $L_{line}$	1 mH (6% p.u.)
Arm Inductance, $L_{arm}$	0.1 $\mu\text{H}$ (0.0006% p.u.)
Submodule Capacitance, $C_i$	85 $\mu\text{F}$ (20% p.u.)
Number of Submodules per Arm	1

where  $i = 1, 2, \dots, 6$ .

**Analysis:** This two-level MMC simulation follows the  $\Gamma$ -Matrix Modulation strategy. The load voltage and current are shown in Figure3.3. The mid-point voltage is shown in Figure3.4. The mid-point voltage of two-level MMC has three levels. Although the mid-point voltage of any single phase,  $v_a$ ,  $v_b$  and  $v_c$ , has only two levels, the differential voltage of any two phases,  $v_{ab}$ ,  $v_{bc}$  and  $v_{ca}$ , has three levels. The submodule capacitor voltage and current are shown in Figure3.5. The capacitor voltage ripple is within 2%. The capacitor current consists mainly of fundamental component and switching-frequency harmonics. Note that the submodule capacitance is only 0.2 p.u.. The energy stored in capacitor is

$$E_i = \frac{1}{2} C_i V_{Ci}^2 = 0.5 \times 85 \times 10^{-6} \times 1000^2 = 42.5 \text{ (J)}. \quad (3.1)$$

The total energy in all submodule capacitors is

$$E_{total} = \sum_{i=1}^6 E_i = 6 \times \frac{1}{2} C_i V_{Ci}^2 = 255 \text{ (J)}. \quad (3.2)$$

The two-level MMC power rating is 50 kVA. The total capacitor energy in respect to MMC power rating is

$$\varepsilon = \frac{E_{total}}{S} = \frac{255 \times 10^{-3}}{50 \times 10^{-3}} = 5.1 \text{ (kJ/MVA)}. \quad (3.3)$$

Typically, the conventional MMC submodule capacitance is chosen such that the total stored energy in all submodule capacitors of the converter is approximately 30 – 40 kJ/MVA, where MVA refers to the converter rating, giving ripple in the range of 10% [35]. To have a voltage ripple within 2%, the conventional MMC needs to have submodule capacitors energy to be 150 – 200 kJ/MVA. Normally, the capacitor energy storage capability is proportional to the capacitor volume. The  $\Gamma$ MM based MMC features an extremely small capacitor volume compared to conventional MMC.

The capacitor voltage is well balanced and converging to the expected value (1000 V) in Figure3.5. However, the fundamental ripples still exist. These fundamental ripples are introduced by the arm inductor and stray resistor. Note that the capacitor voltage balance analysis in previous sections does not consider the voltage drop on arm inductors and stray resistance. The effect of those passive components will be discussed in future work.

Figure3.6 shows line current of phase-A and its corresponding arms' current. The arm current contains not only fundamental component but also switching-frequency harmonics. Normally, the conventional MMC arm current does not contain many switching-frequency harmonics, and the arm inductance follows the equation [36]

$$L_{arm} = \frac{1}{8\omega_0^2 \cdot C_i \cdot V_{Ci}} \left( \frac{S}{3I_{2\omega}} + V_{dc} \right), \quad (3.4)$$

where  $\omega_0 = 2\pi f_0$ ,  $V_{Ci} = 1000$  V, and  $I_{2\omega}$  is the peak value of the  $2-\omega$  component in arm current. For conventional MMC,  $C_i = 150/5.1 \times 85 \mu\text{F} = 2550 \mu\text{F}$  to have a voltage ripple within 2%.  $I_{2\omega}$  is known to be 13.8 A from simulation. The arm inductance of conventional MMC should be  $757 \mu\text{H}$  (4.6% p.u.) according to (3.4). The arm inductor of  $\Gamma\text{MM}$  based MMC is extremely small comparing to conventional MMC. Small arm inductance is critical to balance the capacitor voltage. This will be explained in future work.

Figure3.7 shows the input dc voltage and current. As seen from Figure3.7, the input current consists of dc component and switching-frequency harmonics. These switching-frequency harmonics can be mitigated by adding a decoupling capacitor at dc bus.

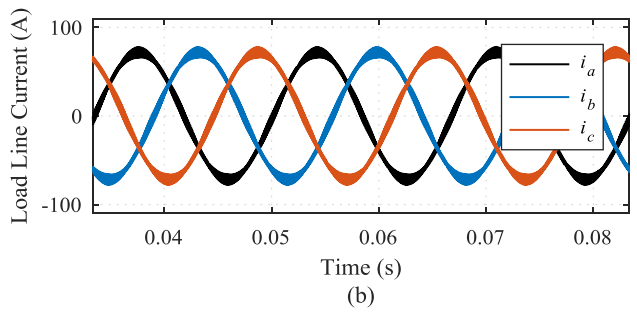
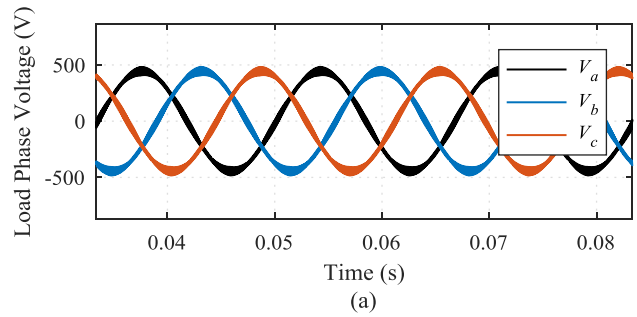
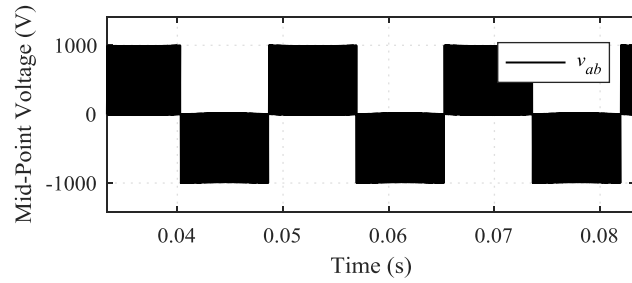
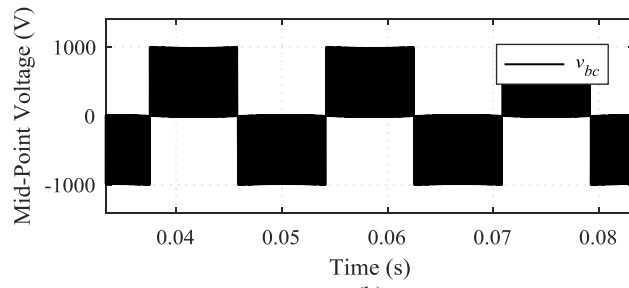


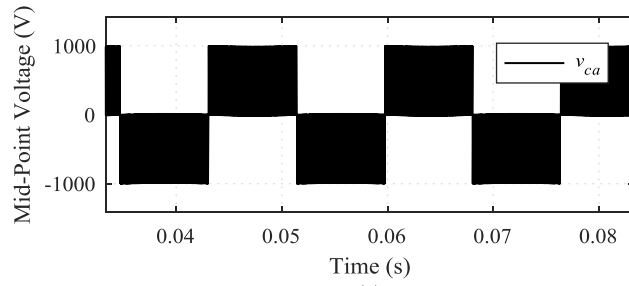
Figure 3.3 Two-level MMC (a) load voltage and (b) load current.



(a)



(b)



(c)

Figure 3.4 Two-level MMC mid-point voltage (a)  $v_{ab}$ ; (b)  $v_{bc}$ ; and (c)  $v_{ca}$ .

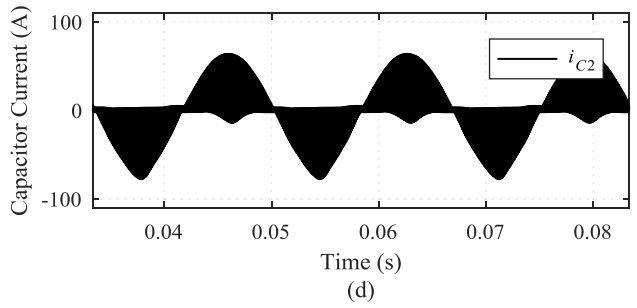
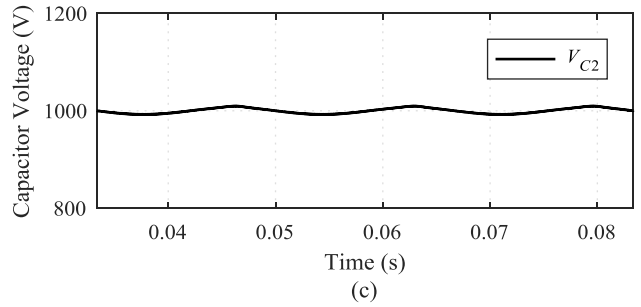
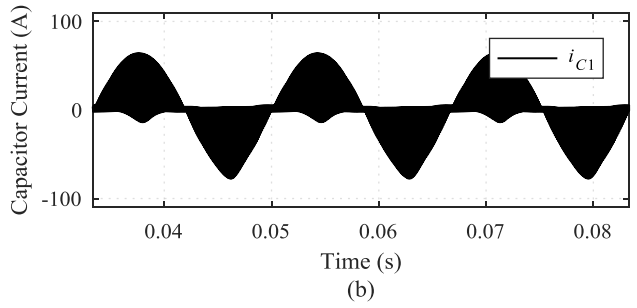
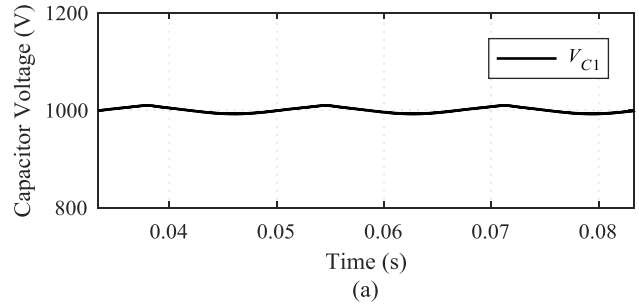


Figure 3.5 Submodule capacitor (a)/(c) voltage; and (b)/(d) current.

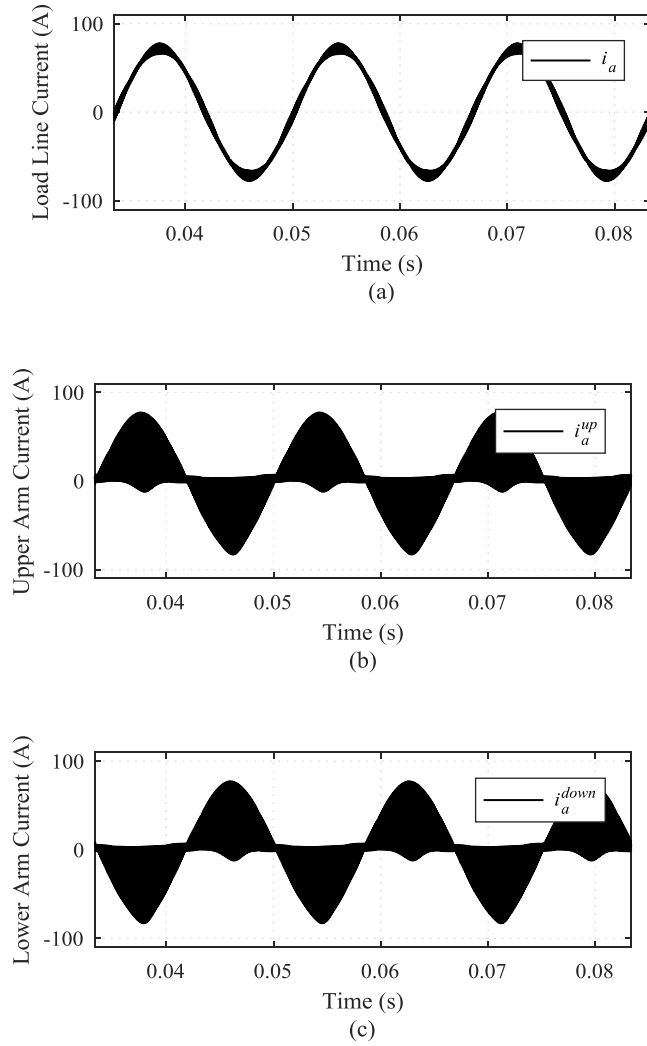


Figure 3.6 (a) Line current of phase-A and its corresponding (b) upper arm current, (c) lower arm current.

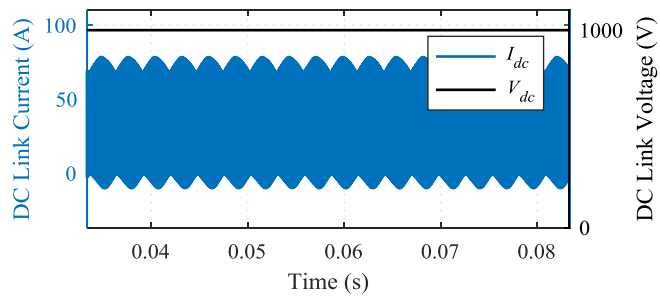


Figure 3.7 Dc input voltage and current.

### 3.3 $\Gamma$ MM BASED THREE-LEVEL MMC

As shown in Figure 2.2, the pole voltage  $v_a$  of a three-level MMC can either be  $V_{dc}$ , zero volt, or  $-V_{dc}$  if all capacitor voltages are  $V_{dc}$ . Assume the expected ac-side voltage to be  $v_s^*$ . The pole voltage  $v_a$  follows the level-shifted modulation strategy. The relationship of  $v_s^*$  and  $v_a$  is plotted in Figure 3.8.

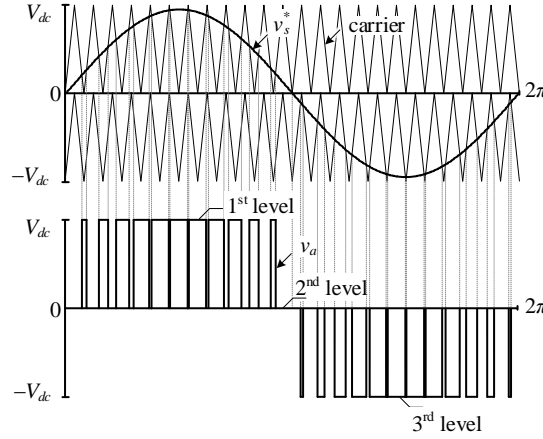


Figure 3.8 Relationship of ac-side voltage  $v_s^*$  and pole voltage  $v_a$ .

When the pole voltage  $v_a$  at first level, one of the rows in  $\Gamma_1^{(3)}$  will be assigned to the MMC as the chosen submodule pattern to realize this first-level pole-voltage. Recall that there is only one row in  $\Gamma_1^{(3)}$ , which is  $[0\ 0\ 1\ 1]$ . This row can be interpreted as this: SM<sub>1</sub> and SM<sub>2</sub> are at by-pass mode, and SM<sub>3</sub> and SM<sub>4</sub> are at inserting mode. The switches of each submodule need to follow this piece of  $\Gamma$ -matrix command accordingly. Similarly, when the pole voltage  $v_a$  at third level, one of the rows in  $\Gamma_3^{(3)}$  will be assigned to MMC as the chosen submodule pattern to realize this third-level pole-voltage. Recall that there is only one row in  $\Gamma_3^{(3)}$ , which is  $[1\ 1\ 0\ 0]$ . This row can be interpreted as this: SM<sub>1</sub> and SM<sub>2</sub> are at inserting mode and SM<sub>3</sub> and SM<sub>4</sub> are at by-pass mode. The switches of each submodule need to follow this piece of  $\Gamma$ -matrix command accordingly.

When the pole voltage  $v_a$  at second level, one of the rows in  $\Gamma_2^{(3)}$  will be assigned to MMC as the chosen submodule pattern to realize this second-level pole-voltage. Recall that there are four rows in  $\Gamma_2^{(3)}$  and the rank of  $\Gamma_2^{(3)}$  is three, which means only three rows in  $\Gamma_2^{(3)}$  are needed to achieve the capacitor voltage balance. There are four combinations of three rows in  $\Gamma_2^{(3)}$  in total and all of them have a rank of three. Hence, we can choose any one of these four submatrices to compose the modulation table. The submatrix  $\hat{\mathbf{Y}}_2^{(3)}$  following (2.16) is selected in this chapter to demonstrate the three-level MMC modulation. The three-level MMC modulation can be explained with the aid of Figure 3.9. When the pole voltage  $v_a$  is determined to be at second level by level-shifted modulation, the level pointer is pointed to Level 2. The gating signal generator is going to grab the current row of  $\hat{\mathbf{Y}}_2^{(3)}$  that the  $\Gamma$ -matrix pointer in level two is pointing to. After feeding the  $\Gamma$ -matrix command to gating signal generator, the level two pointer will point to the next row and wait for the next visit of level pointer. A MATLAB/Simulink simulation is conducted to demonstrate the  $\Gamma$ M based three-level MMC.

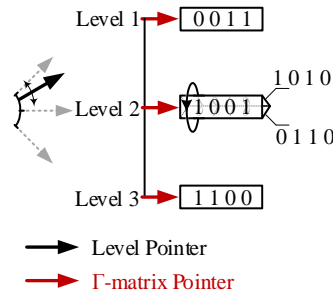


Figure 3.9  $\Gamma$ -matrix modulation strategy for three-level MMC.

### ❖ Case Study 2.2 FMM Based Three-Level MMC

**Objective:** In this case study, the working principle and the performance of FMM based three-level MMC are studied through MATLAB/Simulink. The simulation topology is shown in Figure3.10.

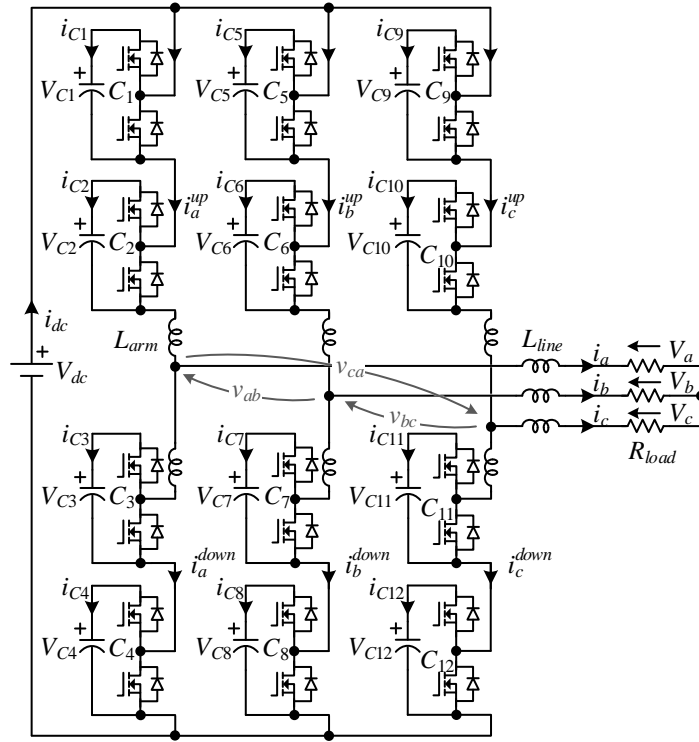


Figure 3.10 Three-level MMC simulation topology.

**Parameters:** The key parameters of the MMC are as follows: rated apparent power  $S = 100$  kVA, output phase voltage  $V_a = V_b = V_c = 643$  V, output line current  $I_a = I_b = I_c = 52$  A, rated output fundamental frequency  $f_0 = 60$  Hz, rated load resistance  $R_{load} = 12.4 \Omega$ , rated dc-bus voltage  $V_{dc} = 2$  kV, number of submodules per arm:  $N - 1 = 2$ , submodule capacitance  $C_i = 85 \mu\text{F}$  ( $i = 1, 2, \dots, 12$ ), line inductance  $L_{line} = 1$  mH, and arm inductance  $L_{arm} = 0.1 \mu\text{H}$ . The switching frequency is  $f_{sw} = 20$  kHz. The definition of switching frequency is the frequency of the MMC pole voltage jumping from one level to the other adjacent level. The key parameters are summarized in Table 2.

Table 2

Three-level MMC simulation key parameters.

Apparent Power, $S$	100 kVA
Fundamental Frequency, $f_0$	60 Hz
Switching Frequency, $f_{sw}$	20 kHz
DC-Bus Voltage, $V_{dc}$	2000 V
Phase Voltage, $V_a, V_b, V_c$	643 V
Line Current, $I_a, I_b, I_c$	52 A
Load Resistance, $R_{load}$	12.4 $\Omega$ (100% p.u.)
Line Inductance, $L_{line}$	1 mH (3% p.u.)
Arm Inductance, $L_{arm}$	0.1 $\mu$ H (0.0003% p.u.)
Submodule Capacitance, $C_i$	85 $\mu$ F (40% p.u.)
Number of Submodules per Arm	2

where  $i = 1, 2, \dots, 12$ .

**Analysis:** This three-level MMC simulation follows the  $\Gamma$ -Matrix Modulation strategy. The submatrix  $\hat{\mathbf{\Gamma}}_2^{(3)}$  extraction follows (2.16). The load voltage and current are shown in Figure3.11. The mid-point voltage is shown in Figure3.12. The mid-point voltage of three-level MMC has five levels. Although the mid-point voltage of any single phase,  $v_a$ ,  $v_b$  or  $v_c$ , has only three levels, the differential voltage of any two phases,  $v_{ab}$ ,  $v_{bc}$  and  $v_{ca}$ , has five levels. The submodule capacitor voltage and current are shown in Figure3.13. The capacitor voltage ripple is within 3%. The capacitor current consists mainly of fundamental

component and switching-frequency harmonics. Note that the submodule capacitance is only 0.4 p.u.. The energy stored in capacitor is

$$E_i = \frac{1}{2} C_i V_{Ci}^2 = 0.5 \times 85 \times 10^{-6} \times 1000^2 = 42.5 \text{ (J)}. \quad (3.5)$$

The total energy in all submodule capacitors is

$$E_{total} = \sum_{i=1}^{12} E_i = 12 \times \frac{1}{2} C_i V_{Ci}^2 = 510 \text{ (J)}. \quad (3.6)$$

The three-level MMC power rating is 100 kVA. The total capacitor energy in respect to MMC power rating is

$$\varepsilon = \frac{E_{total}}{S} = \frac{510 \times 10^{-3}}{100 \times 10^{-3}} = 5.1 \text{ (kJ/MVA)}. \quad (3.7)$$

Typically, the conventional MMC submodule capacitance is chosen such that the total stored energy in all submodule capacitors of the converter is approximately 30 – 40 kJ/MVA, where MVA refers to the converter rating, giving ripple in the range of 10% [37]. To have a voltage ripple within 3%, the conventional MMC needs to have submodule capacitors energy to be 100 – 130 kJ/MVA. Normally, the capacitor energy storage capability is proportional to the capacitor volume. The  $\Gamma$ MM based MMC features an extremely small capacitor volume compared to conventional MMC.

The capacitor voltage is well balanced and converging to the expected value (1000 V) in Figure3.13. However, the fundamental ripples still exist. These fundamental ripples are introduced by the arm inductor and stray resistance. Note that the capacitor voltage balancing analysis in Chapter 1 did not consider the voltage drop on arm inductors and stray resistance. The effect of those passive components will be discussed in future work.

Figure3.14 shows the line current of phase-A and its corresponding arms' current. The arm current contains not only fundamental component but also switching-frequency

harmonics. Normally, the conventional MMC arm current does not contain many switching-frequency harmonics, and the arm inductance follows the equation (3.4) [38], where  $\omega_0 = 2\pi f_0$ ,  $V_{Ci} = 1000$  V, and  $I_{2\omega}$  is the peak value of the  $2-\omega$  component in arm current. For conventional MMC,  $C_i = 100/5.1 \times 85 \mu\text{F} = 16667 \mu\text{F}$  to have a voltage ripple within 3%. Assume  $I_{2\omega}$  to be 13.8 A ( $I_a \times 26.5\%$ ). The arm inductance of conventional MMC should be 2.33 mH (7.1% p.u.) according to (3.4). The arm inductor of  $\Gamma$ MM based MMC is extremely small comparing to conventional MMC. Small arm inductance is critical to balance the capacitor voltage. This will be explained in future work.

Figure 3.15 shows the input dc voltage and current. As seen from Figure 3.15, the input current consists of dc component and switching-frequency harmonics. These switching-frequency harmonics can be mitigated by adding a decoupling capacitor at dc bus.

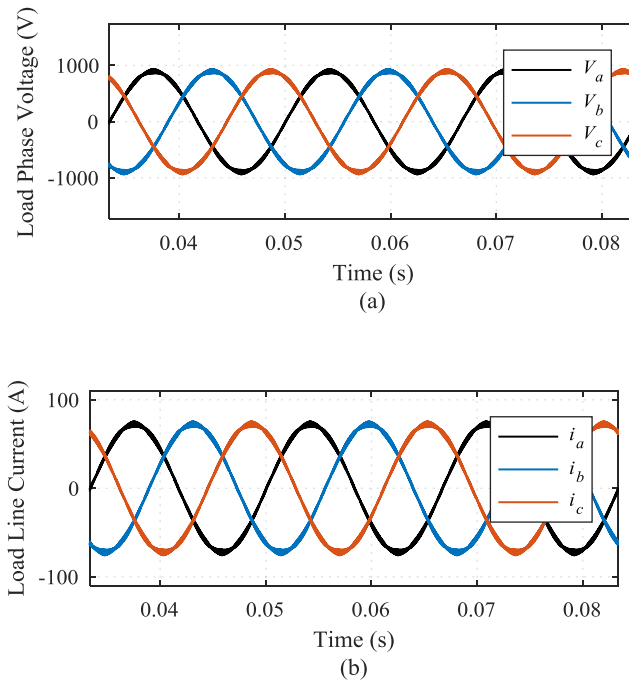


Figure 3.11 Three-level MMC (a) load voltage and (b) load current.

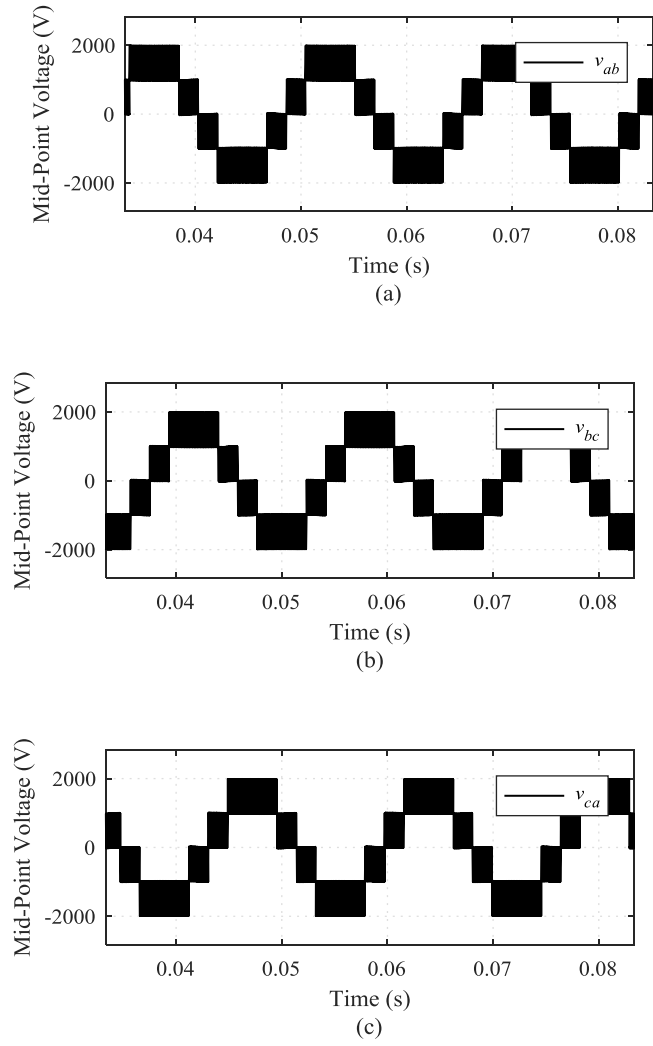


Figure 3.12 Three-level MMC mid-point voltage (a)  $v_{ab}$ ; (b)  $v_{bc}$ ; and (c)  $v_{ca}$ .

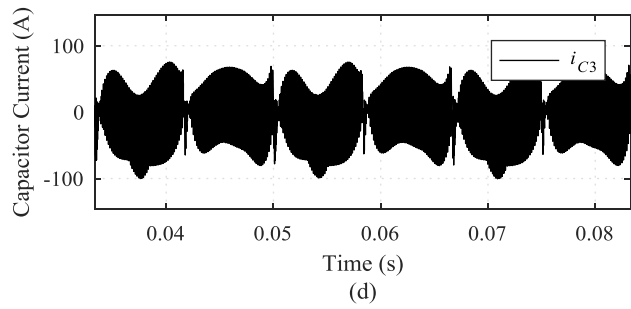
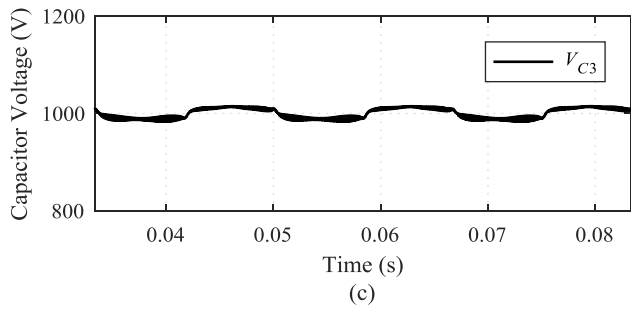
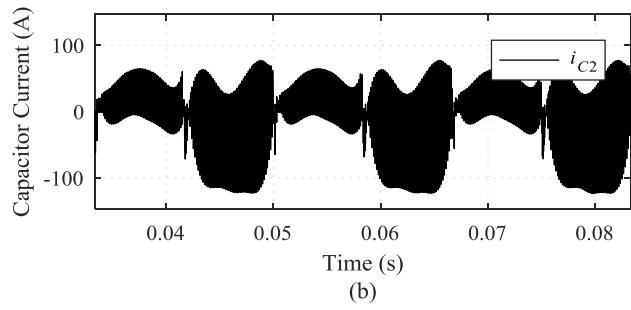
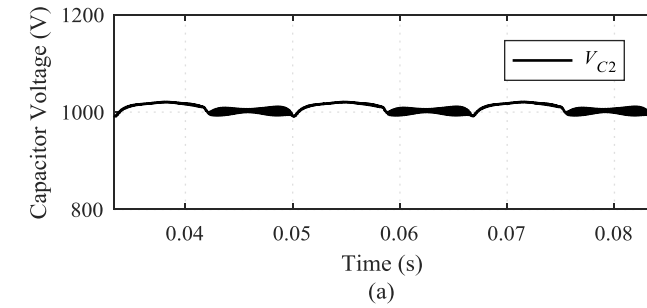


Figure 3.13 Submodule capacitor (a)/(c) voltage; and (b)/(d) current.

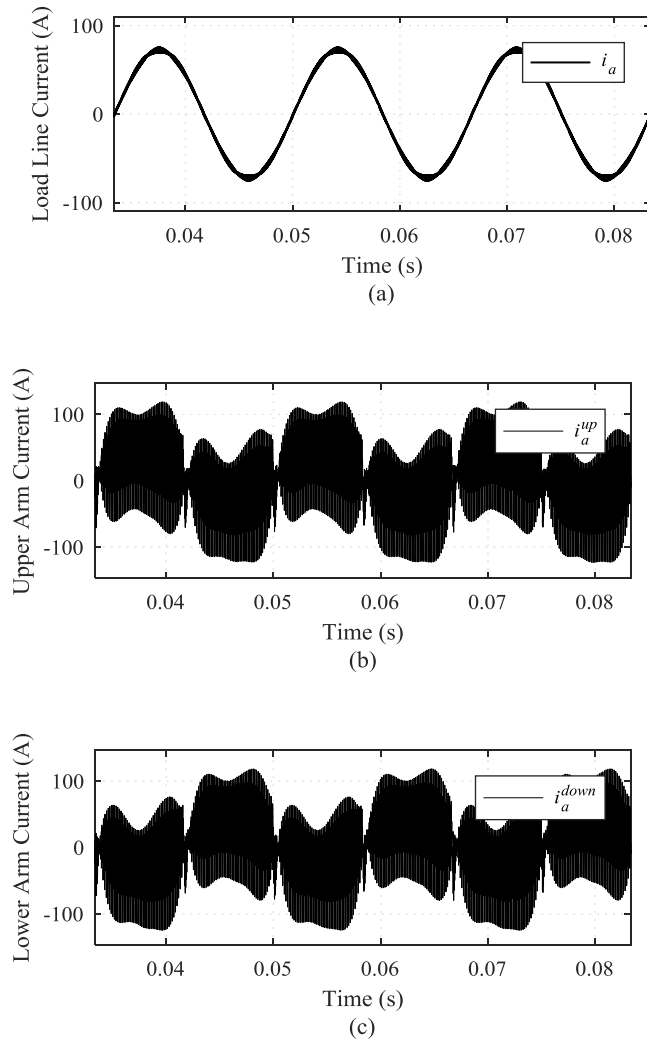


Figure 3.14 (a) Line current of phase-A and its corresponding (b) upper arm current, (c) lower arm current.

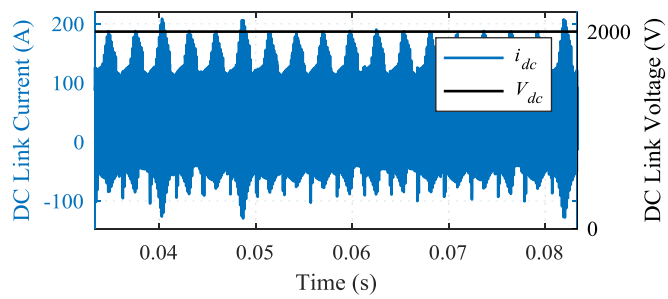


Figure 3.15 Dc input voltage and current.

### 3.4 FMM BASED N-LEVEL MMC

As shown in Figure 2.3, The pole voltage  $v_a$  of an  $N$ -level MMC is an element of  $\{(N-1)V_{dc}/2, (N-3)V_{dc}/2, (N-5)V_{dc}/2, \dots, V_{dc}, 0, -V_{dc}, \dots, -(N-3)V_{dc}/2, -(N-1)V_{dc}/2\}$ , if  $N$  is an odd number. The pole voltage  $v_a$  of an  $N$ -level MMC is an element of  $\{(N-1)V_{dc}/2, (N-3)V_{dc}/2, (N-5)V_{dc}/2, \dots, V_{dc}/2, -V_{dc}/2, \dots, -(N-3)V_{dc}/2, -(N-1)V_{dc}/2\}$ , if  $N$  is an even number. Assume the expected ac-side voltage to be  $v_s^*$ . The pole voltage  $v_a$  follows the level-shifted modulation strategy. As shown in Figure 3.16,  $N - 1$  carriers are needed to determine  $N$ -level shape of  $v_a$ . The relationship of  $v_s^*$  and  $v_a$  is plotted in Figure 3.17.

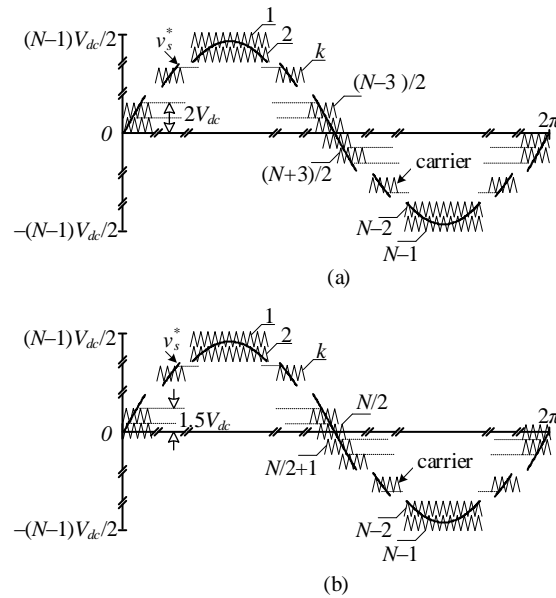


Figure 3.16 Ac-side voltage  $v_s^*$  and carriers, when (a)  $N$  is an odd number; and (b)  $N$  is an even number.

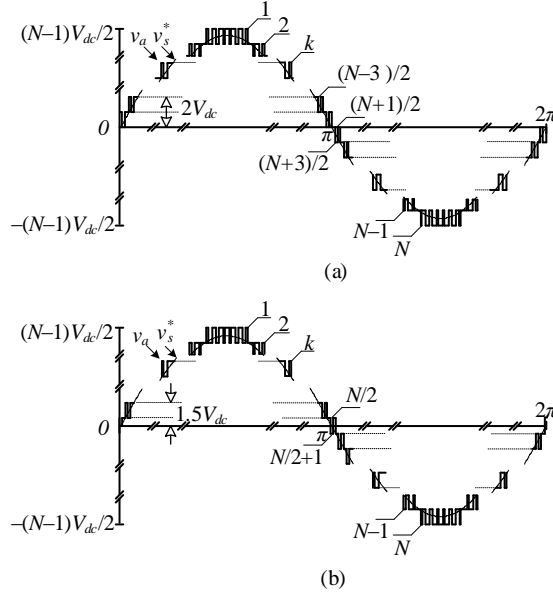


Figure 3.17 Ac-side voltage  $v_s^*$  and pole voltage  $v_a$ , when (a)  $N$  is an odd number; and  
(b)  $N$  is an even number.

When the pole voltage  $v_a$  at first level, one of the rows in  $\Gamma_1^{(N)}$  will be assigned to the MMC as the chosen submodule pattern to realize this first-level pole-voltage. Recall that there is only one row in  $\Gamma_1^{(N)}$ , as formulated in (2.29). This row can be interpreted as this:  $SM_1$  to  $SM_{N-1}$  are at by-pass mode, and  $SM_N$  to  $SM_{2N-2}$  are at inserting mode. The switches of each submodule need to follow this piece of  $\Gamma$ -matrix command accordingly. Similarly, when the pole voltage  $v_a$  at  $N$ -th level, one of the rows in  $\Gamma_N^{(N)}$  will be assigned to MMC as the chosen submodule pattern to realize this  $N$ -th-level pole-voltage. Recall that there is only one row in  $\Gamma_N^{(N)}$ , as formulated in (2.32). This row can be interpreted as this:  $SM_1$  to  $SM_{N-1}$  are at inserting mode and  $SM_N$  and  $SM_{2N-2}$  are at by-pass mode. The switches of each submodule need to follow this piece of  $\Gamma$ -matrix command accordingly.

When the pole voltage  $v_a$  at  $k$ -th level, where  $2 \leq k \leq N-1$ , one of the rows in  $\Gamma_k^{(N)}$  will be assigned to MMC as the chosen submodule pattern to realize this  $k$ -th-level pole-voltage.

Recall that there are  $m_k$  rows in  $\Gamma_k^{(N)}$  where  $m_k = C_{N-1}^{k-1} C_{N-1}^{N-k} = (C_{N-1}^{k-1})^2$ . The rank of  $\Gamma_k^{(N)}$  is  $2N - 3$ , which means only  $2N - 3$  rows in  $\Gamma_k^{(N)}$  are needed to achieve the capacitor voltage balance. There are  $C_{m_k}^{2N-3}$  combinations of  $2N - 3$  rows in  $\Gamma_k^{(N)}$  in total. However, not all of them have a rank of  $2N - 3$ . Unlike two- and three-level MMC,  $N$ -level MMC submatrix,  $\hat{\Gamma}_k^{(N)}$ , needs careful selection. The  $\hat{\Gamma}_k^{(N)}$  extraction in this section follows the  $\hat{\Gamma}_k^{(N)}$  composition in Chapter 2.4 (2.30) - (2.31). The core submatrix,  $\hat{\Gamma}_2^{(3)}$ , of this composition procedure follows (2.16). This submatrix extraction may not be the optimal choice, but it is good enough to demonstrate the self voltage balancing of  $N$ -level MMC. The  $\Gamma$ MM procedure of  $N$ -level MMC are as follows,

- a. Determine the level of  $v_a$  by level-shifted modulation;
- b. Assign the instantaneous level number to the level pointer;
- c. Find the  $\Gamma$ -matrix pointer to which the level pointer points to;
- d. Read the  $\Gamma$ -matrix row (submodule pattern) which the  $\Gamma$ -matrix pointer points to;
- e. Generate the switching function for each submodule according to the current row of  $\Gamma$  matrix;
- f. Update  $\Gamma$ -matrix pointer to next row and wait for next call from level pointer.

The  $N$ -level MMC modulation can also be explained with the aid of Figure 3.18. To fully understand the self voltage balancing of  $N$ -level MMC, MATLAB/Simulink simulations are studied based on the  $\Gamma$ -matrix modulation.

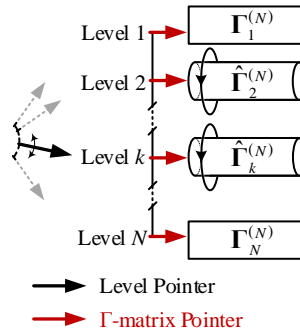


Figure 3.18  $\Gamma$ -matrix modulation strategy for  $N$ -level MMC.

### 3.4.1 CASE STUDY: $\Gamma$ M BASED FOUR-LEVEL MMC

**Objective:** In this case study, the working principle and the performance of  $\Gamma$ M based four-level MMC are studied through MATLAB/Simulink. The simulation topology is shown in Figure3.19.

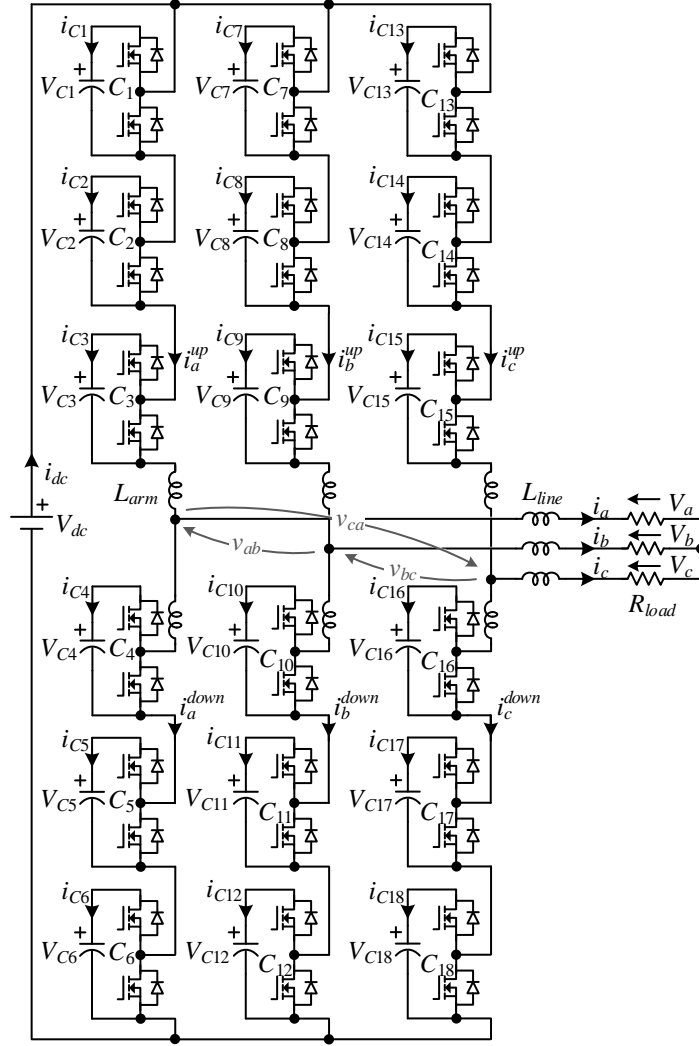


Figure 3.19 Four-level MMC simulation topology.

**Parameters:** The key parameters of the MMC are as follows: rated apparent power  $S = 150$  kVA, output phase voltage  $V_a = V_b = V_c = 964$  V, output line current  $I_a = I_b = I_c = 52$  A, rated output fundamental frequency  $f_0 = 60$  Hz, rated load resistance  $R_{load} = 18.6 \Omega$ , rated dc-bus voltage  $V_{dc} = 3$  kV, number of submodules per arm:  $N - 1 = 3$ , submodule capacitance  $C_i = 171 \mu\text{F}$  ( $i = 1, 2, \dots, 18$ ), line inductance  $L_{line} = 1$  mH, and arm inductance  $L_{arm} = 0.1 \mu\text{H}$ . The switching frequency is  $f_{sw} = 30$  kHz. The definition of switching frequency is the frequency of the MMC pole voltage jumping from one level to the other adjacent level. The key parameters are summarized in Table 3.

Table 3

Four-level MMC simulation key parameters.

Apparent Power, $S$	150 kVA
Fundamental Frequency, $f_0$	60 Hz
Switching Frequency, $f_{sw}$	30 kHz
DC-Bus Voltage, $V_{dc}$	3000 V
Phase Voltage, $V_a, V_b, V_c$	964 V
Line Current, $I_a, I_b, I_c$	52 A
Load Resistance, $R_{load}$	18.6 $\Omega$ (100% p.u.)
Line Inductance, $L_{line}$	1 mH (2% p.u.)
Arm Inductance, $L_{arm}$	0.1 $\mu$ H (0.0002% p.u.)
Submodule Capacitance, $C_i$	171 $\mu$ F (1.2 p.u.)
Number of Submodules per Arm	3

where  $i = 1, 2, \dots, 18$ .

**Analysis:** This four-level MMC simulation follows the  $\Gamma$ -Matrix Modulation strategy, as described in Figure3.20. The submatrices are as follows,

$$\mathbf{\Gamma}_1^{(4)} = [0 \ 0 \ 0 \ 1 \ 1 \ 1], \quad (3.8)$$

$$\hat{\mathbf{\Gamma}}_2^{(4)} = \begin{bmatrix} 0 & 1 & 0 & 1 & 0 & 1 \\ 0 & 1 & 0 & 0 & 1 & 1 \\ 0 & 0 & 1 & 1 & 0 & 1 \\ 1 & 0 & 0 & 1 & 0 & 1 \\ 0 & 1 & 0 & 1 & 1 & 0 \end{bmatrix}, \quad (3.9)$$

$$\hat{\mathbf{\Gamma}}_3^{(4)} = \begin{bmatrix} 1 & 1 & 0 & 1 & 0 & 0 \\ 1 & 1 & 0 & 0 & 1 & 0 \\ 1 & 0 & 1 & 1 & 0 & 0 \\ 1 & 1 & 0 & 0 & 0 & 1 \\ 0 & 1 & 1 & 1 & 0 & 0 \end{bmatrix}, \quad (3.10)$$

$$\mathbf{\Gamma}_4^{(4)} = [1 \ 1 \ 1 \ 0 \ 0 \ 0]. \quad (3.11)$$

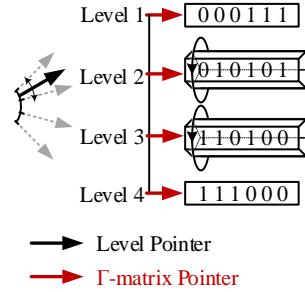


Figure 3.20  $\Gamma$ -matrix modulation strategy for four-level MMC.

All submatrices are full rank. The load voltage and current are shown in Figure 3.21. The mid-point voltage is shown in Figure 3.22. The mid-point voltage of four-level MMC has seven levels. Although the mid-point voltage of any single phase,  $v_a$ ,  $v_b$  or  $v_c$ , has only four levels, the differential voltage of any two phases,  $v_{ab}$ ,  $v_{bc}$  or  $v_{ca}$ , has seven levels. The submodule capacitor voltage and current are shown in Figure 3.23. The capacitor voltage ripple is within 5%. The capacitor current consists mainly of fundamental component and switching-frequency harmonics. Note that the submodule capacitance is only 1.2 p.u.. The energy stored in capacitor is

$$E_i = \frac{1}{2} C_i V_{Ci}^2 = 0.5 \times 171 \times 10^{-6} \times 1000^2 = 85.5 \text{ (J)}. \quad (3.12)$$

The total energy in all submodule capacitors is

$$E_{total} = \sum_{i=1}^{18} E_i = 18 \times \frac{1}{2} C_i V_{Ci}^2 = 1539 \text{ (J)}. \quad (3.13)$$

The four-level MMC power rating is 150 kVA. The total capacitor energy in respect to MMC power rating is

$$\varepsilon = \frac{E_{total}}{S} = \frac{1539 \times 10^{-3}}{150 \times 10^{-3}} = 10.26 \text{ (kJ/MVA)}. \quad (3.14)$$

Typically, the conventional MMC submodule capacitance is chosen such that the total stored energy in all submodule capacitors of the converter is approximately 30 – 40 kJ/MVA, where MVA refers to the converter rating, giving ripple in the range of 10% [37]. To have a voltage ripple within 5%, the conventional MMC needs to have submodule capacitors energy to be 60 – 80 kJ/MVA. Normally, the capacitor energy storage capability is proportional to the capacitor size. The  $\Gamma$ MM based MMC features an extremely small capacitor volume compared to conventional MMC.

The capacitor voltage is well balanced and converging to the expected value (1000 V) in Figure 3.23. However, the fundamental ripples still exist. These fundamental ripples are introduced by the arm inductor and stray resistance. Note that the capacitor voltage balance analysis in Chapter 1 does not consider the voltage drop on arm inductors and stray resistance. The effect of those passive components will be discussed in future work.

Figure 3.24 shows one line current and its corresponding arm current. The arm current contains not only fundamental component but also switching-frequency harmonics. Normally, the conventional MMC arm current does not contain many switching-frequency harmonics, and the arm inductance follows the equation (3.4) [38], where  $\omega_0 = 2\pi f_0$ ,  $V_{Ci} = 1000$  V, and  $I_{2\omega}$  is the peak value of the  $2-\omega$  component in arm current. For conventional MMC,  $C_i = 60/10.26 \times 171 \mu\text{F} = 1000 \mu\text{F}$  is needed to have a voltage ripple within 5%. Assume  $I_{2\omega}$  to be 13.8 A ( $I_a \times 26.5\%$ ). The arm inductance of conventional MMC should be 4.1 mH (8.24% p.u.) according to (3.4). The arm inductor of  $\Gamma$ MM based MMC is

extremely small comparing to conventional MMC. Small arm inductance is critical to balance the capacitor voltage. This will be explained in future work.

Figure3.25 shows the input dc voltage and current. As seen from Figure3.25, the input current consists of dc component and switching-frequency harmonics. These switching-frequency harmonics can be mitigated by adding a decoupling capacitor at dc bus.

Figure3.26 shows all capacitor voltages at phase-A. The capacitor voltages do not deviate from nominal value.

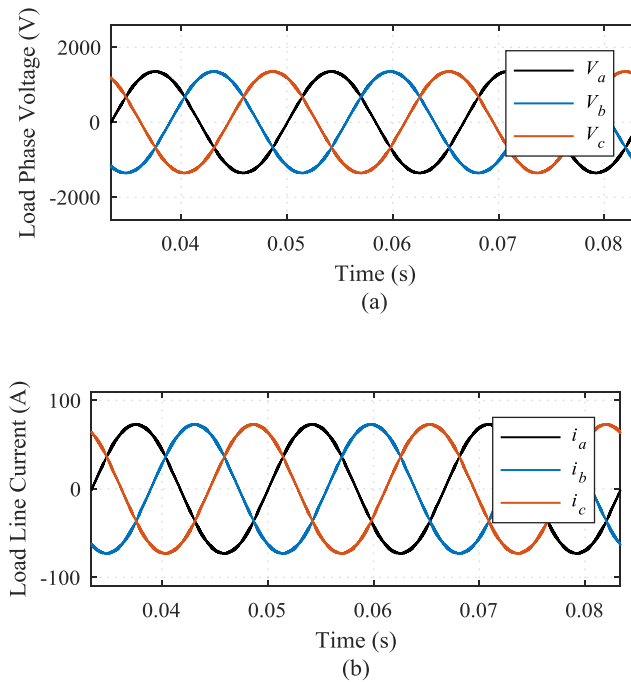
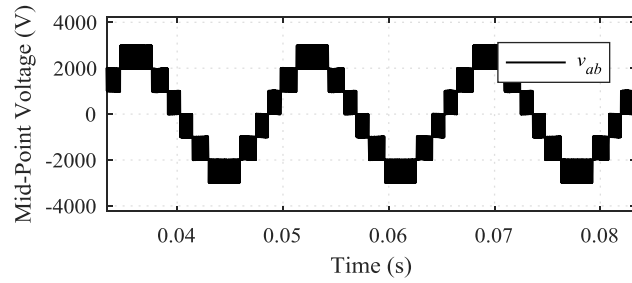
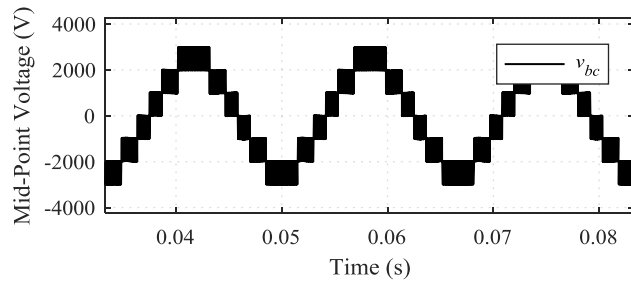


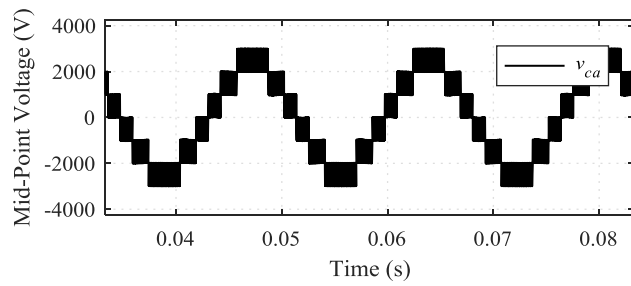
Figure 3.21 Four-level MMC (a) load voltage and (b) load current.



(a)



(b)



(c)

Figure 3.22 Four-level MMC mid-point voltage (a)  $v_{ab}$ ; (b)  $v_{bc}$ ; and (c)  $v_{ca}$ .

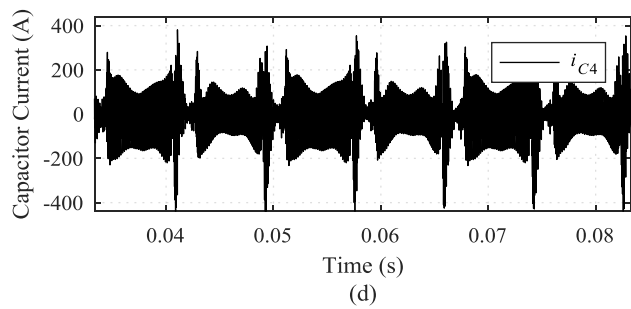
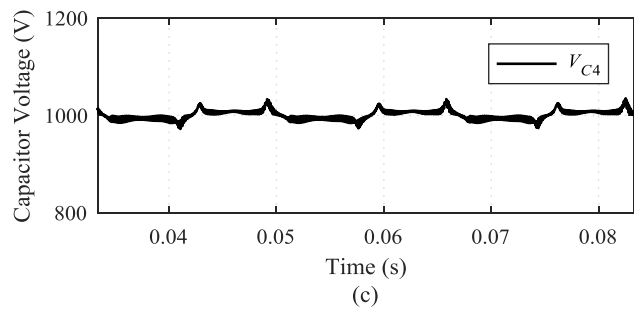
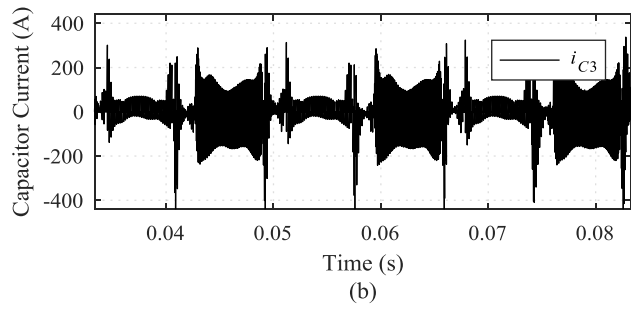
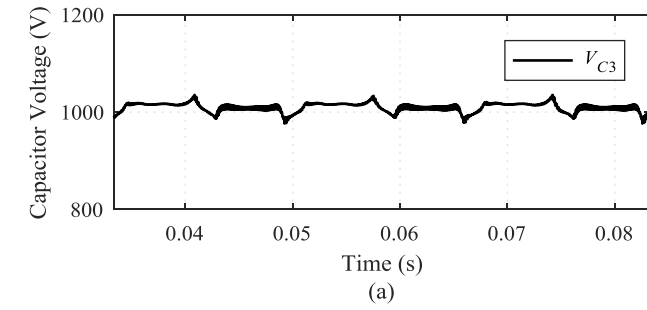


Figure 3.23 Submodule capacitor (a)/(c) voltage; and (b)/(d) current.

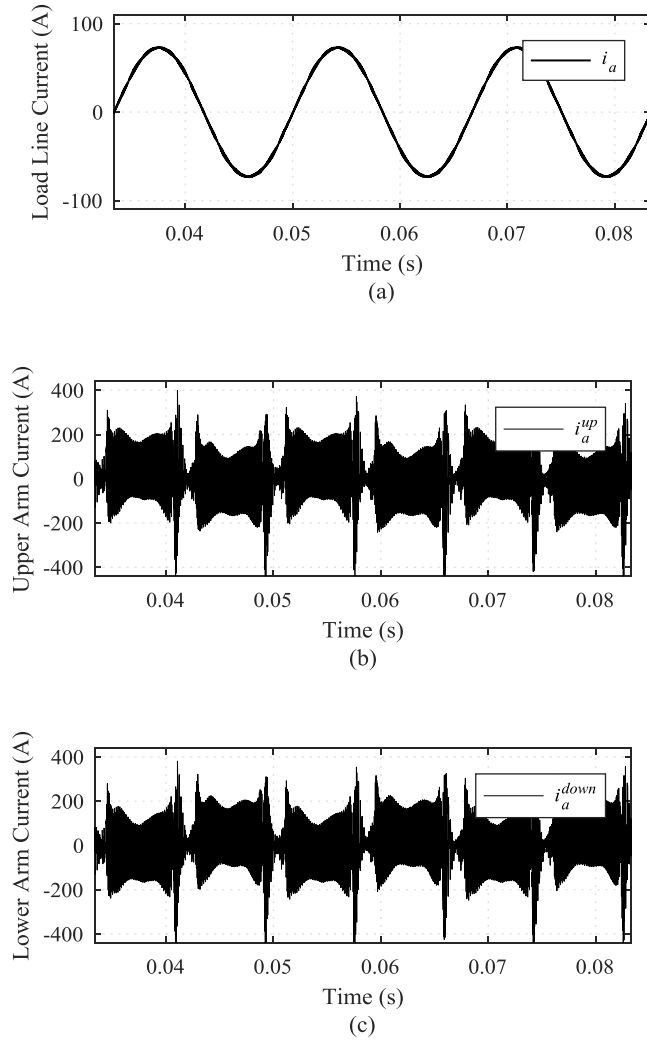


Figure 3.24 (a) Line current in phase-A and its corresponding (b) upper arm current, (c) lower arm current.

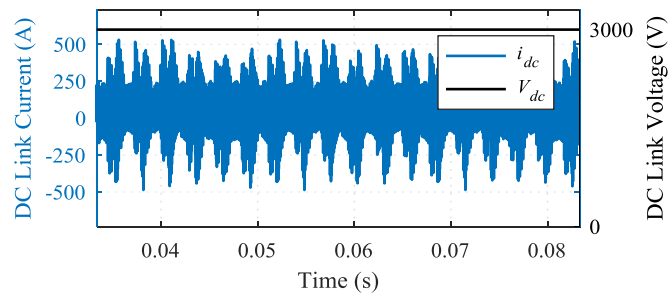


Figure 3.25 Dc input voltage and current.

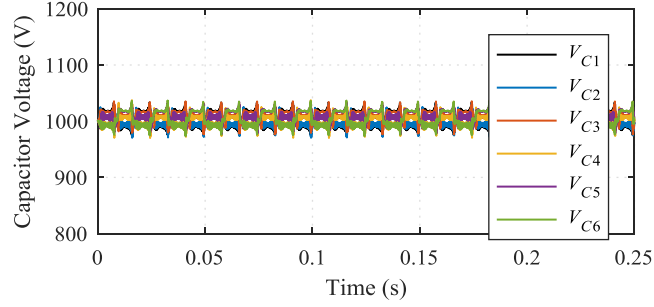


Figure 3.26 All submodule capacitor voltages in phase-A.

### 3.4.2 CASE STUDY: $\Gamma$ MM BASED FOUR-LEVEL MMC WITH NON-FULL-RANK $\Gamma$ MATRIX

**Objective:** In this case study, a non-full-rank  $\Gamma$  matrix is selected for the four-level MMC. Compared with case study in Chapter 3.4.1, the necessity of full-rank  $\Gamma$  matrix selection is addressed. The simulation topology is shown in Figure3.19.

**Parameters:** All the converter parameters are the same as case study in Chapter 3.4.1. The key parameters of the MMC are as follows: rated apparent power  $S = 150$  kVA, output phase voltage  $V_a = V_b = V_c = 964$  V, output line current  $I_a = I_b = I_c = 52$  A, rated output fundamental frequency  $f_0 = 60$  Hz, rated load resistance  $R_{load} = 18.6 \Omega$ , rated dc-bus voltage  $V_{dc} = 3$  kV, number of submodules per arm:  $N - 1 = 3$ , submodule capacitance  $C_i = 171 \mu\text{F}$  ( $i = 1, 2, \dots, 18$ ), line inductance  $L_{line} = 1$  mH, and arm inductance  $L_{arm} = 0.1 \mu\text{H}$ . The switching frequency is  $f_{sw} = 30$  kHz. The definition of switching frequency is the frequency of the MMC pole voltage jumping from one level to the other adjacent level. The key parameters are summarized in Table 3.

**Analysis:** This four-level MMC simulation follows the  $\Gamma$ -Matrix Modulation strategy, as described in Figure3.20. The submatrices are as follows,

$$\Gamma_1^{(4)} = [0 \ 0 \ 0 \ 1 \ 1 \ 1], \quad (3.15)$$

$$\hat{\mathbf{\Gamma}}_2^{(4)} = \begin{bmatrix} 0 & 0 & 1 & 1 & 0 & 1 \\ 0 & 1 & 0 & 0 & 1 & 1 \\ 1 & 0 & 0 & 1 & 1 & 0 \\ 0 & 1 & 0 & 1 & 0 & 1 \\ 0 & 0 & 1 & 0 & 1 & 1 \end{bmatrix}, \quad (3.16)$$

$$\hat{\mathbf{\Gamma}}_3^{(4)} = \begin{bmatrix} 1 & 0 & 1 & 1 & 0 & 0 \\ 1 & 1 & 0 & 0 & 1 & 0 \\ 0 & 1 & 1 & 0 & 0 & 1 \\ 1 & 0 & 1 & 0 & 1 & 0 \\ 1 & 1 & 0 & 1 & 0 & 0 \end{bmatrix}, \quad (3.17)$$

$$\mathbf{\Gamma}_4^{(4)} = [1 \ 1 \ 1 \ 0 \ 0 \ 0]. \quad (3.18)$$

The rank of each matrix are as follows,

$$\text{rank}[\mathbf{\Gamma}_1^{(4)}] = 1, \text{rank}[\hat{\mathbf{\Gamma}}_2^{(4)}] = 4, \text{rank}[\hat{\mathbf{\Gamma}}_3^{(4)}] = 4, \text{ and } \text{rank}[\mathbf{\Gamma}_4^{(4)}] = 1. \quad (3.19)$$

The rank of any two adjacent matrices are as follows,

$$\text{rank} \begin{bmatrix} \mathbf{\Gamma}_1^{(4)} \\ \hat{\mathbf{\Gamma}}_2^{(4)} \end{bmatrix} = 5, \text{rank} \begin{bmatrix} \hat{\mathbf{\Gamma}}_2^{(4)} \\ \hat{\mathbf{\Gamma}}_3^{(4)} \end{bmatrix} = 5, \text{ and } \text{rank} \begin{bmatrix} \hat{\mathbf{\Gamma}}_3^{(4)} \\ \mathbf{\Gamma}_4^{(4)} \end{bmatrix} = 5. \quad (3.20)$$

The load voltage and current are shown in Figure3.27. The mid-point voltage is shown in Figure3.28. The mid-point voltage of four-level MMC has more than seven levels as the capacitor voltage deviates from its nominal value. The submodule capacitor voltage and current are shown in Figure3.29. The capacitor voltage has deviated from its nominal value over 30% after five fundamental cycles.

Figure3.30 shows phase-A line current and its corresponding arms' current.

Figure3.31 shows the input dc voltage and current. As seen from Figure3.31, the input current consists of dc component and switching-frequency harmonics. These switching-frequency harmonics can be mitigated by adding a decoupling capacitor at dc bus.

Figure 3.32 shows all capacitor voltages at phase-A. The initial voltage of all capacitors is 1000 V. Capacitor voltage  $V_{C1}$  and  $V_{C6}$  are gradually reduced to 0 while  $V_{C2}$  to  $V_{C5}$  increase to 1500 V.

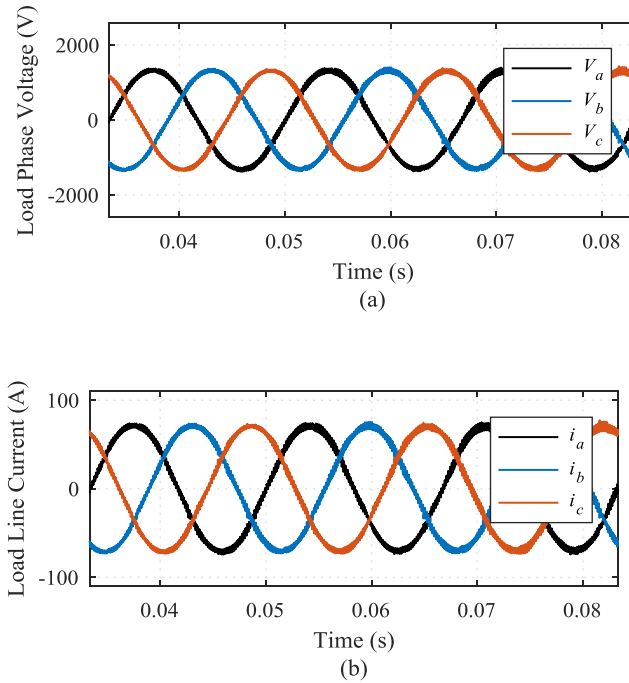
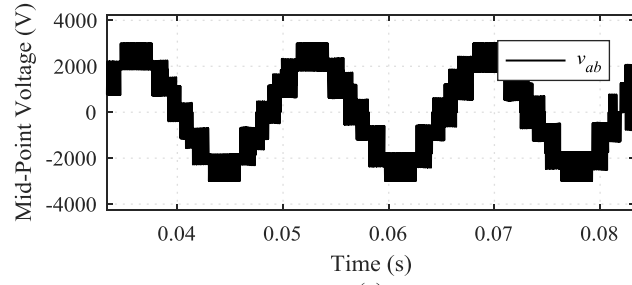
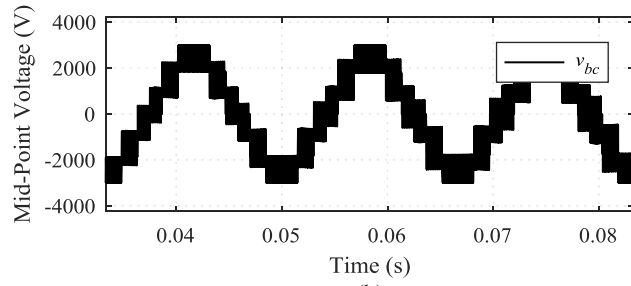


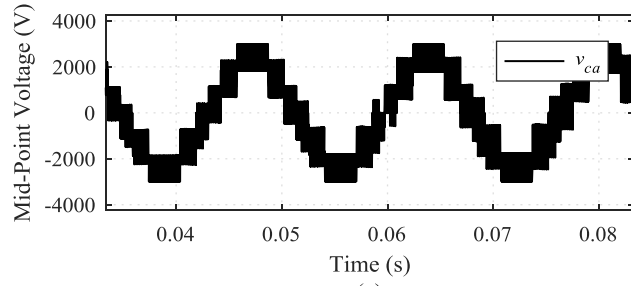
Figure 3.27 Four-level MMC (a) load voltage and (b) load current.



(a)



(b)



(c)

Figure 3.28 Four-level MMC mid-point voltage (a)  $v_{ab}$ ; (b)  $v_{bc}$ ; and (c)  $v_{ca}$ .

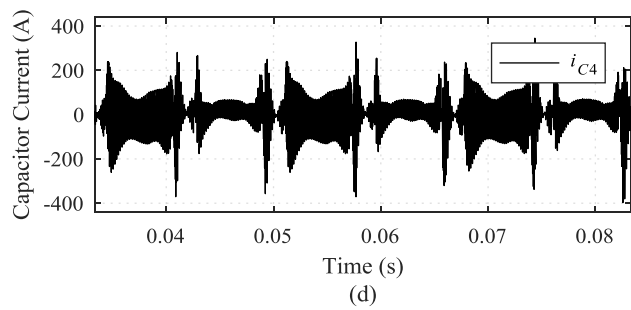
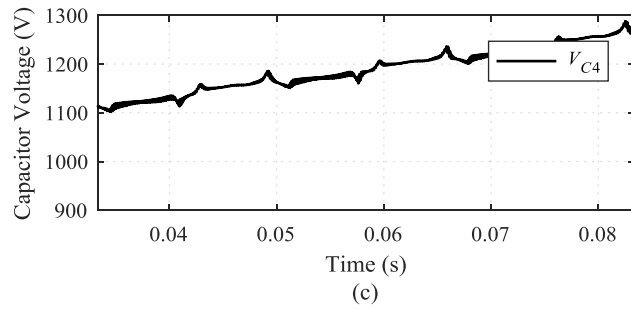
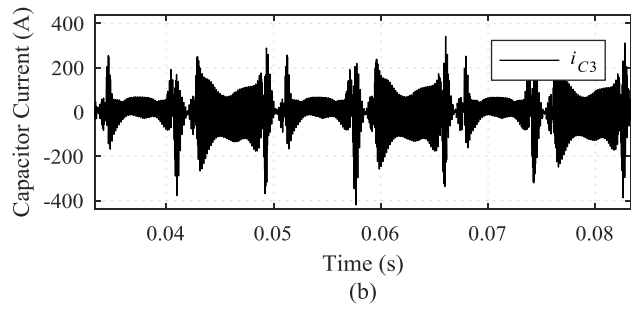
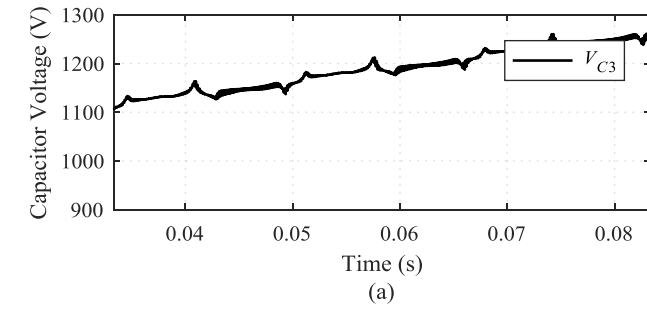
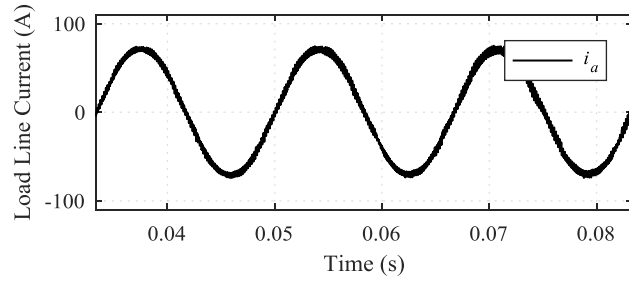
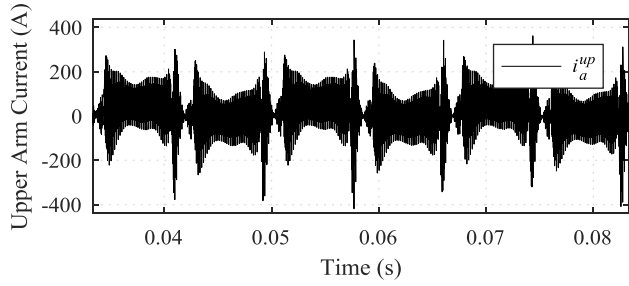


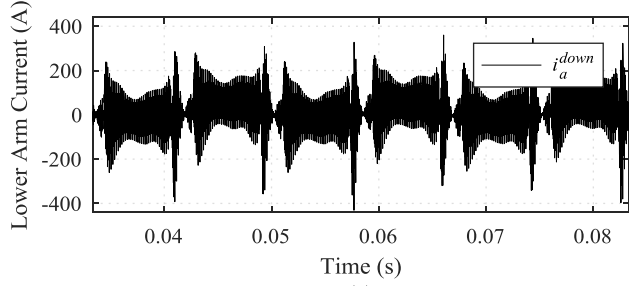
Figure 3.29 Submodule capacitor (a)/(c) voltage; and (b)/(d) current.



(a)



(b)



(c)

Figure 3.30 (a) Line current and its corresponding (b) upper arm current, (c) lower arm current.

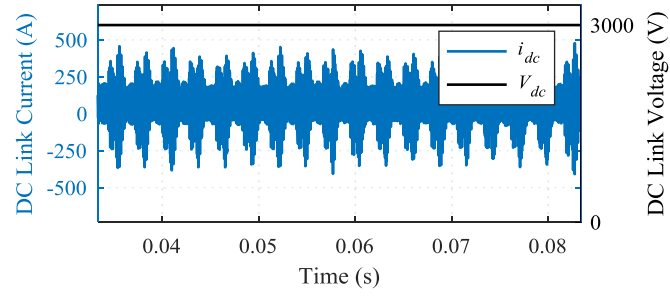


Figure 3.31 Dc input voltage and current.

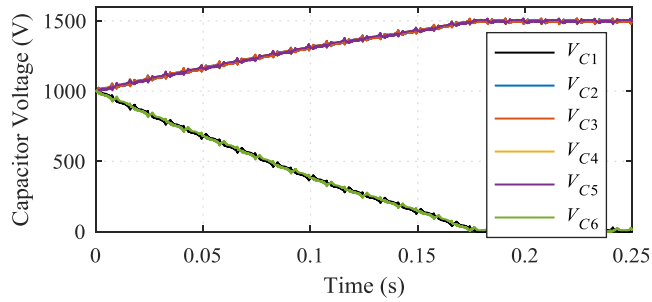


Figure 3.32 All submodule capacitor voltages in phase-A.

### 3.4.3 CASE STUDY: $\Gamma$ MM BASED FOUR-LEVEL MMC WITH CAPACITANCE DEVIATION

In this case study, one submodule capacitance is 50% larger than the other submodules to show that the proposed  $\Gamma$ MM has a good immunity to capacitance deviation. It is common that submodule capacitances are not exactly equal. The simulation topology is shown in Figure 3.19. All the converter parameters and core submatrices are the same as Chapter 3.4.1, except for  $C_3$  is 257  $\mu$ F. The capacitor voltages are self balanced as expected.

The submodule capacitor  $C_3$  voltages is shown in Figure 3.33. Figure 3.34 shows all capacitor voltages in phase-A. All capacitor voltages are well balanced and converging to nominal value (1000 V).

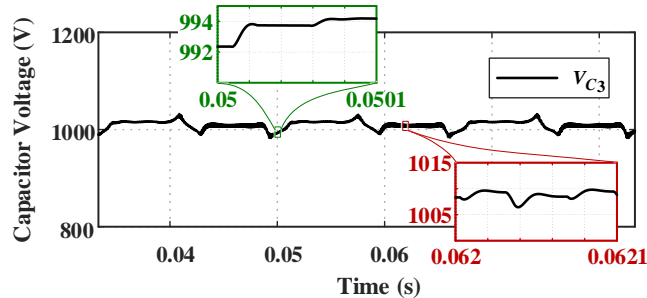


Figure 3.33 Submodule capacitor  $C_3$  voltage.

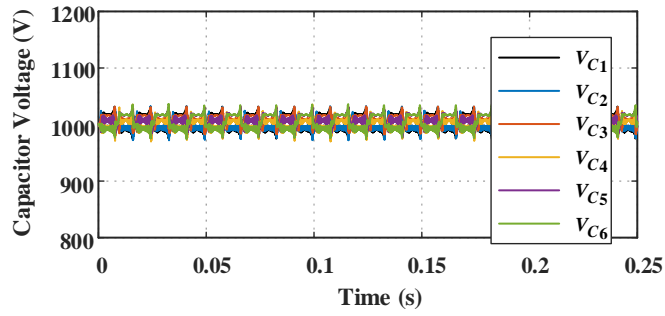


Figure 3.34 All submodule capacitor voltages in phase-A.

### 3.4.4 CASE STUDY: ΓMM BASED ELEVEN-LEVEL MMC

**Objective:** In this case study, the working principle and the performance of  $\Gamma$ MM based eleven-level MMC are studied through MATLAB/Simulink. The simulation topology is shown in Figure3.35.

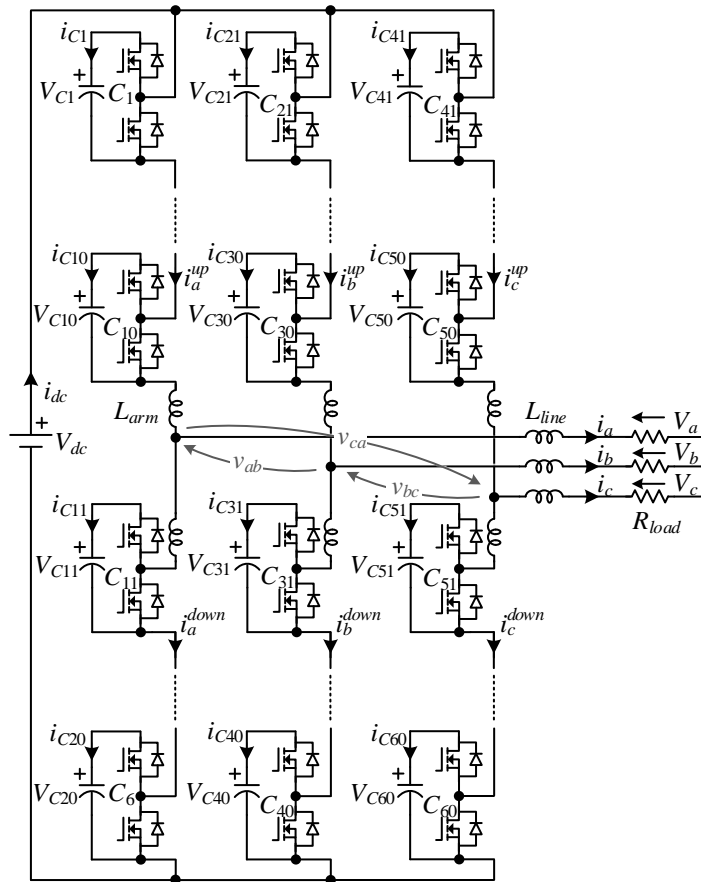


Figure 3.35 Eleven-level MMC simulation topology.

**Parameters:** The key parameters of the MMC are as follows: rated apparent power  $S = 500$  kVA, output phase voltage  $V_a = V_b = V_c = 3200$  V, output line current  $I_a = I_b = I_c = 52$  A, rated output fundamental frequency  $f_0 = 60$  Hz, rated load resistance  $R_{load} = 62 \Omega$ , rated dc-bus voltage  $V_{dc} = 10$  kV, number of submodules per arm:  $N - 1 = 10$ , submodule capacitance  $C_i = 769 \mu\text{F}$  ( $i = 1, 2, \dots, 60$ ), line inductance  $L_{line} = 1$  mH, and arm inductance  $L_{arm} = 0.1 \mu\text{H}$ . The switching frequency is  $f_{sw} = 60$  kHz. The definition of switching frequency is the frequency of the MMC pole voltage jumping from one level to the other adjacent level. The key parameters are summarized in Table 4.

Table 4

Eleven-level MMC simulation key parameters.

Apparent Power, $S$	500 kVA
Fundamental Frequency, $f_0$	60 Hz
Switching Frequency, $f_{sw}$	60 kHz
DC-Bus Voltage, $V_{dc}$	10 kV
Phase Voltage, $V_a, V_b, V_c$	3200 V
Line Current, $I_a, I_b, I_c$	52 A
Load Resistance, $R_{load}$	62 $\Omega$ (100% p.u.)
Line Inductance, $L_{line}$	1 mH (0.61% p.u.)
Arm Inductance, $L_{arm}$	0.1 $\mu\text{H}$ (0.00006% p.u.)
Submodule Capacitance, $C_i$	770 $\mu\text{F}$ (18 p.u.)
Number of Submodules per Arm	10

where  $i = 1, 2, \dots, 60$ .

**Analysis:** This eleven-level MMC simulation follows the  $\Gamma$ -Matrix Modulation strategy, as described in Figure3.18. The  $\hat{\Gamma}_k^{(N)}$  extraction in this section follows the  $\hat{\Gamma}_k^{(N)}$  composition in Chapter 2.4 Eq.(2.30) and (2.31). The initial core submatrix,  $\hat{\Gamma}_2^{(3)}$ , of this composition procedure follows (2.16).

The load voltage and current are shown in Figure3.36. The mid-point voltage is shown in Figure3.37. The mid-point voltage of eleven-level MMC has 17 levels. Although the mid-point voltage of any single phase,  $v_a$   $v_b$  or  $v_c$ , has only 11 levels, the differential voltage of any two phases,  $v_{ab}$   $v_{bc}$  or  $v_{ca}$ , has 17 levels. The submodule capacitor voltage and current are shown in Figure3.38. The capacitor voltage ripple is within 6%. The capacitor current consists mainly of fundamental component and switching-frequency harmonics. Note that the submodule capacitance is 18 p.u.. The energy stored in capacitor is

$$E_i = \frac{1}{2} C_i V_{Ci}^2 = 0.5 \times 770 \times 10^{-6} \times 1000^2 = 385 \text{ (J)} \quad (3.21)$$

The total energy in all submodule capacitors is

$$E_{total} = \sum_{i=1}^{60} E_i = 60 \times \frac{1}{2} C_i V_{Ci}^2 = 23100 \text{ (J)}. \quad (3.22)$$

The eleven-level MMC power rating is 500 kVA. The total capacitor energy in respect to MMC power rating is

$$\varepsilon = \frac{E_{total}}{S} = \frac{23100 \times 10^{-3}}{500 \times 10^{-3}} = 46.2 \text{ (kJ/MVA)}. \quad (3.23)$$

Typically, the conventional MMC submodule capacitance is chosen such that the total stored energy in all submodule capacitors of the converter is approximately 30 – 40 kJ/MVA, where MVA refers to the converter rating, giving ripple in the range of 10% [37].

To have a voltage ripple within 6%, the conventional MMC needs to have submodule capacitors energy to be 50 – 67 kJ/MVA. Normally, the capacitor energy storage capability is proportional to the capacitor size. The  $\Gamma$ MM based MMC features smaller capacitor volume compared to conventional MMC.

The capacitor voltage is well balanced and converging to the expected value (1000 V) in Figure3.38. However, the fundamental ripples still exist. These fundamental ripples are introduced by the arm inductor and stray resistor. Note that the capacitor voltage balance analysis in previous sections did not consider the voltage drop on arm inductors and stray resistors. The effect of those passive components will be discussed in future work.

Figure3.39 shows line current in phase-A and its corresponding arm current. The arm current contains not only fundamental component but also switching-frequency harmonics. Normally, the conventional MMC arm current does not contain many switching-frequency harmonics, and the arm inductance follows the equation (3.4) [38], where  $\omega_0 = 2\pi f_0$ ,  $V_{Ci} = 1000$  V, and  $I_{2\omega}$  is the peak value of the  $2-\omega$  component in arm current. For conventional MMC,  $C_i = 50/46.2 \times 770 \mu\text{F} = 833 \mu\text{F}$  to have a voltage ripple within 6%. Assume  $I_{2\omega}$  to be 13.8 A ( $I_a \times 26.5\%$ ). The arm inductance of conventional MMC should be 23.3 mH (14.2% p.u.) according to (3.4). The arm inductor of  $\Gamma$ MM based MMC is extremely small compared to conventional MMC. Small arm inductance is critical to balance the capacitor voltage. This will be explained in future work.

Figure3.40 shows the input dc voltage and current. As seen from Figure3.40, the input current consists of dc component and switching-frequency harmonics. These switching-frequency harmonics can be mitigated by adding a decoupling capacitor at dc bus.

Figure 3.41 shows all capacitor voltages at phase-A. The capacitor voltages do not deviate from nominal value.

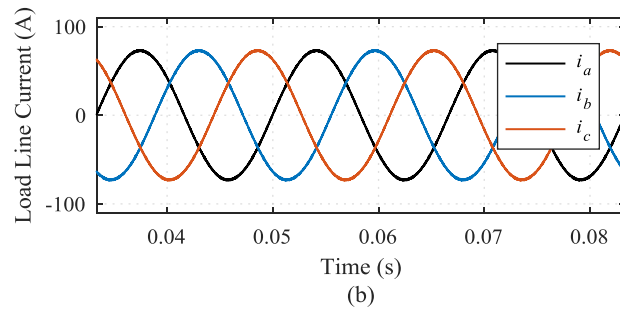
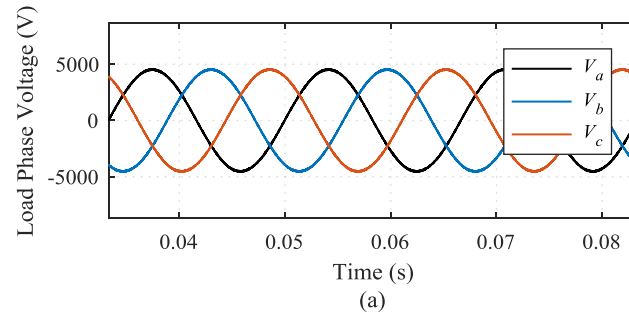


Figure 3.36 Eleven-level MMC (a) load voltage and (b) load current.

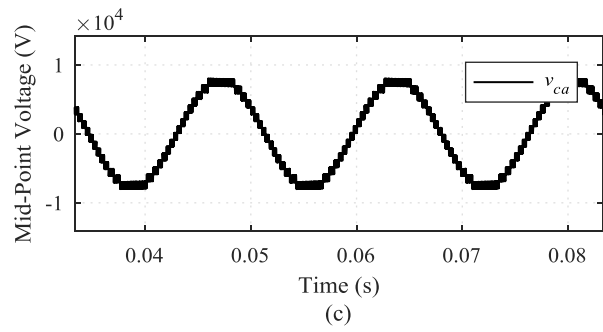
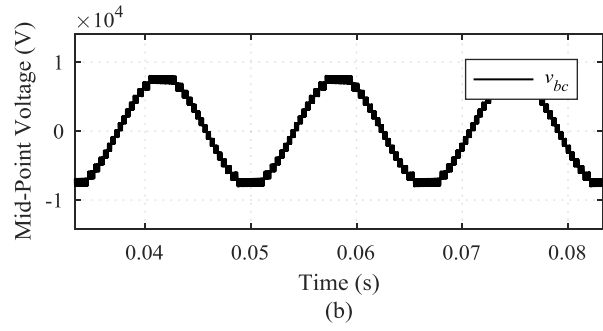
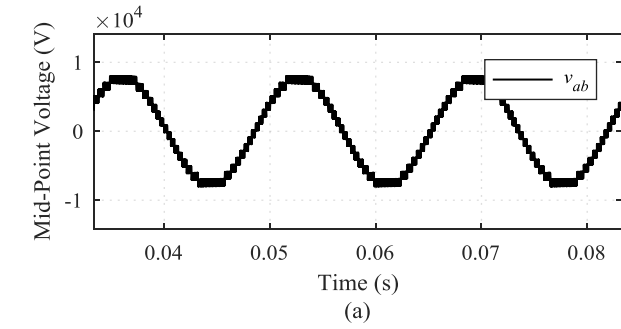


Figure 3.37 Eleven-level MMC mid-point voltage (a)  $v_{ab}$ ; (b)  $v_{bc}$ ; and (c)  $v_{ca}$ .

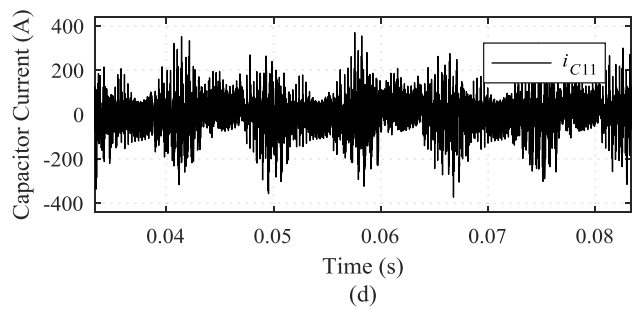
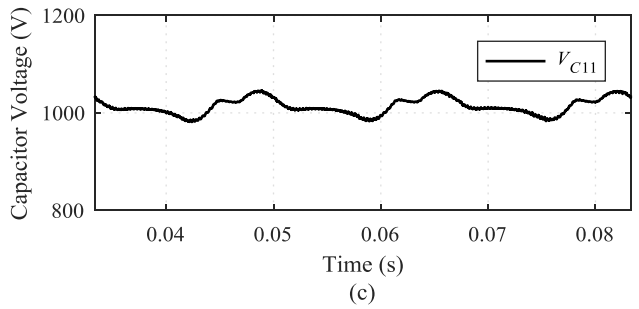
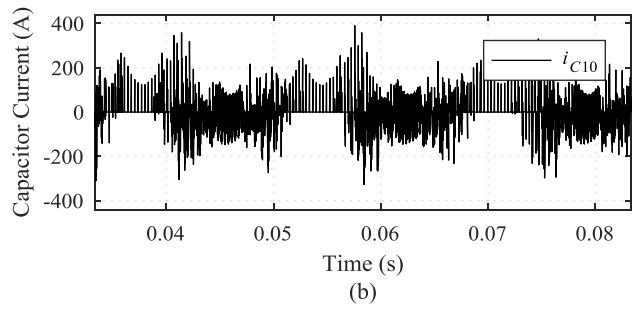
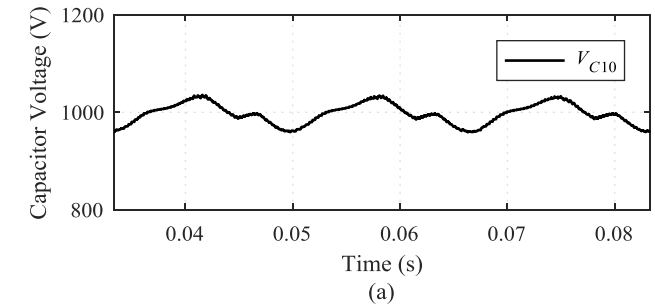


Figure 3.38 Submodule capacitor (a)/(c) voltage; and (b)/(d) current.

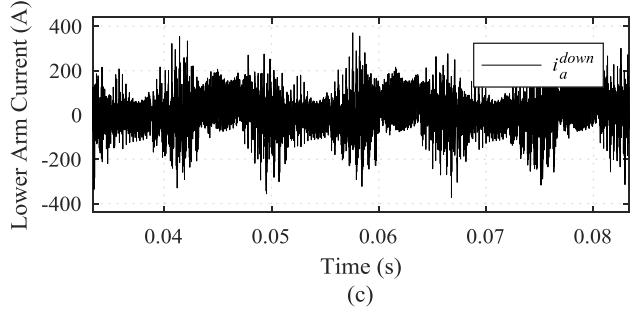
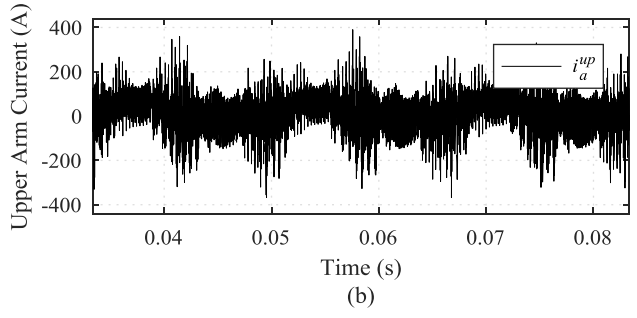
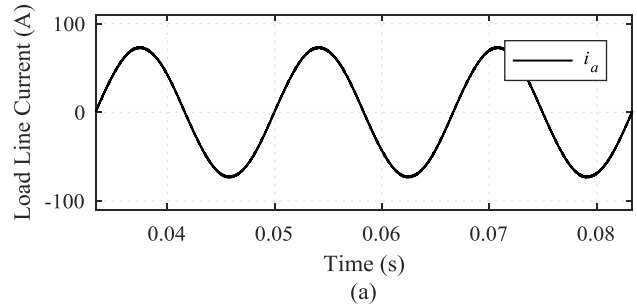


Figure 3.39 (a) Line current in phase-A and its corresponding (b) upper arm current, (c) lower arm current.

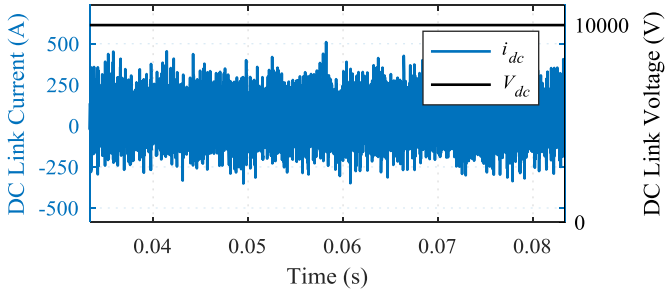


Figure 3.40 Dc input voltage and current.

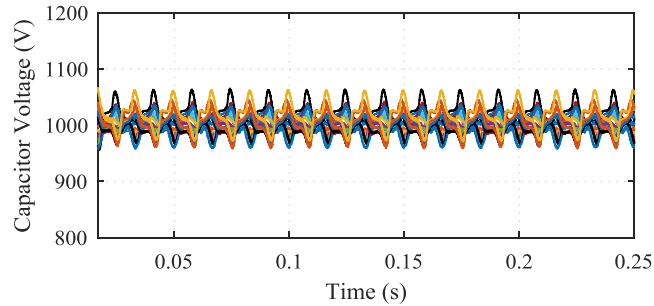


Figure 3.41 All submodule capacitor voltages in phase-A.

### 3.5 DISCUSSIONS

The process of MMC operation is similar to the calculation of the power flow by iterations. In the first iteration of power flow calculation, an initial estimation of the unknowns will be provided to the first equation of the equation set. This initial estimation does not necessarily be the solution for the first equation. A specific iteration law, Newton-Raphson for example, will be provided to find a solution for the first equation based on the initial estimation. Once we have a solution for the first equation, this solution is inserted into the next equation as the initial estimation. Then the iteration law will again be applied to find the solution for the second equation. This iteration will be repeated until the solution converges. That is to say, the solution only makes a slight change each time of the iteration. So, this solution is deemed to be close enough to the analytical solution we are looking for. The difference between power flow calculation and MMC voltage balancing calculation we set up in this Chapter is that the iterations are done by software in power flow calculation, whereas the iterations are done by hardware in MMC. MMC model provides an iteration law, which is equivalent to Newton-Raphson, so that the solution gets closer to the analytical solution after each iteration. In another word, MMC operation is emulating the software iteration to find the solution for capacitor voltage equations set up in Part I.

So, the capacitor voltage equations are actually a virtual equation set. The inductor voltage could be regarded as a computation error, or measurement error, during these iterations. This iteration law provided by MMC physical nature is robust enough to immune to the error introduced by arm inductor.

### **3.6 CONCLUSION**

This Chapter proposed a  $\Gamma$ -Matrix Modulation for MMC. With this novel modulation, the MMC achieves self voltage balancing. This can extremely simplify, or even eliminate, the capacitor voltage balancing control for MMC. Conventionally, either a complicated voltage balancing control, or extra components must be embedded to MMC to balance the capacitor voltage, which increases the MMC cost. Compared to conventional MMC capacitor voltage balancing strategies,  $\Gamma$ MM features extremely simple algorithms and good reachability to high-level MMCs while maintaining the original half-bridge submodule topology. Four- and eleven-level MMC cases are studied to verify the effectiveness of  $\Gamma$ MM.

## 4 THE STATE-SPACE MODEL OF MODULAR MULTILEVEL CONVERTER

### 4.1 MOTIVATIONS

In Figure 3.32, we have seen a mysterious phenomenon: capacitor voltage  $V_{C1}$  and  $V_{C6}$  are gradually reduced to 0 while  $V_{C2}$  to  $V_{C5}$  increase to 1500 V. Although the capacitor voltages diverge as we expect, we do not expect the voltages end up with these values from our previous analysis. The  $\Gamma$ -matrix selected for Chapter 3.4.3 are as follows

$$\mathbf{\Gamma}_1^{(4)} = [0 \ 0 \ 0 \ 1 \ 1 \ 1], \quad (4.1)$$

$$\hat{\mathbf{\Gamma}}_2^{(4)} = \begin{bmatrix} 0 & 0 & 1 & 1 & 0 & 1 \\ 0 & 1 & 0 & 0 & 1 & 1 \\ 1 & 0 & 0 & 1 & 1 & 0 \\ 0 & 1 & 0 & 1 & 0 & 1 \\ 0 & 0 & 1 & 0 & 1 & 1 \end{bmatrix}, \quad (4.2)$$

$$\hat{\mathbf{\Gamma}}_3^{(4)} = \begin{bmatrix} 1 & 0 & 1 & 1 & 0 & 0 \\ 1 & 1 & 0 & 0 & 1 & 0 \\ 0 & 1 & 1 & 0 & 0 & 1 \\ 1 & 0 & 1 & 0 & 1 & 0 \\ 1 & 1 & 0 & 1 & 0 & 0 \end{bmatrix}, \quad (4.3)$$

$$\mathbf{\Gamma}_4^{(4)} = [1 \ 1 \ 1 \ 0 \ 0 \ 0]. \quad (4.4)$$

The rank of each matrix are as follows,

$$\text{rank} [\mathbf{\Gamma}_1^{(4)}] = 1, \text{rank} [\hat{\mathbf{\Gamma}}_2^{(4)}] = 4, \text{rank} [\hat{\mathbf{\Gamma}}_3^{(4)}] = 4, \text{and } \text{rank} [\mathbf{\Gamma}_4^{(4)}] = 1. \quad (4.5)$$

The rank of any two adjacent matrices are as follows,

$$\text{rank} \begin{bmatrix} \mathbf{\Gamma}_1^{(4)} \\ \hat{\mathbf{\Gamma}}_2^{(4)} \end{bmatrix} = 5, \text{rank} \begin{bmatrix} \hat{\mathbf{\Gamma}}_2^{(4)} \\ \hat{\mathbf{\Gamma}}_3^{(4)} \end{bmatrix} = 5, \text{and } \text{rank} \begin{bmatrix} \hat{\mathbf{\Gamma}}_3^{(4)} \\ \mathbf{\Gamma}_4^{(4)} \end{bmatrix} = 5. \quad (4.6)$$

The voltage balancing equations of this  $\Gamma$ -matrix are as follows

$$\begin{bmatrix} 3V_{dc} \\ \vdots \\ 3V_{dc} \end{bmatrix}_{6 \times 1} = \begin{bmatrix} \mathbf{\Gamma}_1^{(4)} \\ \hat{\mathbf{Y}}_2^{(4)} \end{bmatrix} \cdot \begin{bmatrix} V_{C1} \\ V_{C2} \\ \vdots \\ V_{C6} \end{bmatrix} \quad (4.7)$$

$$\begin{bmatrix} 3V_{dc} \\ \vdots \\ 3V_{dc} \end{bmatrix}_{10 \times 1} = \begin{bmatrix} \hat{\mathbf{\Gamma}}_2^{(4)} \\ \hat{\mathbf{\Gamma}}_3^{(4)} \end{bmatrix} \cdot \begin{bmatrix} V_{C1} \\ V_{C2} \\ \vdots \\ V_{C6} \end{bmatrix} \quad (4.8)$$

$$\begin{bmatrix} 3V_{dc} \\ \vdots \\ 3V_{dc} \end{bmatrix}_{6 \times 1} = \begin{bmatrix} \hat{\mathbf{\Gamma}}_3^{(4)} \\ \mathbf{\Gamma}_4^{(4)} \end{bmatrix} \cdot \begin{bmatrix} V_{C1} \\ V_{C2} \\ \vdots \\ V_{C6} \end{bmatrix} \quad (4.9)$$

The solutions of (4.7)-(4.9) are as follows

$$\begin{cases} V_{C1} = V_{C6} \\ V_{C2} = V_{C3} = V_{C4} = V_{C5} \\ V_{C1} + V_{C2} + V_{C3} = 3V_{dc} \end{cases} \quad (4.10)$$

These solutions are not unique. In another word, Eq.(4.7)-(4.9) have infinite many solutions.  $V_{C1}$  and  $V_{C6}$  could be zero as observed in Figure3.32. They could also be other numbers. For example,

$$\begin{cases} V_{C1} = V_{C6} = 3V_{dc} \\ V_{C2} = V_{C3} = V_{C4} = V_{C5} = 0 \end{cases} \quad (4.11)$$

Another example

$$\begin{cases} V_{C1} = V_{C6} = 0.6V_{dc} \\ V_{C2} = V_{C3} = V_{C4} = V_{C5} = 1.2V_{dc} \end{cases} \quad (4.12)$$

Eq.(4.11) and (4.12) are just two possible solutions for (4.7)-(4.9). Actually, (4.7)-(4.9) should have infinite many solutions since they are non-full-rank. Among (4.11) and (4.12), Eq.(4.12) could be observed in Figure3.32 during the transition of the capacitor voltage to

the new steady state. Eq.(4.11) does not ever exist either during the transition or in the steady state. Our previous analysis could not explain this phenomenon. We need to set up a proper dynamic model for MMC to understand this phenomenon, so that we might have a chance to predict and control the behavior of those capacitors in the future.

## 4.2 INTRODUCTION

Many literatures have modeled MMC for different purposes and scenarios. For example,

- i) The MMC is modeled as a whole system in order to understand the interaction between MMCs and other objectives (power grid, load, etc.) [39]-[41]. Normally, this type of models is for system level controller design.
- ii) The MMC is modeled by arm or submodules in order to understand the internal state variables dynamics [42]-[52]. Normally, this type of modeling ends up with internal state variable regulations.
- iii) The MMC is modeled to evaluate a specific state variable at steady state[53]-[55]. This type of MMC modeling loses most of the dynamic properties of MMC but becomes an effective guidance for parameter design.
- iv) The MMC is modeled for real-time simulation [56]-[61]. The existing literature proposes numerous simplified and computationally-efficient equivalent models for MMC to meet with the fast calculation of real-time simulation.

Most of the models developed so far differ from each other on the basis of different degree of assumptions and simplification. This makes them unsuitable for understanding the nature of this circuit from its physical basement. Wang et. [51] proposed a state-space switching model, which is derived from accurate mathematical model without losing any characteristics of MMC. However, the aim of [51] is to develop a control to minimize the

submodule capacitance and arm inductance. Therefore, the state variables selected in [51] are control oriented. This made it unsuitable for understanding the dynamics of MMC.

[45] proved that the arm voltage converges to equilibrium point by nature from Lyapunov method. The model in [45] reduces the dimension of the system by assuming that all submodules per arm have identical dynamics. The Lyapunov energy function proposed in [45] has the potential to evaluate the system stability quantitatively, however, the composition of the Lyapunov energy function is complicated for high order systems. The existing models are not suitable for understanding the MMC circuit from its physical basement. We need to have a model that is accurate enough to demonstrate the mechanism of the self balance nature of MMC.

Switched circuits in power electronics naturally present hybrid behavior. Such circuits can be described by a set of discrete states with associated continuous dynamics. All power electronic systems can be categorized to hybrid system from control theory point of view. However, we seldomly evaluate our power electronic systems using the knowledge from hybrid system analysis. [62] set a good example for how to apply hybrid system analysis on a boost converter.

This Chapter proposes a comprehensive state-space model for MMC system that consistent with hybrid system analysis. With this state-space model, the mechanism of the self balance nature of MMC system could be well explained.

This Chapter is organized as follows:

The prior art of MMC modeling is summarized in Chapter 4.3. The contribution of this Chapter is summarized in Chapter 4.4. The principle of  $\Gamma$ -Matrix Modulation is reviewed in Chapter 4.5. The state-space model of 2-level MMC is derived in Chapter 4.6. The model

is extended to 3-level MMC in Chapter 4.7. A general state-space model of  $N$ -level MMC is derived in Chapter 4.8. The effectiveness of the proposed stability analysis is verified by comparing the proposed state-space model with simulation studies.

### 4.3 PRIOR-ART MMC MODEL

In the stability analysis of an MMC-HVDC system, MMC is normally modeled as a voltage-source converter (VSC) [39]-[41]. The VSC model is shown in Figure 4.1. The model can well interpret the oscillation of a certain state under the controller and the corresponding power network or load. This type of modeling is usually established on the small signal modeling and focused on the phasor/magnitude dynamics. This MMC model can well serve the controller design, especially the DC voltage control (DVC) in timescale around 10Hz. However, the simplified VCS model contains only one equivalent dc link capacitor, either time invariant or time variant. This simplification is suitable for high-level MMC since all the submodule capacitors are reduced to one equivalent dc-link capacitor. One limitation for the VSC model is that the dynamics of individual cells cannot be differentiated from the others in the given model as all of them assumed to be identical.

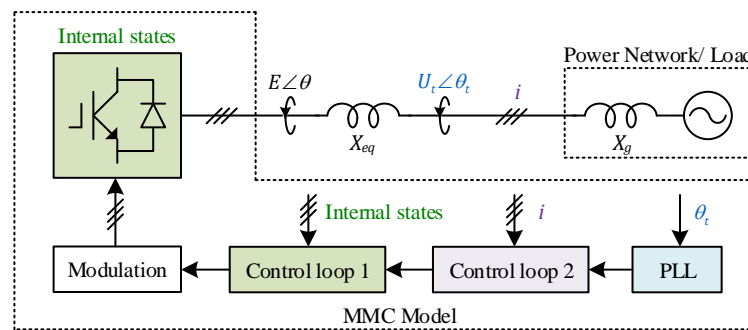


Figure 4.1 The VSC model of MMC.

The MMC is modeled by selecting different internal states in order to understand the internal state variables dynamics [42]-[52]. The selection of the states can be classified into time domain[45]-[52] and frequency domain[42]-[44], [63]-[64]. The frequency domain

state variables contain the independent harmonic states. This will increase the complexity of the Harmonic State Space (HSS). The effects of a zero-sequence voltage are included in some HSS MMC models [63]-[64]. They are all three-phase models with a large number of state variables. Therefore, a single-phase MMC model considering zero-sequence voltage is proposed in [42] to reduce the number of state variables.

The time domain models differ from each other by selecting different state variables. The most common time domain model is arm averaged model (AAM)[45]-[50]. AAM assumes that the voltage distribution among the submodules in each arm is equal. This assumption implies that the capacitor voltage is well balanced among each arm. AAM can significantly reduce the complexity of MMC model while maintaining an accurate representation of the internal dynamics. For three-phase MMC, there are five independent loop currents and six independent node voltages in topology as shown in Figure4.2. These eleven states can be selected as state variables to derive the state-space model of MMC. Other than selecting these eleven state variables, these states can be manipulated into other states by linear operations, for example sum and difference of any two states. Figure4.3 shows several ways to select loop currents. Figure4.4 shows the node voltages are manipulated to be common-mode and differential-mode states. Figure4.5 shows combinations of loop current selection and node voltage selection.

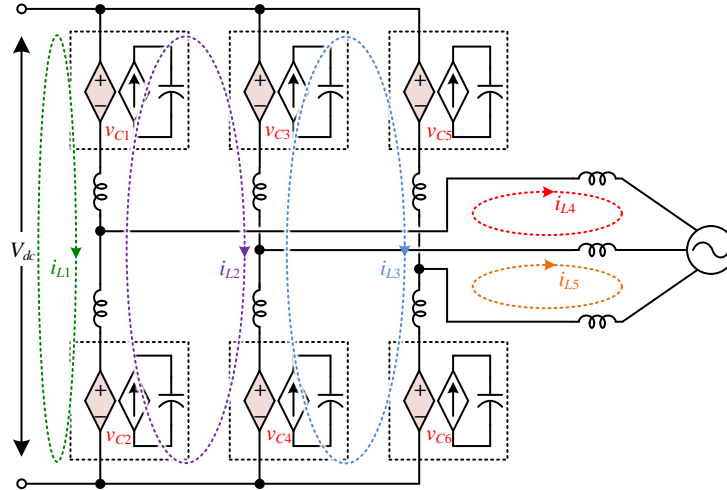


Figure 4.2 Five independent loop currents and six independent node voltages in topology.

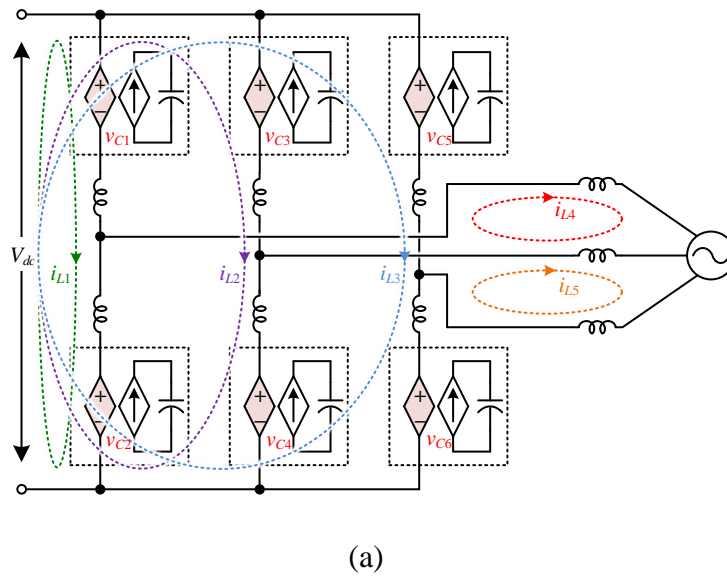
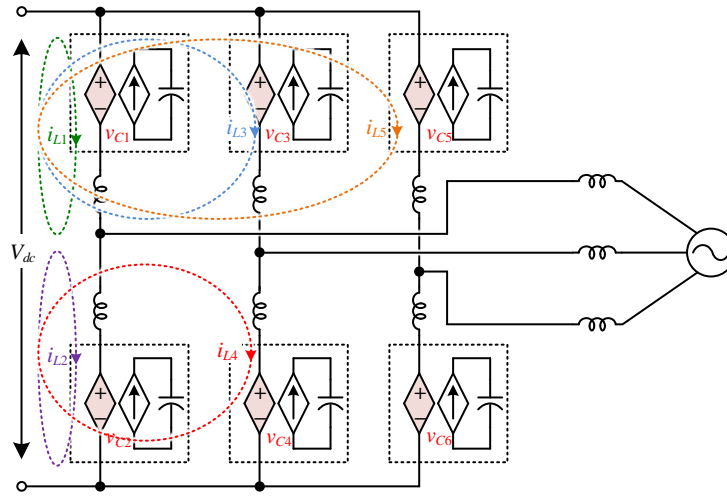
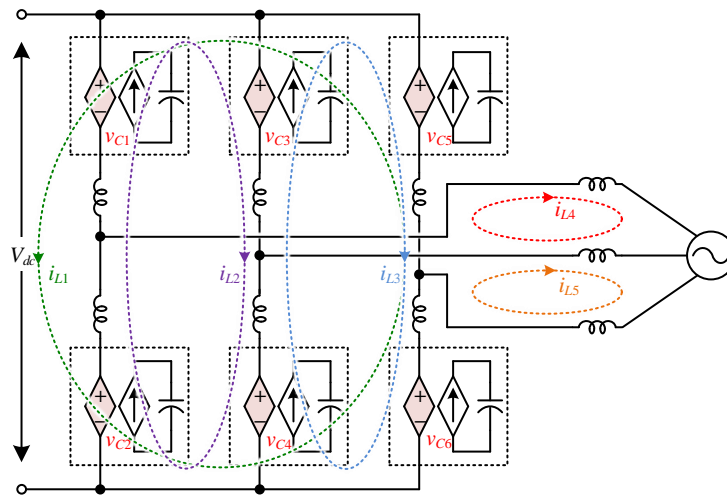


Figure 4.3 Loop current selection (a) single-phase oriented [47]-[48] (b) inductor current oriented [49]-[50] and (c) circulating current oriented [45],[51]-[52].

Figure 4.3 (cont'd)



(b)



(c)

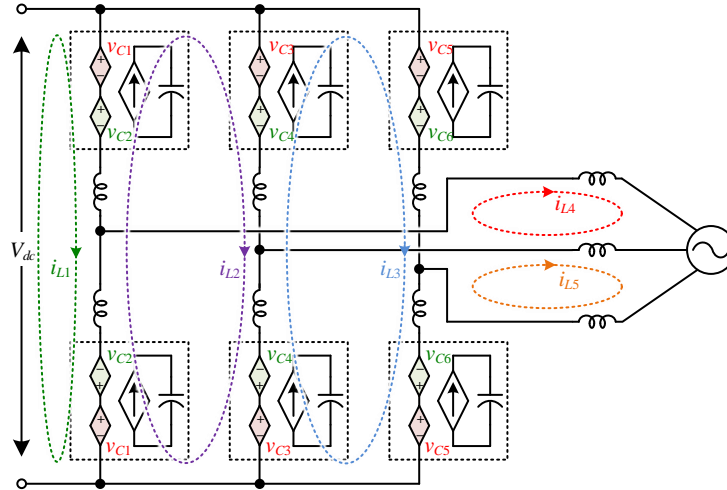
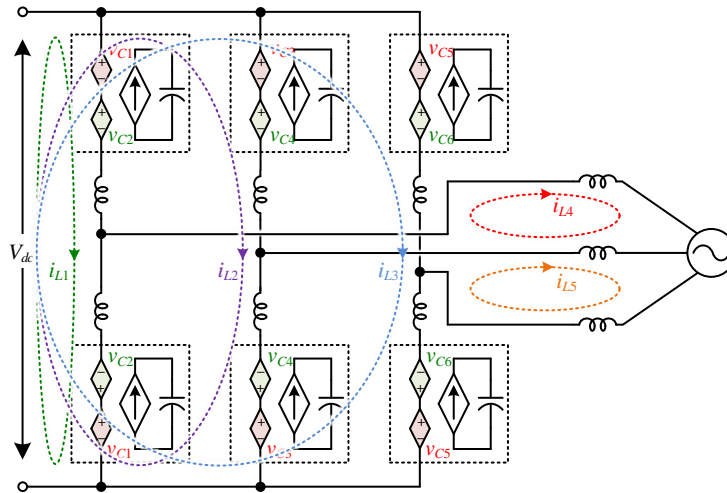


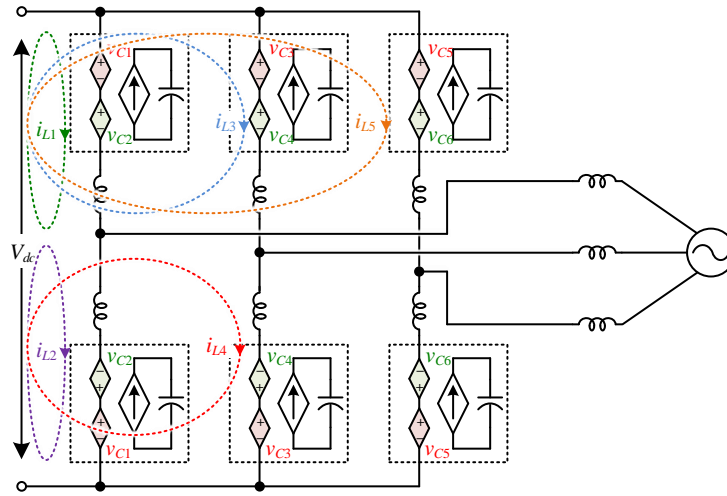
Figure 4.4 Common-mode and differential-mode voltage as state variables [46].



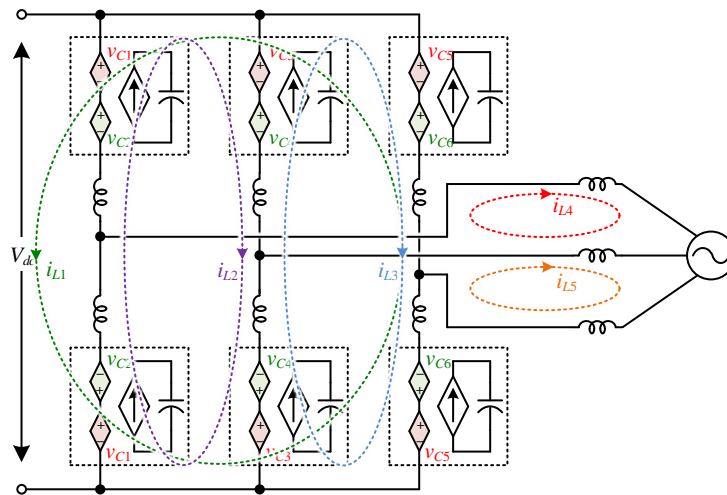
(a)

Figure 4.5 State variable selections (a) dc current + common/differential-mode voltage oriented (b) inductor current + common/differential-mode voltage oriented and (c) circulating current + common/differential-mode voltage oriented.

Figure 4.5 (cont'd)



(b)



(c)

AAM eliminates most of the dynamic difference among the submodule voltages. [51] proposed a switching cycle model (SCM) that discriminates the dynamics of submodule voltages. The SCM assigns each submodule with an independent state.

MMCs are also model for other purposes. The MMC is modeled to evaluate a specific state variable at steady state[53]-[55]. This type of MMC modeling loses most of the dynamic properties of MMC but becomes an effective guidance for parameter design. The

MMC is modeled for real-time simulation [56]-[61]. The existing literature proposes numerous simplified and computationally efficient equivalent models for MMC to meet with the fast calculation of real-time simulation. The selection of MMC internal state variables are summarized in Figure 4.6.

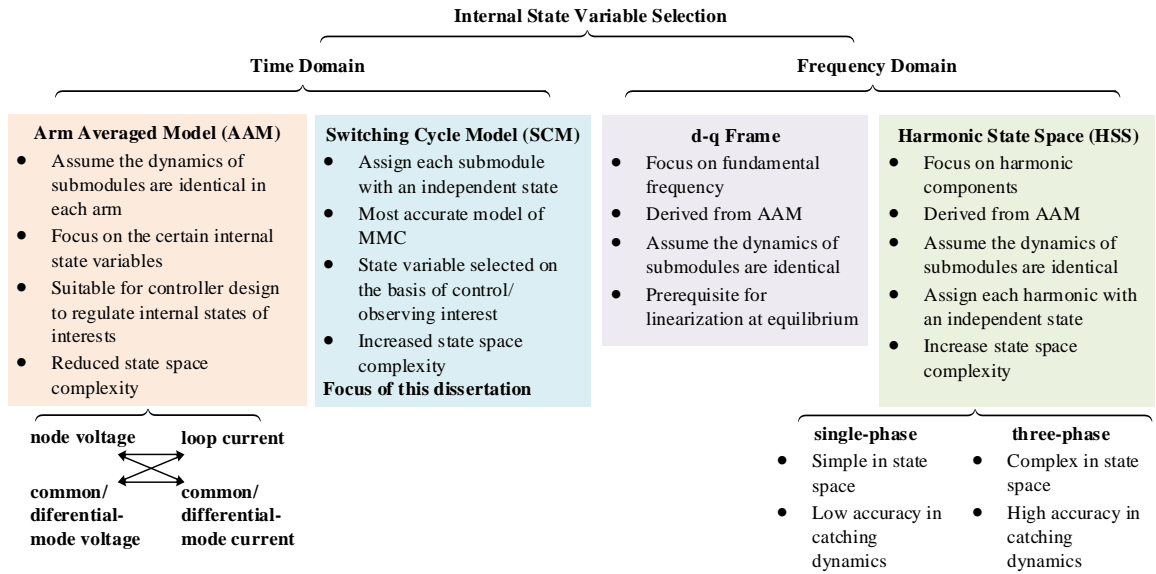


Figure 4.6 The selection of MMC internal state variables.

#### 4.4 CONTRIBUTION

The model proposed in this Chapter falls into the category of SCM. The SCM assigns each submodule with an independent state. The state variables selected in [51] focus on the circulating current and three-phase MMC, which increase the number of state variables. This dissertation proposes a comprehensive state-space model for single-phase MMC system that reduces the number of state variables compared to [51]. With this state-space model, the convergence/divergence of submodule voltage could be well captured. The state variable selection of [51] is shown in Figure 4.7. The selection of state variables of this Chapter is shown in Figure 4.8. For an  $N$ -level MMC, there are  $6N - 1$  states needed in [51], whereas only  $2N$  states needed in this dissertation.

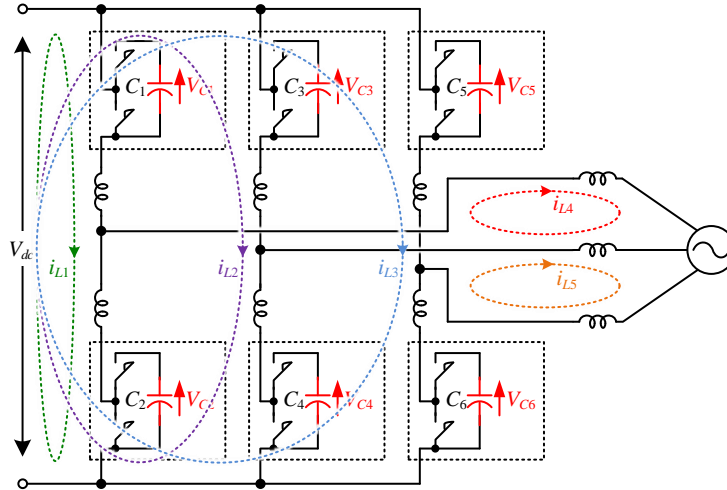


Figure 4.7 The state variable selection of [51].

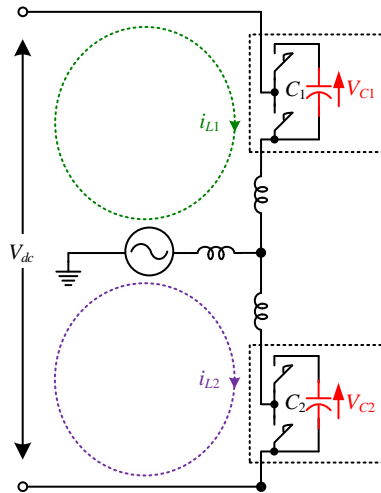


Figure 4.8 The state variable selection of this dissertation.

## 4.5 REVIEW OF $\Gamma$ -MATRIX MODULATION

$\Gamma$ -Matrix Modulation ( $\Gamma$ MM) was proposed in Chapter 3 [65]-[66]. This novel modulation utilizes the self balance nature of MMC so that the voltage balancing control of MMC is eliminated.  $\Gamma$ MM contains two stages. Namely, level pointer preparation and  $\Gamma$ -matrix adaptation.

### 4.5.1 LEVEL POINTER PREPARATION

An  $N$ -level MMC is plotted in Figure 4.9. A  $N$ -level MMC contains  $N - 1$  submodules on upper arm and  $N - 1$  submodules on lower arm. For an  $N$ -level MMC, there are  $N - 1$ , and only  $N - 1$ , out of  $2N - 2$  submodules at inserting mode at a time. The other  $N - 1$  submodules are at by-pass mode meanwhile. Therefore, there are  $N$  possible levels on pole voltage  $v_a$ . The numbering of levels in an  $N$ -level MMC is shown in Figure 4.10.

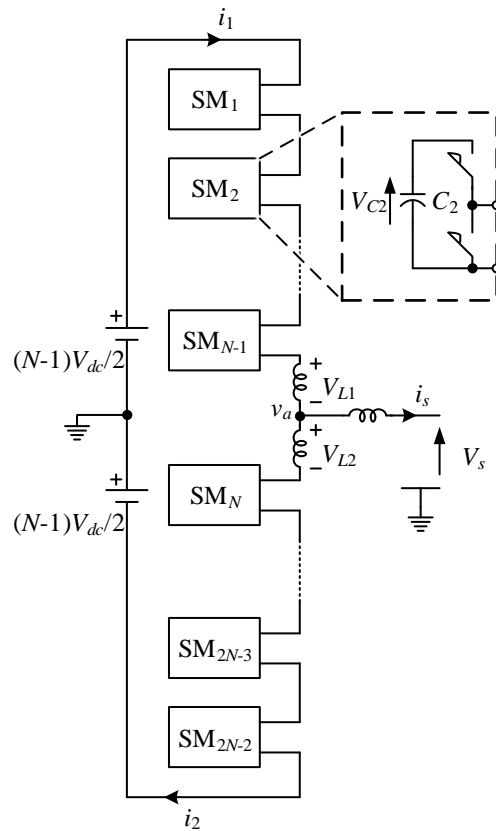


Figure 4.9  $N$ -level MMC circuit.

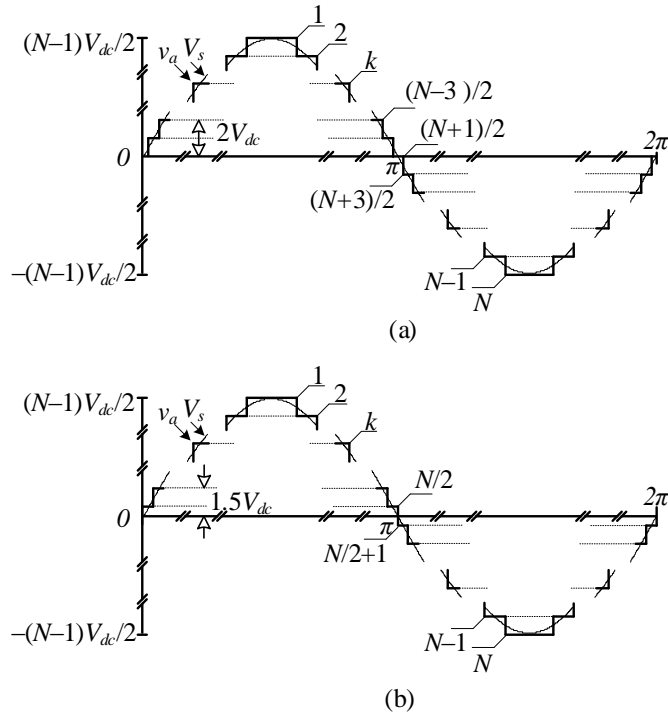


Figure 4.10 Numbering of levels in an  $N$ -level MMC, when (a)  $N$  is an odd number; and (b)  $N$  is an even number.

There are multiple ways to determine the pole voltage level[67]. Phase-disposition (PD) modulation is adopted in this Chapter to determine the pole voltage level. Other methods should also work properly for level pointer preparation.

$N - 1$  carriers are needed to determine  $N$ -level shape of  $v_a$ . The carriers are plotted in Figure4.11. The relationship of  $v_s^*$  and  $v_a$  is plotted in Figure4.12.

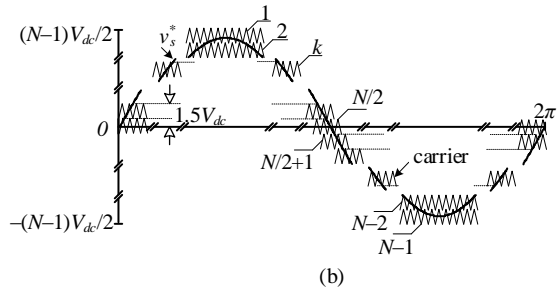
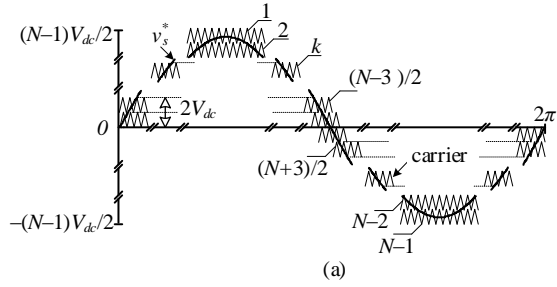


Figure 4.11 ac-side voltage  $v_s^*$  and carriers, when (a)  $N$  is an odd number; and (b)  $N$  is an even number.

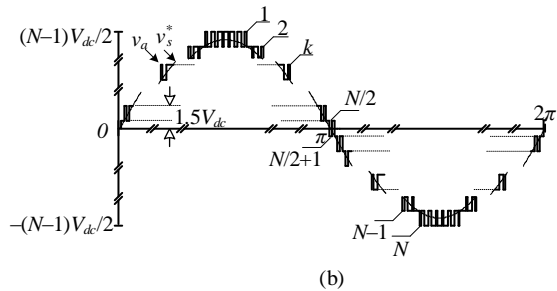
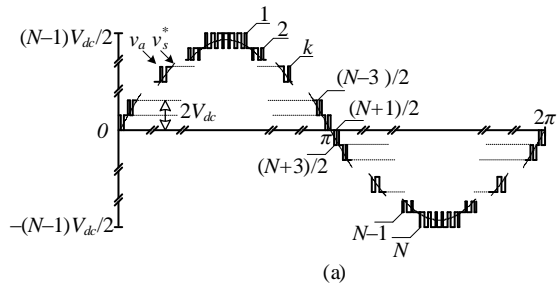


Figure 4.12 ac-side voltage  $v_s^*$  and pole voltage  $v_a$ , when (a)  $N$  is an odd number; and (b)  $N$  is an even number.

The outcome of PD modulation is assigned to the level pointer.

### 4.5.2 $\Gamma$ -MATRIX ADAPTATION

There are always no less than one switching pattern to achieve an arbitrary level of  $v_a$ . One possible selection of switching pattern, namely  $\Gamma$ -Matrix subtraction, is proposed in [61]. The method extremely reduces the  $\Gamma$  dimension to a practical number. MMC achieves self balancing with this  $\Gamma$ -matrix selection[62]. The submatrix  $\hat{\Gamma}$  extracted from  $\Gamma$  is a  $m_k$ -by- $(2N - 2)$  matrix, where  $m_k = C_{N-2}^{k-1} C_{N-2}^{N-k-1}$ . There are still no less than one switching pattern to achieve an arbitrary level of  $v_a$  if using  $\hat{\Gamma}$ . The  $\Gamma$ -matrix adaptor determines the specific row in  $\hat{\Gamma}$  to achieve a certain level of  $v_a$ . Recall that  $\hat{\Gamma}$  of an  $N$ -level MMC are as follows,

$$\hat{\Gamma}^{(N)} = \begin{bmatrix} \Gamma_1^{(N)} \\ \hat{\Gamma}_2^{(N)} \\ \vdots \\ \hat{\Gamma}_k^{(N)} \\ \vdots \\ \hat{\Gamma}_{N-1}^{(N)} \\ \Gamma_N^{(N)} \end{bmatrix} \quad (4.13)$$

$\hat{\Gamma}_k^{(N)}$  is a matrix that contains all the selected switching patterns to achieve level  $k$  for an  $N$ -level MMC.

When the level pointer at first level,  $\Gamma_1^{(N)}$  is chosen as the switching pattern to implement this first-level pole-voltage. Similarly, when the pole voltage  $v_a$  at  $N$ -th level,  $\Gamma_N^{(N)}$  is chosen as the switching pattern to implement this level- $N$  pole-voltage. Recall that  $\Gamma_1^{(N)}$  and  $\Gamma_N^{(N)}$  are as follows,

$$\Gamma_1^{(N)} = [0 \quad \cdots \quad 0 \quad \underbrace{1 \quad \cdots \quad 1}_{N-1}], \quad (4.14)$$

$$\mathbf{\Gamma}_N^{(N)} = [\underbrace{1 \ \cdots \ 1}_{N-1} \ \underbrace{0 \ \cdots \ 0}_{N-1}]. \quad (4.15)$$

When the level pointer at  $k$ -th level, where  $2 \leq k \leq N-1$ ,  $\hat{\mathbf{\Gamma}}_k^{(N)}$  is chosen to implement this  $k$ th-level pole-voltage. There are multiple ways to compose  $\hat{\mathbf{\Gamma}}_k^{(N)}$ . The  $\hat{\mathbf{\Gamma}}_k^{(N)}$  composition in this Chapter follows Chapter 3, which is

$$\hat{\mathbf{\Gamma}}_k^{(N)} = \begin{bmatrix} \mathbf{0} & \hat{\mathbf{\Gamma}}_k^{(N-1)} & \mathbf{1} \\ 1 & \mathbf{T}_{k-1(a)}^{(N-1)} & 1 \\ 0 & \mathbf{T}_{k-1(b)}^{(N-1)} & 0 \end{bmatrix}, \quad (4.16)$$

where  $2 \leq k \leq N-2$ .

$$\hat{\mathbf{\Gamma}}_k^{(N)} = \begin{bmatrix} 1 & \mathbf{T}_{k-1(a)}^{(N-1)} & 1 \\ 0 & \mathbf{T}_{k-1(b)}^{(N-1)} & 0 \\ \mathbf{1} & \hat{\mathbf{\Gamma}}_{k-1}^{(N-1)} & \mathbf{0} \end{bmatrix}, \quad (4.17)$$

where  $k = N-1$ .

$\hat{\mathbf{\Gamma}}_k^{(N-1)}$  and  $\hat{\mathbf{\Gamma}}_{k-1}^{(N-1)}$  are core submatrices from  $(N-1)$ -level MMC.  $\mathbf{T}_{k-1(a)}^{(N-1)}$  is derived from  $\hat{\mathbf{\Gamma}}_{k-1}^{(N-1)}$  by manipulating the right most “1” in first row of  $\hat{\mathbf{\Gamma}}_{k-1}^{(N-1)}$  to “0”.  $\mathbf{T}_{k-1(b)}^{(N-1)}$  is derived from  $\hat{\mathbf{\Gamma}}_{k-1}^{(N-1)}$  by manipulating the left most “0” in first row of  $\hat{\mathbf{\Gamma}}_{k-1}^{(N-1)}$  to “1”.

There are multiple switching patterns to achieve  $k$ -th level.  $\Gamma$ -matrix adaptor determines the exact switching pattern for MMC when level pointer visits level  $k$ .  $\Gamma$ -matrix adaptor reads the current switching pattern that the  $\Gamma$ -matrix pointer points to. Then, reassign the  $\Gamma$ -matrix pointer to the next switching pattern and wait for the next call from level pointer.

The  $\Gamma$ MM for  $N$ -level MMC can also be explained with the aid of Figure4.13.

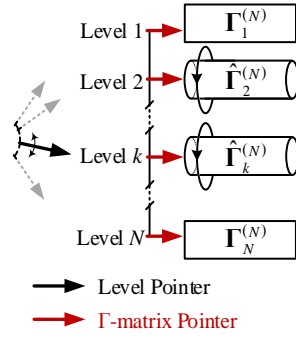


Figure 4.13  $\Gamma$ -matrix modulation for  $N$ -level MMC.

#### 4.6 STATE-SPACE MODEL OF TWO-LEVEL MMC

We need to find the state-space model of MMC to demonstrate the dynamics of the system. Figure 4.14 shows a two-level MMC that is under analysis in this section. Figure 4.15 shows the simplified MMC model. For a two-level MMC, there are two feasible switching patterns. Either the upper submodule or the lower submodule is inserted. The following section will model the two-level MMC for each switching pattern.

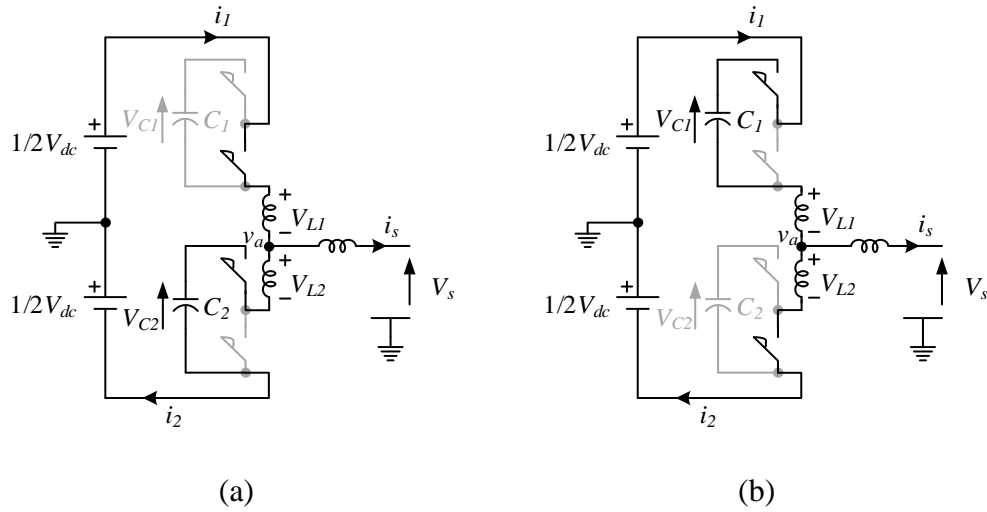


Figure 4.14 two-level MMC with pole connected to (a) positive dc rail (Level 1); and (b) negative dc rail (Level 2).

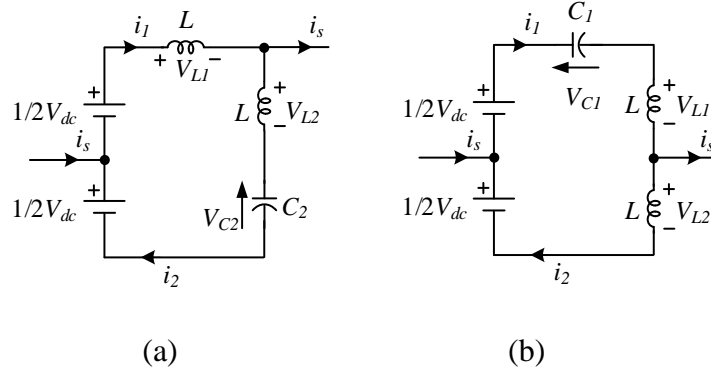


Figure 4.15 two-level MMC model with pole connected to (a) positive dc rail; and (b) negative dc rail.

#### 4.6.1 STATE-SPACE MODEL

Figure 4.15(a) can be formulated as

$$\begin{cases} V_{L1} = L \frac{di_1}{dt} \\ V_{L2} = L \frac{di_2}{dt} \\ i_2 = C_2 \frac{dV_{C2}}{dt} \\ i_1 = i_2 + i_s \\ V_{dc} = V_{L1} + V_{L2} + V_{C2} \end{cases} \quad (4.18)$$

The corresponding switching pattern is

$$\Gamma_1^{(2)} = [0 \quad 1]. \quad (4.19)$$

Define the state variables to be

$$\mathbf{X} = \begin{bmatrix} x_1 \\ x_2 \\ x_3 \\ x_4 \end{bmatrix} = \begin{bmatrix} i_1 \\ i_2 \\ V_{C1} \\ V_{C2} \end{bmatrix}, \quad \dot{\mathbf{X}} = \begin{bmatrix} \dot{x}_1 \\ \dot{x}_2 \\ \dot{x}_3 \\ \dot{x}_4 \end{bmatrix} = \begin{bmatrix} \frac{di_1}{dt} \\ \frac{di_2}{dt} \\ \frac{dV_{C1}}{dt} \\ \frac{dV_{C2}}{dt} \end{bmatrix}. \quad (4.20)$$

Rewrite (4.18) into state equation form,

$$\begin{cases} \dot{x}_1 = -\frac{1}{2L}x_4 + \frac{1}{2L}V_{dc} + \frac{1}{2}\frac{di_s}{dt} \\ \dot{x}_2 = -\frac{1}{2L}x_4 + \frac{1}{2L}V_{dc} - \frac{1}{2}\frac{di_s}{dt}, \\ \dot{x}_4 = \frac{1}{C_2}x_2 \end{cases} \quad (4.21)$$

or

$$\begin{cases} \dot{x}_1 = 0 \cdot x_1 + 0 \cdot x_2 + 0 \cdot \left(-\frac{1}{2L} x_3\right) + 1 \cdot \left(-\frac{1}{2L} x_4\right) + \left(\frac{1}{2L} V_{dc} + \frac{1}{2} \frac{di_s}{dt}\right) \\ \dot{x}_2 = 0 \cdot x_1 + 0 \cdot x_2 + 0 \cdot \left(-\frac{1}{2L} x_3\right) + 1 \cdot \left(-\frac{1}{2L} x_4\right) + \left(\frac{1}{2L} V_{dc} - \frac{1}{2} \frac{di_s}{dt}\right) \\ \dot{x}_3 = 0 \cdot \left(\frac{1}{C_1} x_1\right) + 0 \cdot x_2 + 0 \cdot x_3 + 0 \cdot x_4 + 0 \\ \dot{x}_4 = 0 \cdot x_1 + 1 \cdot \left(\frac{1}{C_2} x_2\right) + 0 \cdot x_3 + 0 \cdot x_4 + 0 \end{cases} \quad (4.22)$$

Rewrite (4.22) into matrix form,

$$\begin{bmatrix} \dot{x}_1 \\ \dot{x}_2 \\ \dot{x}_3 \\ \dot{x}_4 \end{bmatrix} = \begin{bmatrix} 0 & 0 & 0 \cdot \left(-\frac{1}{2L}\right) & 1 \cdot \left(-\frac{1}{2L}\right) \\ 0 & 0 & 0 \cdot \left(-\frac{1}{2L}\right) & 1 \cdot \left(-\frac{1}{2L}\right) \\ 0 \cdot \left(\frac{1}{C_1}\right) & 0 & 0 & 0 \\ 0 & 1 \cdot \left(\frac{1}{C_2}\right) & 0 & 0 \end{bmatrix} \begin{bmatrix} x_1 \\ x_2 \\ x_3 \\ x_4 \end{bmatrix} + \begin{bmatrix} \frac{1}{2L} & \frac{1}{2} \\ \frac{1}{2L} & -\frac{1}{2} \\ 0 & 0 \\ 0 & 0 \end{bmatrix} \begin{bmatrix} V_{dc} \\ \frac{di_s}{dt} \end{bmatrix}. \quad (4.23)$$

The coefficient marked in red contains the information from switching patten  $\Gamma_1^{(2)}$ .

The system matrices are

$$\mathbf{A} = \begin{bmatrix} 0 & 0 & 0 \cdot \left(-\frac{1}{2L}\right) & 1 \cdot \left(-\frac{1}{2L}\right) \\ 0 & 0 & 0 \cdot \left(-\frac{1}{2L}\right) & 1 \cdot \left(-\frac{1}{2L}\right) \\ 0 \cdot \left(\frac{1}{C_1}\right) & 0 & 0 & 0 \\ 0 & 1 \cdot \left(\frac{1}{C_2}\right) & 0 & 0 \end{bmatrix},$$

$$\mathbf{B} = \begin{bmatrix} \frac{1}{2L} & \frac{1}{2} \\ \frac{1}{2L} & -\frac{1}{2} \\ 0 & 0 \\ 0 & 0 \end{bmatrix},$$

$$\text{and } \mathbf{U} = \begin{bmatrix} V_{dc} \\ \frac{di_s}{dt} \end{bmatrix}. \quad (4.24)$$

The coefficient matrix could be decomposed as follows,

$$\mathbf{A} = \begin{bmatrix} 0 & 0 & \mathbf{0} \cdot \left(-\frac{1}{2L}\right) & \mathbf{1} \cdot \left(-\frac{1}{2L}\right) \\ 0 & 0 & \mathbf{0} \cdot \left(-\frac{1}{2L}\right) & \mathbf{1} \cdot \left(-\frac{1}{2L}\right) \\ \mathbf{0} \cdot \left(\frac{1}{C_1}\right) & 0 & 0 & 0 \\ 0 & \mathbf{1} \cdot \left(\frac{1}{C_2}\right) & 0 & 0 \end{bmatrix} = \begin{bmatrix} \mathbf{0} & \mathbf{A}_L \\ \mathbf{A}_C & \mathbf{0} \end{bmatrix}. \quad (4.25)$$

$$\mathbf{A}_L = \begin{bmatrix} \mathbf{0} \cdot \left(-\frac{1}{2L}\right) & \mathbf{1} \cdot \left(-\frac{1}{2L}\right) \\ \mathbf{0} \cdot \left(-\frac{1}{2L}\right) & \mathbf{1} \cdot \left(-\frac{1}{2L}\right) \end{bmatrix} = \begin{bmatrix} -\frac{1}{2L} \\ -\frac{1}{2L} \end{bmatrix} \cdot [\mathbf{0} \ \mathbf{1}] = \hat{\mathbf{A}}_L \cdot \mathbf{\Gamma}_1^{(2)}. \quad (4.26)$$

$$\mathbf{A}_C = \begin{bmatrix} \mathbf{0} \cdot \left(\frac{1}{C_1}\right) & 0 \\ 0 & \mathbf{1} \cdot \left(\frac{1}{C_2}\right) \end{bmatrix} = [\hat{\mathbf{A}}_C \ \bar{\mathbf{A}}_C]. \quad (4.27)$$

$$\hat{\mathbf{A}}_C = \text{diag} \left( \begin{bmatrix} \frac{1}{C_1} \\ 0 \end{bmatrix} \cdot [\mathbf{0} \ \mathbf{1}] \right) = \text{diag} (\hat{\mathbf{A}}'_C \cdot \mathbf{\Gamma}_1^{(2)}). \quad (4.28)$$

$$\bar{\mathbf{A}}_C = \text{diag} \left( \begin{bmatrix} 0 \\ \frac{1}{C_2} \end{bmatrix} \cdot [\mathbf{0} \ \mathbf{1}] \right) = \text{diag} (\bar{\mathbf{A}}'_C \cdot \mathbf{\Gamma}_1^{(2)}). \quad (4.29)$$

*diag* operator returns a column vector of the main diagonal elements of the objective matrix.  $\hat{\mathbf{A}}_L$  contains the parameters from arm inductance.  $\hat{\mathbf{A}}'_C$  and  $\bar{\mathbf{A}}'_C$  contains the parameters from submodule capacitance. The reason to decompose the state space in such form is to save the work for programming. It will be easy to extent to high level state space by decomposing the matrix into such form.

Note that  $\mathbf{U}$  contains  $\frac{di_s}{dt}$ .  $\frac{di_s}{dt}$  reflects the voltage across the load inductor. That is

$$L_a \frac{di_s}{dt} = v_a - V_s, \quad (4.30)$$

as modeled in Figure 4.16.

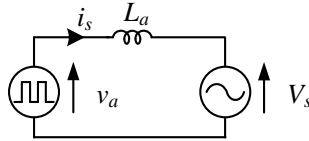


Figure 4.16 Load inductor voltage modeling.

If the pole is attached to the positive dc rail, as shown in Figure 4.14(a) and Figure 4.15(a),  $v_a = 1/2V_{dc}$ . Eq.(4.30) can be modified as

$$\frac{di_s}{dt} = \frac{1}{L_a} \left( \frac{1}{2} V_{dc} - V_s \right). \quad (4.31)$$

Replace the  $\frac{di_s}{dt}$  in (4.23) by (4.31)

$$\mathbf{U} = \left[ \begin{array}{c} V_{dc} \\ \frac{1}{L_a} \left( \frac{1}{2} V_{dc} - V_s \right) \end{array} \right]. \quad (4.32)$$

Figure 4.15(b) can be formulated as

$$\left\{ \begin{array}{l} V_{L1} = L \frac{di_1}{dt} \\ V_{L2} = L \frac{di_2}{dt} \\ i_1 = C_1 \frac{dV_{C1}}{dt} \\ i_1 = i_2 + i_s \\ V_{dc} = V_{L1} + V_{L2} + V_{C1} \end{array} \right. . \quad (4.33)$$

The corresponding switching pattern is

$$\Gamma_2^{(2)} = [1 \ 0]. \quad (4.34)$$

Define the state variables to be

$$\mathbf{X} = \begin{bmatrix} x_1 \\ x_2 \\ x_3 \\ x_4 \end{bmatrix} = \begin{bmatrix} i_1 \\ i_2 \\ V_{C1} \\ V_{C2} \end{bmatrix}, \quad \dot{\mathbf{X}} = \begin{bmatrix} \dot{x}_1 \\ \dot{x}_2 \\ \dot{x}_3 \\ \dot{x}_4 \end{bmatrix} = \begin{bmatrix} \frac{di_1}{dt} \\ \frac{di_2}{dt} \\ \frac{dV_{C1}}{dt} \\ \frac{dV_{C2}}{dt} \end{bmatrix}. \quad (4.35)$$

Rewrite (4.33) into state equation,

$$\begin{cases} \dot{x}_1 = -\frac{1}{2L}x_3 + \frac{1}{2L}V_{dc} + \frac{1}{2}\frac{di_s}{dt} \\ \dot{x}_2 = -\frac{1}{2L}x_3 + \frac{1}{2L}V_{dc} - \frac{1}{2}\frac{di_s}{dt} \\ \dot{x}_3 = \frac{1}{C_1}x_1 \end{cases} \quad (4.36)$$

or

$$\left\{ \begin{array}{l} \dot{x}_1 = 0 \cdot x_1 + 0 \cdot x_2 + 1 \cdot \left( -\frac{1}{2L} x_3 \right) + 0 \cdot \left( -\frac{1}{2L} x_4 \right) + \left( \frac{1}{2L} V_{dc} + \frac{1}{2} \frac{di_s}{dt} \right) \\ \dot{x}_2 = 0 \cdot x_1 + 0 \cdot x_2 + 1 \cdot \left( -\frac{1}{2L} x_3 \right) + 0 \cdot \left( -\frac{1}{2L} x_4 \right) + \left( \frac{1}{2L} V_{dc} - \frac{1}{2} \frac{di_s}{dt} \right) \\ \dot{x}_3 = 1 \cdot \left( \frac{1}{C_1} x_1 \right) + 0 \cdot x_2 + 0 \cdot x_3 + 0 \cdot x_4 + 0 \\ \dot{x}_4 = 0 \cdot x_1 + 0 \cdot \left( \frac{1}{C_2} x_2 \right) + 0 \cdot x_3 + 0 \cdot x_4 + 0 \end{array} \right. \quad (4.37)$$

Rewrite (4.37) into matrix form,

$$\begin{bmatrix} \dot{x}_1 \\ \dot{x}_2 \\ \dot{x}_3 \\ \dot{x}_4 \end{bmatrix} = \begin{bmatrix} 0 & 0 & \mathbf{1} \cdot \left(-\frac{1}{2L}\right) & \mathbf{0} \cdot \left(-\frac{1}{2L}\right) \\ 0 & 0 & \mathbf{1} \cdot \left(-\frac{1}{2L}\right) & \mathbf{0} \cdot \left(-\frac{1}{2L}\right) \\ \mathbf{1} \cdot \left(\frac{1}{C_1}\right) & 0 & 0 & 0 \\ 0 & \mathbf{0} \cdot \left(\frac{1}{C_2}\right) & 0 & 0 \end{bmatrix} \begin{bmatrix} x_1 \\ x_2 \\ x_3 \\ x_4 \end{bmatrix} + \begin{bmatrix} \frac{1}{2L} & \frac{1}{2} \\ \frac{1}{2L} & -\frac{1}{2} \\ 0 & 0 \\ 0 & 0 \end{bmatrix} \begin{bmatrix} V_{dc} \\ \frac{di_s}{dt} \end{bmatrix}. \quad (4.38)$$

The coefficient marked in red contains the information from switching patten  $\Gamma_2^{(2)}$ .

The system matrices are

$$\mathbf{A} = \begin{bmatrix} 0 & 0 & \mathbf{1} \cdot \left(-\frac{1}{2L}\right) & \mathbf{0} \cdot \left(-\frac{1}{2L}\right) \\ 0 & 0 & \mathbf{1} \cdot \left(-\frac{1}{2L}\right) & \mathbf{0} \cdot \left(-\frac{1}{2L}\right) \\ \mathbf{1} \cdot \left(\frac{1}{C_1}\right) & 0 & 0 & 0 \\ 0 & \mathbf{0} \cdot \left(\frac{1}{C_2}\right) & 0 & 0 \end{bmatrix},$$

$$\mathbf{B} = \begin{bmatrix} \frac{1}{2L} & \frac{1}{2} \\ \frac{1}{2L} & -\frac{1}{2} \\ 0 & 0 \\ 0 & 0 \end{bmatrix},$$

$$\text{and } \mathbf{U} = \begin{bmatrix} V_{dc} \\ \frac{di_s}{dt} \end{bmatrix}. \quad (4.39)$$

The coefficient matrix could be decomposed as follows,

$$\mathbf{A} = \left[ \begin{array}{cc|cc} 0 & 0 & \mathbf{1} \cdot \left(-\frac{1}{2L}\right) & \mathbf{0} \cdot \left(-\frac{1}{2L}\right) \\ 0 & 0 & \mathbf{1} \cdot \left(-\frac{1}{2L}\right) & \mathbf{0} \cdot \left(-\frac{1}{2L}\right) \\ \hline \mathbf{1} \cdot \left(\frac{1}{C_1}\right) & 0 & 0 & 0 \\ 0 & \mathbf{0} \cdot \left(\frac{1}{C_2}\right) & 0 & 0 \end{array} \right] = \left[ \begin{array}{c|c} \mathbf{0} & \mathbf{A}_L \\ \hline \mathbf{A}_C & \mathbf{0} \end{array} \right]. \quad (4.40)$$

$$\mathbf{A}_L = \left[ \begin{array}{cc} \mathbf{1} \cdot \left(-\frac{1}{2L}\right) & \mathbf{0} \cdot \left(-\frac{1}{2L}\right) \\ \mathbf{1} \cdot \left(-\frac{1}{2L}\right) & \mathbf{0} \cdot \left(-\frac{1}{2L}\right) \end{array} \right] = \left[ \begin{array}{c} -\frac{1}{2L} \\ -\frac{1}{2L} \end{array} \right] \cdot [\mathbf{1} \ \mathbf{0}] = \hat{\mathbf{A}}_L \cdot \mathbf{\Gamma}_1^{(2)}. \quad (4.41)$$

$$\mathbf{A}_C = \left[ \begin{array}{c|c} \mathbf{1} \cdot \left(\frac{1}{C_1}\right) & 0 \\ \hline 0 & \mathbf{0} \cdot \left(\frac{1}{C_2}\right) \end{array} \right] = [\hat{\mathbf{A}}_C \ | \ \bar{\mathbf{A}}_C]. \quad (4.42)$$

$$\hat{\mathbf{A}}_C = \text{diag} \left( \left[ \begin{array}{c} \frac{1}{C_1} \\ 0 \end{array} \right] \cdot [\mathbf{1} \ \mathbf{0}] \right) = \text{diag} \left( \hat{\mathbf{A}}'_C \cdot \mathbf{\Gamma}_2^{(2)} \right). \quad (4.43)$$

$$\bar{\mathbf{A}}_C = \text{diag} \left( \left[ \begin{array}{c} 0 \\ \frac{1}{C_2} \end{array} \right] \cdot [\mathbf{1} \ \mathbf{0}] \right) = \text{diag} \left( \bar{\mathbf{A}}'_C \cdot \mathbf{\Gamma}_2^{(2)} \right). \quad (4.44)$$

*diag* operator returns a column vector of the main diagonal elements of the objective matrix.  $\hat{\mathbf{A}}_L$  contains the parameters from arm inductance.  $\hat{\mathbf{A}}'_C$  and  $\bar{\mathbf{A}}'_C$  contains the parameters from submodule capacitance. The reason to decompose the state space in such form is to save the work for programming. It will be easy to extent to high level state space by decomposing the matrix into such form.

Note that  $\mathbf{U}$  contains  $\frac{di_s}{dt}$ .  $\frac{di_s}{dt}$  reflects the voltage across the load inductor. That is

$$L_a \frac{di_s}{dt} = v_a - V_s, \quad (4.45)$$

as modeled in Figure4.16.

If the pole is attached to the negative dc rail, as shown in Figure4.14(b) and Figure4.15(b),  $v_a = -1/2V_{dc}$ . Eq.(4.45) can be modified as

$$\frac{di_s}{dt} = \frac{1}{L_a} \left( -\frac{1}{2}V_{dc} - V_s \right). \quad (4.46)$$

Replace the  $\frac{di_s}{dt}$  in (4.39) by (4.46)

$$\mathbf{U} = \begin{bmatrix} V_{dc} \\ \frac{1}{L_a} \left( -\frac{1}{2}V_{dc} - V_s \right) \end{bmatrix}. \quad (4.47)$$

#### 4.6.2 STATE-SPACE MODEL WITH STRAY RESISTANCE

The stray resistance is essential in the real MMC installations or simulations. The pole voltage  $v_a$  of a two-level MMC can either be  $1/2V_{dc}$  or  $-1/2V_{dc}$  as shown in Figure4.17. To calculate the arm inductor voltage, we need to find the state equation of MMC. Figure4.18 shows the simplified MMC model. Figure4.18(a) can be formulated as

$$\begin{cases} V_{L1} = L \frac{di_1}{dt} \\ V_{L2} = L \frac{di_2}{dt} \\ i_2 = C_2 \frac{dV_{C2}}{dt} \\ i_1 = i_2 + i_s \\ V_{dc} = V_{L1} + V_{R1} + V_{R2} + V_{L2} + V_{C2} \end{cases} \cdot \quad (4.48)$$

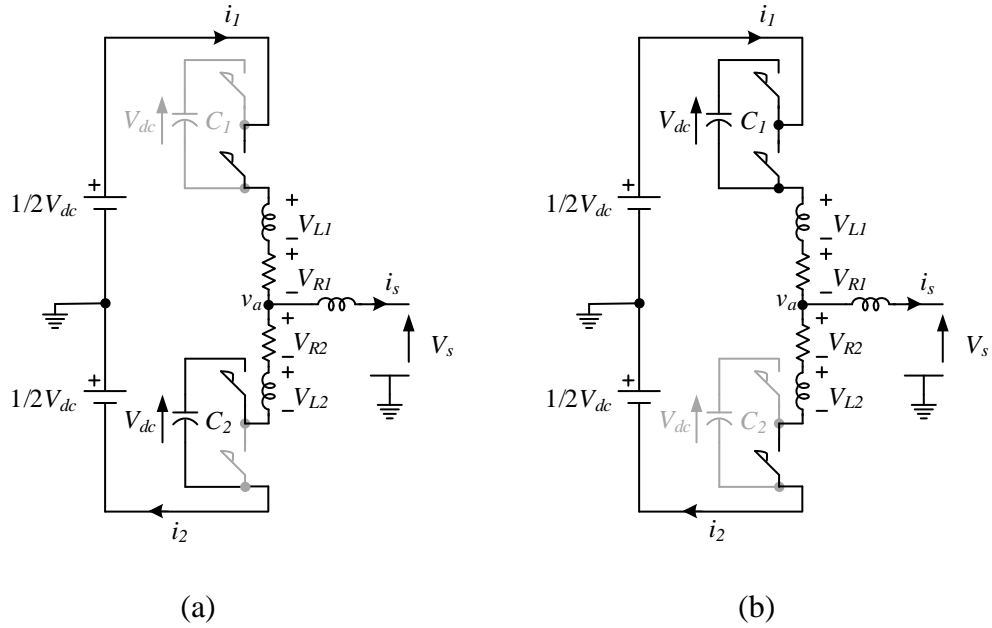


Figure 4.17 Two-level MMC with pole connected to (a) positive dc rail (Level 1); and (b) negative dc rail (Level 2).

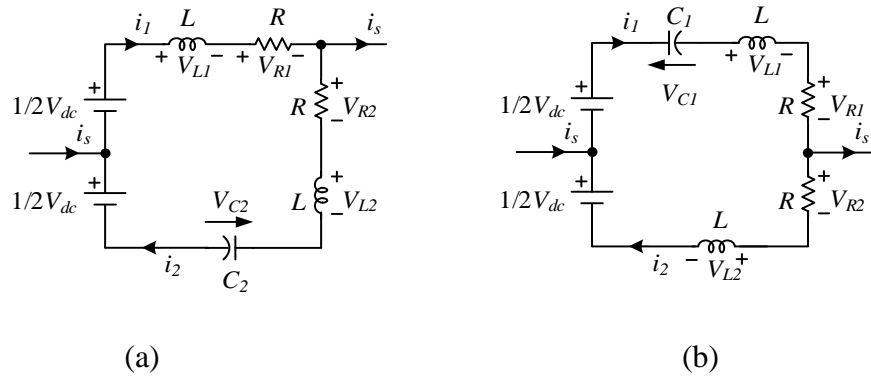


Figure 4.18 Two-level MMC model with pole connected to (a) positive dc rail; and (b) negative dc rail.

The corresponding switching pattern is

$$\Gamma_1^{(2)} = [0 \ 1]. \tag{4.49}$$

Define the state variables to be

$$\mathbf{X} = \begin{bmatrix} x_1 \\ x_2 \\ x_3 \\ x_4 \end{bmatrix} = \begin{bmatrix} i_1 \\ i_2 \\ V_{C1} \\ V_{C2} \end{bmatrix}, \quad \dot{\mathbf{X}} = \begin{bmatrix} \dot{x}_1 \\ \dot{x}_2 \\ \dot{x}_3 \\ \dot{x}_4 \end{bmatrix} = \begin{bmatrix} \frac{di_1}{dt} \\ \frac{di_2}{dt} \\ \frac{dV_{C1}}{dt} \\ \frac{dV_{C2}}{dt} \end{bmatrix}. \quad (4.50)$$

Rewrite (4.48) into state equation form,

$$\begin{cases} \dot{x}_1 = -\frac{R}{2L}x_1 - \frac{R}{2L}x_2 - \frac{1}{2L}x_4 + \frac{1}{2L}V_{dc} + \frac{1}{2}\frac{di_s}{dt} \\ \dot{x}_2 = -\frac{R}{2L}x_1 - \frac{R}{2L}x_2 - \frac{1}{2L}x_4 + \frac{1}{2L}V_{dc} - \frac{1}{2}\frac{di_s}{dt}, \\ \dot{x}_4 = \frac{1}{C_2}x_2 \end{cases}, \quad (4.51)$$

or

$$\begin{cases} \dot{x}_1 = \left(-\frac{R}{2L}\right) \cdot x_1 + \left(-\frac{R}{2L}\right) \cdot x_2 + \mathbf{0} \cdot \left(-\frac{1}{2L} x_3\right) + \mathbf{1} \cdot \left(-\frac{1}{2L} x_4\right) + \left(\frac{1}{2L} V_{dc} + \frac{1}{2} \frac{di_s}{dt}\right) \\ \dot{x}_2 = \left(-\frac{R}{2L}\right) \cdot x_1 + \left(-\frac{R}{2L}\right) \cdot x_2 + \mathbf{0} \cdot \left(-\frac{1}{2L} x_3\right) + \mathbf{1} \cdot \left(-\frac{1}{2L} x_4\right) + \left(\frac{1}{2L} V_{dc} - \frac{1}{2} \frac{di_s}{dt}\right) \\ \dot{x}_3 = \mathbf{0} \cdot \left(\frac{1}{C_1} x_1\right) + 0 \cdot x_2 + 0 \cdot x_3 + 0 \cdot x_4 + 0 \\ \dot{x}_4 = 0 \cdot x_1 + \mathbf{1} \cdot \left(\frac{1}{C_2} x_2\right) + 0 \cdot x_3 + 0 \cdot x_4 + 0 \end{cases} \quad (4.52)$$

Rewrite (4.52) into matrix form,

$$\begin{bmatrix} \dot{x}_1 \\ \dot{x}_2 \\ \dot{x}_3 \\ \dot{x}_4 \end{bmatrix} = \begin{bmatrix} -\frac{R}{2L} & -\frac{R}{2L} & 0 \cdot \left(-\frac{1}{2L}\right) & 1 \cdot \left(-\frac{1}{2L}\right) \\ -\frac{R}{2L} & -\frac{R}{2L} & 0 \cdot \left(-\frac{1}{2L}\right) & 1 \cdot \left(-\frac{1}{2L}\right) \\ 0 \cdot \left(\frac{1}{C_1}\right) & 0 & 0 & 0 \\ 0 & 1 \cdot \left(\frac{1}{C_2}\right) & 0 & 0 \end{bmatrix} \begin{bmatrix} x_1 \\ x_2 \\ x_3 \\ x_4 \end{bmatrix} + \begin{bmatrix} \frac{1}{2L} & \frac{1}{2} \\ \frac{1}{2L} & -\frac{1}{2} \\ 0 & 0 \\ 0 & 0 \end{bmatrix} \begin{bmatrix} V_{dc} \\ \frac{di_s}{dt} \end{bmatrix}. \quad (4.53)$$

The coefficient marked in red contains the information from switching patten  $\Gamma_1^{(2)}$ .

The system matrices are

$$\mathbf{A} = \begin{bmatrix} -\frac{R}{2L} & -\frac{R}{2L} & 0 \cdot \left(-\frac{1}{2L}\right) & 1 \cdot \left(-\frac{1}{2L}\right) \\ -\frac{R}{2L} & -\frac{R}{2L} & 0 \cdot \left(-\frac{1}{2L}\right) & 1 \cdot \left(-\frac{1}{2L}\right) \\ 0 \cdot \left(\frac{1}{C_1}\right) & 0 & 0 & 0 \\ 0 & 1 \cdot \left(\frac{1}{C_2}\right) & 0 & 0 \end{bmatrix},$$

$$\mathbf{B} = \begin{bmatrix} \frac{1}{2L} & \frac{1}{2} \\ \frac{1}{2L} & -\frac{1}{2} \\ 0 & 0 \\ 0 & 0 \end{bmatrix},$$

$$\text{and } \mathbf{U} = \begin{bmatrix} V_{dc} \\ \frac{di_s}{dt} \end{bmatrix}. \quad (4.54)$$

The coefficient matrix could be decomposed as follows,

$$\mathbf{A} = \begin{bmatrix} -\frac{R}{2L} & -\frac{R}{2L} & \mathbf{0} \cdot \left(-\frac{1}{2L}\right) & \mathbf{1} \cdot \left(-\frac{1}{2L}\right) \\ -\frac{R}{2L} & -\frac{R}{2L} & \mathbf{0} \cdot \left(-\frac{1}{2L}\right) & \mathbf{1} \cdot \left(-\frac{1}{2L}\right) \\ \mathbf{0} \cdot \left(\frac{1}{C_1}\right) & 0 & 0 & 0 \\ 0 & \mathbf{1} \cdot \left(\frac{1}{C_2}\right) & 0 & 0 \end{bmatrix} = \begin{bmatrix} \mathbf{A}_R & \mathbf{A}_L \\ \mathbf{A}_C & \mathbf{0} \end{bmatrix}. \quad (4.55)$$

$$\mathbf{A}_R = \begin{bmatrix} -\frac{R}{2L} & -\frac{R}{2L} \\ -\frac{R}{2L} & -\frac{R}{2L} \end{bmatrix}. \quad (4.56)$$

$$\mathbf{A}_L = \begin{bmatrix} \mathbf{0} \cdot \left(-\frac{1}{2L}\right) & \mathbf{1} \cdot \left(-\frac{1}{2L}\right) \\ \mathbf{0} \cdot \left(-\frac{1}{2L}\right) & \mathbf{1} \cdot \left(-\frac{1}{2L}\right) \end{bmatrix} = \begin{bmatrix} -\frac{1}{2L} \\ -\frac{1}{2L} \end{bmatrix} \cdot [\mathbf{0} \ \mathbf{1}] = \hat{\mathbf{A}}_L \cdot \Gamma_1^{(2)}. \quad (4.57)$$

$$\mathbf{A}_C = \begin{bmatrix} \mathbf{0} \cdot \left(\frac{1}{C_1}\right) & 0 \\ 0 & \mathbf{1} \cdot \left(\frac{1}{C_2}\right) \end{bmatrix} = [\hat{\mathbf{A}}_C \ \bar{\mathbf{A}}_C]. \quad (4.58)$$

$$\hat{\mathbf{A}}_C = \text{diag} \left( \begin{bmatrix} \frac{1}{C_1} \\ 0 \end{bmatrix} \cdot [\mathbf{0} \ \mathbf{1}] \right) = \text{diag} (\hat{\mathbf{A}}'_C \cdot \Gamma_1^{(2)}). \quad (4.59)$$

$$\bar{\mathbf{A}}_C = \text{diag} \left( \begin{bmatrix} 0 \\ \frac{1}{C_2} \end{bmatrix} \cdot [\mathbf{0} \ \mathbf{1}] \right) = \text{diag} (\bar{\mathbf{A}}'_C \cdot \Gamma_1^{(2)}). \quad (4.60)$$

*diag* operator returns a column vector of the main diagonal elements of the objective matrix.  $\hat{\mathbf{A}}_L$  contains the parameters from arm inductance.  $\hat{\mathbf{A}}'_C$  and  $\bar{\mathbf{A}}'_C$  contains the parameters from submodule capacitance. The reason to decompose the state space in such

form is to save the work for programming. It will be easy to extent to high level state space by decomposing the matrix into such form.

Note that  $\mathbf{U}$  contains  $\frac{di_s}{dt}$ .  $\frac{di_s}{dt}$  reflects the voltage across the load inductor. That is

$$L_a \frac{di_s}{dt} = v_a - V_s, \quad (4.61)$$

as modeled in Figure4.16.

If the pole is attached to the positive dc rail, as shown in Figure4.17(a) and Figure4.18(a),  $v_a = 1/2V_{dc}$ . Eq.(4.61) can be modified as

$$\frac{di_s}{dt} = \frac{1}{L_a} \left( \frac{1}{2} V_{dc} - V_s \right). \quad (4.62)$$

Replace the  $\frac{di_s}{dt}$  in (4.54) by (4.62)

$$\mathbf{U} = \begin{bmatrix} V_{dc} \\ \frac{1}{L_a} \left( \frac{1}{2} V_{dc} - V_s \right) \end{bmatrix}. \quad (4.63)$$

Figure4.18(b) can be formulated as

$$\begin{cases} V_{L1} = L \frac{di_1}{dt} \\ V_{L2} = L \frac{di_2}{dt} \\ i_2 = C_1 \frac{dV_{C1}}{dt} \\ i_1 = i_2 + i_s \\ V_{dc} = V_{L1} + V_{R1} + V_{R2} + V_{L2} + V_{C1} \end{cases}. \quad (4.64)$$

The corresponding switching pattern is

$$\mathbf{\Gamma}_2^{(2)} = [1 \ 0]. \quad (4.65)$$

Define the state variables to be

$$\mathbf{X} = \begin{bmatrix} x_1 \\ x_2 \\ x_3 \\ x_4 \end{bmatrix} = \begin{bmatrix} i_1 \\ i_2 \\ V_{C1} \\ V_{C2} \end{bmatrix}, \quad \dot{\mathbf{X}} = \begin{bmatrix} \dot{x}_1 \\ \dot{x}_2 \\ \dot{x}_3 \\ \dot{x}_4 \end{bmatrix} = \begin{bmatrix} \frac{di_1}{dt} \\ \frac{di_2}{dt} \\ \frac{dV_{C1}}{dt} \\ \frac{dV_{C2}}{dt} \end{bmatrix}. \quad (4.66)$$

Rewrite (4.64) into state equation,

$$\begin{cases} \dot{x}_1 = -\frac{R}{2L}x_1 - \frac{R}{2L}x_2 - \frac{1}{2L}x_3 + \frac{1}{2L}V_{dc} + \frac{1}{2}\frac{di_s}{dt} \\ \dot{x}_2 = -\frac{R}{2L}x_1 - \frac{R}{2L}x_2 - \frac{1}{2L}x_3 + \frac{1}{2L}V_{dc} - \frac{1}{2}\frac{di_s}{dt} \\ \dot{x}_3 = \frac{1}{C_1}x_1 \end{cases} \quad (4.67)$$

or

$$\begin{cases} \dot{x}_1 = \left(-\frac{R}{2L}\right) \cdot x_1 + \left(-\frac{R}{2L}\right) \cdot x_2 + \mathbf{1} \cdot \left(-\frac{1}{2L} x_3\right) + \mathbf{0} \cdot \left(-\frac{1}{2L} x_4\right) + \left(\frac{1}{2L} V_{dc} + \frac{1}{2} \frac{di_s}{dt}\right) \\ \dot{x}_2 = \left(-\frac{R}{2L}\right) \cdot x_1 + \left(-\frac{R}{2L}\right) \cdot x_2 + \mathbf{1} \cdot \left(-\frac{1}{2L} x_3\right) + \mathbf{0} \cdot \left(-\frac{1}{2L} x_4\right) + \left(\frac{1}{2L} V_{dc} - \frac{1}{2} \frac{di_s}{dt}\right) \\ \dot{x}_3 = \mathbf{1} \cdot \left(\frac{1}{C_1} x_1\right) + \mathbf{0} \cdot x_2 + \mathbf{0} \cdot x_3 + \mathbf{0} \cdot x_4 + \mathbf{0} \\ \dot{x}_4 = \mathbf{0} \cdot x_1 + \mathbf{0} \cdot \left(\frac{1}{C_2} x_2\right) + \mathbf{0} \cdot x_3 + \mathbf{0} \cdot x_4 + \mathbf{0} \end{cases} \quad (4.68)$$

Rewrite (4.68) into matrix form,

$$\begin{bmatrix} \dot{x}_1 \\ \dot{x}_2 \\ \dot{x}_3 \\ \dot{x}_4 \end{bmatrix} = \begin{bmatrix} -\frac{R}{2L} & -\frac{R}{2L} & \mathbf{1} \cdot \left(-\frac{1}{2L}\right) & \mathbf{0} \cdot \left(-\frac{1}{2L}\right) \\ -\frac{R}{2L} & -\frac{R}{2L} & \mathbf{1} \cdot \left(-\frac{1}{2L}\right) & \mathbf{0} \cdot \left(-\frac{1}{2L}\right) \\ \mathbf{1} \cdot \left(\frac{1}{C_1}\right) & 0 & 0 & 0 \\ 0 & \mathbf{0} \cdot \left(\frac{1}{C_2}\right) & 0 & 0 \end{bmatrix} \begin{bmatrix} x_1 \\ x_2 \\ x_3 \\ x_4 \end{bmatrix} + \begin{bmatrix} \frac{1}{2L} & \frac{1}{2} \\ \frac{1}{2L} & -\frac{1}{2} \\ 0 & 0 \\ 0 & 0 \end{bmatrix} \begin{bmatrix} V_{dc} \\ \frac{di_s}{dt} \end{bmatrix}. \quad (4.69)$$

The coefficient marked in red contains the information from switching pattern  $\Gamma_2^{(2)}$ .

The system matrices are

$$\mathbf{A} = \begin{bmatrix} -\frac{R}{2L} & -\frac{R}{2L} & \mathbf{1} \cdot \left(-\frac{1}{2L}\right) & \mathbf{0} \cdot \left(-\frac{1}{2L}\right) \\ -\frac{R}{2L} & -\frac{R}{2L} & \mathbf{1} \cdot \left(-\frac{1}{2L}\right) & \mathbf{0} \cdot \left(-\frac{1}{2L}\right) \\ \mathbf{1} \cdot \left(\frac{1}{C_1}\right) & 0 & 0 & 0 \\ 0 & \mathbf{0} \cdot \left(\frac{1}{C_2}\right) & 0 & 0 \end{bmatrix},$$

$$\mathbf{B} = \begin{bmatrix} \frac{1}{2L} & \frac{1}{2} \\ \frac{1}{2L} & -\frac{1}{2} \\ 0 & 0 \\ 0 & 0 \end{bmatrix},$$

$$\text{and } \mathbf{U} = \begin{bmatrix} V_{dc} \\ \frac{di_s}{dt} \end{bmatrix}. \quad (4.70)$$

The coefficient matrix could be decomposed as follows,

$$\mathbf{A} = \left[ \begin{array}{cc|cc} -\frac{R}{2L} & -\frac{R}{2L} & \mathbf{1} \cdot \left(-\frac{1}{2L}\right) & \mathbf{0} \cdot \left(-\frac{1}{2L}\right) \\ -\frac{R}{2L} & -\frac{R}{2L} & \mathbf{1} \cdot \left(-\frac{1}{2L}\right) & \mathbf{0} \cdot \left(-\frac{1}{2L}\right) \\ \hline \mathbf{1} \cdot \left(\frac{1}{C_1}\right) & 0 & 0 & 0 \\ 0 & \mathbf{0} \cdot \left(\frac{1}{C_2}\right) & 0 & 0 \end{array} \right] = \left[ \begin{array}{c|c} \mathbf{A}_R & \mathbf{A}_L \\ \hline \mathbf{A}_C & \mathbf{0} \end{array} \right]. \quad (4.71)$$

$$\mathbf{A}_R = \begin{bmatrix} -\frac{R}{2L} & -\frac{R}{2L} \\ -\frac{R}{2L} & -\frac{R}{2L} \end{bmatrix}. \quad (4.72)$$

$$\mathbf{A}_L = \begin{bmatrix} \mathbf{1} \cdot \left(-\frac{1}{2L}\right) & \mathbf{0} \cdot \left(-\frac{1}{2L}\right) \\ \mathbf{1} \cdot \left(-\frac{1}{2L}\right) & \mathbf{0} \cdot \left(-\frac{1}{2L}\right) \end{bmatrix} = \begin{bmatrix} -\frac{1}{2L} \\ -\frac{1}{2L} \end{bmatrix} \cdot [\mathbf{1} \ \mathbf{0}] = \hat{\mathbf{A}}_L \cdot \Gamma_2^{(2)}. \quad (4.73)$$

$$\mathbf{A}_C = \left[ \begin{array}{c|c} \mathbf{1} \cdot \left(\frac{1}{C_1}\right) & 0 \\ \hline 0 & \mathbf{0} \cdot \left(\frac{1}{C_2}\right) \end{array} \right] = [\hat{\mathbf{A}}_C \ \bar{\mathbf{A}}_C]. \quad (4.74)$$

$$\hat{\mathbf{A}}_C = \text{diag} \left( \begin{bmatrix} \frac{1}{C_1} \\ 0 \end{bmatrix} \cdot [\mathbf{1} \ \mathbf{0}] \right) = \text{diag} (\hat{\mathbf{A}}'_C \cdot \Gamma_2^{(2)}). \quad (4.75)$$

$$\bar{\mathbf{A}}_C = \text{diag} \left( \begin{bmatrix} 0 \\ \frac{1}{C_2} \end{bmatrix} \cdot [\mathbf{1} \ \mathbf{0}] \right) = \text{diag} (\bar{\mathbf{A}}'_C \cdot \Gamma_2^{(2)}). \quad (4.76)$$

*diag* operator returns a column vector of the main diagonal elements of the objective matrix.  $\hat{\mathbf{A}}_L$  contains the parameters from arm inductance.  $\hat{\mathbf{A}}'_C$  and  $\bar{\mathbf{A}}'_C$  contains the parameters from submodule capacitance. The reason to decompose the state space in such

form is to save the work for programming. It will be easy to extent to high level state space by decomposing the matrix into such form.

Note that  $\mathbf{U}$  contains  $\frac{di_s}{dt}$ .  $\frac{di_s}{dt}$  reflects the voltage across the load inductor. That is

$$L_a \frac{di_s}{dt} = v_a - V_s, \quad (4.77)$$

as modeled in Figure4.16.

If the pole is attached to the negative dc rail, as shown in Figure4.17(b) and Figure4.18 (b),  $v_a = -1/2V_{dc}$ . Eq.(4.77) can be modified as

$$\frac{di_s}{dt} = \frac{1}{L_a} \left( -\frac{1}{2}v_a - V_s \right). \quad (4.78)$$

Replace the  $\frac{di_s}{dt}$  in (4.70) by (4.78)

$$\mathbf{U} = \begin{bmatrix} V_{dc} \\ \frac{1}{L_a} \left( -\frac{1}{2}V_{dc} - V_s \right) \end{bmatrix}. \quad (4.79)$$

### 4.6.3 MODEL ANALYSIS AND SIMULATION

To prove the correctness of the proposed state-space model, the simulation of a two-level single phase MMC model in MATLAB/Simulink is conducted for comparison.

To simulate the proposed model, the differential equations of the state-space model (4.53) and (4.69) are discretized as follows,

$$\frac{d\mathbf{X}}{dt} = \mathbf{A} \cdot \mathbf{X} + \mathbf{B} \cdot \mathbf{U}, \quad (4.80)$$

$$d\mathbf{X} = \mathbf{A} \cdot \mathbf{X} \cdot dt + \mathbf{B} \cdot \mathbf{U} \cdot dt, \quad (4.81)$$

$$\mathbf{X}(k) - \mathbf{X}(k-1) = \mathbf{A}(k-1) \cdot \mathbf{X}(k-1) \cdot \Delta T + \mathbf{B} \cdot \mathbf{U}(k-1) \cdot \Delta T, \quad (4.82)$$

$$\mathbf{X}(k) = \mathbf{A}(k-1) \cdot \mathbf{X}(k-1) \cdot \Delta T + \mathbf{B} \cdot \mathbf{U}(k-1) \cdot \Delta T + \mathbf{X}(k-1), \quad (4.83)$$

A time-step of  $\Delta T = 0.1 \mu\text{s}$  was used to make sure the approximation is accurate enough. The system matrix  $\mathbf{A}$  is a function of switching patterns. The switching pattern of this modeling follows the modulation discussed Chapter 3. The initial values of the state space are extracted from the simulations. Four initial times are selected. The state space values at the specific time are extracted from simulation and substituted into (4.83) as initial state. The state space initial values are summarized in Table 5. Four initial times are selected to verify the state space derivation with the MATLAB/Simulink simulation.

Table 5  
Initial values of state space at four time instants.

	$t_1 = 10 \text{ ms}$	$t_2 = 15 \text{ ms}$	$t_3 = 20 \text{ ms}$	$t_4 = 25 \text{ ms}$
$i_1 \text{ (A)}$	-39.5	-48.7	66.9	4.2
$i_2 \text{ (A)}$	-1.4	-3.7	-0.2	-1.0
$V_{C1} \text{ (V)}$	995.6	994.8	1007.9	999.9
$V_{C2} \text{ (V)}$	1004.1	1005.2	993.3	999.7

A switching model is built in MATLAB/Simulink. The simulation circuit is shown in Figure 4.19. The key parameters of the system are summarized in Table 6. Ideal switches, inductors, and capacitors with no parasitic parameters as well as ideal voltage sources were used. Any controller delays are not included in the model. In the simulation setup, discrete-Tustin/Backward Euler (TBE) with a sample time of  $0.1 \mu\text{s}$  is selected. The initial values of capacitor voltages are 1000V. The initial values of the inductor current are determined by MATLAB/Simulink.

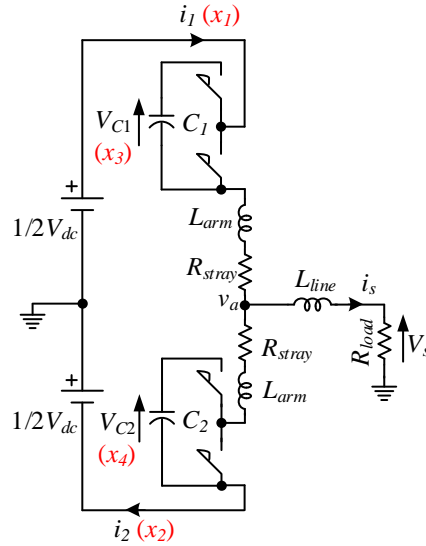


Figure 4.19 Two-level single-phase MMC circuit for simulation study.

The comparison results are shown in Figs. 4.20-4.23. The proposed state space model and the simulation results are matched at  $t_1$ ,  $t_2$ , and  $t_4$ , whereas a minor mismatch happens at  $t_3$ . This mismatch at  $t_3$  accumulated along with time. This is caused by the  $di_s/dt$  term in  $\mathbf{U}$ . We treat  $di_s/dt$  as an input since this term contains information from load instead of the information from MMC. We could have an even accurate state-space model by adding  $di_s/dt$  as the fifth state variable. This accumulation error becomes notable in a long run. Figure 4.24 shows the Simulink simulation along with the state-space model in two fundamental cycles. The accumulated error can be observed from this figure. Although there is minor mismatch between the simulation and the state-space model in this specific case study, the main features of the simulation curves are well captured by state-space model. This indicates that the mathematical derivation of the proposed model is correct. The  $di_s/dt$  term contains the information of load. This term could vary from load to load. But this has nothing to do with the MMC parameters. It is better to regard the  $di_s/dt$  as an input instead of a state variable when later on we move on to the stability analysis. Please

notice that stability analysis should have a general idea of how MMC respond to a specific load model and its load change.

Table 6

Two-level MMC simulation key parameters.

Fundamental Frequency, $f_0$	60 Hz
Switching Frequency, $f_{sw}$	10 kHz
DC-Bus Voltage, $V_{dc}$	1000 V
Load Resistance, $R_{load}$	6.2 $\Omega$ (100% p.u.)
Line Inductance, $L_{line}$	1 mH (6% p.u.)
Arm Inductance, $L_{arm}$	0.1 $\mu$ H (0.0006% p.u.)
Stray Resistance, $R_{stray}$	0.1 $\Omega$ (1.6% p.u.)
Submodule Capacitance, $C_i$	85 $\mu$ F (20% p.u.)
Number of Submodules per Arm	1

where  $i = 1, 2$ .

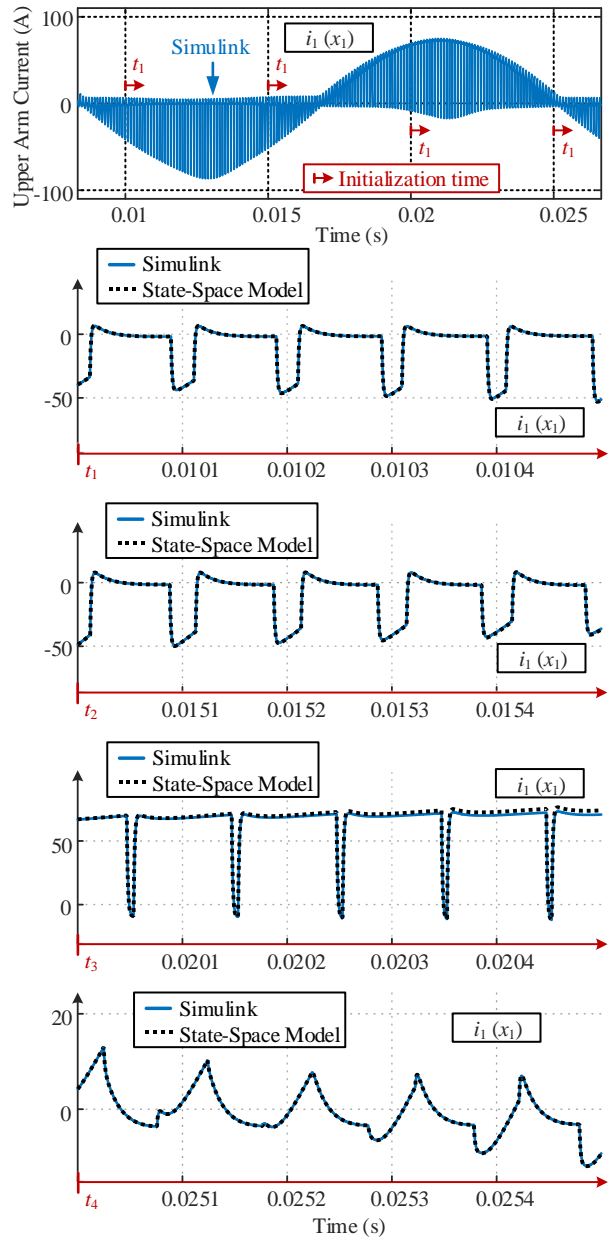


Figure 4.20 Upper arm current ( $x_1$ ) simulation and state-space model comparison.

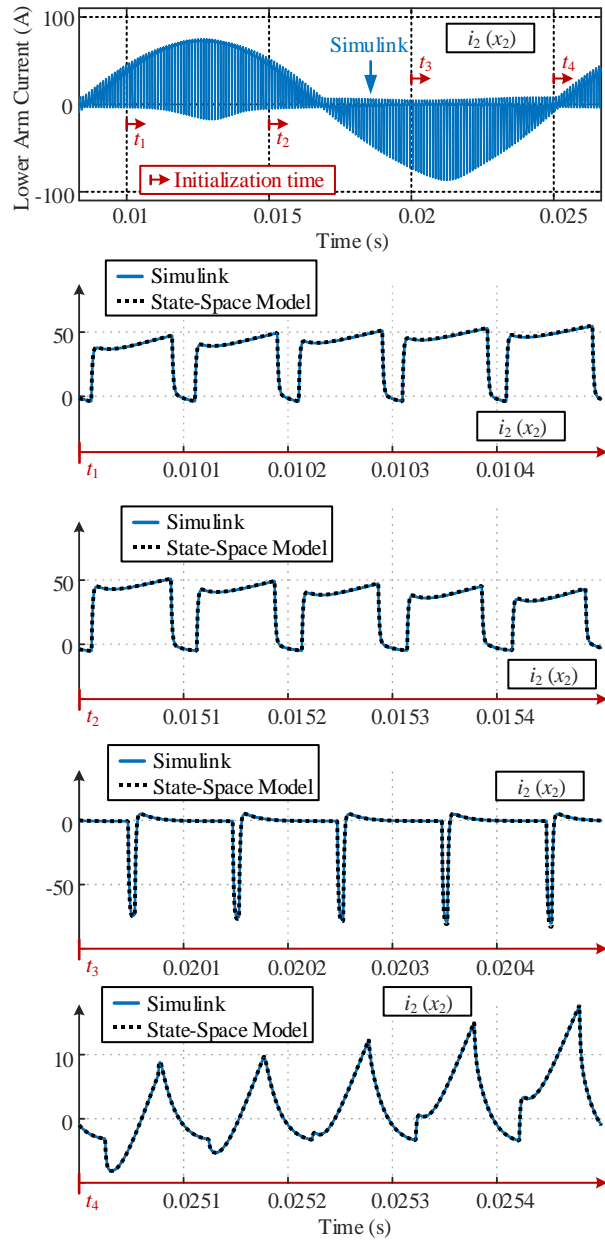


Figure 4.21 Lower arm current ( $x_2$ ) simulation and state-space model comparison.

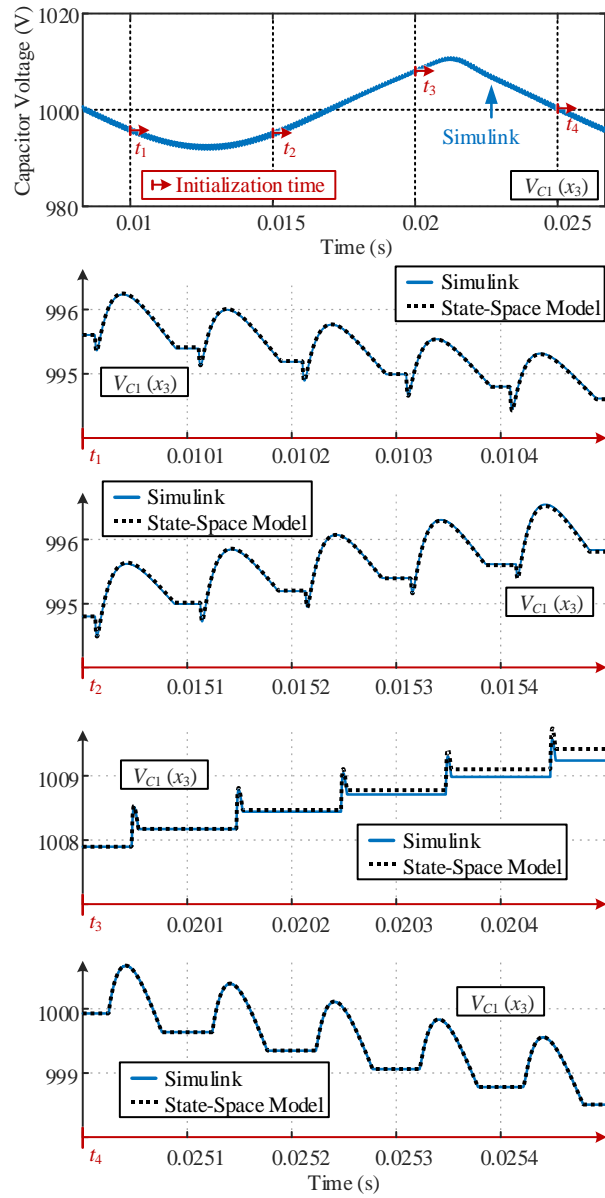


Figure 4.22 Capacitor voltage ( $x_3$ ) simulation and state-space model comparison.

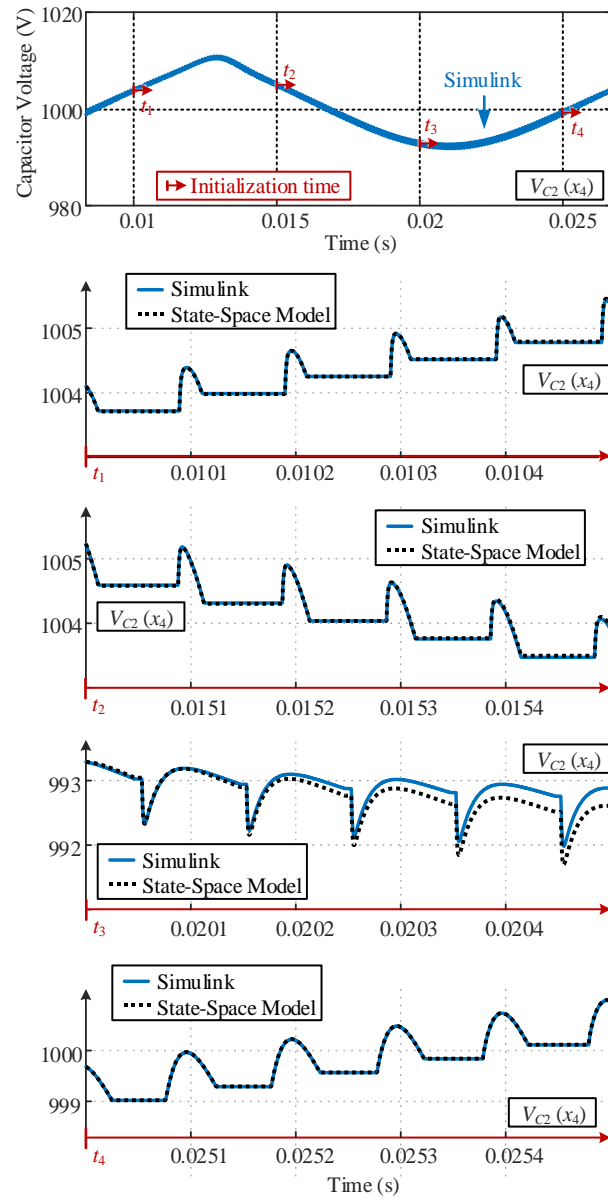
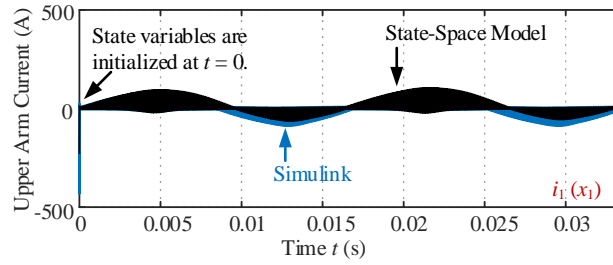
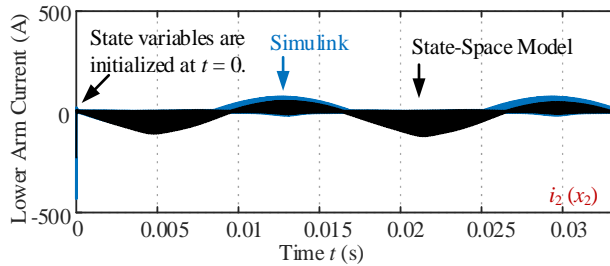


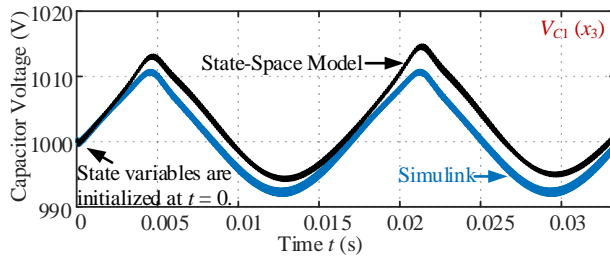
Figure 4.23 Capacitor voltage ( $x_4$ ) simulation and state-space model comparison.



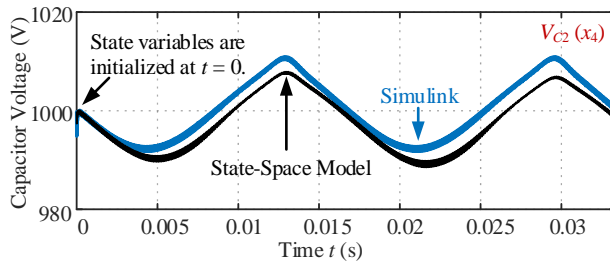
(a)



(b)



(c)



(d)

Figure 4.24 Comparison of simulation and state-space model in a long run. (a) upper arm current; (b) lower arm current; (c) capacitor voltage  $V_{C1}$ ; (d) capacitor voltage  $V_{C2}$ .

#### 4.6.4 STATE-SPACE MODEL WITH LOAD AS STATE VARIABLE

This section includes the derivation of the state space when considering the load as a state variable. We can see how complicated the state space could be.

The pole voltage  $v_a$  of a two-level MMC can either be  $1/2V_{dc}$  or  $-1/2V_{dc}$  as shown in Figure4.25. To calculate the arm inductor voltage, we need to find the state equation of MMC. Figure4.26 shows the simplified MMC model. Figure4.26(a) can be formulated as

$$\left\{ \begin{array}{l} V_{L1} = L \frac{di_1}{dt} \\ V_{L2} = L \frac{di_2}{dt} \\ i_2 = C_2 \frac{dV_{C2}}{dt} \\ i_1 = i_2 + i_s \\ V_{dc} = V_{L1} + V_{R1} + V_{R2} + V_{L2} + V_{C2} \\ V_{La} = L_a \frac{di_s}{dt} \\ 0 = 1/2V_{dc} - V_{dc} - V_{L2} - V_{R2} + V_{La} + V_s \\ V_s = i_s \cdot R_s \end{array} \right. \quad (4.84)$$

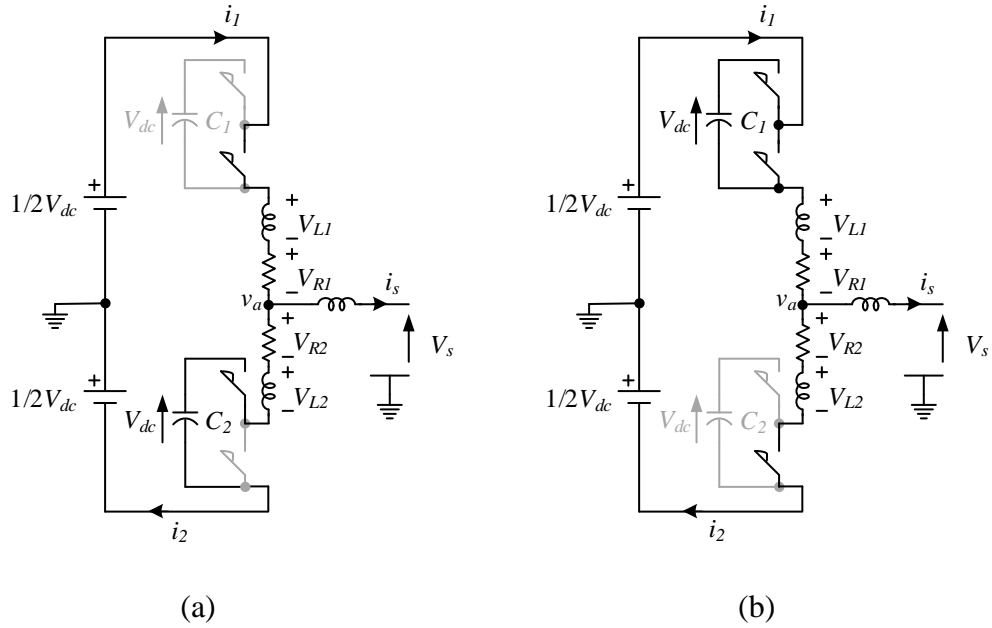


Figure 4.25 Two-level MMC with pole connected to (a) positive dc rail (Level 1); and (b) negative dc rail (Level 2).

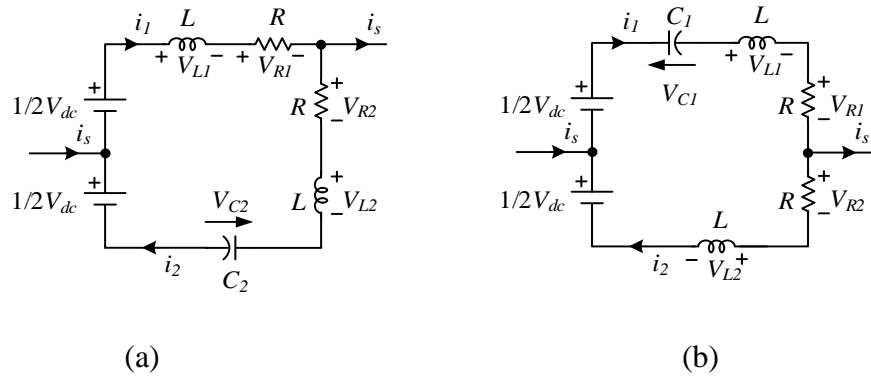


Figure 4.26 Two-level MMC model with pole connected to (a) positive dc rail; and (b) negative dc rail.

The corresponding switching pattern is

$$\Gamma_1^{(2)} = [0 \ 1]. \tag{4.85}$$

Define the state variables to be

$$\mathbf{X} = \begin{bmatrix} x_1 \\ x_2 \\ x_3 \\ x_4 \\ x_5 \end{bmatrix} = \begin{bmatrix} i_1 \\ i_2 \\ V_{C1} \\ V_{C2} \\ i_s \end{bmatrix}, \quad \dot{\mathbf{X}} = \begin{bmatrix} \dot{x}_1 \\ \dot{x}_2 \\ \dot{x}_3 \\ \dot{x}_4 \\ \dot{x}_5 \end{bmatrix} = \begin{bmatrix} \frac{di_1}{dt} \\ \frac{di_2}{dt} \\ \frac{dV_{C1}}{dt} \\ \frac{dV_{C2}}{dt} \\ \frac{di_s}{dt} \end{bmatrix}. \quad (4.86)$$

Rewrite (4.84) into state equation form,

$$\left\{ \begin{array}{l} V_{L1} = L \cdot \dot{x}_1 \\ V_{L2} = L \cdot \dot{x}_2 \\ x_2 = C_2 \cdot \dot{x}_4 \\ i_1 = i_2 + i_s \\ V_{dc} = V_{L1} + V_{R1} + V_{R2} + V_{L2} + x_4 \\ V_{La} = L_a \cdot \dot{x}_5 \\ 0 = -1/2V_{dc} - V_{L2} - V_{R2} + V_{La} + V_s \\ V_s = x_5 \cdot R_s \end{array} \right.$$

$$\left\{ \begin{array}{l} x_2 = C_2 \cdot \dot{x}_4 \\ i_1 = i_2 + i_s \\ V_{dc} = L \cdot \dot{x}_1 + R \cdot x_1 + R \cdot x_2 + L \cdot \dot{x}_2 + x_4 \\ 0 = -1/2V_{dc} - L \cdot \dot{x}_2 - R \cdot x_2 + L_a \cdot \dot{x}_5 + R_s \cdot x_5 \end{array} \right.$$

$$\left\{ \begin{array}{l} x_2 = C_2 \cdot \dot{x}_4 \\ \dot{x}_1 = \dot{x}_2 + \dot{x}_5 \\ V_{dc} = L \cdot (\dot{x}_2 + \dot{x}_5) + R \cdot x_1 + R \cdot x_2 + L \cdot \dot{x}_2 + x_4 \\ 0 = -1/2V_{dc} - L \cdot \dot{x}_2 - R \cdot x_2 + L_a \cdot \dot{x}_5 + R_s \cdot x_5 \end{array} \right.$$

$$\left\{ \begin{array}{l} x_2 = C_2 \cdot \dot{x}_4 \\ \dot{x}_1 = \dot{x}_2 + \dot{x}_5 \\ V_{dc} = 2L \cdot \dot{x}_2 + L \cdot \dot{x}_5 + R \cdot x_1 + R \cdot x_2 + x_4 \\ V_{dc} = -2L \cdot \dot{x}_2 + 2L_a \cdot \dot{x}_5 + 2R_s \cdot x_5 - 2R \cdot x_2 \\ 2V_{dc} = (L + 2L_a) \cdot \dot{x}_5 + R \cdot x_1 - R \cdot x_2 + x_4 + 2R_s \cdot x_5 \end{array} \right.$$

$$\left\{ \begin{array}{l} x_2 = C_2 \cdot \dot{x}_4 \\ \dot{x}_1 = \dot{x}_2 + \dot{x}_5 \\ V_{dc} = 2L \cdot \dot{x}_2 + L \cdot \dot{x}_5 + R \cdot x_1 + R \cdot x_2 + x_4 \\ V_{dc} = -2L \cdot \dot{x}_2 + 2L_a \cdot \dot{x}_5 + 2R_s \cdot x_5 - 2R \cdot x_2 \\ \dot{x}_5 = \frac{-R}{(L + 2L_a)} \cdot x_1 + \frac{R}{(L + 2L_a)} \cdot x_2 + \frac{-1}{(L + 2L_a)} x_4 + \frac{-2R_s}{(L + 2L_a)} \cdot x_5 + \frac{2}{(L + 2L_a)} V_{dc} \end{array} \right.$$

$$\left\{ \begin{array}{l} x_2 = C_2 \cdot \dot{x}_4 \\ \dot{x}_1 = \dot{x}_2 + \dot{x}_5 \\ V_{dc} = 2L \cdot \dot{x}_2 + L \cdot \dot{x}_5 + R \cdot x_1 + R \cdot x_2 + x_4 \\ \dot{x}_2 = \frac{-1}{2} \cdot \dot{x}_5 + \frac{-R}{2L} \cdot x_1 + \frac{-R}{2L} \cdot x_2 + \frac{-1}{2L} x_4 + \frac{1}{2L} V_{dc} \\ \dot{x}_5 = \frac{-R}{(L + 2L_a)} \cdot x_1 + \frac{R}{(L + 2L_a)} \cdot x_2 + \frac{-1}{(L + 2L_a)} x_4 + \frac{-2R_s}{(L + 2L_a)} \cdot x_5 + \frac{2}{(L + 2L_a)} V_{dc} \end{array} \right.$$

$$\left\{ \begin{array}{l} x_2 = C_2 \cdot \dot{x}_4 \\ \dot{x}_1 = \dot{x}_2 + \dot{x}_5 \\ V_{dc} = 2L \cdot \dot{x}_2 + L \cdot \dot{x}_5 + R \cdot x_1 + R \cdot x_2 + x_4 \\ \dot{x}_2 = \frac{-RL_a}{L(L+2L_a)} \cdot x_1 + \frac{-RL_a}{L(L+2L_a)} \cdot x_2 + \frac{-L_a}{L(L+2L_a)} x_4 + \frac{R_s}{(L+2L_a)} \cdot x_5 + \frac{-L+2L_a}{2L(L+2L_a)} V_{dc} \\ \dot{x}_5 = \frac{-R}{(L+2L_a)} \cdot x_1 + \frac{R}{(L+2L_a)} \cdot x_2 + \frac{-1}{(L+2L_a)} x_4 + \frac{-2R_s}{(L+2L_a)} \cdot x_5 + \frac{2}{(L+2L_a)} V_{dc} \end{array} \right.$$

$$\left\{ \begin{array}{l} x_2 = C_2 \cdot \dot{x}_4 \\ \dot{x}_1 = \frac{-R(L_a+L)}{L(L+2L_a)} \cdot x_1 + \frac{-R(L_a+L)}{L(L+2L_a)} \cdot x_2 + \frac{-L_a-L}{L(L+2L_a)} x_4 + \frac{-R_s}{(L+2L_a)} \cdot x_5 + \frac{3L+2L_a}{2L(L+2L_a)} V_{dc} \\ \dot{x}_2 = \frac{-RL_a}{L(L+2L_a)} \cdot x_1 + \frac{-RL_a}{L(L+2L_a)} \cdot x_2 + \frac{-L_a}{L(L+2L_a)} x_4 + \frac{R_s}{(L+2L_a)} \cdot x_5 + \frac{-L+2L_a}{2L(L+2L_a)} V_{dc} \\ \dot{x}_5 = \frac{-R}{(L+2L_a)} \cdot x_1 + \frac{R}{(L+2L_a)} \cdot x_2 + \frac{-1}{(L+2L_a)} x_4 + \frac{-2R_s}{(L+2L_a)} \cdot x_5 + \frac{2}{(L+2L_a)} V_{dc} \end{array} \right.$$

$$\begin{cases}
\dot{x}_1 = \frac{-R(L_a + L)}{L(L + 2L_a)} \cdot x_1 + \frac{-R(L_a + L)}{L(L + 2L_a)} \cdot x_2 + \frac{-L_a - L}{L(L + 2L_a)} x_4 + \frac{-R_s}{(L + 2L_a)} \cdot x_5 + \frac{3L + 2L_a}{2L(L + 2L_a)} V_{dc} \\
\dot{x}_2 = \frac{-RL_a}{L(L + 2L_a)} \cdot x_1 + \frac{-RL_a}{L(L + 2L_a)} \cdot x_2 + \frac{-L_a}{L(L + 2L_a)} x_4 + \frac{R_s}{(L + 2L_a)} \cdot x_5 + \frac{-L + 2L_a}{2L(L + 2L_a)} V_{dc} \\
\dot{x}_4 = \frac{1}{C_2} \cdot x_2 \\
\dot{x}_5 = \frac{-R}{(L + 2L_a)} \cdot x_1 + \frac{R}{(L + 2L_a)} \cdot x_2 + \frac{-1}{(L + 2L_a)} x_4 + \frac{-2R_s}{(L + 2L_a)} \cdot x_5 + \frac{2}{(L + 2L_a)} V_{dc}
\end{cases} \quad (4.87)$$

Where  $R_s$  is the load resistance, and  $L_a$  is the load inductance.

Figure 4.26(b) can be formulated as

$$\left\{ \begin{array}{l} V_{L1} = L \frac{di_1}{dt} \\ V_{L2} = L \frac{di_2}{dt} \\ i_1 = C_1 \frac{dV_{C1}}{dt} \\ i_1 = i_2 + i_s \\ V_{dc} = V_{L1} + V_{R1} + V_{R2} + V_{L2} + V_{C1} \\ V_{La} = L_a \frac{di_s}{dt} \\ 0 = 1/2V_{dc} - V_{L2} - V_{R2} + V_{La} + V_s \\ V_s = i_s \cdot R_s \end{array} \right.$$

$$\left\{ \begin{array}{l} V_{L1} = L \cdot \dot{x}_1 \\ V_{L2} = L \cdot \dot{x}_2 \\ x_1 = C_1 \cdot \dot{x}_3 \\ x_1 = x_2 + x_5 \\ V_{dc} = V_{L1} + V_{R1} + V_{R2} + V_{L2} + x_3 \\ V_{La} = L_a \cdot \dot{x}_5 \\ 0 = 1/2V_{dc} - V_{L2} - V_{R2} + V_{La} + V_s \\ V_s = x_5 \cdot R_s \end{array} \right.$$

$$\left\{ \begin{array}{l} x_1 = C_1 \cdot \dot{x}_3 \\ x_1 = x_2 + x_5 \\ V_{dc} = L \cdot \dot{x}_1 + R \cdot x_1 + R \cdot x_2 + L \cdot \dot{x}_2 + x_3 \\ 0 = 1/2V_{dc} - L \cdot \dot{x}_2 - R \cdot x_2 + L_a \cdot \dot{x}_5 + x_5 \cdot R_s \end{array} \right.$$

$$\left\{ \begin{array}{l} x_1 = C_1 \cdot \dot{x}_3 \\ \dot{x}_1 = (\dot{x}_2 + \dot{x}_5) \\ V_{dc} = L \cdot \dot{x}_1 + R \cdot x_1 + R \cdot x_2 + L \cdot \dot{x}_2 + x_3 \\ 0 = 1/2V_{dc} - L \cdot \dot{x}_2 - R \cdot x_2 + L_a \cdot \dot{x}_5 + x_5 \cdot R_s \end{array} \right.$$

$$\left\{ \begin{array}{l} x_1 = C_1 \cdot \dot{x}_3 \\ \dot{x}_1 = (\dot{x}_2 + \dot{x}_5) \\ V_{dc} = 2L \cdot \dot{x}_2 + L \cdot \dot{x}_5 + R \cdot x_1 + R \cdot x_2 + x_3 \\ V_{dc} = 2L \cdot \dot{x}_2 + 2R \cdot x_2 - 2L_a \cdot \dot{x}_5 - 2x_5 \cdot R_s \end{array} \right.$$

$$\left\{ \begin{array}{l} x_1 = C_1 \cdot \dot{x}_3 \\ \dot{x}_1 = \dot{x}_2 + \dot{x}_5 \\ V_{dc} = 2L \cdot \dot{x}_2 + L \cdot \dot{x}_5 + R \cdot x_1 + R \cdot x_2 + x_3 \\ V_{dc} = 2L \cdot \dot{x}_2 - 2L_a \cdot \dot{x}_5 + 2R \cdot x_2 - 2x_5 \cdot R_s \\ 0 = -(2L_a + L) \cdot \dot{x}_5 - R \cdot x_1 + R \cdot x_2 - x_3 - 2x_5 \cdot R_s \end{array} \right.$$

$$\left\{ \begin{array}{l} x_1 = C_1 \cdot \dot{x}_3 \\ \dot{x}_1 = \dot{x}_2 + \dot{x}_5 \\ V_{dc} = 2L \cdot \dot{x}_2 + L \cdot \dot{x}_5 + R \cdot x_1 + R \cdot x_2 + x_3 \\ V_{dc} = 2L \cdot \dot{x}_2 - 2L_a \cdot \dot{x}_5 + 2R \cdot x_2 - 2x_5 \cdot R_s \\ \dot{x}_5 = \frac{-R}{(2L_a + L)} \cdot x_1 + \frac{R}{(2L_a + L)} \cdot x_2 + \frac{-1}{(2L_a + L)} \cdot x_3 + \frac{-2R_s}{(2L_a + L)} \cdot x_5 \end{array} \right.$$

$$\left\{ \begin{array}{l} x_1 = C_1 \cdot \dot{x}_3 \\ \dot{x}_1 = \dot{x}_2 + \dot{x}_5 \\ V_{dc} = 2L \cdot \dot{x}_2 + L \cdot \dot{x}_5 + R \cdot x_1 + R \cdot x_2 + x_3 \\ V_{dc} = 2L \cdot \dot{x}_2 - 2L_a \cdot \dot{x}_5 + 2R \cdot x_2 - 2x_5 \cdot R_s \\ \dot{x}_5 = \frac{-R}{(2L_a + L)} \cdot x_1 + \frac{R}{(2L_a + L)} \cdot x_2 + \frac{-1}{(2L_a + L)} \cdot x_3 + \frac{-2R_s}{(2L_a + L)} \cdot x_5 \end{array} \right.$$

$$\left\{ \begin{array}{l} x_1 = C_1 \cdot \dot{x}_3 \\ \dot{x}_1 = \dot{x}_2 + \dot{x}_5 \\ \dot{x}_2 = \frac{-1}{2} \cdot \dot{x}_5 + \frac{-R}{2L} \cdot x_1 + \frac{-R}{2L} \cdot x_2 + \frac{-1}{2L} x_3 + \frac{1}{2L} V_{dc} \\ V_{dc} = 2L \cdot \dot{x}_2 - 2L_a \cdot \dot{x}_5 + 2R \cdot x_2 - 2x_5 \cdot R_s \\ \dot{x}_5 = \frac{-R}{(2L_a + L)} \cdot x_1 + \frac{R}{(2L_a + L)} \cdot x_2 + \frac{-1}{(2L_a + L)} \cdot x_3 + \frac{-2R_s}{(2L_a + L)} \cdot x_5 \end{array} \right.$$

$$\left\{ \begin{array}{l}
x_1 = C_1 \cdot \dot{x}_3 \\
\dot{x}_1 = \frac{-R(L_a + L)}{L(2L_a + L)} \cdot x_1 + \frac{-RL_a}{L(2L_a + L)} \cdot x_2 + \frac{-L_a - L}{L(2L_a + L)} \cdot x_3 + \frac{-R_s}{(2L_a + L)} \cdot x_5 + \frac{1}{2L} V_{dc} \\
\dot{x}_2 = \frac{-RL_a}{L(2L_a + L)} \cdot x_1 + \frac{-R(L + L_a)}{L(2L_a + L)} \cdot x_2 + \frac{-L_a}{L(2L_a + L)} \cdot x_3 + \frac{R_s}{(2L_a + L)} \cdot x_5 + \frac{1}{2L} V_{dc} \\
\dot{x}_5 = \frac{-R}{(2L_a + L)} \cdot x_1 + \frac{R}{(2L_a + L)} \cdot x_2 + \frac{-1}{(2L_a + L)} \cdot x_3 + \frac{-2R_s}{(2L_a + L)} \cdot x_5
\end{array} \right.$$
  

$$\left\{ \begin{array}{l}
\dot{x}_1 = \frac{-R(L_a + L)}{L(2L_a + L)} \cdot x_1 + \frac{-RL_a}{L(2L_a + L)} \cdot x_2 + \frac{-L_a - L}{L(2L_a + L)} \cdot x_3 + \frac{-R_s}{(2L_a + L)} \cdot x_5 + \frac{1}{2L} V_{dc} \\
\dot{x}_2 = \frac{-RL_a}{L(2L_a + L)} \cdot x_1 + \frac{-R(L + L_a)}{L(2L_a + L)} \cdot x_2 + \frac{-L_a}{L(2L_a + L)} \cdot x_3 + \frac{R_s}{(2L_a + L)} \cdot x_5 + \frac{1}{2L} V_{dc} \\
\dot{x}_3 = \frac{1}{C_1} x_1 \\
\dot{x}_5 = \frac{-R}{(2L_a + L)} \cdot x_1 + \frac{R}{(2L_a + L)} \cdot x_2 + \frac{-1}{(2L_a + L)} \cdot x_3 + \frac{-2R_s}{(2L_a + L)} \cdot x_5
\end{array} \right. \tag{4.88}$$

The corresponding switching pattern is

$$\mathbf{\Gamma}_2^{(2)} = [1 \ 0]. \quad (4.89)$$

Equation (4.87) and (4.88) has a complete representation of MMC and RL load together. However, they are hard to decompose as we did in previous sections. Analyzing the dynamics and stability of the system considering load model is worth doing. I would like to leave this for future work.

#### **4.7 STATE-SPACE MODEL OF THREE-LEVEL MMC**

We are going to derive the state-space model for three-level MMC in this section. Figure 4.27 shows a single-phase three-level MMC that is under analysis. For a three-level MMC, there are six feasible switching patterns. The following section will model the three-level MMC for each switching pattern.

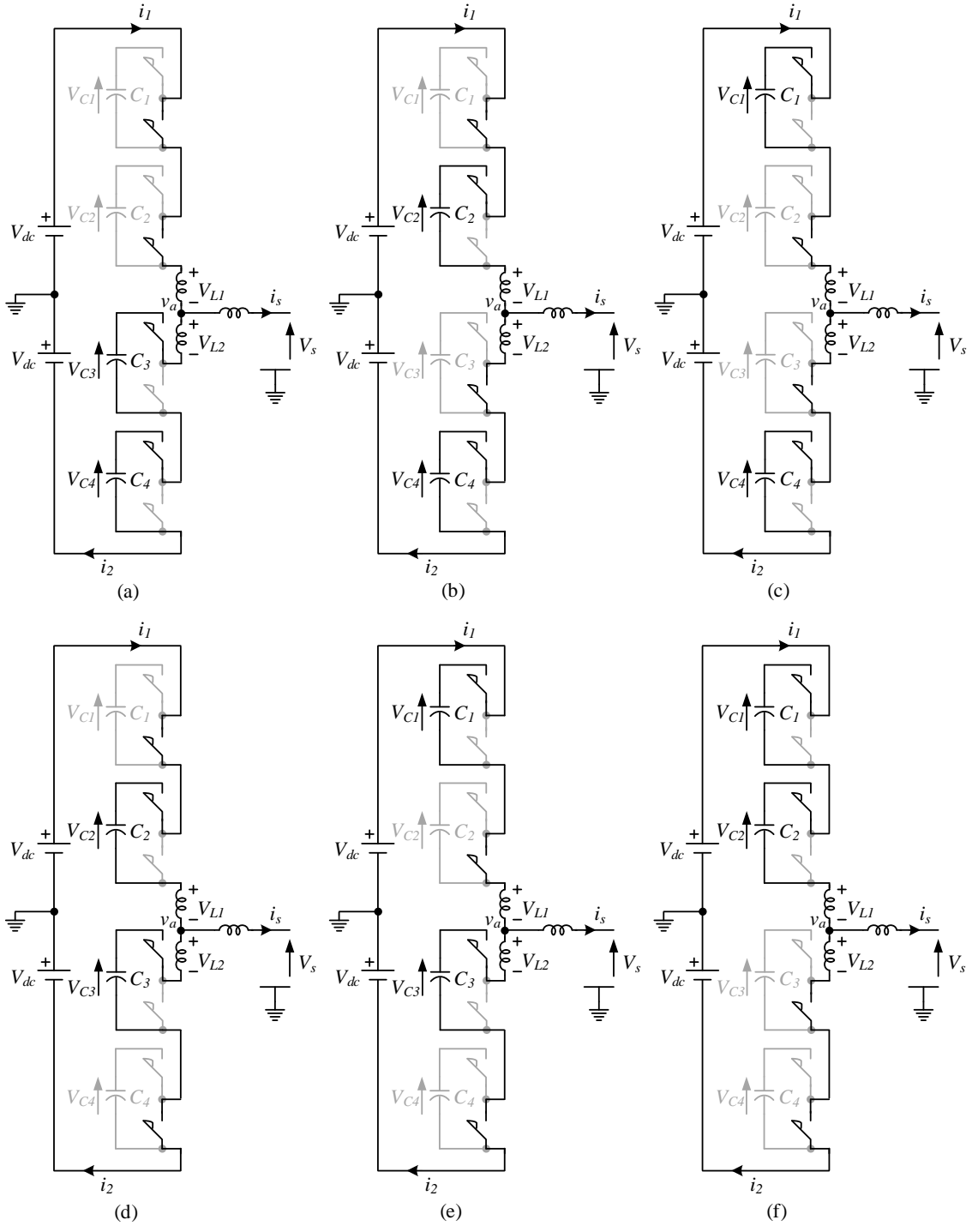


Figure 4.27 Three-level MMC with pole voltage of (a)  $V_{dc}$  (Level I); (b)(c)(d)(e) zero volt (Level II); and (f)  $-V_{dc}$  (Level III).

### 4.7.1 STATE-SPACE MODEL

Figure 4.27(a) can be formulated as

$$\left\{ \begin{array}{l} V_{L1} = L \frac{di_1}{dt} \\ V_{L2} = L \frac{di_2}{dt} \\ i_2 = C_3 \frac{dV_{C3}}{dt} \\ i_2 = C_4 \frac{dV_{C4}}{dt} \\ i_1 = i_2 + i_s \\ V_{dc} = V_{L1} + V_{L2} + V_{C3} + V_{C4} \end{array} \right. \quad (4.90)$$

The corresponding switching pattern is

$$\Gamma_1^{(3)} = [0 \ 0 \ 1 \ 1]. \quad (4.91)$$

Define the state variables to be

$$\mathbf{X} = \begin{bmatrix} x_1 \\ x_2 \\ x_3 \\ x_4 \\ x_5 \\ x_6 \end{bmatrix} = \begin{bmatrix} i_1 \\ i_2 \\ V_{C1} \\ V_{C2} \\ V_{C3} \\ V_{C4} \end{bmatrix}, \quad \dot{\mathbf{X}} = \begin{bmatrix} \dot{x}_1 \\ \dot{x}_2 \\ \dot{x}_3 \\ \dot{x}_4 \\ \dot{x}_5 \\ \dot{x}_6 \end{bmatrix} = \begin{bmatrix} \frac{di_1}{dt} \\ \frac{di_2}{dt} \\ \frac{dV_{C1}}{dt} \\ \frac{dV_{C2}}{dt} \\ \frac{dV_{C3}}{dt} \\ \frac{dV_{C4}}{dt} \end{bmatrix}. \quad (4.92)$$

Rewrite (4.90) into state equation form,

$$\begin{cases} V_{L1} = L \cdot \dot{x}_1 \\ V_{L2} = L \cdot \dot{x}_2 \\ x_2 = C_3 \cdot \dot{x}_5 \\ x_2 = C_4 \cdot \dot{x}_6 \\ x_1 = x_2 + i_s \\ V_{dc} = V_{L1} + V_{L2} + x_5 + x_6 \end{cases}$$

$$\begin{cases} \dot{x}_1 = \frac{1}{2} \cdot \frac{di_s}{dt} + \frac{-1}{2L} x_5 + \frac{-1}{2L} x_6 + \frac{V_{dc}}{2L} \\ \dot{x}_2 = \frac{-1}{2} \cdot \frac{di_s}{dt} + \frac{-1}{2L} x_5 + \frac{-1}{2L} x_6 + \frac{V_{dc}}{2L} \\ \dot{x}_5 = \frac{1}{C_3} x_2 \\ \dot{x}_6 = \frac{1}{C_4} x_2 \end{cases}, \quad (4.93)$$

Or

$$\left\{ \begin{array}{l}
 \dot{x}_1 = 0 \cdot x_1 + 0 \cdot x_2 + 0 \cdot \left(-\frac{1}{2L} x_3\right) + 0 \cdot \left(-\frac{1}{2L} x_4\right) + 1 \cdot \left(-\frac{1}{2L} x_5\right) + 1 \cdot \left(-\frac{1}{2L} x_6\right) + \left(\frac{1}{2L} V_{dc} + \frac{1}{2} \frac{di_s}{dt}\right) \\
 \dot{x}_2 = 0 \cdot x_1 + 0 \cdot x_2 + 0 \cdot \left(-\frac{1}{2L} x_3\right) + 0 \cdot \left(-\frac{1}{2L} x_4\right) + 1 \cdot \left(-\frac{1}{2L} x_5\right) + 1 \cdot \left(-\frac{1}{2L} x_6\right) + \left(\frac{1}{2L} V_{dc} - \frac{1}{2} \frac{di_s}{dt}\right) \\
 \dot{x}_3 = 0 \cdot \left(\frac{1}{C_1} x_1\right) + 0 \cdot x_2 + 0 \cdot x_3 + 0 \cdot x_4 + 0 \cdot x_5 + 0 \cdot x_6 + 0 \\
 \dot{x}_4 = 0 \cdot \left(\frac{1}{C_2} x_1\right) + 0 \cdot x_2 + 0 \cdot x_3 + 0 \cdot x_4 + 0 \cdot x_5 + 0 \cdot x_6 + 0 \\
 \dot{x}_5 = 0 \cdot x_1 + 1 \cdot \left(\frac{1}{C_3} x_2\right) + 0 \cdot x_3 + 0 \cdot x_4 + 0 \cdot x_5 + 0 \cdot x_6 + 0 \\
 \dot{x}_6 = 0 \cdot x_1 + 1 \cdot \left(\frac{1}{C_4} x_2\right) + 0 \cdot x_3 + 0 \cdot x_4 + 0 \cdot x_5 + 0 \cdot x_6 + 0
 \end{array} \right.$$

(4.94)

Rewrite (4.94) into matrix form,

$$\begin{bmatrix} \dot{x}_1 \\ \dot{x}_2 \\ \dot{x}_3 \\ \dot{x}_4 \\ \dot{x}_5 \\ \dot{x}_6 \end{bmatrix} = \begin{bmatrix} 0 & 0 & 0 \cdot \left(-\frac{1}{2L}\right) & 0 \cdot \left(-\frac{1}{2L}\right) & 1 \cdot \left(-\frac{1}{2L}\right) & 1 \cdot \left(-\frac{1}{2L}\right) \\ 0 & 0 & 0 \cdot \left(-\frac{1}{2L}\right) & 0 \cdot \left(-\frac{1}{2L}\right) & 1 \cdot \left(-\frac{1}{2L}\right) & 1 \cdot \left(-\frac{1}{2L}\right) \\ 0 \cdot \left(\frac{1}{C_1}\right) & 0 & 0 & 0 & 0 & 0 \\ 0 \cdot \left(\frac{1}{C_2}\right) & 0 & 0 & 0 & 0 & 0 \\ 0 & 1 \cdot \left(\frac{1}{C_3}\right) & 0 & 0 & 0 & 0 \\ 0 & 1 \cdot \left(\frac{1}{C_4}\right) & 0 & 0 & 0 & 0 \end{bmatrix} \begin{bmatrix} x_1 \\ x_2 \\ x_3 \\ x_4 \\ x_5 \\ x_6 \end{bmatrix} + \begin{bmatrix} \frac{1}{2L} & \frac{1}{2} \\ \frac{1}{2L} & -\frac{1}{2} \\ 0 & 0 \\ 0 & 0 \\ 0 & 0 \\ 0 & 0 \end{bmatrix} \begin{bmatrix} V_{dc} \\ \frac{di_s}{dt} \end{bmatrix}. \quad (4.95)$$

The coefficient marked in red contains the information from switching patten  $\Gamma_1^{(3)}$ .

The system matrices are

$$\mathbf{A} = \begin{bmatrix} 0 & 0 & 0 \cdot \left(-\frac{1}{2L}\right) & 0 \cdot \left(-\frac{1}{2L}\right) & 1 \cdot \left(-\frac{1}{2L}\right) & 1 \cdot \left(-\frac{1}{2L}\right) \\ 0 & 0 & 0 \cdot \left(-\frac{1}{2L}\right) & 0 \cdot \left(-\frac{1}{2L}\right) & 1 \cdot \left(-\frac{1}{2L}\right) & 1 \cdot \left(-\frac{1}{2L}\right) \\ 0 \cdot \left(\frac{1}{C_1}\right) & 0 & 0 & 0 & 0 & 0 \\ 0 \cdot \left(\frac{1}{C_2}\right) & 0 & 0 & 0 & 0 & 0 \\ 0 & 1 \cdot \left(\frac{1}{C_3}\right) & 0 & 0 & 0 & 0 \\ 0 & 1 \cdot \left(\frac{1}{C_4}\right) & 0 & 0 & 0 & 0 \end{bmatrix},$$

$$\mathbf{B} = \begin{bmatrix} \frac{1}{2L} & \frac{1}{2} \\ \frac{1}{2L} & -\frac{1}{2} \\ 0 & 0 \\ 0 & 0 \\ 0 & 0 \\ 0 & 0 \end{bmatrix},$$

$$\mathbf{U} = \begin{bmatrix} V_{dc} \\ \frac{di_s}{dt} \end{bmatrix}. \quad (4.96)$$

The coefficient matrix could be decomposed as follows,

$$\mathbf{A} = \left[ \begin{array}{cc|cccc}
0 & 0 & 0 \cdot \left(-\frac{1}{2L}\right) & 0 \cdot \left(-\frac{1}{2L}\right) & 1 \cdot \left(-\frac{1}{2L}\right) & 1 \cdot \left(-\frac{1}{2L}\right) \\
0 & 0 & 0 \cdot \left(-\frac{1}{2L}\right) & 0 \cdot \left(-\frac{1}{2L}\right) & 1 \cdot \left(-\frac{1}{2L}\right) & 1 \cdot \left(-\frac{1}{2L}\right) \\
\hline
0 \cdot \left(\frac{1}{C_1}\right) & 0 & 0 & 0 & 0 & 0 \\
0 \cdot \left(\frac{1}{C_2}\right) & 0 & 0 & 0 & 0 & 0 \\
0 & 1 \cdot \left(\frac{1}{C_3}\right) & 0 & 0 & 0 & 0 \\
0 & 1 \cdot \left(\frac{1}{C_4}\right) & 0 & 0 & 0 & 0
\end{array} \right] \cdot \quad (4.97)$$

$$= \left[ \begin{array}{c|c}
\mathbf{0} & \mathbf{A}_L \\
\hline
\mathbf{A}_C & \mathbf{0}
\end{array} \right]$$

$$\mathbf{A}_L = \left[ \begin{array}{cccc}
0 \cdot \left(-\frac{1}{2L}\right) & 0 \cdot \left(-\frac{1}{2L}\right) & 1 \cdot \left(-\frac{1}{2L}\right) & 1 \cdot \left(-\frac{1}{2L}\right) \\
0 \cdot \left(-\frac{1}{2L}\right) & 0 \cdot \left(-\frac{1}{2L}\right) & 1 \cdot \left(-\frac{1}{2L}\right) & 1 \cdot \left(-\frac{1}{2L}\right)
\end{array} \right] \cdot \quad (4.98)$$

$$= \begin{bmatrix} -\frac{1}{2L} \\ -\frac{1}{2L} \end{bmatrix} \cdot [\mathbf{0} \quad \mathbf{0} \quad \mathbf{1} \quad \mathbf{1}] = \hat{\mathbf{A}}_L \cdot \Gamma_1^{(3)}$$

$$\mathbf{A}_C = \left[ \begin{array}{c|c}
0 \cdot \left(\frac{1}{C_1}\right) & 0 \\
0 \cdot \left(\frac{1}{C_2}\right) & 0 \\
\hline
0 & 1 \cdot \left(\frac{1}{C_3}\right) \\
0 & 1 \cdot \left(\frac{1}{C_4}\right)
\end{array} \right] = [\hat{\mathbf{A}}_C \mid \bar{\mathbf{A}}_C] \cdot \quad (4.99)$$

$$\hat{\mathbf{A}}_c = \text{diag} \left( \begin{bmatrix} \frac{1}{C_1} \\ \frac{1}{C_2} \\ 0 \\ 0 \end{bmatrix} \cdot [\mathbf{0} \quad \mathbf{0} \quad \mathbf{1} \quad \mathbf{1}] \right) = \text{diag}(\hat{\mathbf{A}}'_c \cdot \mathbf{\Gamma}_1^{(3)}). \quad (4.100)$$

$$\bar{\mathbf{A}}_c = \text{diag} \left( \begin{bmatrix} 0 \\ 0 \\ \frac{1}{C_3} \\ \frac{1}{C_4} \end{bmatrix} \cdot [\mathbf{0} \quad \mathbf{0} \quad \mathbf{1} \quad \mathbf{1}] \right) = \text{diag}(\bar{\mathbf{A}}'_c \cdot \mathbf{\Gamma}_1^{(2)}). \quad (4.101)$$

*diag* operator returns a column vector of the main diagonal elements of the objective matrix.  $\hat{\mathbf{A}}_L$  contains the parameters from arm inductance.  $\hat{\mathbf{A}}'_c$  and  $\bar{\mathbf{A}}'_c$  contain the parameters from submodule capacitance.  $\hat{\mathbf{A}}'_c$  contain the parameters from upper arm submodules.  $\bar{\mathbf{A}}'_c$  contains the parameters from lower arm submodules. The reason to decompose the state space in such form is to save the work for programming. It will be easy to extent to high level state space by decomposing the matrix into such form.

Note that  $\mathbf{U}$  contains  $\frac{di_s}{dt}$ .  $\frac{di_s}{dt}$  reflects the voltage across the load inductor. That is

$$L_a \frac{di_s}{dt} = v_a - V_s, \quad (4.102)$$

as modeled in Figure4.28.

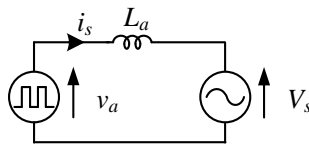


Figure 4.28 Load inductor voltage modeling.

If the pole is attached to the positive dc rail, as shown in Figure4.27(a),  $v_a = V_{dc}$ .

Eq.(4.102) can be modified as

$$\frac{di_s}{dt} = \frac{1}{L_a}(V_{dc} - V_s). \quad (4.103)$$

Replace the  $\frac{di_s}{dt}$  in (4.96) by (4.103)

$$\mathbf{U} = \begin{bmatrix} V_{dc} \\ \frac{1}{L_a}(V_{dc} - V_s) \end{bmatrix}. \quad (4.104)$$

The other five feasible state space models [Figure4.27(b)-(f)] are omitted since the derivations are similar.

#### 4.7.2 STATE SPACE MODEL WITH STRAY RESISTANCE

The stray resistance always exists in the real MMC installations or simulations. Figure4.29 shows single-phase MMC model with stray resistance  $R$ . Figure4.29 can be formulated as

$$\left\{ \begin{array}{l} V_{L1} = L \frac{di_1}{dt} \\ V_{L2} = L \frac{di_2}{dt} \\ i_2 = C_3 \frac{dV_{C3}}{dt} \\ i_2 = C_4 \frac{dV_{C4}}{dt} \\ i_1 = i_2 + i_s \\ V_{dc} = V_{L1} + V_{R1} + V_{R2} + V_{L2} + V_{C2} \end{array} \right. \quad (4.105)$$

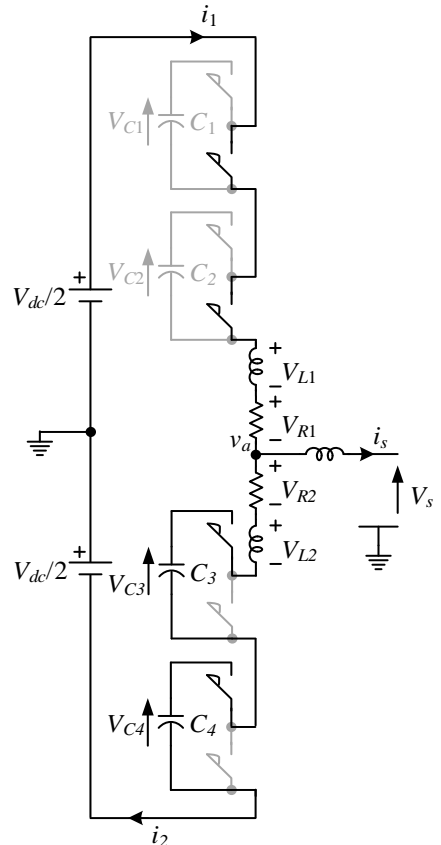


Figure 4.29 Three-level MMC with pole connected to positive dc rail (Level 1).

The corresponding switching pattern is

$$\Gamma_1^{(3)} = [0 \ 0 \ 1 \ 1]. \tag{4.106}$$

Define the state variables to be

$$\mathbf{X} = \begin{bmatrix} x_1 \\ x_2 \\ x_3 \\ x_4 \\ x_5 \\ x_6 \end{bmatrix} = \begin{bmatrix} i_1 \\ i_2 \\ V_{C1} \\ V_{C2} \\ V_{C3} \\ V_{C4} \end{bmatrix}, \quad \dot{\mathbf{X}} = \begin{bmatrix} \dot{x}_1 \\ \dot{x}_2 \\ \dot{x}_3 \\ \dot{x}_4 \\ \dot{x}_5 \\ \dot{x}_6 \end{bmatrix} = \begin{bmatrix} \frac{di_1}{dt} \\ \frac{di_2}{dt} \\ \frac{dV_{C1}}{dt} \\ \frac{dV_{C2}}{dt} \\ \frac{dV_{C3}}{dt} \\ \frac{dV_{C4}}{dt} \end{bmatrix}. \quad (4.107)$$

Rewrite (4.105) into state equation form,

$$\left\{ \begin{array}{l} \dot{x}_1 = -\frac{R}{2L}x_1 - \frac{R}{2L}x_2 + \frac{1}{2} \cdot \frac{di_s}{dt} + \frac{-1}{2L}x_5 + \frac{-1}{2L}x_6 + \frac{V_{dc}}{2L} \\ \dot{x}_2 = -\frac{R}{2L}x_1 - \frac{R}{2L}x_2 + \frac{-1}{2} \cdot \frac{di_s}{dt} + \frac{-1}{2L}x_5 + \frac{-1}{2L}x_6 + \frac{V_{dc}}{2L} \\ \dot{x}_5 = \frac{1}{C_3}x_2 \\ \dot{x}_6 = \frac{1}{C_4}x_2 \end{array} \right., \quad (4.108)$$

or

$$\begin{cases}
 \dot{x}_1 = \left(-\frac{R}{2L}\right) \cdot x_1 + \left(-\frac{R}{2L}\right) \cdot x_2 + 0 \cdot \left(-\frac{1}{2L} x_3\right) + 0 \cdot \left(-\frac{1}{2L} x_4\right) + 1 \cdot \left(-\frac{1}{2L} x_5\right) + 1 \cdot \left(-\frac{1}{2L} x_6\right) + \left(\frac{1}{2L} V_{dc} + \frac{1}{2} \frac{di_s}{dt}\right) \\
 \dot{x}_2 = \left(-\frac{R}{2L}\right) \cdot x_1 + \left(-\frac{R}{2L}\right) \cdot x_2 + 0 \cdot \left(-\frac{1}{2L} x_3\right) + 0 \cdot \left(-\frac{1}{2L} x_4\right) + 1 \cdot \left(-\frac{1}{2L} x_5\right) + 1 \cdot \left(-\frac{1}{2L} x_6\right) + \left(\frac{1}{2L} V_{dc} - \frac{1}{2} \frac{di_s}{dt}\right) \\
 \dot{x}_3 = 0 \cdot \left(\frac{1}{C_1} x_1\right) + 0 \cdot x_2 + 0 \cdot x_3 + 0 \cdot x_4 + 0 \cdot x_5 + 0 \cdot x_6 + 0 \\
 \dot{x}_4 = 0 \cdot \left(\frac{1}{C_2} x_1\right) + 0 \cdot x_2 + 0 \cdot x_3 + 0 \cdot x_4 + 0 \cdot x_5 + 0 \cdot x_6 + 0 \\
 \dot{x}_5 = 0 \cdot x_1 + 1 \cdot \left(\frac{1}{C_3} x_2\right) + 0 \cdot x_3 + 0 \cdot x_4 + 0 \cdot x_5 + 0 \cdot x_6 + 0 \\
 \dot{x}_6 = 0 \cdot x_1 + 1 \cdot \left(\frac{1}{C_4} x_2\right) + 0 \cdot x_3 + 0 \cdot x_4 + 0 \cdot x_5 + 0 \cdot x_6 + 0
 \end{cases}$$

(4.109)

Rewrite (4.109) into matrix form,

$$\begin{bmatrix} \dot{x}_1 \\ \dot{x}_2 \\ \dot{x}_3 \\ \dot{x}_4 \\ \dot{x}_5 \\ \dot{x}_6 \end{bmatrix} = \begin{bmatrix} -\frac{R}{2L} & -\frac{R}{2L} & 0 \cdot \left(-\frac{1}{2L}\right) & 0 \cdot \left(-\frac{1}{2L}\right) & 1 \cdot \left(-\frac{1}{2L}\right) & 1 \cdot \left(-\frac{1}{2L}\right) \\ -\frac{R}{2L} & -\frac{R}{2L} & 0 \cdot \left(-\frac{1}{2L}\right) & 0 \cdot \left(-\frac{1}{2L}\right) & 1 \cdot \left(-\frac{1}{2L}\right) & 1 \cdot \left(-\frac{1}{2L}\right) \\ 0 \cdot \left(\frac{1}{C_1}\right) & 0 & 0 & 0 & 0 & 0 \\ 0 \cdot \left(\frac{1}{C_2}\right) & 0 & 0 & 0 & 0 & 0 \\ 0 & 1 \cdot \left(\frac{1}{C_3}\right) & 0 & 0 & 0 & 0 \\ 0 & 1 \cdot \left(\frac{1}{C_4}\right) & 0 & 0 & 0 & 0 \end{bmatrix} \begin{bmatrix} x_1 \\ x_2 \\ x_3 \\ x_4 \\ x_5 \\ x_6 \end{bmatrix} + \begin{bmatrix} \frac{1}{2L} & \frac{1}{2} \\ \frac{1}{2L} & -\frac{1}{2} \\ 0 & 0 \\ 0 & 0 \\ 0 & 0 \\ 0 & 0 \end{bmatrix} \begin{bmatrix} V_{dc} \\ \frac{di_s}{dt} \end{bmatrix}. \quad (4.110)$$

The coefficient marked in red contains the information from switching patten  $\Gamma_1^{(3)}$ .

The system matrices are

$$\mathbf{A} = \begin{bmatrix} -\frac{R}{2L} & -\frac{R}{2L} & 0 \cdot \left(-\frac{1}{2L}\right) & 0 \cdot \left(-\frac{1}{2L}\right) & 1 \cdot \left(-\frac{1}{2L}\right) & 1 \cdot \left(-\frac{1}{2L}\right) \\ -\frac{R}{2L} & -\frac{R}{2L} & 0 \cdot \left(-\frac{1}{2L}\right) & 0 \cdot \left(-\frac{1}{2L}\right) & 1 \cdot \left(-\frac{1}{2L}\right) & 1 \cdot \left(-\frac{1}{2L}\right) \\ 0 \cdot \left(\frac{1}{C_1}\right) & 0 & 0 & 0 & 0 & 0 \\ 0 \cdot \left(\frac{1}{C_2}\right) & 0 & 0 & 0 & 0 & 0 \\ 0 & 1 \cdot \left(\frac{1}{C_3}\right) & 0 & 0 & 0 & 0 \\ 0 & 1 \cdot \left(\frac{1}{C_4}\right) & 0 & 0 & 0 & 0 \end{bmatrix},$$

$$\mathbf{B} = \begin{bmatrix} \frac{1}{2L} & \frac{1}{2} \\ \frac{1}{2L} & -\frac{1}{2} \\ 0 & 0 \\ 0 & 0 \\ 0 & 0 \\ 0 & 0 \end{bmatrix},$$

$$\mathbf{U} = \begin{bmatrix} V_{dc} \\ \frac{di_s}{dt} \end{bmatrix}. \quad (4.111)$$

The coefficient matrix could be decomposed as follows,

$$\mathbf{A} = \left[ \begin{array}{cc|cccc}
 -\frac{R}{2L} & -\frac{R}{2L} & 0 \cdot \left(-\frac{1}{2L}\right) & 0 \cdot \left(-\frac{1}{2L}\right) & 1 \cdot \left(-\frac{1}{2L}\right) & 1 \cdot \left(-\frac{1}{2L}\right) \\
 -\frac{R}{2L} & -\frac{R}{2L} & 0 \cdot \left(-\frac{1}{2L}\right) & 0 \cdot \left(-\frac{1}{2L}\right) & 1 \cdot \left(-\frac{1}{2L}\right) & 1 \cdot \left(-\frac{1}{2L}\right) \\
 \hline
 0 \cdot \left(\frac{1}{C_1}\right) & 0 & 0 & 0 & 0 & 0 \\
 0 \cdot \left(\frac{1}{C_2}\right) & 0 & 0 & 0 & 0 & 0 \\
 0 & 1 \cdot \left(\frac{1}{C_3}\right) & 0 & 0 & 0 & 0 \\
 0 & 1 \cdot \left(\frac{1}{C_4}\right) & 0 & 0 & 0 & 0
 \end{array} \right] \quad (4.112)$$

$$= \left[ \begin{array}{c|c}
 \mathbf{A}_R & \mathbf{A}_L \\
 \hline
 \mathbf{A}_C & \mathbf{0}
 \end{array} \right]$$

$$\mathbf{A}_L = \left[ \begin{array}{cccc}
 0 \cdot \left(-\frac{1}{2L}\right) & 0 \cdot \left(-\frac{1}{2L}\right) & 1 \cdot \left(-\frac{1}{2L}\right) & 1 \cdot \left(-\frac{1}{2L}\right) \\
 0 \cdot \left(-\frac{1}{2L}\right) & 0 \cdot \left(-\frac{1}{2L}\right) & 1 \cdot \left(-\frac{1}{2L}\right) & 1 \cdot \left(-\frac{1}{2L}\right)
 \end{array} \right] \quad (4.113)$$

$$= \begin{bmatrix} -\frac{1}{2L} \\ -\frac{1}{2L} \end{bmatrix} \cdot [0 \quad 0 \quad 1 \quad 1] = \hat{\mathbf{A}}_L \cdot \mathbf{\Gamma}_1^{(3)}$$

$$\mathbf{A}_C = \left[ \begin{array}{c|c}
 0 \cdot \left(\frac{1}{C_1}\right) & 0 \\
 0 \cdot \left(\frac{1}{C_2}\right) & 0 \\
 0 & 1 \cdot \left(\frac{1}{C_3}\right) \\
 0 & 1 \cdot \left(\frac{1}{C_4}\right)
 \end{array} \right] = [\hat{\mathbf{A}}_C \quad \bar{\mathbf{A}}_C] \quad (4.114)$$

$$\hat{\mathbf{A}}_c = \text{diag} \left( \begin{bmatrix} \frac{1}{C_1} \\ \frac{1}{C_2} \\ 0 \\ 0 \end{bmatrix} \cdot [\mathbf{0} \ \mathbf{0} \ \mathbf{1} \ \mathbf{1}] \right) = \text{diag}(\hat{\mathbf{A}}'_c \cdot \mathbf{\Gamma}_1^{(3)}). \quad (4.115)$$

$$\bar{\mathbf{A}}_c = \text{diag} \left( \begin{bmatrix} 0 \\ 0 \\ \frac{1}{C_3} \\ \frac{1}{C_4} \end{bmatrix} \cdot [\mathbf{0} \ \mathbf{0} \ \mathbf{1} \ \mathbf{1}] \right) = \text{diag}(\bar{\mathbf{A}}'_c \cdot \mathbf{\Gamma}_1^{(2)}). \quad (4.116)$$

*diag* operator returns a column vector of the main diagonal elements of the objective matrix.  $\hat{\mathbf{A}}_L$  contains the parameters from arm inductance.  $\hat{\mathbf{A}}'_c$  and  $\bar{\mathbf{A}}'_c$  contain the parameters from submodule capacitance.  $\hat{\mathbf{A}}'_c$  contain the parameters from upper arm submodules.  $\bar{\mathbf{A}}'_c$  contains the parameters from lower arm submodules. The reason to decompose the state space in such form is to save the work for programming. It will be easy to extent to high level state space by decomposing the matrix into such form.

Note that  $\mathbf{U}$  contains  $\frac{di_s}{dt} \cdot \frac{di_s}{dt}$  reflects the voltage across the load inductor. That is

$$L_a \frac{di_s}{dt} = v_a - V_s, \quad (4.117)$$

as modeled in Figure4.28.

If the pole is attached to the positive dc rail, as shown in Figure4.29,  $v_a = 1/2V_{dc}$ .

Eq.(4.117) can be modified as

$$\frac{di_s}{dt} = \frac{1}{L_a} (V_{dc} - V_s). \quad (4.118)$$

Replace the  $\frac{di_s}{dt}$  in (4.111) by (4.118)

$$\mathbf{U} = \begin{bmatrix} V_{dc} \\ \frac{1}{L_a}(V_{dc} - V_s) \end{bmatrix}. \quad (4.119)$$

The other five feasible state space models [Figure 4.27(b)-(f)] are omitted since the derivations are similar.

### 4.7.3 MODEL ANALYSIS AND SIMULATION

To prove the correctness of the proposed state-space model, the simulation of a three-level single phase MMC model in MATLAB/Simulink is conducted for comparison.

To simulate the proposed model, the differential equations of the state-space model (4.110) are discretized as follows,

$$\frac{d\mathbf{X}}{dt} = \mathbf{A} \cdot \mathbf{X} + \mathbf{B} \cdot \mathbf{U}, \quad (4.120)$$

$$d\mathbf{X} = \mathbf{A} \cdot \mathbf{X} \cdot dt + \mathbf{B} \cdot \mathbf{U} \cdot dt, \quad (4.121)$$

$$\mathbf{X}(k) - \mathbf{X}(k-1) = \mathbf{A}(k-1) \cdot \mathbf{X}(k-1) \cdot \Delta T + \mathbf{B} \cdot \mathbf{U}(k-1) \cdot \Delta T, \quad (4.122)$$

$$\mathbf{X}(k) = \mathbf{A}(k-1) \cdot \mathbf{X}(k-1) \cdot \Delta T + \mathbf{B} \cdot \mathbf{U}(k-1) \cdot \Delta T + \mathbf{X}(k-1), \quad (4.123)$$

A time-step of  $\Delta T = 0.1 \mu\text{s}$  was used to make sure the approximation is accurate enough. The system matrix  $\mathbf{A}$  is a function of switching patterns. The switching pattern of this modeling follows the modulation discussed in Chapter 3. The initial values of the state space are extracted from the simulations. Four initial times are selected. The state space values at the specific time are extracted from simulation and substituted into (4.123) as initial state. The state space initial values are summarized in Table 7. Four initial times are selected to verify the state space derivation with the MATLAB/Simulink simulation.

Table 7

Initial values of state space at four time instants.

	$t_1 = 10$ ms	$t_2 = 15$ ms	$t_3 = 20$ ms	$t_4 = 25$ ms
$i_1$ (A)	-34.5	60.6	70.7	0.7
$i_2$ (A)	5.6	16.9	2.2	-0.7
$V_{C1}$ (V)	984.8	983.3	1012.5	1009.5
$V_{C2}$ (V)	1004.1	999.0	1018.7	1011.0
$V_{C3}$ (V)	1012.3	1007.9	988.9	990.5
$V_{C4}$ (V)	1017.8	1023.4	1003.7	994.0

A switching model is built in MATLAB/Simulink. The simulation circuit is shown in Figure4.30. The key parameters of the system are summarized in Table 8. Ideal switches, inductors, and capacitors with no parasitic parameters as well as ideal voltage sources were used. Any controller delays are not included in the model. In the simulation setup, discrete-Tustin/Backward Euler (TBE) with a sample time of  $0.1 \mu\text{s}$  is selected. The initial values of capacitor voltages are 1000V. The initial values of the inductor current are determined by MATLAB/Simulink.

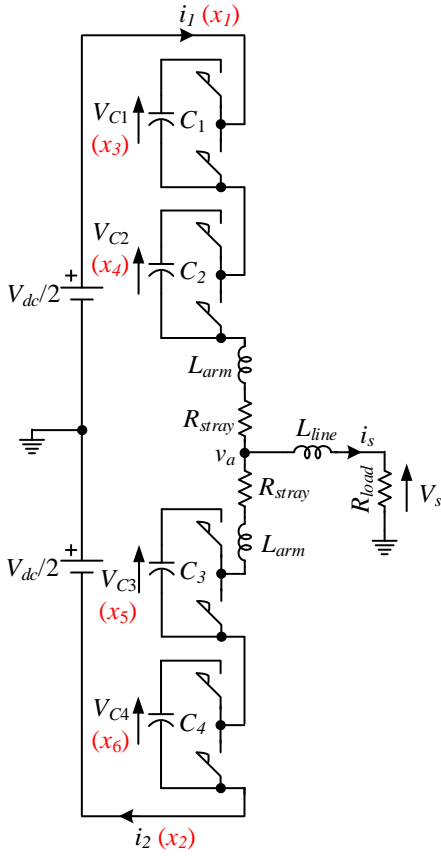


Figure 4.30 Three-level single-phase MMC circuit for simulation study.

The comparison results are shown in Figs. 4.31-4.36. The proposed state space model and the simulation results are matched at  $t_1$ ,  $t_2$ , and  $t_4$ , whereas a minor mismatch happens at  $t_3$ . This mismatch at  $t_3$  accumulated along with time. This is caused by the  $di_s/dt$  term in  $\mathbf{U}$ . We treat  $di_s/dt$  as an input since this term contains information from load instead of the information from MMC. We could have a more accurate state-space model by adding  $di_s/dt$  as the fifth state variable. This accumulation error becomes notable in a long run. Figure 4.37 shows the Simulink simulation along with the state-space model in five fundamental cycles. The accumulated error can be observed from this figure. Figure 4.38 shows the load current derived from the state space model ( $x_1 - x_2$ ). The load current has a dc offset. This is because the state space model only catches the derivative of load current

( $di_s/dt$ ). The dc component of load current is neglected. This is the major weakness of this model. Although there is minor mismatch between the simulation and the state-space model in this specific case study, the main features of the simulation curves are well captured by state-space model. This indicates that the mathematical derivation of the proposed model is correct. The  $di_s/dt$  term contains the information of load. This term could vary from load to load. But this has nothing to do with the MMC parameters. It is better to regard the  $di_s/dt$  as an input instead of a state variable when later on we move on to the stability analysis. Please notice that stability analysis should have a general idea of how MMC respond to a specific load model and its load change.

Table 8

Three-level MMC simulation key parameters.

Fundamental Frequency, $f_0$	60 Hz
Switching Frequency, $f_{sw}$	20 kHz
DC-Bus Voltage, $V_{dc}$	2000 V
Load Resistance, $R_{load}$	12.4 $\Omega$ (100% p.u.)
Line Inductance, $L_{line}$	1 mH (3% p.u.)
Arm Inductance, $L_{arm}$	0.1 $\mu$ H (0.0003% p.u.)
Stray Resistance, $R_{stray}$	0.1 $\Omega$ (0.8% p.u.)
Submodule Capacitance, $C_i$	85 $\mu$ F (40% p.u.)
Number of Submodules per Arm	2

where  $i = 1, 2, \dots, 4$ .

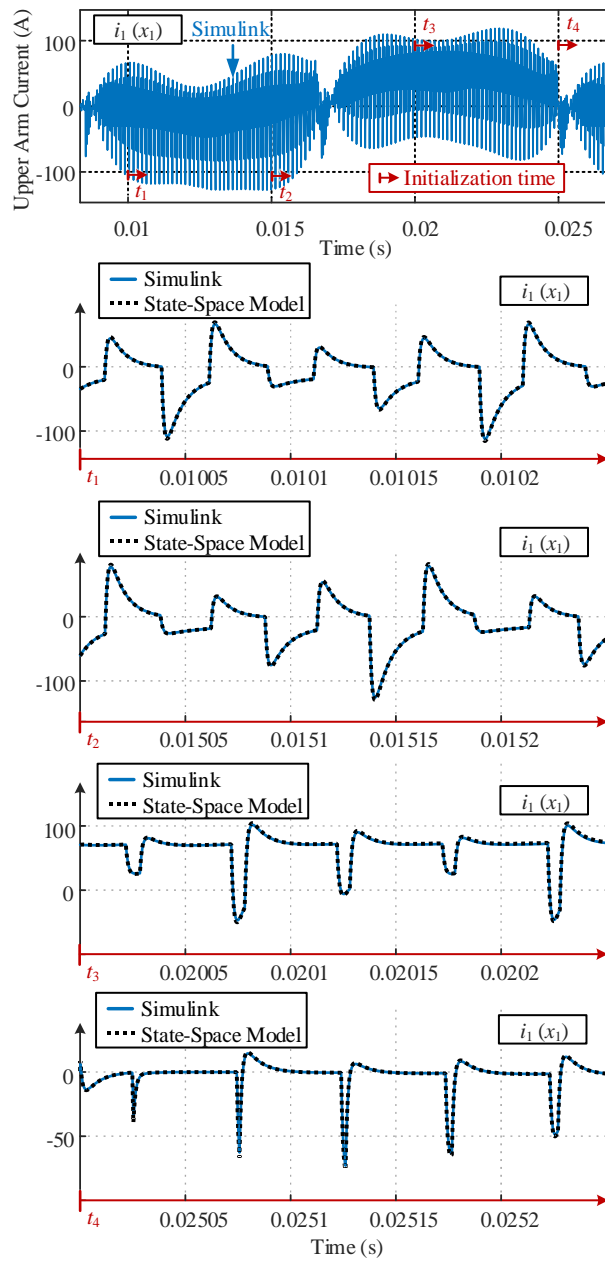


Figure 4.31 Upper arm current ( $x_1$ ) simulation and state-space model comparison.

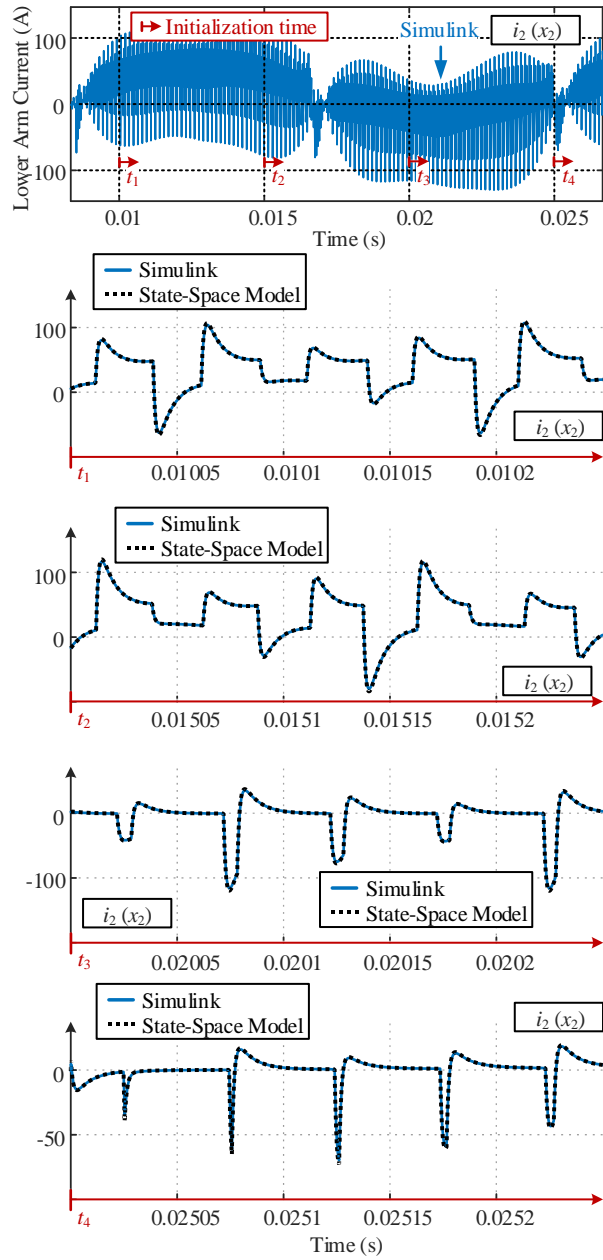


Figure 4.32 Lower arm current ( $x_2$ ) simulation and state-space model comparison.

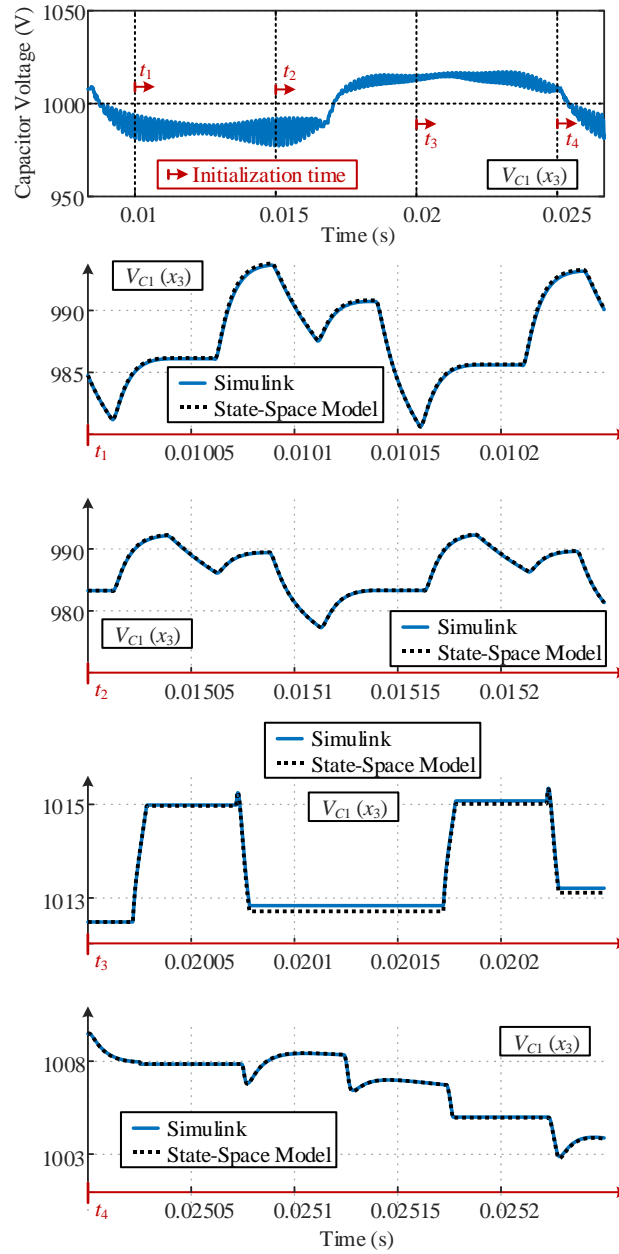


Figure 4.33 Capacitor voltage ( $x_3$ ) simulation and state-space model comparison.

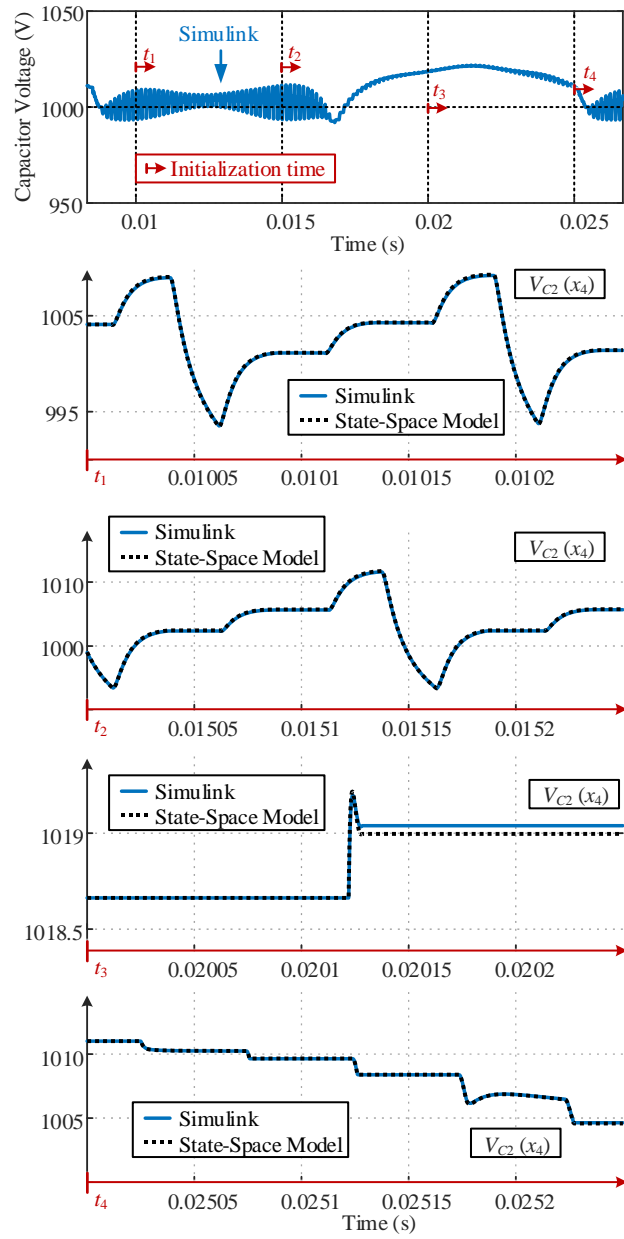


Figure 4.34 Capacitor voltage ( $x_4$ ) simulation and state-space model comparison.

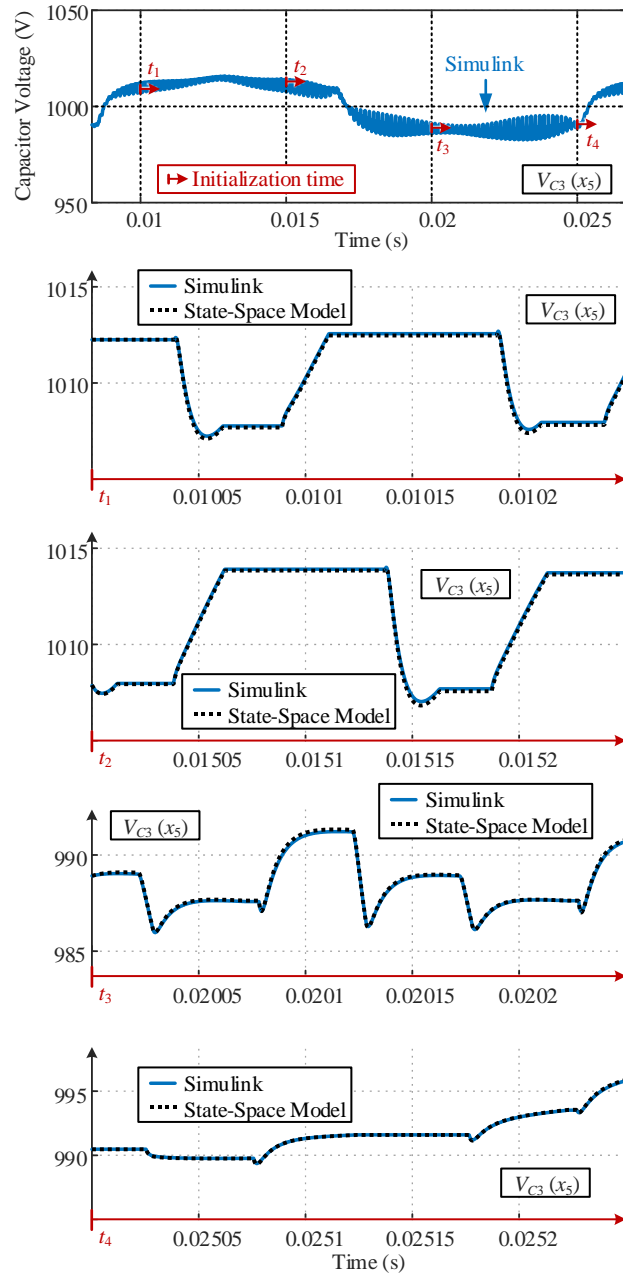


Figure 4.35 Capacitor voltage ( $x_5$ ) simulation and state-space model comparison.

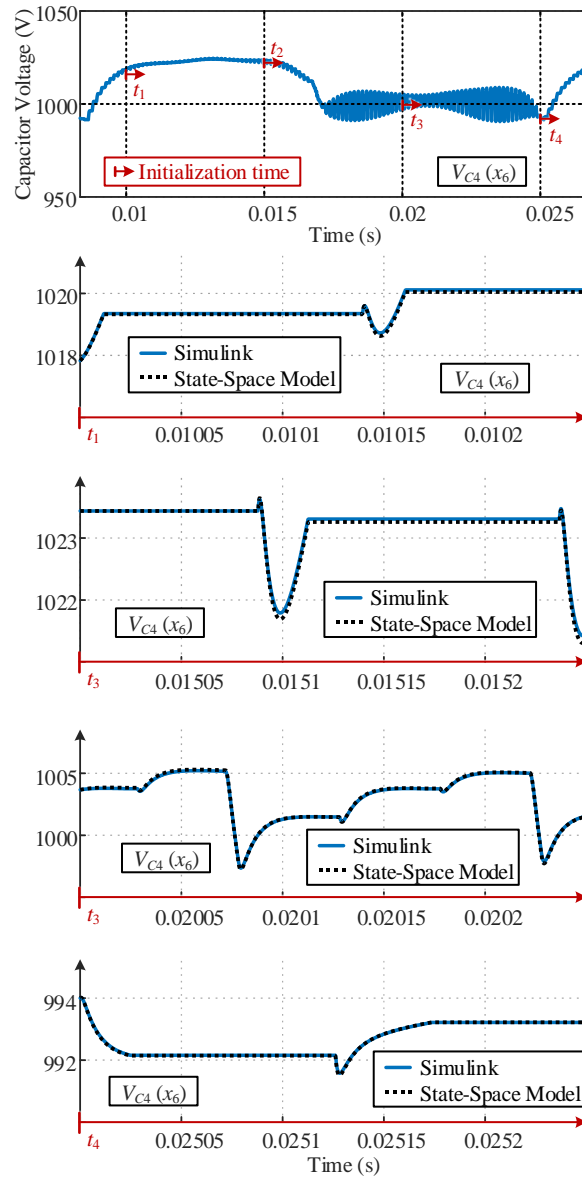
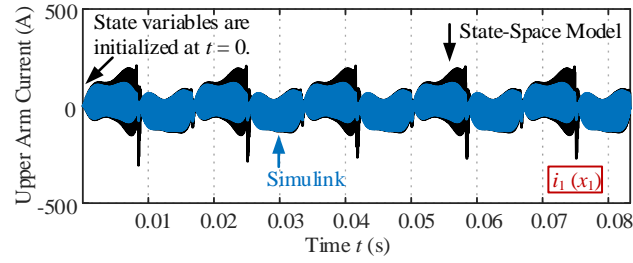
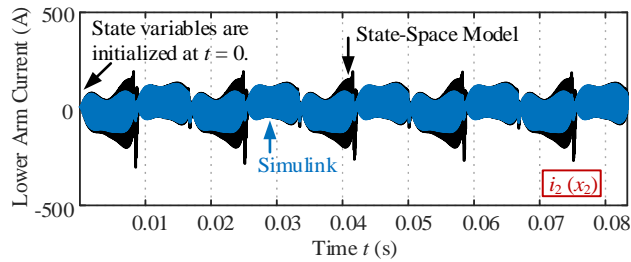


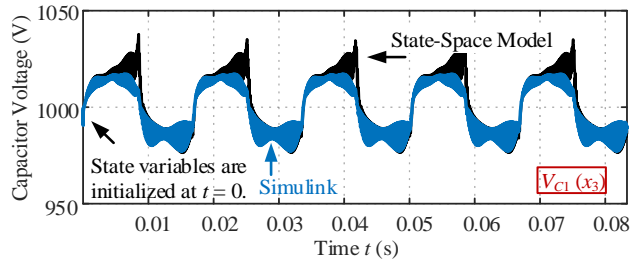
Figure 4.36 Capacitor voltage ( $x_6$ ) simulation and state-space model comparison.



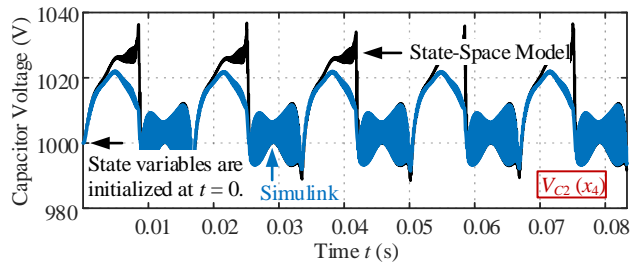
(a)



(b)



(c)

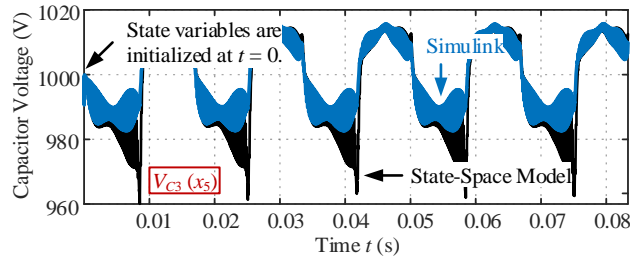


(d)

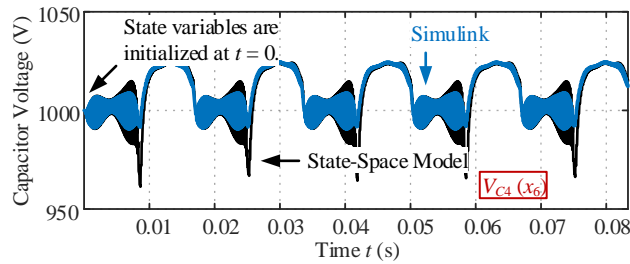
Figure 4.37 Comparison of simulation and state-space model in a long run. (a) upper arm current; (b) lower arm current; (c) capacitor voltage  $V_{C1}$ ; (d) capacitor voltage  $V_{C2}$ ;

(e) capacitor voltage  $V_{C3}$ ; (f) capacitor voltage  $V_{C4}$ .

Figure 4.37 (cont'd)



(e)



(f)

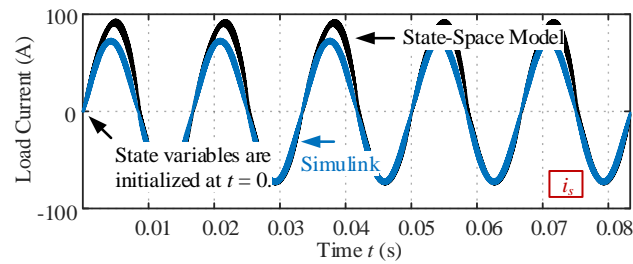


Figure 4.38 Accumulated error on load current.

#### 4.8 STATE-SPACE MODEL OF $N$ -LEVEL MMC

We are going to derive the state-space model for  $N$ -level MMC in this section. Figure 4.39 shows the single-phase  $N$ -level MMC under analysis. We have derived the state-space model for two-level and three-level MMC in previous sections. There are some common in their derivations. The law of derivations is summarized in this chapter.

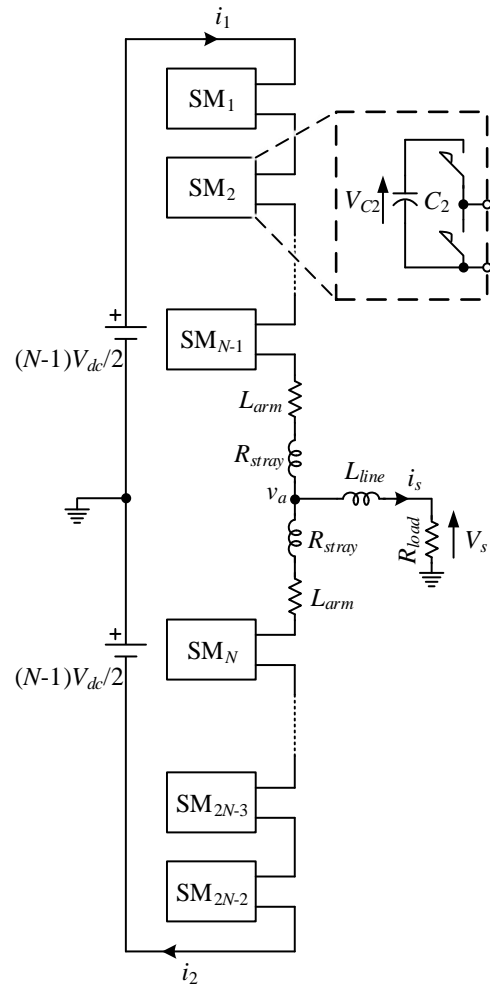


Figure 4.39 A single-phase  $N$ -level MMC.

#### 4.8.1 STATE-SPACE MODEL

Define the state variables to be

$$\mathbf{X} = \begin{bmatrix} x_1 \\ x_2 \\ x_3 \\ x_4 \\ \vdots \\ x_{2N} \end{bmatrix} = \begin{bmatrix} i_1 \\ i_2 \\ V_{C1} \\ V_{C2} \\ \vdots \\ V_{C(2N-2)} \end{bmatrix}, \quad \dot{\mathbf{X}} = \begin{bmatrix} \dot{x}_1 \\ \dot{x}_2 \\ \dot{x}_3 \\ \dot{x}_4 \\ \vdots \\ \dot{x}_{2N} \end{bmatrix} = \begin{bmatrix} \frac{di_1}{dt} \\ \frac{di_2}{dt} \\ \frac{dV_{C1}}{dt} \\ \frac{dV_{C2}}{dt} \\ \vdots \\ \frac{dV_{C(2N-2)}}{dt} \end{bmatrix}. \quad (4.124)$$

The state equation are as follows,

$$\dot{\mathbf{X}} = \mathbf{A} \cdot \mathbf{X} + \mathbf{B} \cdot \mathbf{U}. \quad (4.125)$$

Where

$$\mathbf{A} = \begin{bmatrix} -\frac{R}{2L} & -\frac{R}{2L} & \gamma_1 \cdot \left(-\frac{1}{2L}\right) & \gamma_2 \cdot \left(-\frac{1}{2L}\right) & \cdots & \gamma_{2N-2} \cdot \left(-\frac{1}{2L}\right) \\ -\frac{R}{2L} & -\frac{R}{2L} & \gamma_1 \cdot \left(-\frac{1}{2L}\right) & \gamma_2 \cdot \left(-\frac{1}{2L}\right) & \cdots & \gamma_{2N-2} \cdot \left(-\frac{1}{2L}\right) \\ \gamma_1 \cdot \left(\frac{1}{C_1}\right) & 0 & 0 & 0 & 0 & 0 \\ \vdots & \vdots & \vdots & \vdots & \vdots & \vdots \\ \gamma_{N-1} \cdot \left(\frac{1}{C_{N-1}}\right) & 0 & 0 & 0 & 0 & 0 \\ 0 & \gamma_N \cdot \left(\frac{1}{C_N}\right) & 0 & 0 & 0 & 0 \\ \vdots & \vdots & \vdots & \vdots & \vdots & \vdots \\ 0 & \gamma_{2N-2} \cdot \left(\frac{1}{C_{2N-2}}\right) & 0 & 0 & 0 & 0 \end{bmatrix}_{2N \times 2N}. \quad (4.126)$$

$y_m$  is an element of switching pattern; and

$$\mathbf{B} = \begin{bmatrix} \frac{1}{2L} & \frac{1}{2} \\ \frac{1}{2L} & -\frac{1}{2} \\ 0 & 0 \\ 0 & 0 \\ \vdots & \vdots \\ 0 & 0 \end{bmatrix}_{2N \times 2}, \quad (4.127)$$

$$\mathbf{U} = \begin{bmatrix} V_{dc} \\ \frac{di_s}{dt} \end{bmatrix}. \quad (4.128)$$

The coefficient matrix could be decomposed as follows,

$$\mathbf{A} = \begin{bmatrix} -\frac{R}{2L} & -\frac{R}{2L} & \gamma_1 \cdot \left(-\frac{1}{2L}\right) & \gamma_2 \cdot \left(-\frac{1}{2L}\right) & \cdots & \gamma_{2N-2} \cdot \left(-\frac{1}{2L}\right) \\ -\frac{R}{2L} & -\frac{R}{2L} & \gamma_1 \cdot \left(-\frac{1}{2L}\right) & \gamma_2 \cdot \left(-\frac{1}{2L}\right) & \cdots & \gamma_{2N-2} \cdot \left(-\frac{1}{2L}\right) \\ \hline \gamma_1 \cdot \left(\frac{1}{C_1}\right) & 0 & 0 & 0 & 0 & 0 \\ \vdots & \vdots & \vdots & \vdots & \vdots & \vdots \\ \gamma_{N-1} \cdot \left(\frac{1}{C_{N-1}}\right) & 0 & 0 & 0 & 0 & 0 \\ 0 & \gamma_N \cdot \left(\frac{1}{C_N}\right) & 0 & 0 & 0 & 0 \\ \vdots & \vdots & \vdots & \vdots & \vdots & \vdots \\ 0 & \gamma_{2N-2} \cdot \left(\frac{1}{C_{2N-2}}\right) & 0 & 0 & 0 & 0 \end{bmatrix}_{2N \times 2N}$$

$$= \begin{bmatrix} \mathbf{A}_R & \mathbf{A}_L \\ \hline \mathbf{A}_C & \mathbf{0} \end{bmatrix}.$$

(4.129)

$$\begin{aligned}
\mathbf{A}_L &= \begin{bmatrix} \gamma_1 \cdot \left(-\frac{1}{2L}\right) & \gamma_2 \cdot \left(-\frac{1}{2L}\right) & \cdots & \gamma_{2N-2} \cdot \left(-\frac{1}{2L}\right) \\ \gamma_1 \cdot \left(-\frac{1}{2L}\right) & \gamma_2 \cdot \left(-\frac{1}{2L}\right) & \cdots & \gamma_{2N-2} \cdot \left(-\frac{1}{2L}\right) \end{bmatrix} \\
&= \begin{bmatrix} -\frac{1}{2L} \\ -\frac{1}{2L} \end{bmatrix} \cdot [\gamma_1 \quad \gamma_2 \quad \cdots \quad \gamma_{2N-2}] = \hat{\mathbf{A}}_L \cdot \mathbf{\Gamma}_y^{(N)}
\end{aligned} \tag{4.130}$$

$$\mathbf{A}_C = \begin{bmatrix} \gamma_1 \cdot \left(\frac{1}{C_1}\right) & 0 \\ \vdots & \vdots \\ \gamma_{N-1} \cdot \left(\frac{1}{C_{N-1}}\right) & 0 \\ 0 & \gamma_N \cdot \left(\frac{1}{C_N}\right) \\ \vdots & \vdots \\ 0 & \gamma_{2N-2} \cdot \left(\frac{1}{C_{2N-2}}\right) \end{bmatrix} = [\hat{\mathbf{A}}_C \quad \bar{\mathbf{A}}_C] \tag{4.131}$$

$$\hat{\mathbf{A}}_C = \text{diag} \left( \begin{bmatrix} \frac{1}{C_1} \\ \vdots \\ \frac{1}{C_{N-1}} \\ 0 \\ \vdots \\ 0 \end{bmatrix}_{(2N-2) \times 1} \cdot [\gamma_1 \quad \gamma_2 \quad \cdots \quad \gamma_{2N-2}] \right) = \text{diag} \left( \hat{\mathbf{A}}_C' \cdot \mathbf{Y}_y^{(N)} \right) \tag{4.132}$$

$$\bar{\mathbf{A}}_C = \text{diag} \left( \begin{bmatrix} 0 \\ \vdots \\ 0 \\ \frac{1}{C_N} \\ \vdots \\ \frac{1}{C_{2N-2}} \end{bmatrix}_{(2N-2) \times 1} \cdot [\gamma_1 \quad \gamma_2 \quad \cdots \quad \gamma_{2N-2}] \right) = \text{diag} \left( \bar{\mathbf{A}}_C' \cdot \mathbf{\Gamma}_y^{(N)} \right) \tag{4.133}$$

*diag* operator returns a column vector of the main diagonal elements of the objective matrix.  $\hat{\mathbf{A}}_L$  contains the parameters from arm inductance.  $\hat{\mathbf{A}}'_C$  and  $\bar{\mathbf{A}}'_C$  contain the parameters from submodule capacitance.  $\hat{\mathbf{A}}'_C$  contain the parameters from upper arm submodules.  $\bar{\mathbf{A}}'_C$  contains the parameters from lower arm submodules. The reason to decompose the state space in such form is to save the work for programming. It will be easy to extent to high level state space by decomposing the matrix into such form.

Note that  $\mathbf{U}$  contains  $\frac{di_s}{dt}$ .  $\frac{di_s}{dt}$  reflects the voltage across the load inductor. That is

$$L_a \frac{di_s}{dt} = v_a - V_s, \quad (4.134)$$

as modeled in Figure4.40.

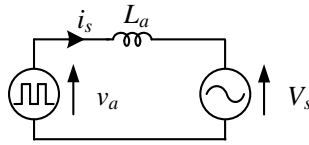


Figure 4.40 Load inductor voltage modeling.

If the pole is attached to the positive dc rail,  $v_a = (N - 1)V_{dc}/2$ . Eq.(4.124) can be modified as

$$\frac{di_s}{dt} = \frac{1}{L_a} \left( (N-1)V_{dc} / 2 - V_s \right). \quad (4.135)$$

For other switching patterns,  $v_a$  is determined by the number of the submodule at inserted mode in upper arm. Replace the  $\frac{di_s}{dt}$  in (4.128) by (4.134)

$$\mathbf{U} = \begin{bmatrix} V_{dc} \\ \frac{1}{L_a} (v_a - V_s) \end{bmatrix}. \quad (4.136)$$

## 4.8.2 MODEL ANALYSIS AND SIMULATION

To simulate the proposed model, the differential equations of the state-space model (4.125) are discretized as follows,

$$\frac{d\mathbf{X}}{dt} = \mathbf{A} \cdot \mathbf{X} + \mathbf{B} \cdot \mathbf{U}, \quad (4.137)$$

$$d\mathbf{X} = \mathbf{A} \cdot \mathbf{X} \cdot dt + \mathbf{B} \cdot \mathbf{U} \cdot dt, \quad (4.138)$$

$$\mathbf{X}(k) - \mathbf{X}(k-1) = \mathbf{A}(k-1) \cdot \mathbf{X}(k-1) \cdot \Delta T + \mathbf{B} \cdot \mathbf{U}(k-1) \cdot \Delta T, \quad (4.139)$$

$$\mathbf{X}(k) = \mathbf{A}(k-1) \cdot \mathbf{X}(k-1) \cdot \Delta T + \mathbf{B} \cdot \mathbf{U}(k-1) \cdot \Delta T + \mathbf{X}(k-1), \quad (4.140)$$

The system matrix  $\mathbf{A}$  is a function of switching patterns. The switching pattern of this modeling follows the modulation discussed in [62].

### 4.8.2.1 CASE STUDY: $\Gamma$ MM BASED FOUR-LEVEL MMC

To prove the correctness of the proposed state-space model, the simulation of a single-phase four-level MMC model in MATLAB/Simulink is conducted for comparison. This four-level MMC simulation follows the  $\Gamma$ MM strategy. The submatrices are as follows,

$$\mathbf{\Gamma}_1^{(4)} = [0 \ 0 \ 0 \ 1 \ 1 \ 1], \quad (4.141)$$

$$\hat{\mathbf{\Gamma}}_2^{(4)} = \begin{bmatrix} 0 & 1 & 0 & 1 & 0 & 1 \\ 0 & 1 & 0 & 0 & 1 & 1 \\ 0 & 0 & 1 & 1 & 0 & 1 \\ 1 & 0 & 0 & 1 & 0 & 1 \\ 0 & 1 & 0 & 1 & 1 & 0 \end{bmatrix}, \quad (4.142)$$

$$\hat{\mathbf{\Gamma}}_3^{(4)} = \begin{bmatrix} 1 & 1 & 0 & 1 & 0 & 0 \\ 1 & 1 & 0 & 0 & 1 & 0 \\ 1 & 0 & 1 & 1 & 0 & 0 \\ 1 & 1 & 0 & 0 & 0 & 1 \\ 0 & 1 & 1 & 1 & 0 & 0 \end{bmatrix}, \quad (4.143)$$

$$\mathbf{\Gamma}_4^{(4)} = [1 \ 1 \ 1 \ 0 \ 0 \ 0]. \quad (4.144)$$

Eq.(4.141)-(4.144) are all in full rank.

The initial values of the state space are extracted from the simulations. Four initial times are selected. The state space values at the specific time are extracted from simulation and substituted into (4.140) as initial state. The state space initial values are summarized in Table 9. Four initial times are selected to verify the state space derivation with the MATLAB/Simulink simulation.

Table 9

Initial values of state space at four time instants.

	$t_1 = 10 \text{ ms}$	$t_2 = 15 \text{ ms}$	$t_3 = 20 \text{ ms}$	$t_4 = 25 \text{ ms}$
$i_1 \text{ (A)}$	- 3.4	- 14.8	70.1	27.9
$i_2 \text{ (A)}$	37.7	28.8	0.8	26.5
$V_{C1} \text{ (V)}$	991.0	989.4	1016.7	994.2
$V_{C2} \text{ (V)}$	986.3	985.6	1008.2	1010.6
$V_{C3} \text{ (V)}$	1001.3	1005.0	1014.1	1008.4
$V_{C4} \text{ (V)}$	1003.9	1001.8	995.5	988.9
$V_{C5} \text{ (V)}$	1019.7	1020.9	1006.9	991.6
$V_{C6} \text{ (V)}$	1019.1	1020.2	995.4	999.9

A simulation is built in MATLAB/Simulink. The simulation circuit is shown in Figure4.41. The key parameters of the system are summarized in Table 10. Ideal switches, inductors, and capacitors with no parasitic parameters as well as ideal voltage sources were used. Any controller delays are not included in the model. In the simulation setup, discrete-

Tustin/Backward Euler (TBE) with a sample time of  $0.167 \mu\text{s}$  is selected. The initial values of capacitor voltages are 1000V. The initial values of the inductor current are determined by MATLAB/Simulink.

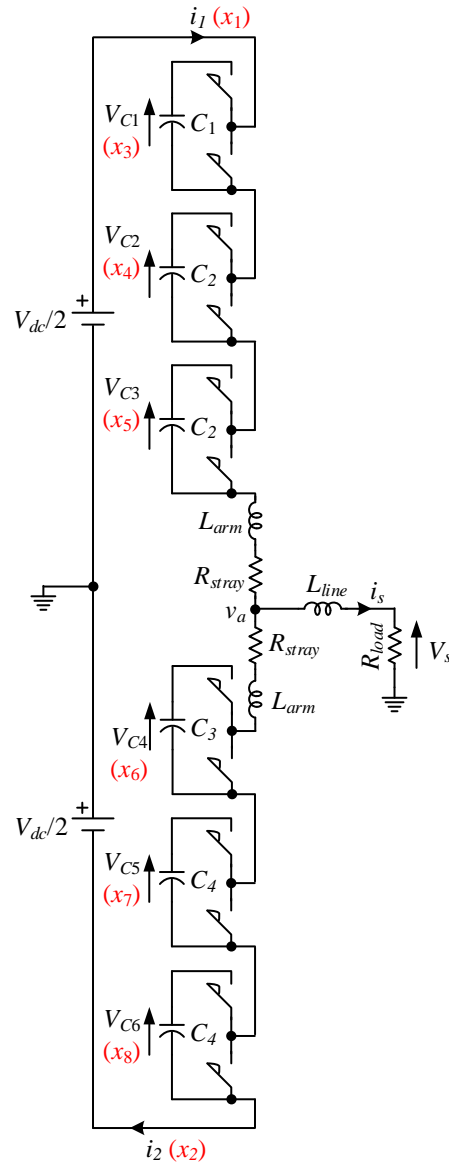


Figure 4.41 Four-level single-phase MMC circuit for simulation study.

The comparison results are shown in Figs. 4.42-4.45. The proposed state space model and the simulation results are matched at all time slots. Figure 4.46 shows the Simulink simulation along with the state-space model in five fundamental cycles. The proposed

state-space model matches with simulation in a long run. Figure 4.47 shows the load current derived from the state space model ( $x_1 - x_2$ ). This indicates that the mathematical derivation of the proposed model is correct. The  $di_s/dt$  term contains the information of load. This term could vary from load to load. But this has nothing to do with the MMC parameters. It is better to regard the  $di_s/dt$  as an input instead of a state variable when later on we move on to the stability analysis. Please notice that stability analysis should have a general idea of how MMC respond to a specific load model and its load change.

Table 10

Four-level MMC simulation key parameters.

Fundamental Frequency, $f_0$	60 Hz
Switching Frequency, $f_{sw}$	30 kHz
DC-Bus Voltage, $V_{dc}$	3000 V
Load Resistance, $R_{load}$	18.6 $\Omega$ (100% p.u.)
Line Inductance, $L_{line}$	1 mH (3% p.u.)
Arm Inductance, $L_{arm}$	0.1 $\mu$ H (0.0002% p.u.)
Stray Resistance, $R_{stray}$	0.1 $\Omega$ (0.5% p.u.)
Submodule Capacitance, $C_i$	171 $\mu$ F (1.2 p.u.)
Number of Submodules per Arm	3

where  $i = 1, 2, \dots, 6$ .

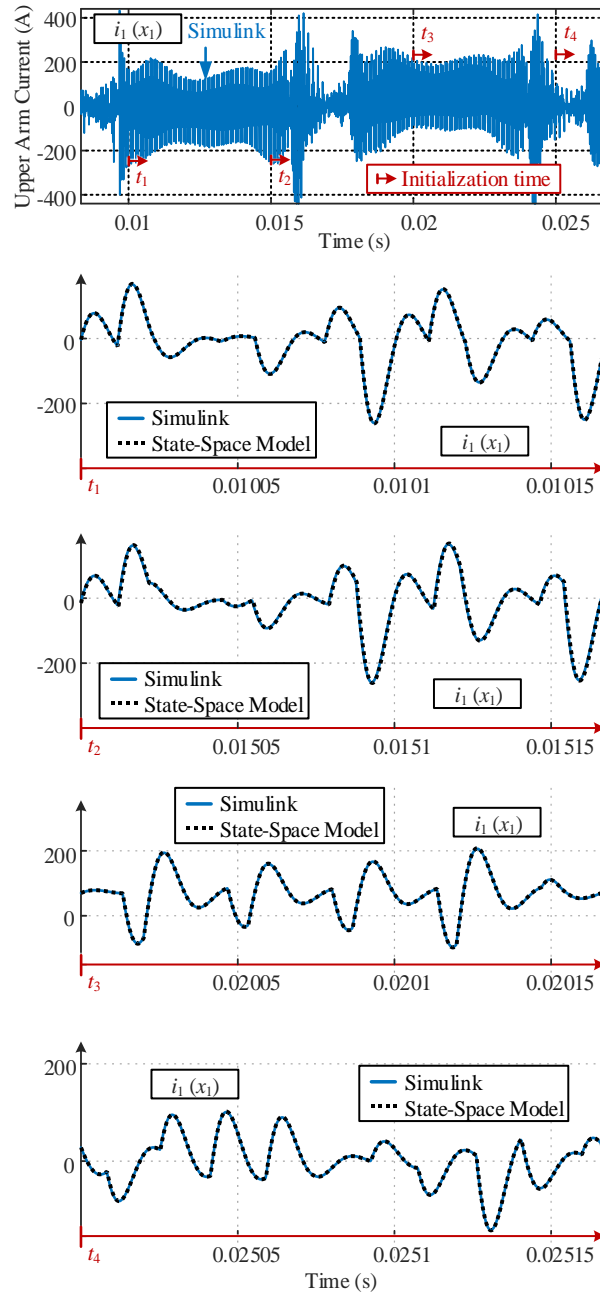


Figure 4.42 Upper arm current ( $x_1$ ) simulation and state-space model comparison.

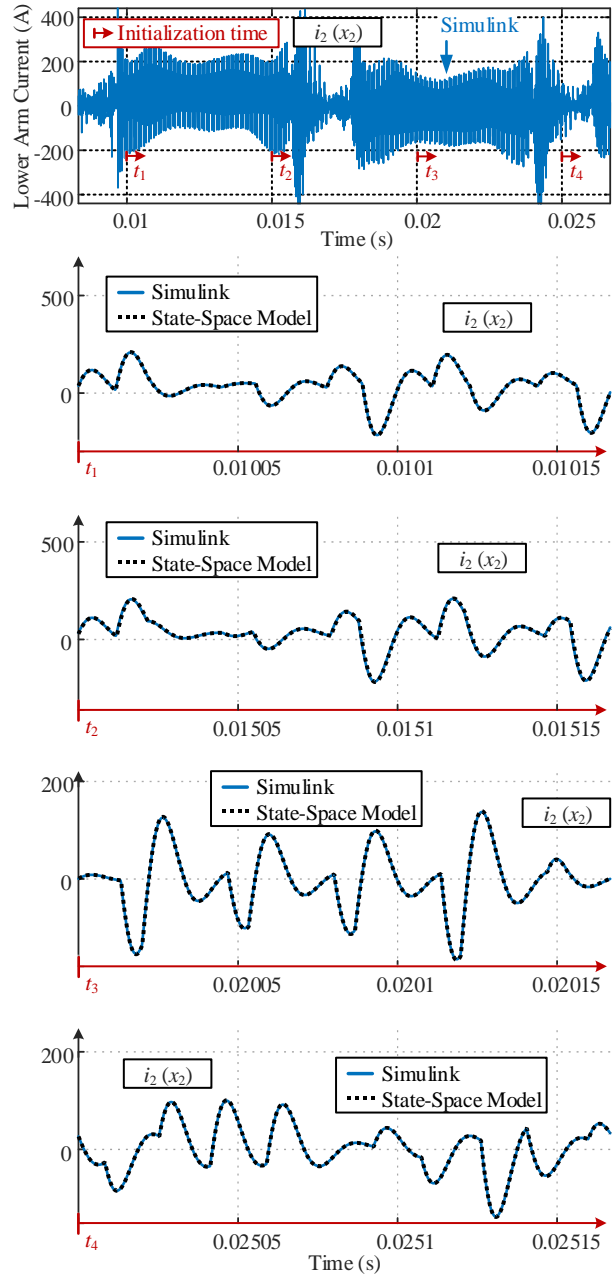


Figure 4.43 Lower arm current ( $x_2$ ) simulation and state-space model comparison.

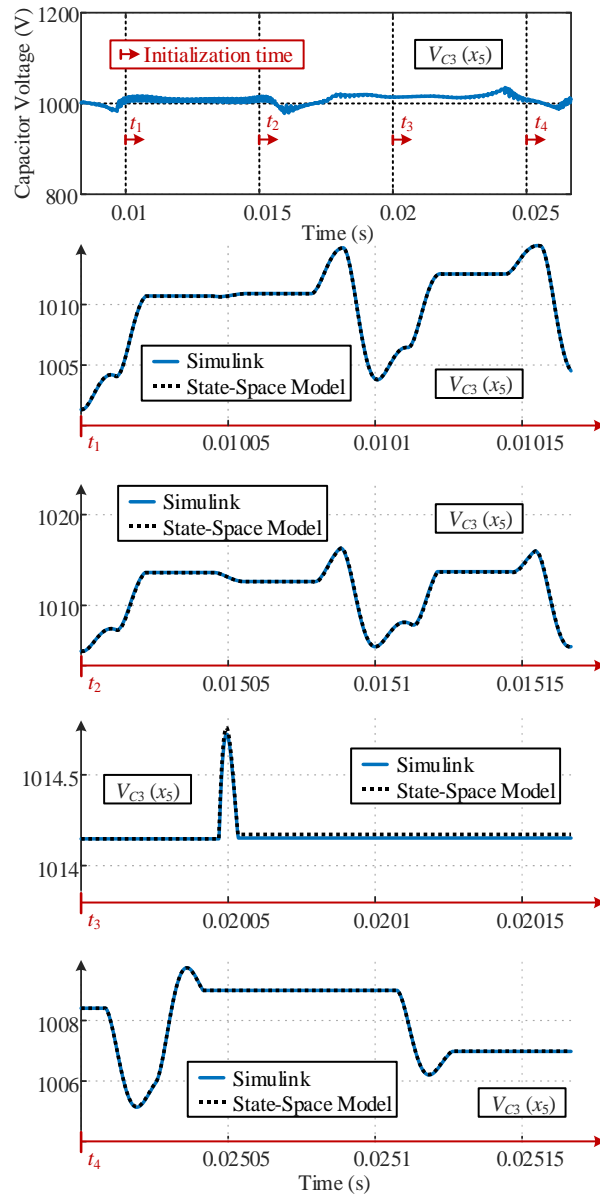


Figure 4.44 Capacitor voltage ( $x_5$ ) simulation and state-space model comparison.

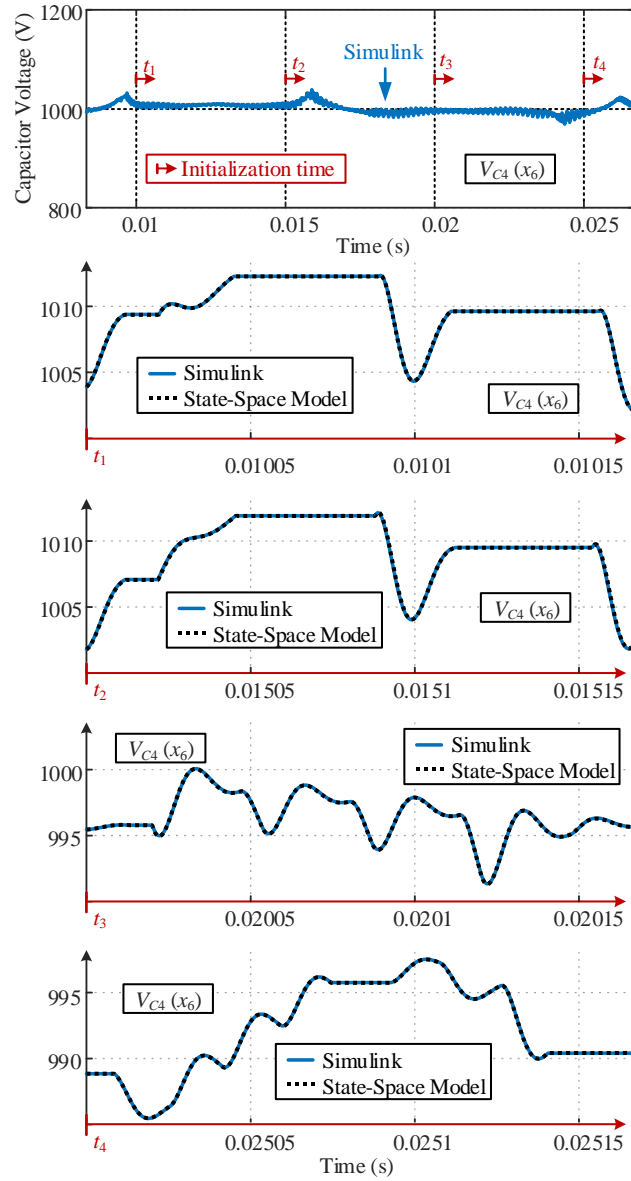
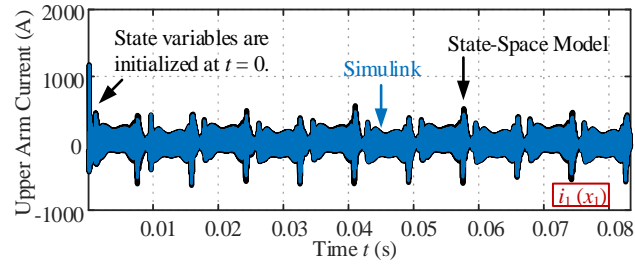
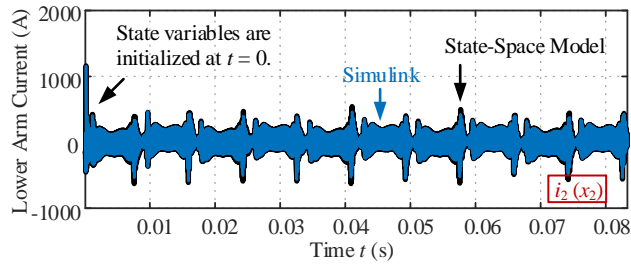


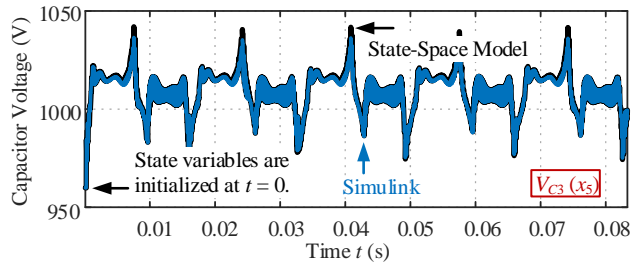
Figure 4.45 Capacitor voltage ( $x_6$ ) simulation and state-space model comparison.



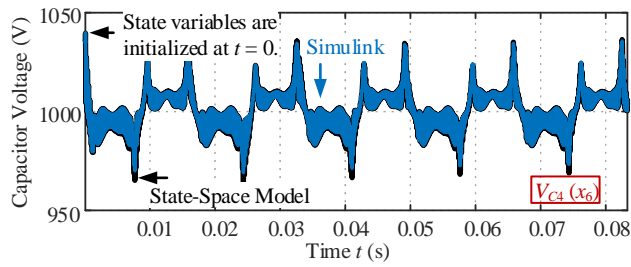
(a)



(b)



(c)



(d)

Figure 4.46 Comparison of simulation and state-space model in a long run. (a) upper arm current; (b) lower arm current; (c) capacitor voltage  $V_{C3}$ ; (d) capacitor voltage  $V_{C4}$ .

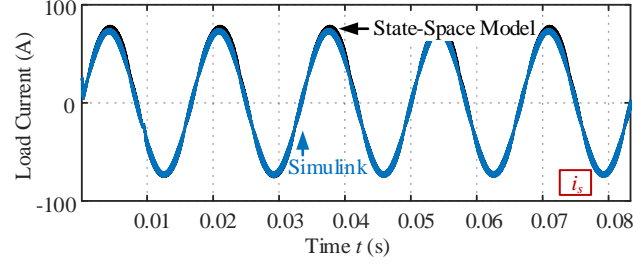


Figure 4.47 Load current  $i_s = x_1 - x_2$ .

#### 4.8.2.2 CASE STUDY: $\Gamma$ MM BASED FOUR-LEVEL MMC WITH NON-FULL-RANK MATRIX

To prove the proposed state-space model can effectively demonstrate the deviation of the non-full-rank  $\Gamma$  matrix, the simulation of a single-phase four-level MMC model in MATLAB/Simulink is conducted for comparison. This four-level MMC simulation follows the  $\Gamma$ MM strategy. The submatrices are as follows,

$$\mathbf{\Gamma}_1^{(4)} = [0 \ 0 \ 0 \ 1 \ 1 \ 1], \quad (4.145)$$

$$\hat{\mathbf{\Gamma}}_2^{(4)} = \begin{bmatrix} 0 & 0 & 1 & 1 & 0 & 1 \\ 0 & 1 & 0 & 0 & 1 & 1 \\ 1 & 0 & 0 & 1 & 1 & 0 \\ 0 & 1 & 0 & 1 & 0 & 1 \\ 0 & 0 & 1 & 0 & 1 & 1 \end{bmatrix}, \quad (4.146)$$

$$\hat{\mathbf{\Gamma}}_3^{(4)} = \begin{bmatrix} 1 & 0 & 1 & 1 & 0 & 0 \\ 1 & 1 & 0 & 0 & 1 & 0 \\ 0 & 1 & 1 & 0 & 0 & 1 \\ 1 & 0 & 1 & 0 & 1 & 0 \\ 1 & 1 & 0 & 1 & 0 & 0 \end{bmatrix}, \quad (4.147)$$

$$\mathbf{\Gamma}_4^{(4)} = [1 \ 1 \ 1 \ 0 \ 0 \ 0]. \quad (4.148)$$

Eq.(4.145)-(4.148) are non-full-rank. The rank of each matrix are as follows,

$$\text{rank}[\mathbf{\Gamma}_1^{(4)}] = 1, \text{rank}[\hat{\mathbf{\Gamma}}_2^{(4)}] = 4, \text{rank}[\hat{\mathbf{\Gamma}}_3^{(4)}] = 4, \text{and } \text{rank}[\mathbf{\Gamma}_4^{(4)}] = 1. \quad (4.149)$$

The rank of any two adjacent matrices are as follows,

$$\text{rank} \begin{bmatrix} \mathbf{\Gamma}_1^{(4)} \\ \hat{\mathbf{\Gamma}}_2^{(4)} \end{bmatrix} = 5, \text{rank} \begin{bmatrix} \hat{\mathbf{\Gamma}}_2^{(4)} \\ \hat{\mathbf{\Gamma}}_3^{(4)} \end{bmatrix} = 5, \text{ and } \text{rank} \begin{bmatrix} \hat{\mathbf{\Gamma}}_3^{(4)} \\ \mathbf{\Gamma}_4^{(4)} \end{bmatrix} = 5. \quad (4.150)$$

The initial values of the state space are extracted from the simulations. Four initial times are selected. The state space values at the specific time are extracted from simulation and substituted into (4.140) as initial state. The state space initial values are summarized in Table 11. Four initial times are selected to verify the state space derivation with the MATLAB/Simulink simulation.

Table 11

Initial values of state space at four time instants.

	$t_1 = 10 \text{ ms}$	$t_2 = 15 \text{ ms}$	$t_3 = 20 \text{ ms}$	$t_4 = 25 \text{ ms}$
$i_1 \text{ (A)}$	-9.8	-19.7	67.3	18.0
$i_2 \text{ (A)}$	30.7	23.2	-1.4	18.0
$V_{C1} \text{ (V)}$	921.9	888.9	868.2	829.2
$V_{C2} \text{ (V)}$	1028.6	1048.9	1075.4	1087.2
$V_{C3} \text{ (V)}$	1032.9	1051.0	1075.7	1089.2
$V_{C4} \text{ (V)}$	1042.6	1057.7	1069.8	1082.2
$V_{C5} \text{ (V)}$	1046.7	1061.5	1071.1	1083.2
$V_{C6} \text{ (V)}$	958.9	906.8	860.1	830.2

A simulation is built in MATLAB/Simulink. The simulation circuit is shown in Figure4.41. The key parameters of the system are the same as Chapter 4.8.2.1, which is summarized in Table 10. Ideal switches, inductors, and capacitors with no parasitic

parameters as well as ideal voltage sources were used. Any controller delays are not included in the model. In the simulation setup, discrete-Tustin/Backward Euler (TBE) with a sample time of  $0.167 \mu\text{s}$  is selected. The initial values of capacitor voltages are  $1000\text{V}$ . The initial values of the inductor current are determined by MATLAB/Simulink.

The comparison results are shown in Figs. 4.48-4.51. The proposed state-space model and the simulation results are matched at all time slots. Figure 4.52 shows the Simulink simulation along with the state-space model in five fundamental cycles. The proposed state-space model matches with simulation in a long run. Figure 4.53 shows the load current derived from the state variables ( $x_1 - x_2$ ). This indicates that the mathematical derivation of the proposed model is correct. The  $di_s/dt$  term contains the information of load. This term could vary from load to load. But this has nothing to do with the MMC parameters. It is better to regard the  $di_s/dt$  as an input instead of a state variable when later on we move on to the stability analysis. Please notice that stability analysis should have a general idea of how MMC responds to a specific load model and its load change.

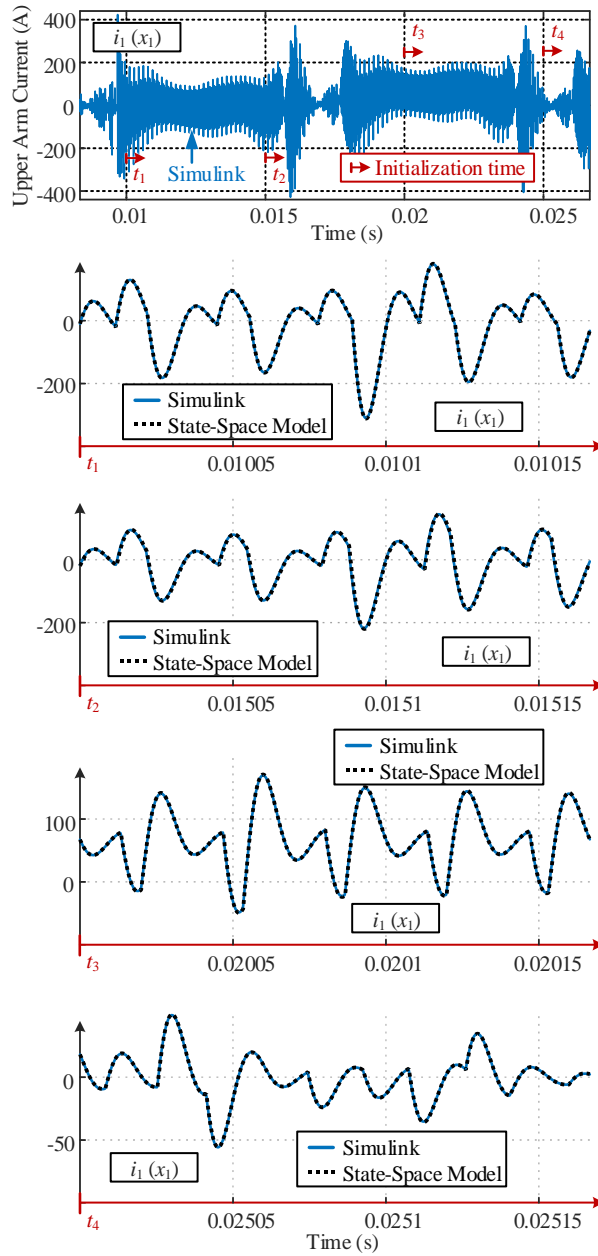


Figure 4.48 Upper arm current ( $x_1$ ) simulation and state-space model comparison.

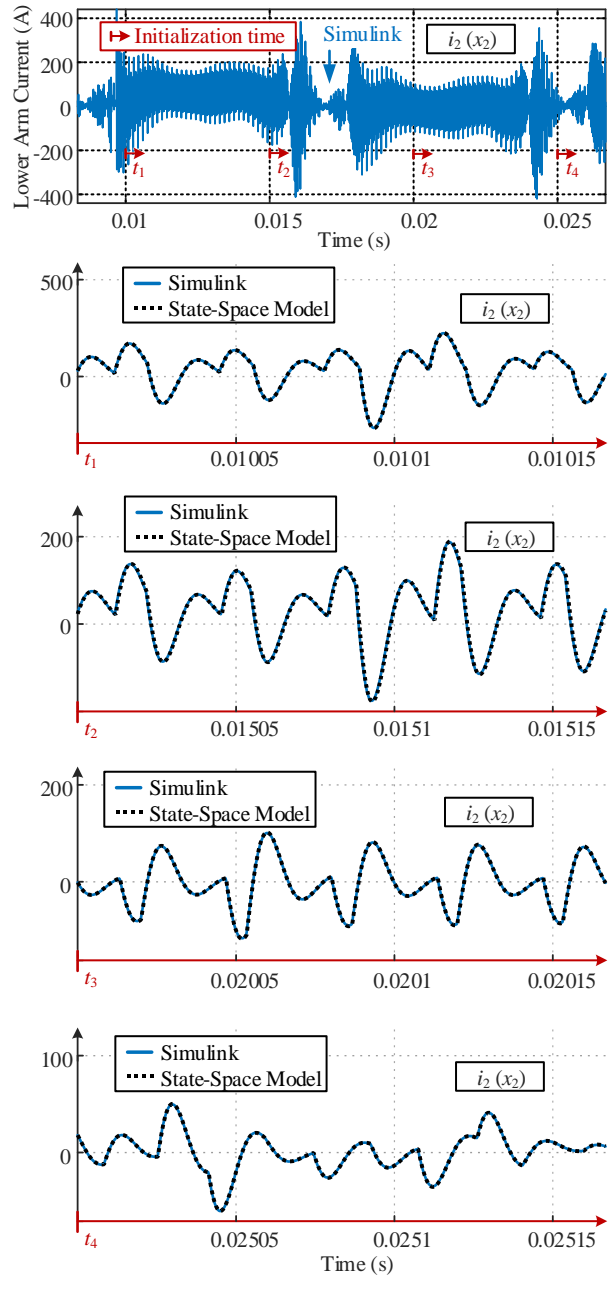


Figure 4.49 Lower arm current ( $x_2$ ) simulation and state-space model comparison.

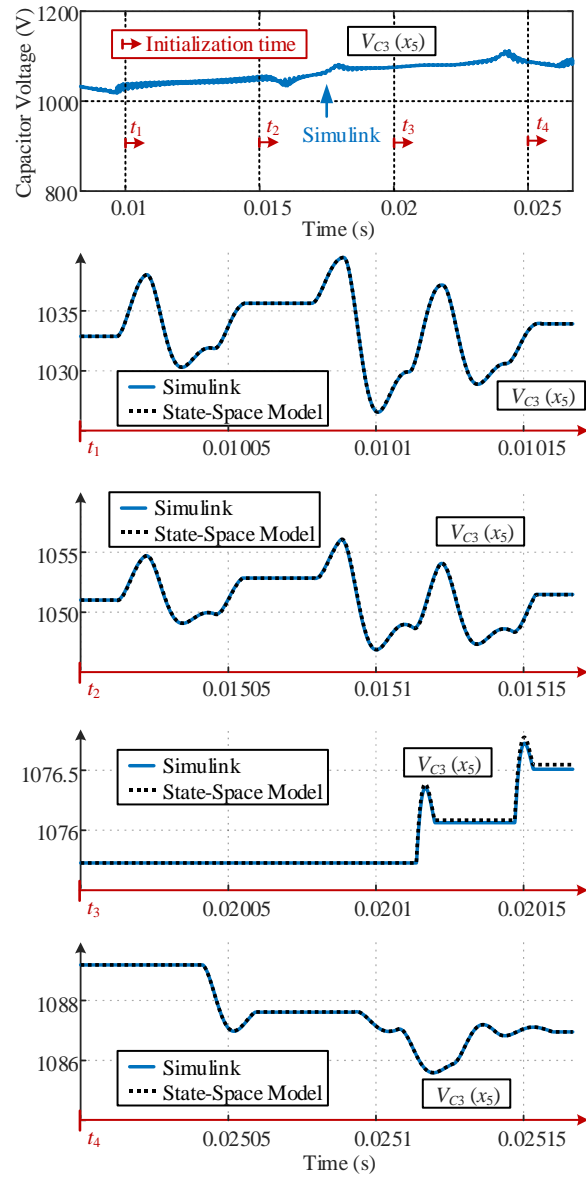


Figure 4.50 Capacitor voltage ( $x_5$ ) simulation and state-space model comparison.

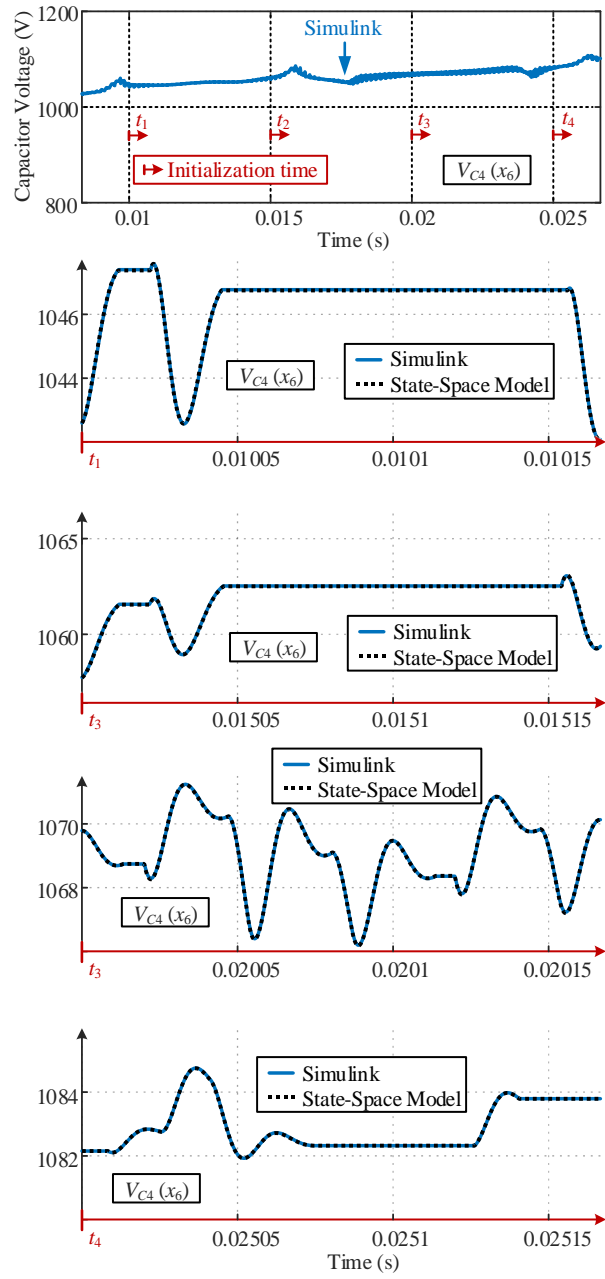
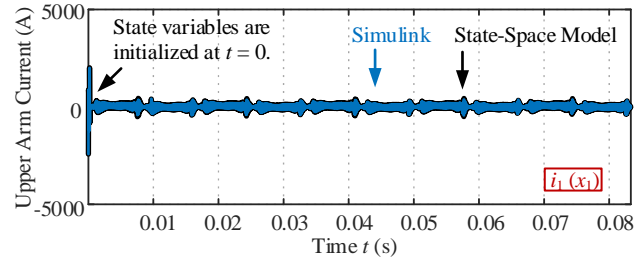
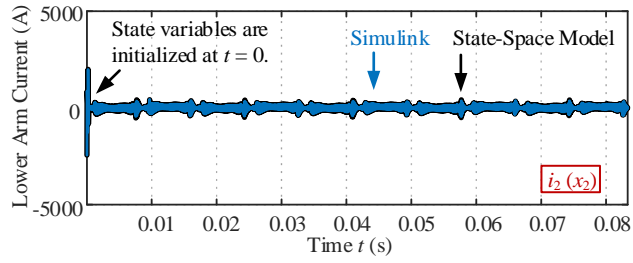


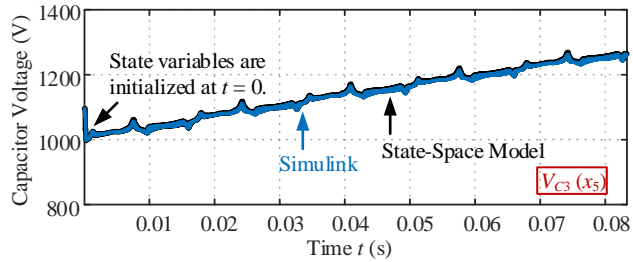
Figure 4.51 Capacitor voltage ( $x_6$ ) simulation and state-space model comparison.



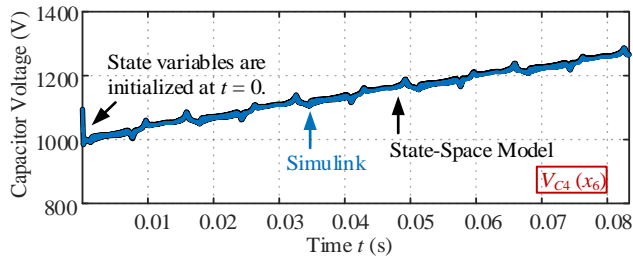
(a)



(b)



(c)



(d)

Figure 4.52 Comparison of simulation and state-space model in a long run. (a) upper arm current; (b) lower arm current; (c) capacitor voltage  $V_{C3}$ ; (d) capacitor voltage  $V_{C4}$ .

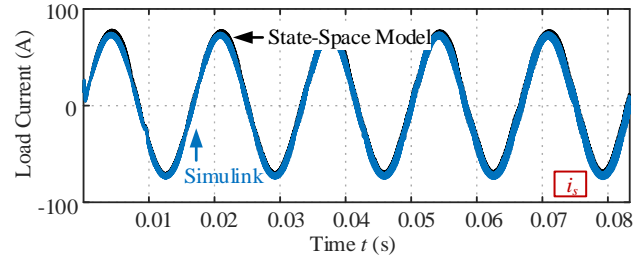


Figure 4.53 Load current  $i_s = x_1 - x_2$ .

#### 4.8.2.3 CASE STUDY: $\Gamma$ MM BASED ELEVEN-LEVEL MMC

To prove that this model can be extended to higher level a simulation of a single-phase eleven-level MMC model in MATLAB/Simulink is conducted for comparison with the proposed state-space model. This eleven-level MMC simulation follows the  $\Gamma$ MM strategy. The submatrices extraction follows the case study in Chapter 3.4.4.

The initial values of the state space are extracted from the simulations. Four initial times are selected. The state space values at the specific time are extracted from simulation and substituted into (4.140) as initial state. The state space initial values are summarized in Table 12. Four initial times are selected to verify the state space derivation with the MATLAB/Simulink simulation.

Table 12

Initial values of state variables at four time instants.

	$t_1 = 25$ ms	$t_2 = 30$ ms	$t_3 = 35$ ms	$t_4 = 40$ ms
$i_1$ (A)	76.1	- 18.8	127.3	180.1
$i_2$ (A)	77.5	50.8	84.3	137.5
$V_{C1}$ (V)	1017.5	1001.7	1001.6	1015.3
$V_{C2}$ (V)	1023.5	998.2	1010.2	1023.6
$V_{C3}$ (V)	1020.0	997.7	1002.4	1020.3
$V_{C4}$ (V)	1025.7	997.4	1000.8	1023.6
$V_{C5}$ (V)	1012.5	995.9	995.8	1021.6
$V_{C6}$ (V)	1013.2	996.8	996.0	1024.4
$V_{C7}$ (V)	1019.0	998.8	999.2	1023.9
$V_{C8}$ (V)	1029.4	1002.1	1003.1	1024.1
$V_{C9}$ (V)	1040.1	1002.0	992.3	1039.7
$V_{C10}$ (V)	1033.1	1005.0	994.3	1029.5
$V_{C11}$ (V)	989.4	1012.2	1008.4	998.4
$V_{C12}$ (V)	1000.0	1011.4	1018.5	1012.3
$V_{C13}$ (V)	997.7	1009.4	1007.6	999.7
$V_{C14}$ (V)	1001.4	1010.8	1003.0	990.9
$V_{C15}$ (V)	995.8	1013.2	995.2	987.9
$V_{C16}$ (V)	998.4	1014.0	996.4	990.7
$V_{C17}$ (V)	971.4	1013.8	995.6	984.0
$V_{C18}$ (V)	973.0	1013.0	1.0020	991.3

Table 12 (cont'd)

$V_{C19}$ (V)	968.1	1015.1	998.1	982.1
$V_{C20}$ (V)	970.0	1017.8	1012.5	989.3

A simulation is built in MATLAB/Simulink. The simulation circuit is shown in Figure 4.54. The key parameters of the system are summarized in Table 13. Ideal switches, inductors, and capacitors with no parasitic parameters as well as ideal voltage sources were used. Any controller delays are not included in the model. In the simulation setup, discrete-Tustin/Backward Euler (TBE) with a sample time of  $0.167 \mu\text{s}$  is selected. The initial values of capacitor voltages are 1000V. The initial values of the inductor current are determined by MATLAB/Simulink.

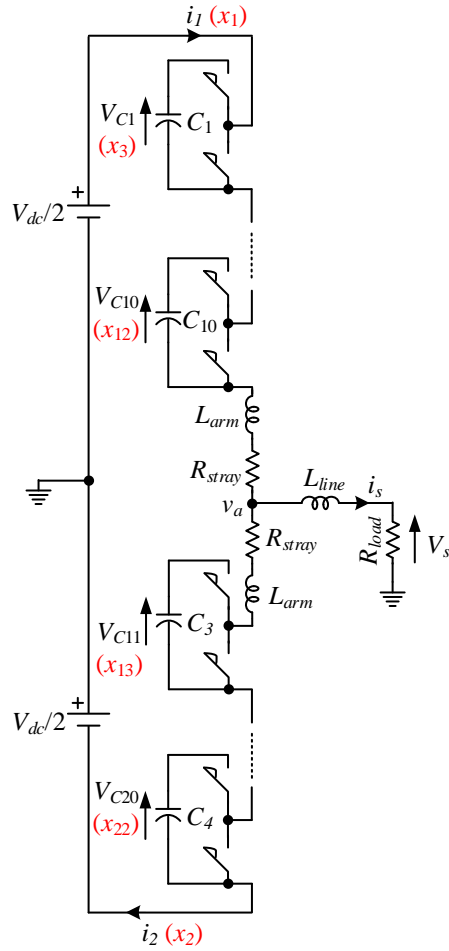


Figure 4.54 Eleven-level single-phase MMC circuit for state-space model study.

The comparison results are shown in Figs. 4.55-4.58. The proposed state space model and the simulation results are matched at all time slots. Figure 4.59 shows the Simulink simulation along with the state-space model in four fundamental cycles. The proposed state-space model matches with simulation in a long run. Figure 4.60 shows the load current derived from the state variables  $(x_1 - x_2)$ . This indicates that the mathematical derivation of the proposed model is correct. The  $di_s/dt$  term contains the information of load. This term could vary from load to load. But this has nothing to do with the MMC parameters. It is better to regard the  $di_s/dt$  as an input instead of a state variable when later on we move

on to the stability analysis. Please notice that stability analysis should have a general idea of how MMC respond to a specific load model and its load change.

Table 13

Eleven-level MMC simulation key parameters.

Fundamental Frequency, $f_0$	60 Hz
Switching Frequency, $f_{sw}$	60 kHz
DC-Bus Voltage, $V_{dc}$	10 kV
Load Resistance, $R_{load}$	62 $\Omega$ (100% p.u.)
Line Inductance, $L_{line}$	1 mH (0.61% p.u.)
Arm Inductance, $L_{arm}$	0.1 $\mu$ H (0.00006% p.u.)
Stray Resistance, $R_{stray}$	0.2 $\Omega$ (0.32% p.u.)
Submodule Capacitance, $C_i$	770 $\mu$ F (18 p.u.)
Number of Submodules per Arm	10

where  $i = 1, 2, \dots, 20$ .

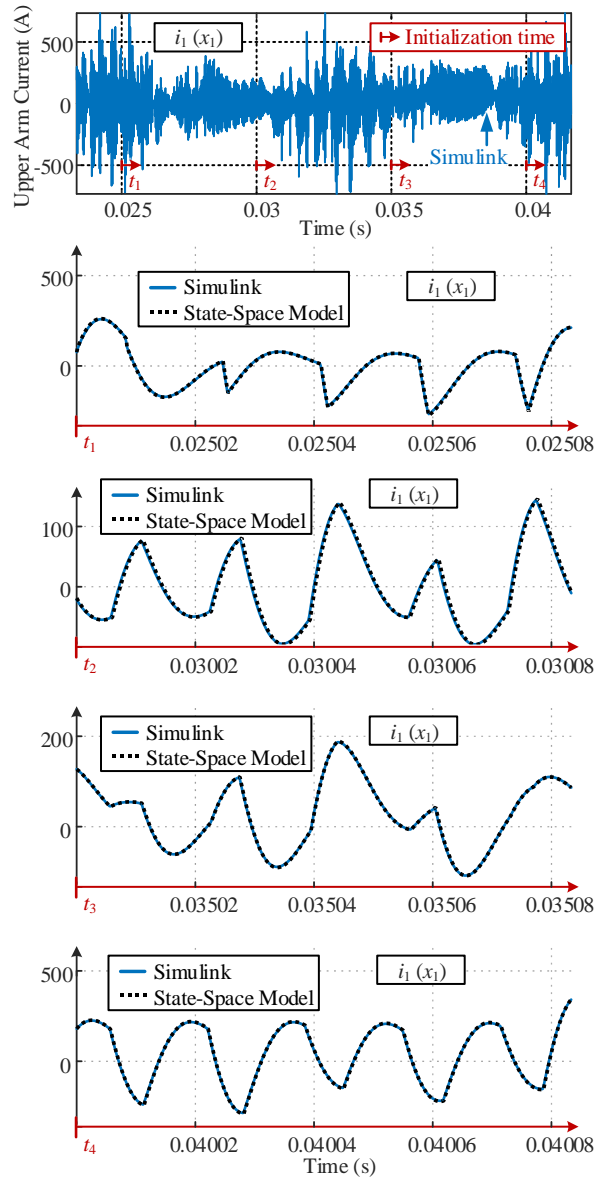


Figure 4.55 Upper arm current ( $x_1$ ) simulation and state-space model comparison.

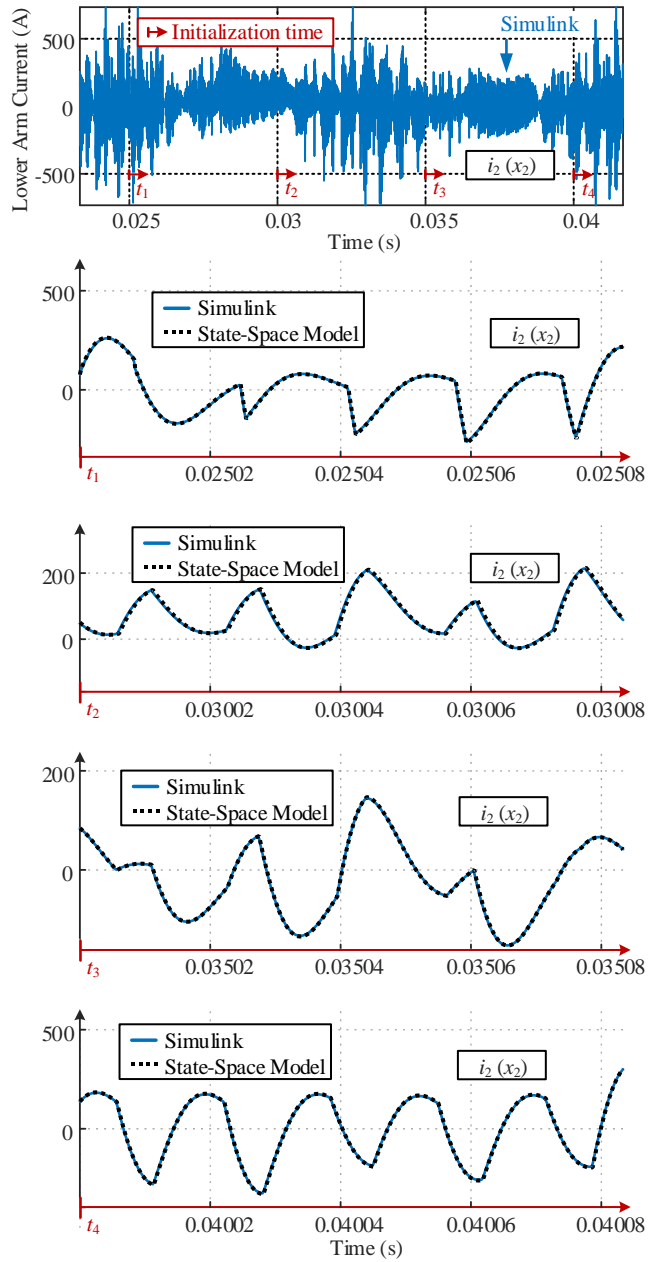


Figure 4.56 Lower arm current ( $x_2$ ) simulation and state-space model comparison.

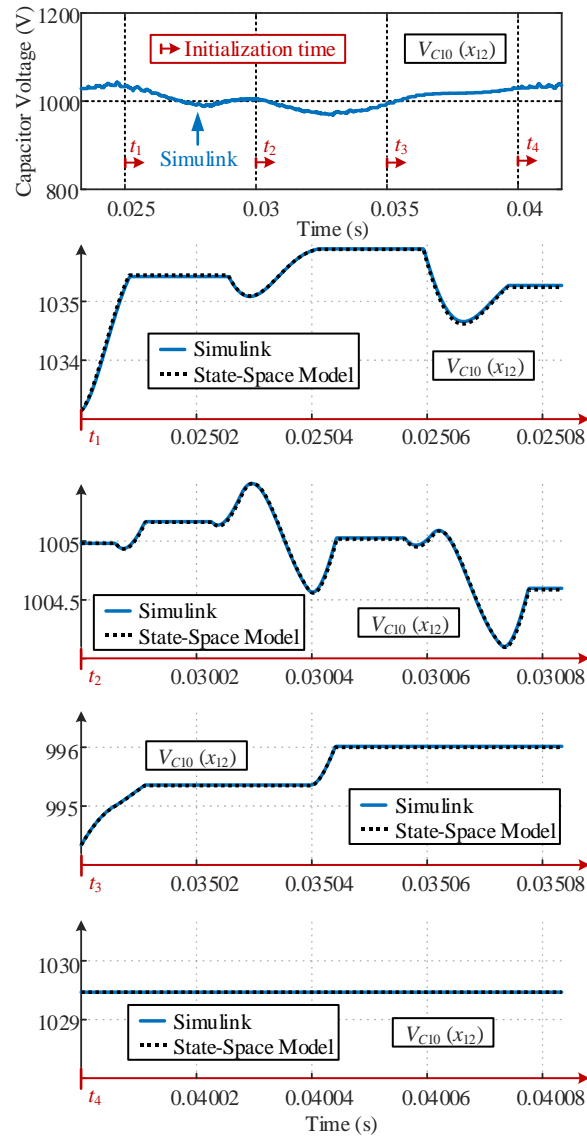


Figure 4.57 Capacitor voltage ( $x_{12}$ ) simulation and state-space model comparison.

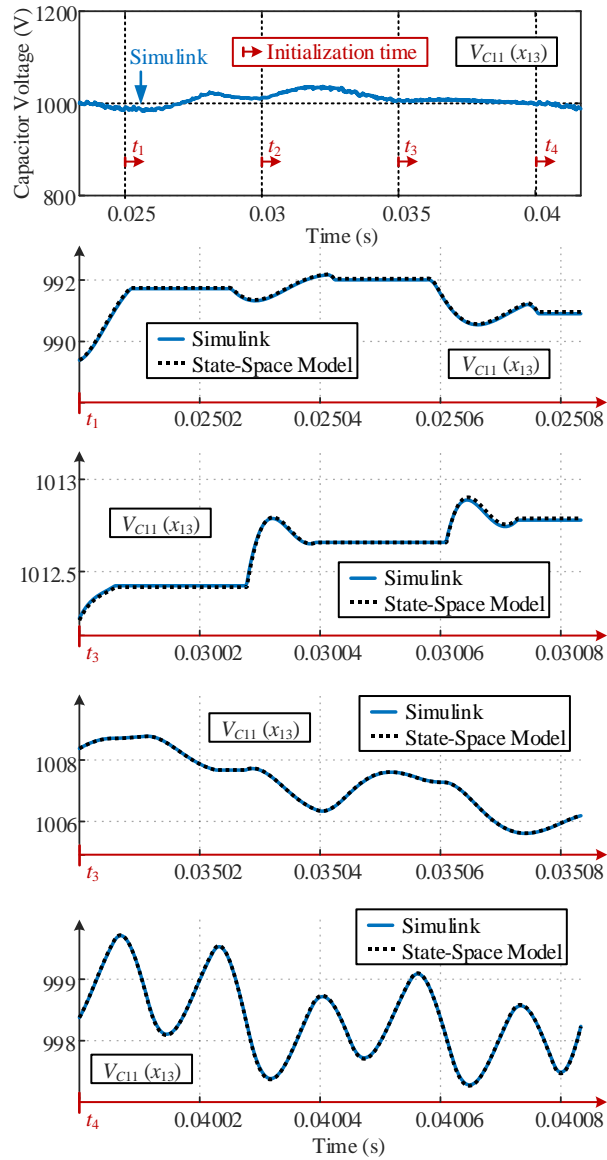
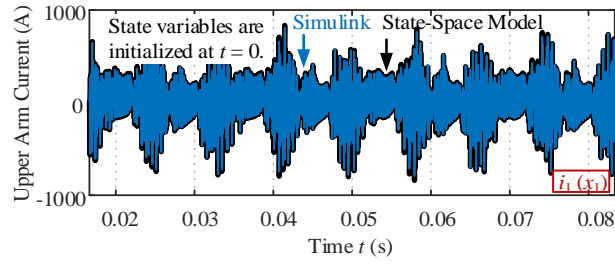
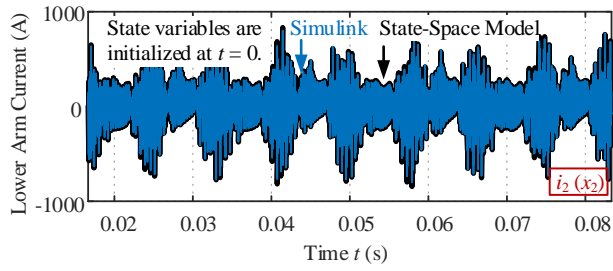


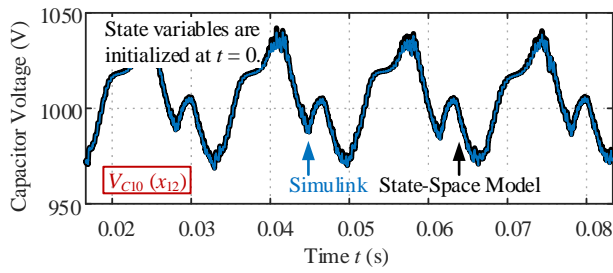
Figure 4.58 Capacitor voltage ( $x_{13}$ ) simulation and state-space model comparison.



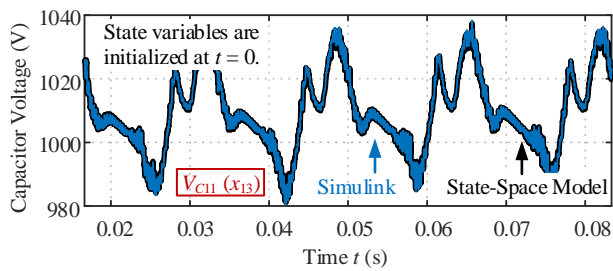
(a)



(b)



(c)



(d)

Figure 4.59 Comparison of simulation and state-space model in a long run. (a) Upper arm current; (b) lower arm current; (c) capacitor voltage  $V_{C10}$ ; (d) capacitor voltage  $V_{C11}$ .

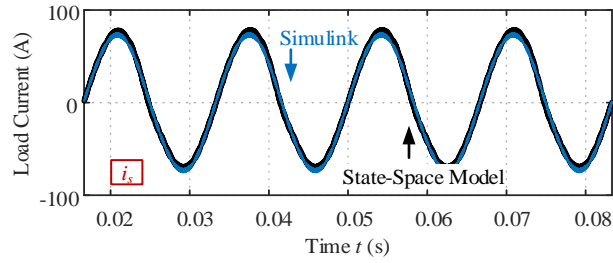


Figure 4.60 Load current  $i_s = x_1 - x_2$ .

## 4.9 CONCLUSION

This Chapter proposed a state-space model for MMC. With this state-space model, the MMC capacitor voltage convergence and divergence can be well captured. This state-space model can be used for stability analysis and understanding the mechanism of the self balance phenomenon in the future. The existing MMC modeling are developed on the basis of certain degree of assumptions and simplification. This makes them unsuitable for understanding the nature of this circuit from its physical basement. Compared to existing MMC modeling, the proposed state-space model well captured the MMC dynamics. Four-level MMC with both full-rank  $\Gamma$  and non-full-rank  $\Gamma$  are studied to demonstrate that this model could explain both convergence and divergence of the capacitor voltage. A generalized MMC model is derived, which can be applied to higher level. An eleven-level MMC case study is provided to verify the proposed model when extended to higher level.

## 5 THE ARM INDUCTORS VOLTAGE DROP ASSUMPTION

### 5.1 INTRODUCTION

The arm inductors are assumed to have zero voltage drop in the analysis of previous Chapters. This Chapter is going to address the critical value of inductor in terms of validating the assumption. In another word, this Chapter will address how large is this arm inductor to drive the system from convergence to divergence. This Chapter will start with the assumption of  $V_L=0$ . Then some simulations will be provided to verify the analysis.

### 5.2 DYNAMIC RESPONSE OF MMC IN SWITCHING CYCLES

To calculate the arm inductor voltage, we need to find the state equation of MMC. Figure5.1 shows the simplified MMC model. For a two-level MMC, there are two states at steady state, either the upper sub-module inserted, or the lower sub-module inserted. The following section will model the two-level MMC for each state.

#### 5.2.1 STATE I

Figure5.1(a) can be formulated as

$$\begin{cases} V_{L1} = L \frac{di_1}{dt} \\ V_{L2} = L \frac{di_2}{dt} \\ i_2 = C_2 \frac{dV_{C2}}{dt} \\ i_1 = i_2 + i_s \\ V_{dc} = V_{L1} + V_{L2} + V_{C2} \end{cases} \quad (5.1)$$

Define the state variables to be

$$\mathbf{X} = \begin{bmatrix} x_1 \\ x_2 \\ x_3 \end{bmatrix} = \begin{bmatrix} i_1 \\ i_2 \\ V_{C2} \end{bmatrix}, \quad \dot{\mathbf{X}} = \begin{bmatrix} \dot{x}_1 \\ \dot{x}_2 \\ \dot{x}_3 \end{bmatrix} = \begin{bmatrix} \frac{di_1}{dt} \\ \frac{di_2}{dt} \\ \frac{dV_{C2}}{dt} \end{bmatrix}. \quad (5.2)$$

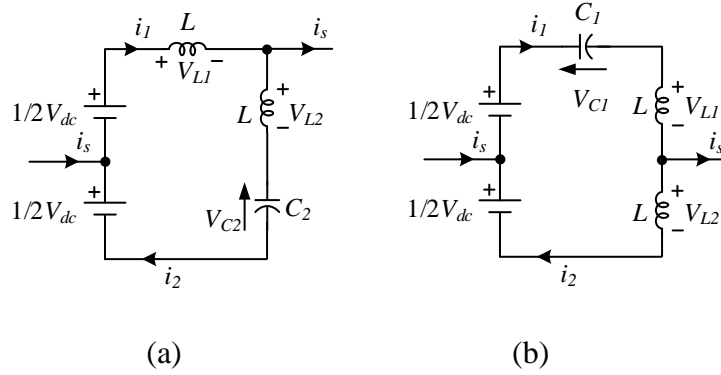


Figure 5.1 Two-level MMC model with pole connected to (a) positive dc rail; and (b) negative dc rail.

Rewrite (5.1) into state equation form,

$$\begin{cases} \dot{x}_1 = -\frac{1}{2L}x_3 + \frac{1}{2L}V_{dc} + \frac{1}{2}\frac{di_s}{dt} \\ \dot{x}_2 = -\frac{1}{2L}x_3 + \frac{1}{2L}V_{dc} - \frac{1}{2}\frac{di_s}{dt} \\ \dot{x}_3 = \frac{1}{C_2}x_2 \end{cases}, \quad (5.3)$$

$$\begin{bmatrix} \dot{x}_1 \\ \dot{x}_2 \\ \dot{x}_3 \end{bmatrix} = \begin{bmatrix} 0 & 0 & -\frac{1}{2L} \\ 0 & 0 & -\frac{1}{2L} \\ 0 & \frac{1}{C_2} & 0 \end{bmatrix} \begin{bmatrix} x_1 \\ x_2 \\ x_3 \end{bmatrix} + \begin{bmatrix} \frac{1}{2L} & \frac{1}{2} \\ \frac{1}{2L} & -\frac{1}{2} \\ 0 & 0 \end{bmatrix} \begin{bmatrix} V_{dc} \\ \frac{di_s}{dt} \end{bmatrix}. \quad (5.4)$$

Notice that  $\frac{di_s}{dt}$  reflects the voltage across the phase inductor. That is

$$L_a \frac{di_s}{dt} = v_a - V_s, \quad (5.5)$$

as modeled in Figure 5.2.

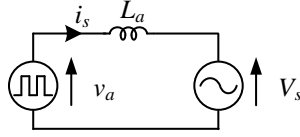


Figure 5.2 Phase inductor voltage modeling.

If the pole is attached to the positive dc rail, as shown in Figure 5.1(a),  $v_a = 1/2V_{dc}$ .

Eq.(5.5) can be modified as

$$\frac{di_s}{dt} = \frac{1}{L_a} \left( \frac{1}{2} V_{dc} - V_s \right). \quad (5.6)$$

Replace the  $\frac{di_s}{dt}$  in (5.4) by (5.6)

$$\begin{bmatrix} \dot{x}_1 \\ \dot{x}_2 \\ \dot{x}_3 \end{bmatrix} = \begin{bmatrix} 0 & 0 & -\frac{1}{2L} \\ 0 & 0 & -\frac{1}{2L} \\ 0 & \frac{1}{C_2} & 0 \end{bmatrix} \begin{bmatrix} x_1 \\ x_2 \\ x_3 \end{bmatrix} + \begin{bmatrix} \frac{1}{2L} & \frac{1}{2} \\ \frac{1}{2L} & -\frac{1}{2} \\ 0 & 0 \end{bmatrix} \begin{bmatrix} V_{dc} \\ \frac{1}{L_a} \left( \frac{1}{2} V_{dc} - V_s \right) \end{bmatrix}. \quad (5.7)$$

The system matrices are

$$\mathbf{A} = \begin{bmatrix} 0 & 0 & -\frac{1}{2L} \\ 0 & 0 & -\frac{1}{2L} \\ 0 & \frac{1}{C_2} & 0 \end{bmatrix}, \quad \mathbf{B} = \begin{bmatrix} \frac{1}{2L} & \frac{1}{2} \\ \frac{1}{2L} & -\frac{1}{2} \\ 0 & 0 \end{bmatrix}, \quad \text{and } \mathbf{U} = \begin{bmatrix} V_{dc} \\ \frac{1}{L_a} \left( \frac{1}{2} V_{dc} - V_s \right) \end{bmatrix}. \quad (5.8)$$

State equation (5.7) could be re-written as

$$\dot{\mathbf{X}} = \mathbf{A}\mathbf{X} + \mathbf{B}\mathbf{U}. \quad (5.9)$$

Apply the Laplace transform to (5.2), (5.8), and (5.9)

$$\mathcal{L}[\mathbf{X}(t)] = \mathbf{X}(s), \quad \mathcal{L}[\dot{\mathbf{X}}(t)] = s\mathbf{X}(s) - \mathbf{x}(0), \quad (5.10)$$

$$\mathcal{L}[\mathbf{U}(t)] = \mathbf{U}(s) = \begin{bmatrix} \frac{V_{dc}}{s} \\ \frac{1}{sL_a} \left( \frac{1}{2}V_{dc} - V_s \right) \end{bmatrix}, \quad (5.11)$$

$$s\mathbf{X}(s) - \mathbf{x}(0) = \mathbf{A}\mathbf{X}(s) + \mathbf{B}\mathbf{U}(s), \quad (5.12)$$

where  $\mathbf{x}(0) = [0 \quad -i_s \quad V_{dc}]^T$ . To solve for  $\mathbf{X}(s)$ ,

$$(s\mathbf{I} - \mathbf{A})\mathbf{X}(s) = \mathbf{x}(0) + \mathbf{B}\mathbf{U}(s), \quad (5.13)$$

$$\mathbf{X}(s) = (s\mathbf{I} - \mathbf{A})^{-1} (\mathbf{x}(0) + \mathbf{B}\mathbf{U}(s)), \quad (5.14)$$

$$\mathbf{X}(s) = \mathbf{\Phi}(\mathbf{x}(0) + \mathbf{B}\mathbf{U}(s)), \quad (5.15)$$

where  $\mathbf{\Phi} = (s\mathbf{I} - \mathbf{A})^{-1}$ .

$$\mathbf{\Phi} = \begin{bmatrix} \frac{1}{s} & \frac{-1}{s(2s^2LC_2 + 1)} & \frac{-C_2}{2s^2LC_2 + 1} \\ 0 & \frac{2sLC_2}{2s^2LC_2 + 1} & \frac{-C_2}{2s^2LC_2 + 1} \\ 0 & \frac{2L}{2s^2LC_2 + 1} & \frac{2sLC_2}{2s^2LC_2 + 1} \end{bmatrix}, \quad (5.16)$$

$$\begin{aligned} \mathbf{x}(0) + \mathbf{B}\mathbf{U}(s) &= \begin{bmatrix} 0 \\ -i_s \\ V_{dc} \end{bmatrix} + \begin{bmatrix} \frac{1}{2L} & \frac{1}{2} \\ \frac{1}{2L} & -\frac{1}{2} \\ 0 & 0 \end{bmatrix} \cdot \begin{bmatrix} \frac{V_{dc}}{s} \\ \frac{1}{sL_a} \left( \frac{1}{2}V_{dc} - V_s \right) \end{bmatrix} \\ &= \begin{bmatrix} \frac{V_{dc}}{2sL} + \frac{0.5V_{dc} - V_s}{2sL_a} \\ -i_s + \frac{V_{dc}}{2sL} - \frac{0.5V_{dc} - V_s}{2sL_a} \\ V_{dc} \end{bmatrix}, \end{aligned} \quad (5.17)$$

Hence,

$$\mathbf{X}(s) = \Phi(\mathbf{x}(0) + \mathbf{B}U(s)) = \begin{bmatrix} \frac{-2V_s + V_{dc} - 2sL_a i_s + s^2 LC_2 V_{dc} - 2s^2 LC_2 V_s}{2s^2 L_a \cdot (2s^2 LC_2 + 1)} \\ \frac{LC_2 \cdot (2V_s - V_{dc} - 4sL_a i_s)}{2L_a \cdot (2s^2 LC_2 + 1)} \\ \frac{4s^2 L_a LC_2 V_{dc} - 4sL_a L i_s - LV_{dc} + 2LV_s + 2L_a V_{dc}}{2sL_a \cdot (2s^2 LC_2 + 1)} \end{bmatrix}. \quad (5.18)$$

Laplace inverse transform,

$$\mathbf{X}(t) = \mathcal{L}^{-1}(\mathbf{X}(s))$$

$$= \begin{bmatrix} \frac{2L_a i_s \cos\left(\frac{t}{\sqrt{2LC_2}}\right) + \frac{\sqrt{2LC_2} \cdot V_{dc} \sin\left(\frac{t}{\sqrt{2LC_2}}\right)}{2} - \sqrt{2LC_2} \cdot V_s \sin\left(\frac{t}{\sqrt{2LC_2}}\right)}{2L_a} + i_s + \frac{(0.5V_{dc} - V_s) \cdot t}{L_a} \\ \frac{-2L_a i_s \cos\left(\frac{t}{\sqrt{2LC_2}}\right) + \frac{\sqrt{2LC_2} \cdot V_{dc} \sin\left(\frac{t}{\sqrt{2LC_2}}\right)}{2} - \sqrt{2LC_2} \cdot V_s \sin\left(\frac{t}{\sqrt{2LC_2}}\right)}{2L_a} \\ \frac{LV_s - 0.5LV_{dc} + L_a V_{dc}}{L_a} + \frac{L\sqrt{C_2} \cdot V_{dc} \cos\left(\frac{t}{\sqrt{2LC_2}}\right) - 2L\sqrt{C_2} \cdot V_s \cos\left(\frac{t}{\sqrt{2LC_2}}\right) - 2\sqrt{2L} \cdot L_a i_s \sin\left(\frac{t}{\sqrt{2LC_2}}\right)}{2L_a \sqrt{C_2}} \end{bmatrix} \quad (5.19)$$

$$i_1(t) = \underbrace{-i_s \cos\left(\frac{t}{\sqrt{2LC_2}}\right) - \frac{(0.5V_{dc} - V_s) \cdot \sqrt{2LC_2} \cdot \sin\left(\frac{t}{\sqrt{2LC_2}}\right)}{2L_a}}_{\text{Transient}} + \underbrace{i_s + \frac{(0.5V_{dc} - V_s) \cdot t}{L_a}}_{\text{Steady State}}, \quad (5.20)$$

$$i_2(t) = \underbrace{-i_s \cos\left(\frac{t}{\sqrt{2LC_2}}\right) - \frac{(0.5V_{dc} - V_s) \cdot \sqrt{2LC_2} \cdot \sin\left(\frac{t}{\sqrt{2LC_2}}\right)}{2L_a}}_{\text{Transient}} + \underbrace{0}_{\text{Steady State}}, \quad (5.21)$$

$$V_{C_2}(t) = \underbrace{\frac{L}{L_a} \cdot (0.5V_{dc} - V_s) \cdot \cos\left(\frac{t}{\sqrt{2LC_2}}\right) - \sqrt{\frac{2L}{C_2}} \cdot i_s \sin\left(\frac{t}{\sqrt{2LC_2}}\right)}_{\text{Transient}} + \underbrace{V_{dc} - \frac{L}{L_a} (0.5V_{dc} - V_s)}_{\text{Steady State}}. \quad (5.22)$$

Eq. (5.20), (5.21), and (5.22) are the dynamic response of upper arm current, lower arm current, and  $C_2$  voltage, respectively, in State I. All these three functions can be divided by two components, the transient component and the steady-state components.

### 5.2.2 STATE II

The dynamic response of State II is similar to State I. Therefore, the derivation is omitted. Figure 5.1(b) can be formulated by

$$\begin{bmatrix} \dot{x}_1 \\ \dot{x}_2 \\ \dot{x}_3 \end{bmatrix} = \begin{bmatrix} 0 & 0 & -\frac{1}{2L} \\ 0 & 0 & -\frac{1}{2L} \\ \frac{1}{C_1} & 0 & 0 \end{bmatrix} \begin{bmatrix} x_1 \\ x_2 \\ x_3 \end{bmatrix} + \begin{bmatrix} \frac{1}{2L} & \frac{1}{2} \\ \frac{1}{2L} & -\frac{1}{2} \\ 0 & 0 \end{bmatrix} \begin{bmatrix} V_{dc} \\ \frac{di_s}{dt} \end{bmatrix}. \quad (5.23)$$

Apply the Laplace transform and Laplace inverse transform to (5.23), yields

$$\mathbf{X}(t) = \mathcal{L}^{-1}(\mathbf{X}(s))$$

$$= \begin{bmatrix} \frac{-\left(\sqrt{2LC_1} \cdot V_{dc} \sin\left(\frac{t}{\sqrt{2LC_1}}\right) - 4L_a i_s \cos\left(\frac{t}{\sqrt{2LC_1}}\right) + 2\sqrt{2LC_1} \cdot V_s \sin\left(\frac{t}{\sqrt{2LC_1}}\right)\right)}{4L_a} \\ \frac{(0.5V_{dc} + V_s)t}{L_a} - i_s - \frac{\left(\sqrt{2LC_1} \cdot V_{dc} \sin\left(\frac{t}{\sqrt{2LC_1}}\right) - 4L_a i_s \cos\left(\frac{t}{\sqrt{2LC_1}}\right) + 2\sqrt{2LC_1} \cdot V_s \sin\left(\frac{t}{\sqrt{2LC_1}}\right)\right)}{4L_a} \\ - \frac{LV_s + 0.5LV_{dc} - L_a V_{dc}}{L_a} + \frac{L\sqrt{C_1} \cdot V_{dc} \cos\left(\frac{t}{\sqrt{2LC_1}}\right) + 2L\sqrt{C_1} \cdot V_s \cos\left(\frac{t}{\sqrt{2LC_1}}\right) + 2\sqrt{2L} \cdot L_a i_s \sin\left(\frac{t}{\sqrt{2LC_1}}\right)}{2L_a \sqrt{C_1}} \end{bmatrix} \quad (5.24)$$

$$i_1(t) = \underbrace{i_s \cos\left(\frac{t}{\sqrt{2LC_1}}\right)}_{\text{Transient}} - \frac{(0.5V_{dc} + V_s)\sqrt{2LC_1} \cdot \sin\left(\frac{t}{\sqrt{2LC_1}}\right)}{2L_a} + \underbrace{0}_{\text{Steady State}}, \quad (5.25)$$

$$i_2(t) = \underbrace{i_s \cos\left(\frac{t}{\sqrt{2LC_1}}\right)}_{\text{Transient}} - \frac{(0.5V_{dc} + V_s)\sqrt{2LC_1} \cdot \sin\left(\frac{t}{\sqrt{2LC_1}}\right)}{2L_a} + \underbrace{\frac{(0.5V_{dc} + V_s)t}{L_a} - i_s}_{\text{Steady State}}, \quad (5.26)$$

$$V_{C1}(t) = \underbrace{\frac{L}{L_a} \cdot (0.5V_{dc} + V_s) \cdot \cos\left(\frac{t}{\sqrt{2LC_1}}\right)}_{\text{Transient}} + \underbrace{\sqrt{\frac{2L}{C_1}} \cdot i_s \sin\left(\frac{t}{\sqrt{2LC_1}}\right) + V_{dc} - \frac{L}{L_a} (0.5V_{dc} + V_s)}_{\text{Steady State}}. \quad (5.27)$$

Eq.(25), (26), and (27) are the dynamic response of upper arm current, lower arm current, and  $C_1$  voltage, respectively, in State II. All these three functions can be divided by two components, the transient component and the steady-state components. The transient component will be damped with a coefficient of  $e^{-t/\tau}$ , where  $\tau = 2L/R_{eq}$ .  $L$  is the arm inductance and  $R_{eq}$  is the equivalent resistance of power loss.

### 5.3 ZERO VOLTAGE DROP ASSUMPTION

The transient component should be damped down to zero if resistance exists in circuit. In real MMC prototype, there always 2-4% power loss and this power dissipation can be modeled by resistance.

In order to assume the inductor voltage to be zero, the transient needs to be much faster than the switching frequency. From (5.20)-(5.22) and (5.25)-(5.27), we can see that the oscillation frequency and the damping time constant of the transient are

$$\omega_0 = \sqrt{\frac{1}{LC_{eq}}} \quad (5.28)$$

$$\tau = 2L/R_{eq} \quad (5.29)$$

Where  $\omega_0$  is the resonance frequency.  $L$  is the arm inductor and  $C_{eq}$  is the equivalent capacitance of the submodules.  $\tau$  is the time constant.  $R_{eq}$  is the equivalent converter loss. Therefore,  $\tau < T_{sw}$  is the condition that guarantees the assumption to hold true, where  $T_{sw}$  is the switching period.

When  $L$  is small, e.g., zero, then the above condition will automatically hold true. and at each switching instant, charging balance occurs. However, the charging and discharging current would be inrush (or impulse) current that may be not good for devices and noises. Then in order to limit inrush charging/discharging current, we have to have a minimum

inductance to make sure the inrush charging/discharging current below 3 times rated load current.

## 5.4 SIMULATION

In this chapter, several simulations with various arm inductances are examined to verify the analysis in Chapter 5.3 and 5.4. The simulation topology is shown in Figure 5.3.

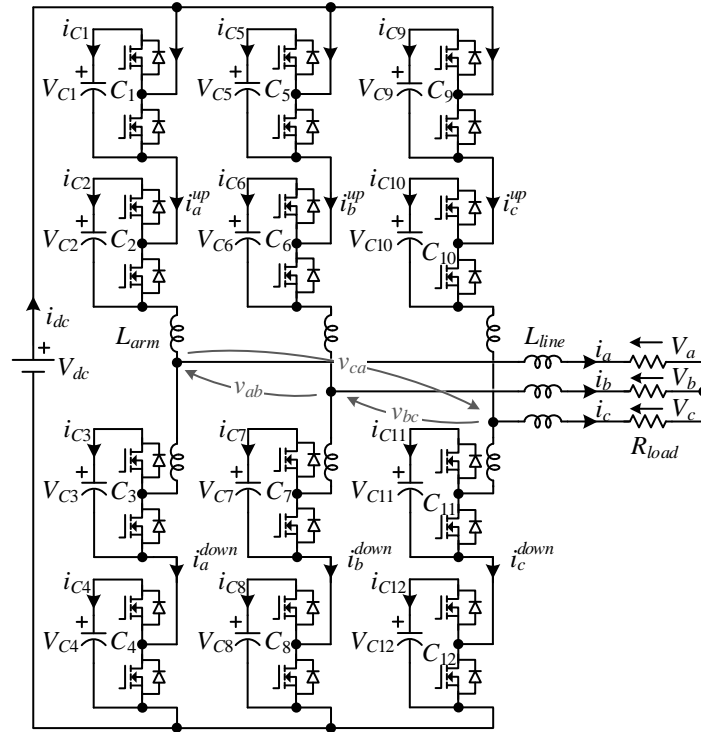


Figure 5.3 Three-level MMC simulation topology.

**Parameters:** The key parameters of the MMC are as follows: rated apparent power  $S = 100$  kVA, output phase voltage  $V_a = V_b = V_c = 643$  V, output line current  $I_a = I_b = I_c = 52$  A, rated output fundamental frequency  $f_0 = 60$  Hz, rated load resistance  $R_{load} = 12.4 \Omega$ , rated dc-bus voltage  $V_{dc} = 2$  kV, number of sub-modules per arm:  $N - 1 = 2$ , sub-module capacitance  $C_i = 85 \mu\text{F}$  ( $i = 1, 2, \dots, 12$ ), line inductance  $L_{line} = 4$  mH. The switching frequency is  $f_{sw} = 5$  kHz. The power loss is modeled by a stray resistor  $R = 0.4 \Omega$  (3.6% p.u.). The arm inductance  $L_{arm}$  varies case by case.

### 5.4.1 $\tau / T_{sw} = 0.02$

The time constant of the system is smaller than switching period in this case study.  $V_L = 0$  holds true in this case. The key parameters are summarized in Table 14.

Table 14

Three-level MMC simulation key parameters.

Apparent Power, $S$	100 kVA
Fundamental Frequency, $f_0$	60 Hz
Switching Frequency, $f_{sw}$	5 kHz
DC-Bus Voltage, $V_{dc}$	2000 V
Phase Voltage, $V_a, V_b, V_c$	643 V
Line Current, $I_a, I_b, I_c$	52 A
Load Resistance, $R_{load}$	12.4 $\Omega$
Line Inductance, $L_{line}$	4 mH
Arm Inductance, $L_{arm}$	0.8 $\mu$ H
Stray Resistance, $R$	0.4 $\Omega$ (3.2% p.u.)
Sub-Module Capacitance, $C_i$	85 $\mu$ F
Number of Sub-Modules per Arm	2
Time Ratio $\tau / T_{sw}$	0.02
Resonant Frequency, $f_0$	27 kHz

where  $i = 1, 2, \dots, 12$ .

The capacitor voltage is well balanced and converging to the expected dc voltage (1000 V) in Figure5.6. The load voltage and current are shown in Figure5.4. The mid-point voltage is shown in Figure5.5. The sub-module capacitor voltage and current are shown in

Figure 5.6 The arm inductor current is shown in Figure 5.7. The arm inductor current is limited within 2 times the load current.

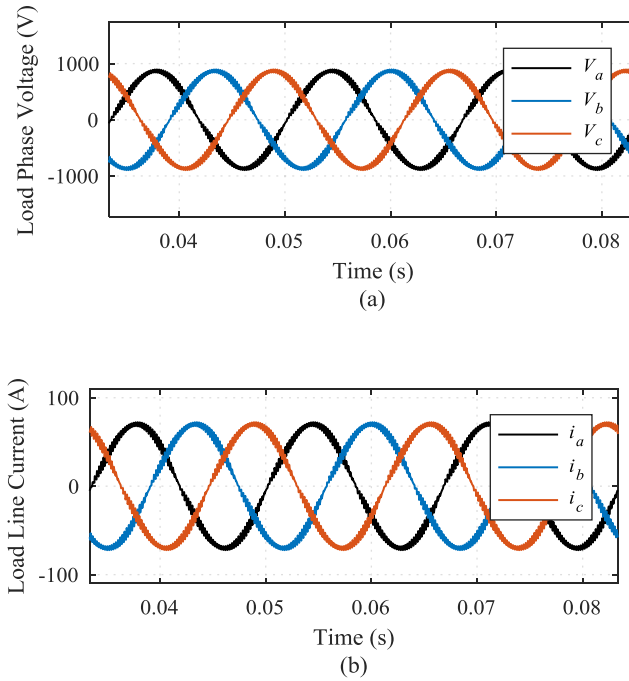


Figure 5.4 Three-level MMC (a) load voltage and (b) load current.

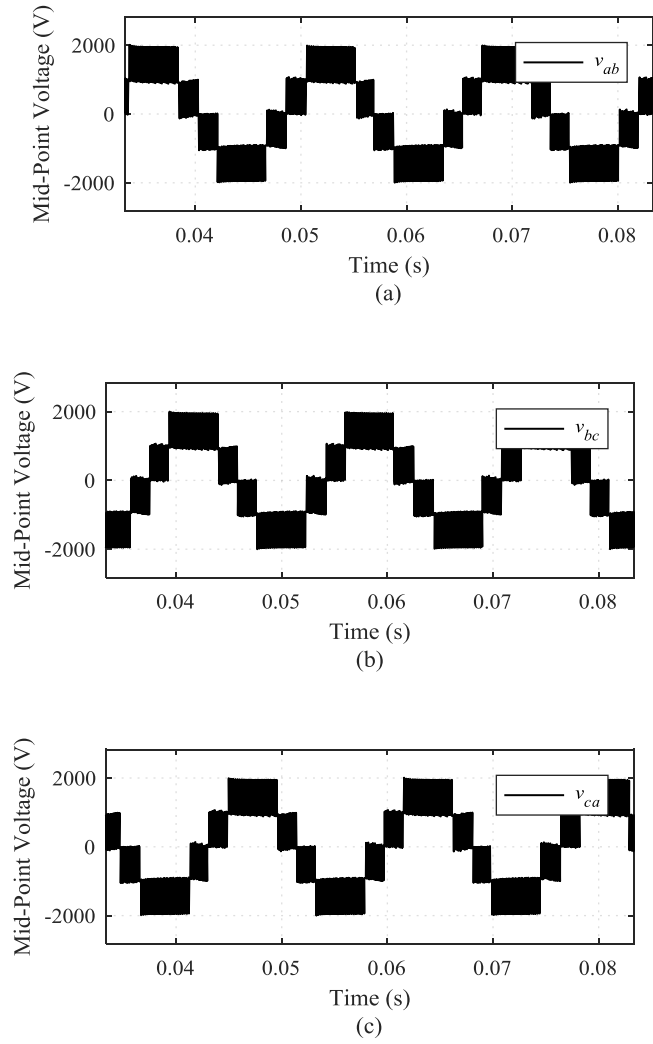


Figure 5.5 Three-level MMC mid-point voltage (a)  $v_{ab}$ ; (b)  $v_{bc}$ ; and (c)  $v_{ca}$ .

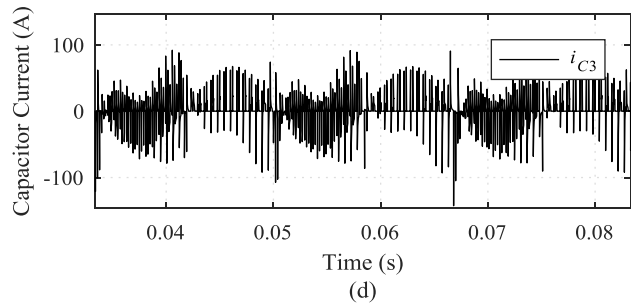
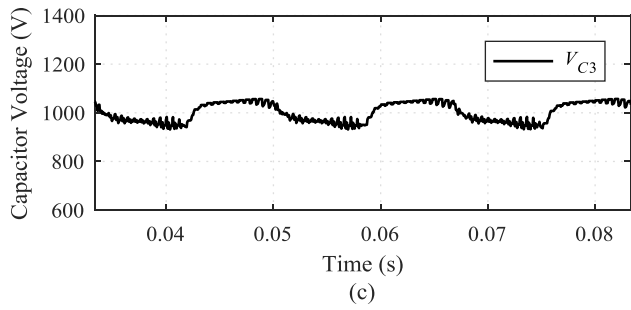
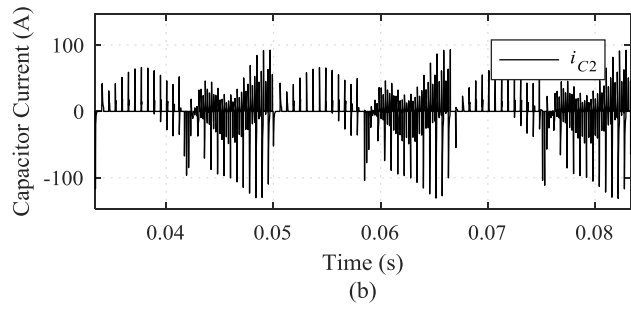
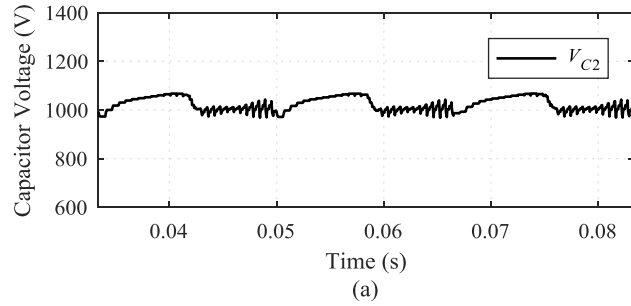


Figure 5.6 Sub-module capacitor (a)/(c) voltage; and (b)/(d) current.

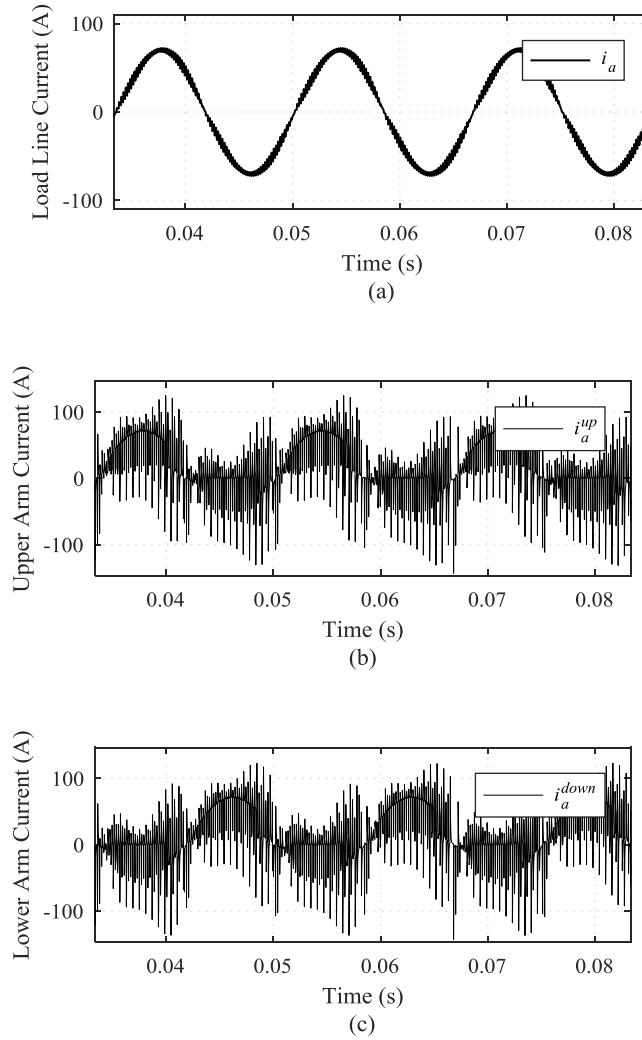


Figure 5.7 (a) Line current and its corresponding (b) upper arm current, (c) lower arm current.

#### 5.4.2 $\tau / T_{sw} = 0.25$

The time constant of the system is smaller than switching period in this case study.  $V_L = 0$  holds true in this case. The key parameters are summarized in Table 15.

Table 15

Three-level MMC simulation key parameters.

Apparent Power, $S$	100 kVA
Fundamental Frequency, $f_0$	60 Hz
Switching Frequency, $f_{sw}$	5 kHz
DC-Bus Voltage, $V_{dc}$	2000 V
Phase Voltage, $V_a, V_b, V_c$	643 V
Line Current, $I_a, I_b, I_c$	52 A
Load Resistance, $R_{load}$	12.4 $\Omega$
Line Inductance, $L_{line}$	4 mH
Arm Inductance, $L_{arm}$	10 $\mu$ H
Stray Resistance, $R$	0.4 $\Omega$ (3.2% p.u.)
Sub-Module Capacitance, $C_i$	85 $\mu$ F
Number of Sub-Modules per Arm	2
Time Ratio $\tau / T_{sw}$	0.25
Resonant Frequency, $f_0$	7.7 kHz

where  $i = 1, 2, \dots, 12$ .

The capacitor voltage is well balanced and converging to the expected dc voltage (1000 V) in Figure5.10. The load voltage and current are shown in Figure5.8. The mid-point voltage is shown in Figure5.9. The sub-module capacitor voltage and current are shown in Figure5.10. The arm inductor current is shown in Figure5.11. The arm inductor current is limited within 2 times the load current.

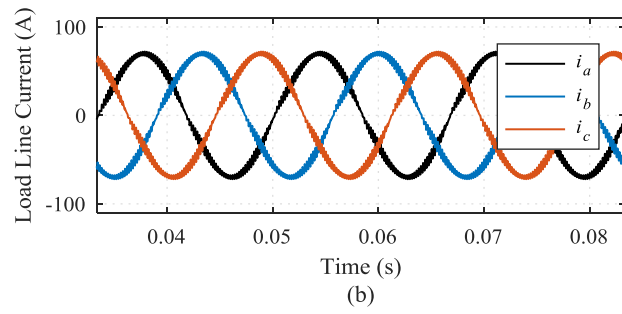
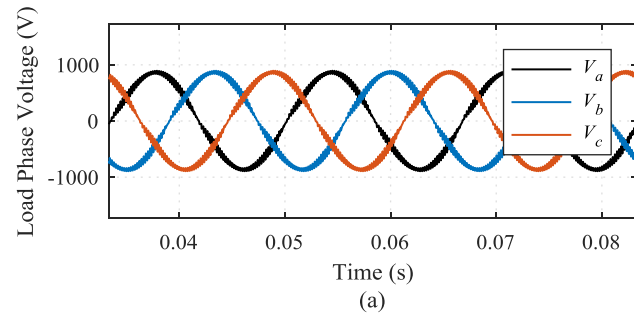


Figure 5.8 Three-level MMC (a) load voltage and (b) load current.

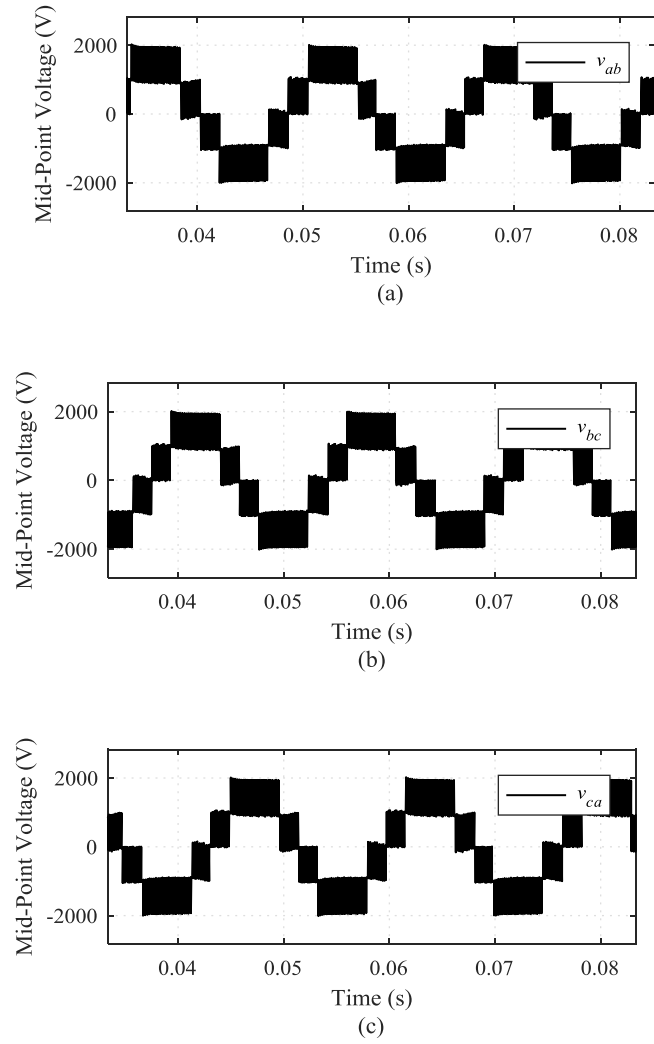


Figure 5.9 Three-level MMC mid-point voltage (a)  $v_{ab}$ ; (b)  $v_{bc}$ ; and (c)  $v_{ca}$ .

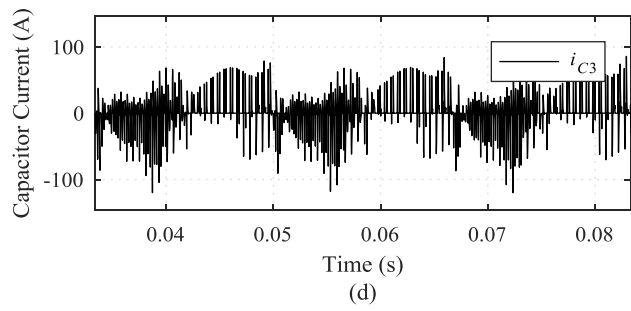
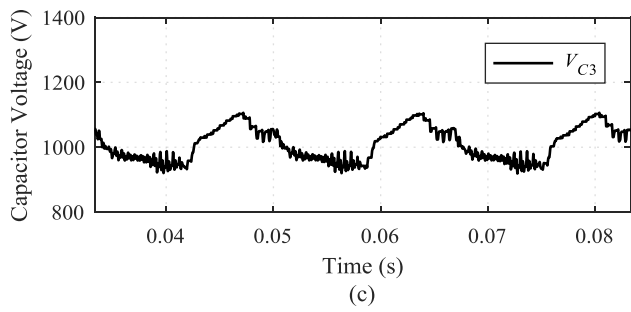
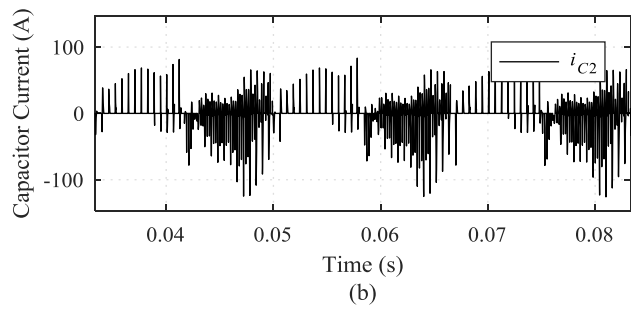
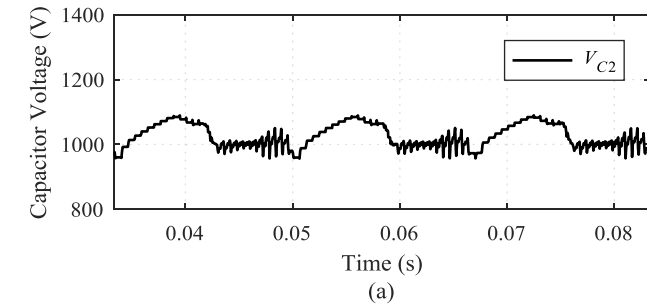


Figure 5.10 Sub-module capacitor (a)/(c) voltage; and (b)/(d) current.

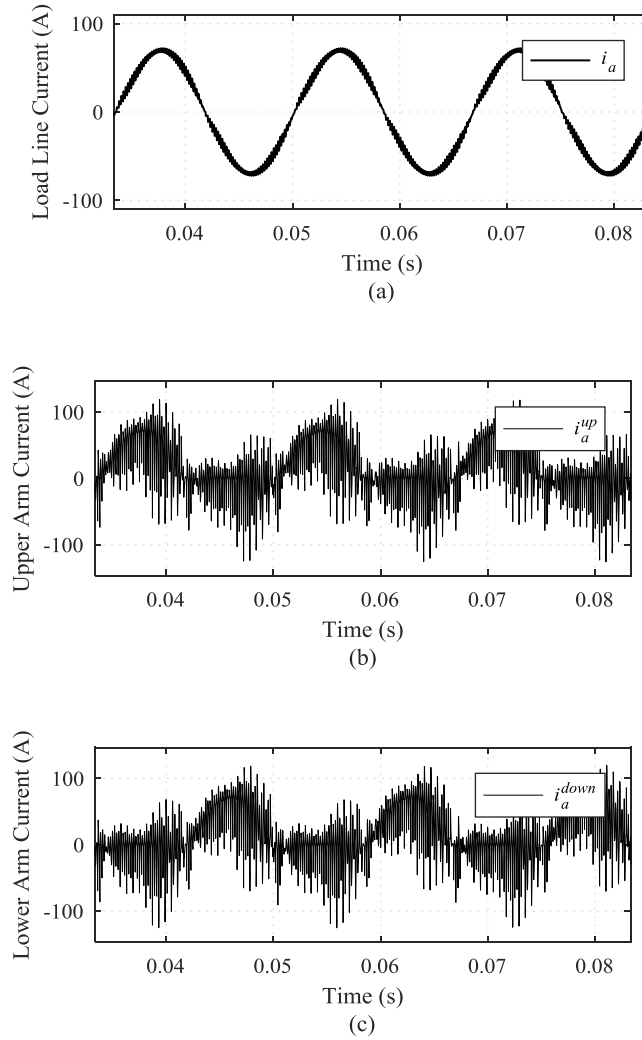


Figure 5.11 (a) Line current and its corresponding (b) upper arm current, (c) lower arm current.

### 5.4.3 $\tau / T_{sw} = 1$

The time constant of the system is equal to the switching period in this case study.  $V_L = 0$  does not hold true in this case. The key parameters are summarized in Table 16.

Table 16

Three-level MMC simulation key parameters.

Apparent Power, $S$	100 kVA
Fundamental Frequency, $f_0$	60 Hz
Switching Frequency, $f_{sw}$	5 kHz
DC-Bus Voltage, $V_{dc}$	2000 V
Phase Voltage, $V_a, V_b, V_c$	643 V
Line Current, $I_a, I_b, I_c$	52 A
Load Resistance, $R_{load}$	12.4 $\Omega$
Line Inductance, $L_{line}$	4 mH
Arm Inductance, $L_{arm}$	40 $\mu$ H
Stray Resistance, $R$	0.4 $\Omega$ (3.2% p.u.)
Sub-Module Capacitance, $C_i$	85 $\mu$ F
Number of Sub-Modules per Arm	2
Time Ratio $\tau / T_{sw}$	1
Resonant Frequency, $f_0$	3.8 kHz

where  $i = 1, 2, \dots, 12$ .

The capacitor voltage is well balanced and converging to the expected dc voltage (1000 V) in Figure5.14. However, the voltage ripple is around 40%. Normally, this voltage ripple is deemed to be abnormal operation. The load voltage and current are shown in Figure5.12. The load voltage and current are distorted since the high voltage ripple on capacitors. The mid-point voltage is shown in Figure5.13. The sub-module capacitor voltage and current

are shown in Figure 5.14. The arm inductor current is shown in Figure 5.15. The arm inductor current is limited within 2 times the load current.

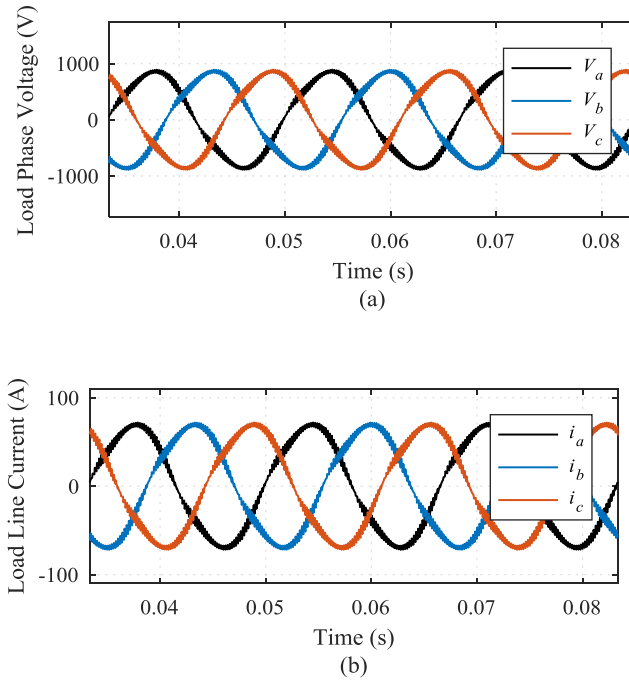


Figure 5.12 Three-level MMC (a) load voltage and (b) load current.

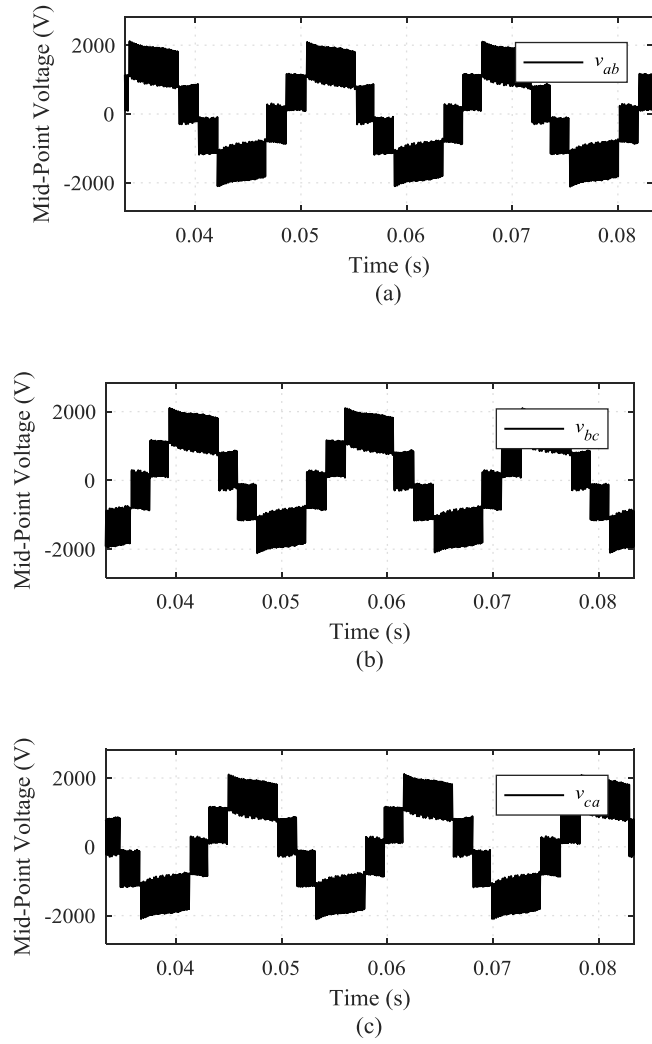


Figure 5.13 Three-level MMC mid-point voltage (a)  $v_{ab}$ ; (b)  $v_{bc}$ ; and (c)  $v_{ca}$ .

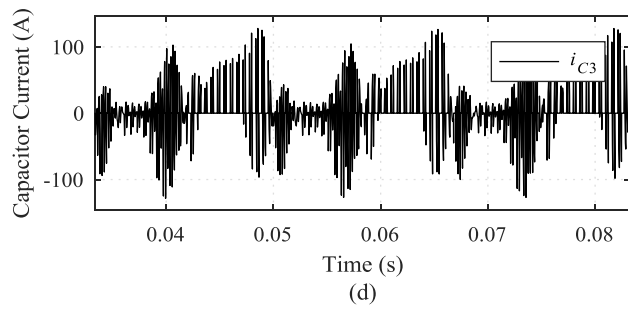
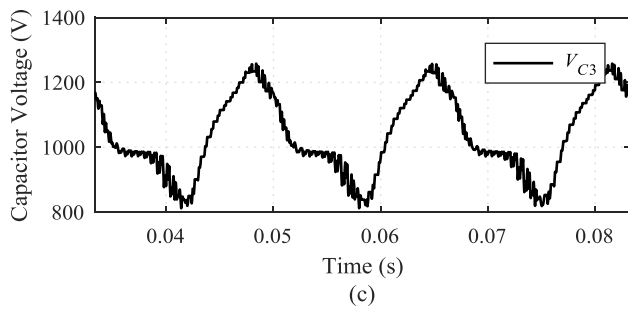
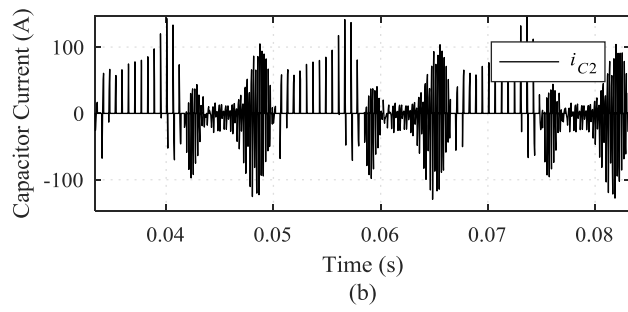
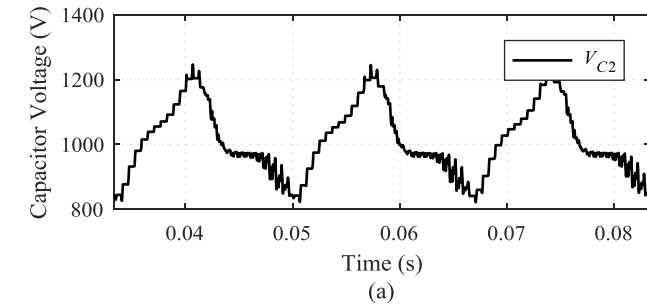


Figure 5.14 Sub-module capacitor (a)/(c) voltage; and (b)/(d) current.

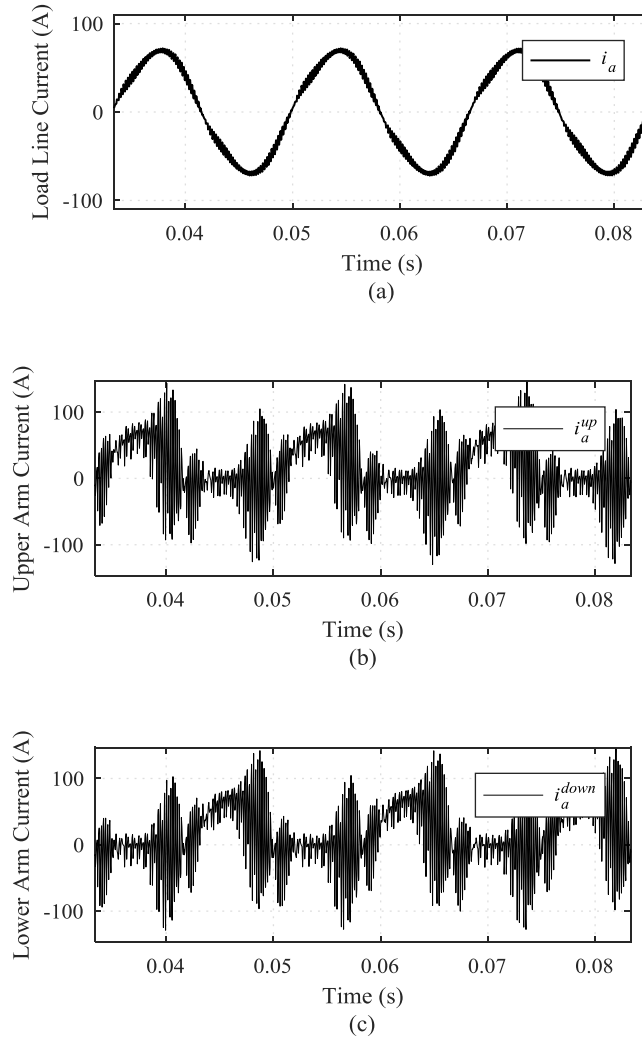


Figure 5.15 (a) Line current and its corresponding (b) upper arm current, (c) lower arm current.

#### 5.4.4 $\tau / T_{sw} = 2$

The time constant of the system is greater than switching period in this case study.  $V_L = 0$  does not hold true in this case. The key parameters are summarized in Table 17.

Table 17

Three-level MMC simulation key parameters.

Apparent Power, $S$	100 kVA
Fundamental Frequency, $f_0$	60 Hz
Switching Frequency, $f_{sw}$	5 kHz
DC-Bus Voltage, $V_{dc}$	2000 V
Phase Voltage, $V_a, V_b, V_c$	643 V
Line Current, $I_a, I_b, I_c$	52 A
Load Resistance, $R_{load}$	12.4 $\Omega$
Line Inductance, $L_{line}$	4 mH
Arm Inductance, $L_{arm}$	80 $\mu$ H
Stray Resistance, $R$	0.4 $\Omega$ (3.2% p.u.)
Sub-Module Capacitance, $C_i$	85 $\mu$ F
Number of Sub-Modules per Arm	2
Time Ratio $\tau / T_{sw}$	2
Resonant Frequency, $f_0$	2.7 kHz

where  $i = 1, 2, \dots, 12$ .

The capacitor voltage is well balanced and converging to the expected dc voltage (1000 V) in Figure5.18. However, the voltage ripple is around 40%. Normally, this voltage ripple is deemed to be abnormal operation. The load voltage and current are shown in Figure5.16. The load voltage and current are distorted since the high voltage ripple on capacitors. The mid-point voltage is shown in Figure5.17. The sub-module capacitor voltage and current

are shown in Figure 5.18. The arm inductor current is shown in Figure 5.19. The arm inductor current is limited within 1.5 times the load current.

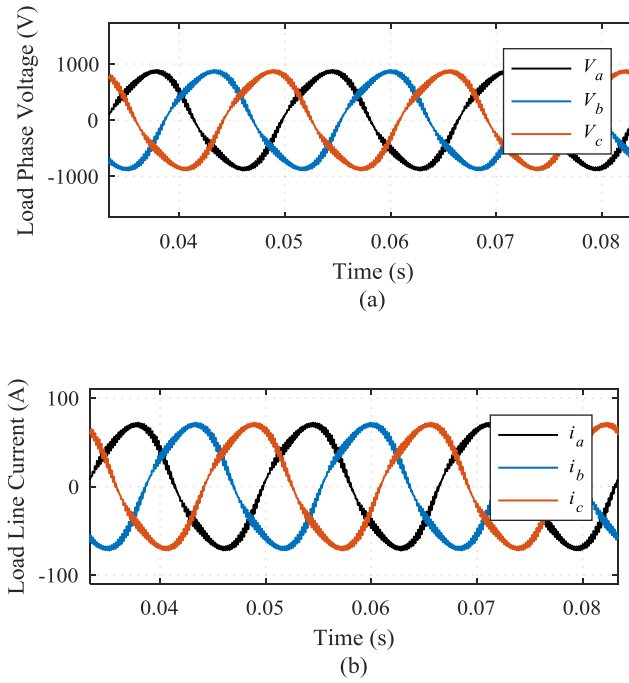
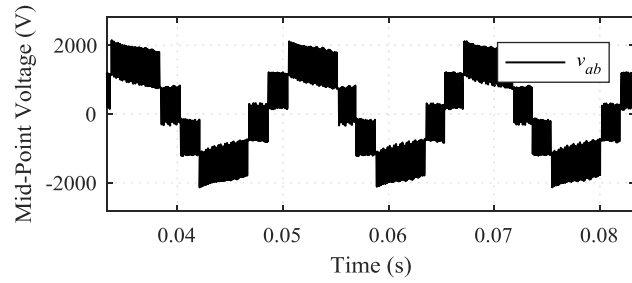
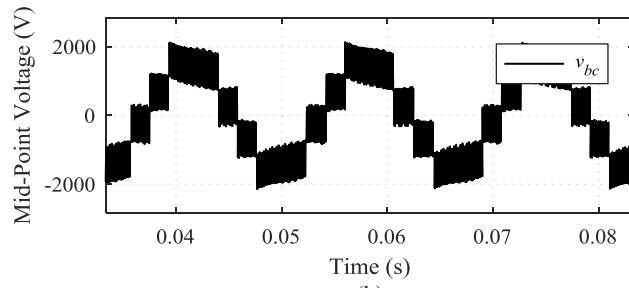


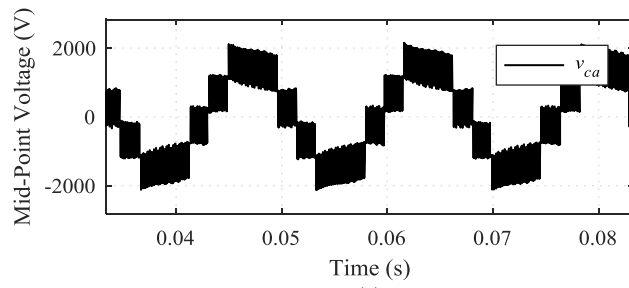
Figure 5.16 Three-level MMC (a) load voltage and (b) load current.



(a)



(b)



(c)

Figure 5.17 Three-level MMC mid-point voltage (a)  $v_{ab}$ ; (b)  $v_{bc}$ ; and (c)  $v_{ca}$ .

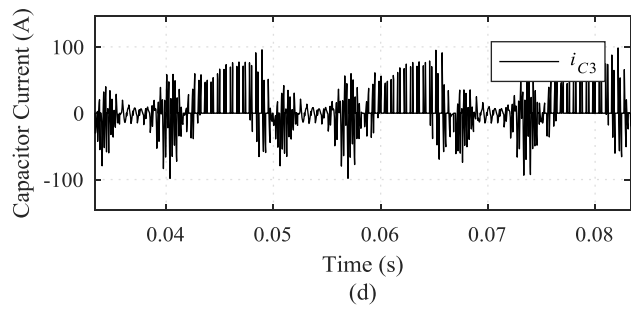
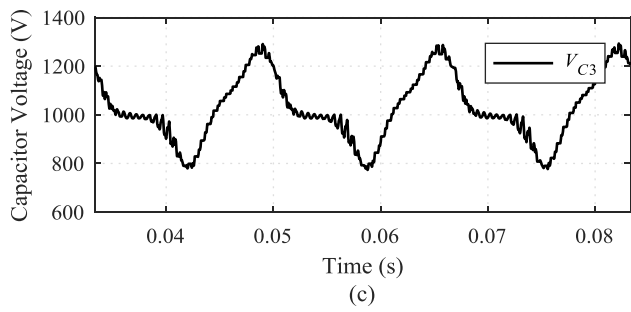
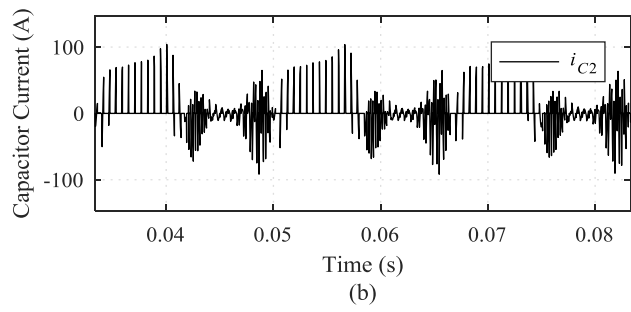
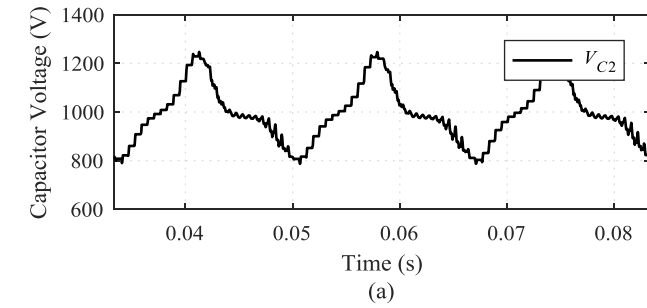


Figure 5.18 Sub-module capacitor (a)/(c) voltage; and (b)/(d) current.

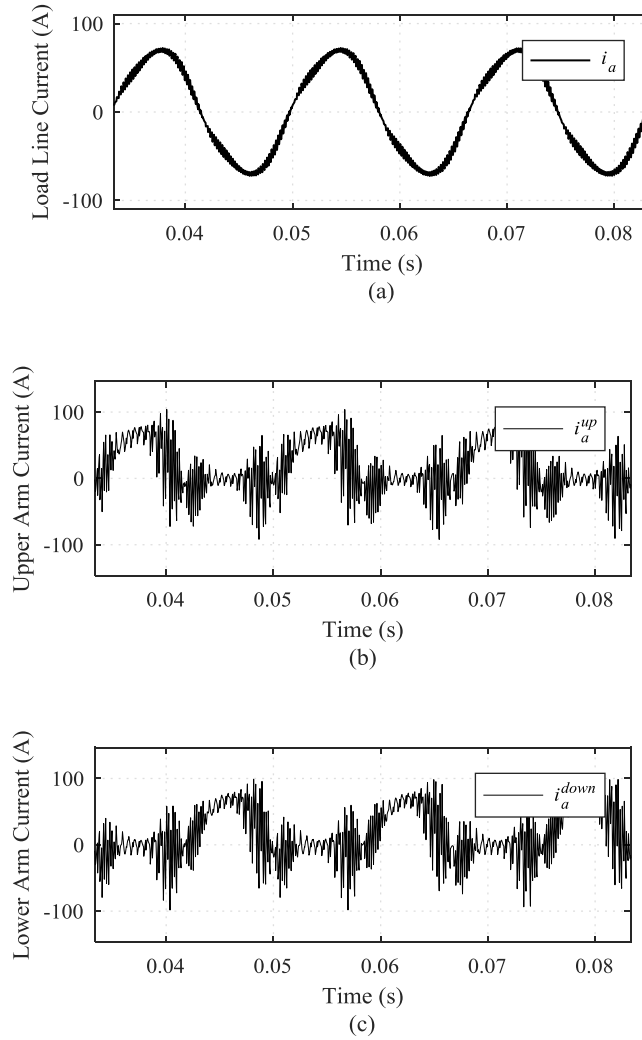


Figure 5.19 (a) Line current and its corresponding (b) upper arm current, (c) lower arm current.

#### 5.4.5 $\tau / T_{sw} = 10$

The time constant of the system is smaller than switching period in this case study.  $V_L = 0$  does not hold true in this case. The key parameters are summarized in Table 18.

Table 18

Three-level MMC simulation key parameters.

Apparent Power, $S$	100 kVA
Fundamental Frequency, $f_0$	60 Hz
Switching Frequency, $f_{sw}$	5 kHz
DC-Bus Voltage, $V_{dc}$	2000 V
Phase Voltage, $V_a, V_b, V_c$	643 V
Line Current, $I_a, I_b, I_c$	52 A
Load Resistance, $R_{load}$	12.4 $\Omega$
Line Inductance, $L_{line}$	4 mH
Arm Inductance, $L_{arm}$	400 $\mu$ H
Stray Resistance, $R$	0.4 $\Omega$ (3.2% p.u.)
Sub-Module Capacitance, $C_i$	85 $\mu$ F
Number of Sub-Modules per Arm	2
Time Ratio $\tau / T_{sw}$	10
Resonant Frequency, $f_0$	1.2 kHz

where  $i = 1, 2, \dots, 12$ .

The capacitor voltage is diverging from the nominal dc voltage (1000 V) in Figure5.22. Normally, this voltage ripple is deemed to be abnormal operation. The load voltage and current are shown in Figure5.20. The load voltage and current are distorted since the high voltage ripple on capacitors. The mid-point voltage is shown in Figure5.21. The sub-module capacitor voltage and current are shown in Figure5.22. The arm inductor current is shown in Figure5.23.

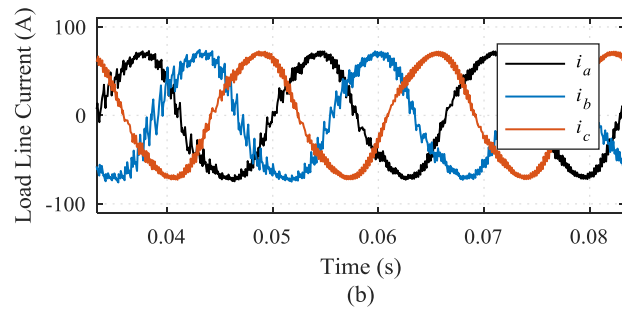
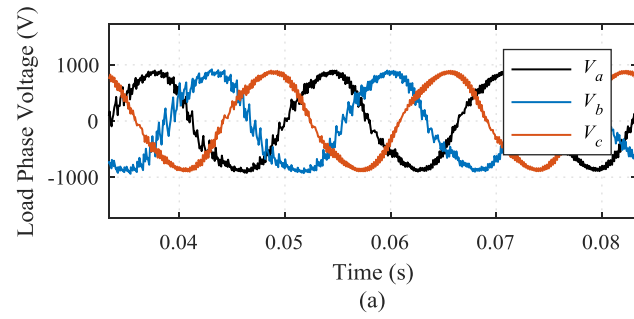


Figure 5.20 Three-level MMC (a) load voltage and (b) load current.

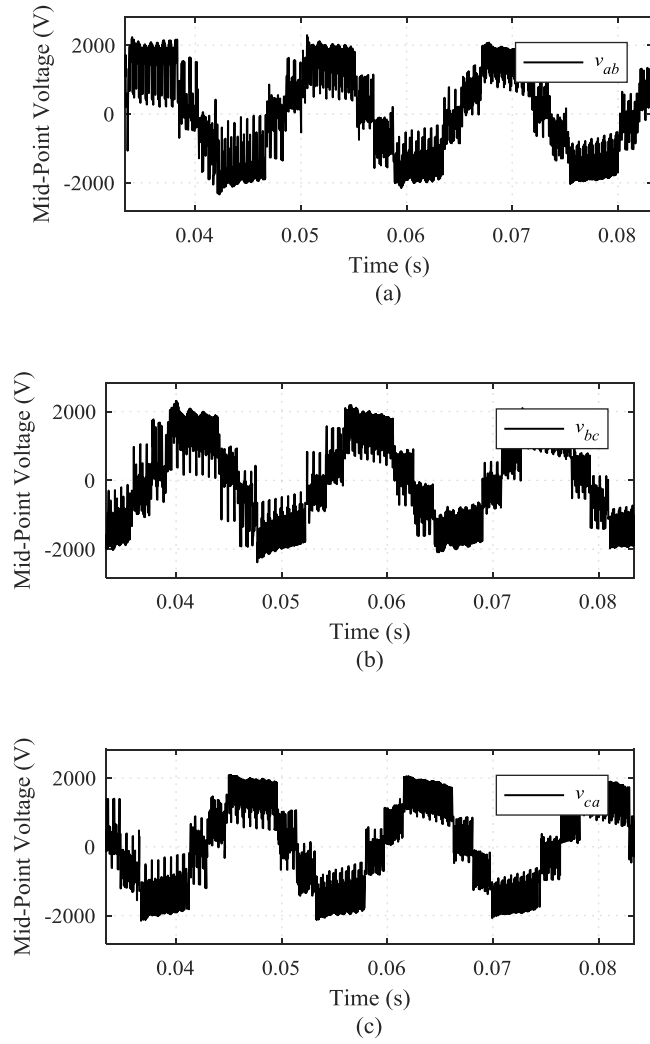


Figure 5.21 Three-level MMC mid-point voltage (a)  $v_{ab}$ ; (b)  $v_{bc}$ ; and (c)  $v_{ca}$ .

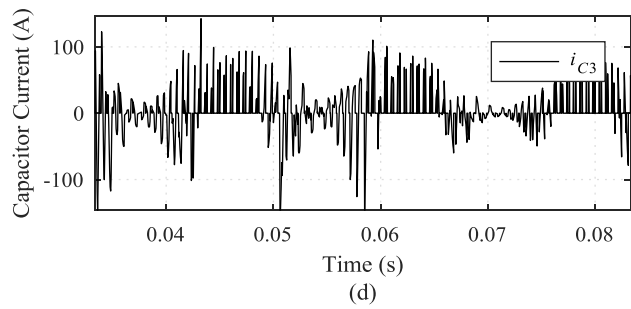
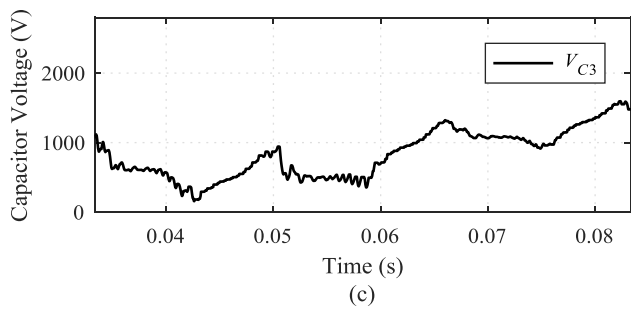
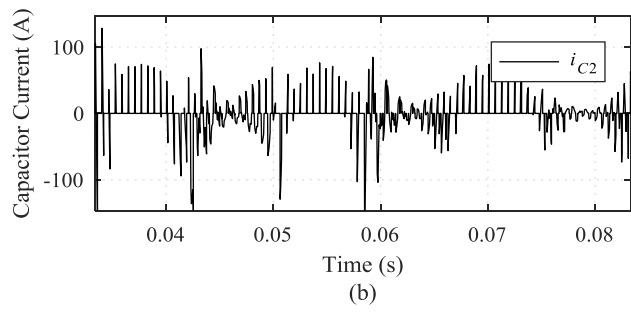
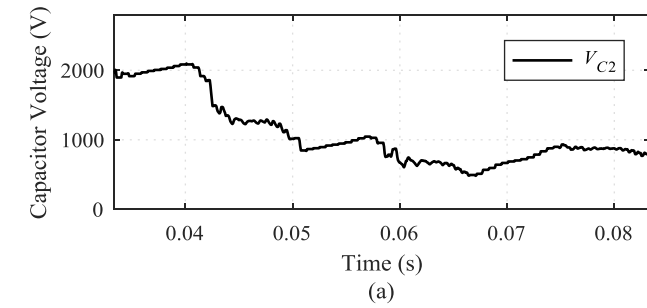


Figure 5.22 Sub-module capacitor (a)/(c) voltage; and (b)/(d) current.

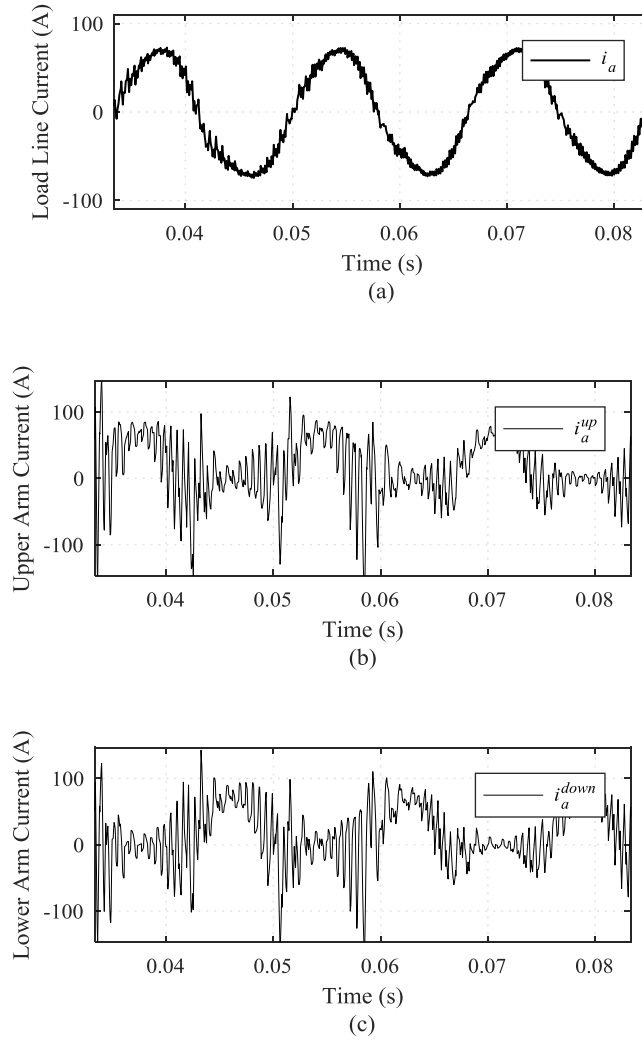


Figure 5.23 (a) Line current and its corresponding (b) upper arm current, (c) lower arm current.

## 5.5 CONCLUSION

This Chapter theoretically analyzes the dynamic response of the MMC in switching cycles. To assume the voltage drop on inductor to be zero, transient should be faster than the switching period. In another word,  $\tau < T_{sw}$ . Some simulations results are provided to verify the analysis.

## 6 CONCLUSIONS AND RECOMMENDATIONS FOR FUTURE WORK

### 6.1 CONCLUSIONS

This dissertation presents a modular multilevel converter with self voltage balancing.

This work has made the following contributions:

- ❖ This dissertation mathematically proves that MMC capacitor voltage is self-balanced by nature if considering certain submodule patterns. This implies that MMC could achieve the submodule capacitor voltage balancing without any monitoring or control. The mathematical proof starts from observing the two- and three-level MMCs. Mathematically, two- and three-level MMCs are proved to be self-balanced. Then, the similar observation is extended to  $N$ -level MMC. A computer-aid procedure is given to prove that  $N$ -level MMC, where  $N \leq 533$ , is self balanced by nature. This dissertation conjectures that this observation can be extended to arbitrary-level of MMC.
- ❖ To utilize this merit of MMC, a novel modulation, namely  $\Gamma$ -Matrix Modulation ( $\Gamma$ MM), is proposed to transform the math analysis of Chapter 2 into modulation practice. With the proposed  $\Gamma$ MM, MMCs are secured self voltage balancing. Conventionally, either a complicated voltage balancing control, or extra components must be embedded to MMC to balance the capacitor voltage. Compared to conventional MMC capacitor voltage balancing strategies,  $\Gamma$ MM features extremely simple algorithms and good reachability to high-level MMCs while maintaining the original half-bridge submodule topology. To simplify the analysis,  $\Gamma$ MM is introduced to two-level and three-level MMCs as examples. Then,

the generalized  $\Gamma$ MM is derived, which is suitable for high-level MMCs. Several  $\Gamma$ MM based MMC case studies are provided for verification purposes.

- ❖ The general state-space model of MMC is proposed to understand the mechanisms of the self balance phenomena of MMC. The existing MMC modeling are developed on different degrees of assumptions and simplification. This makes them unsuitable for understanding the nature of this circuit from its physical basement. Compared to existing MMC modeling, the proposed state-space model well captured the MMC dynamics. With this state-space model, the MMC capacitor voltage convergence and divergence can be well observed. Four-level MMC with both full-rank  $\Gamma$  and non-full-rank  $\Gamma$  are studied to demonstrate that this model could explain both convergence and divergence of the capacitor voltage. In addition, a generalized MMC model is derived. The generalized model can be applied to higher level MMC. An eleven-level MMC case study is provided to verify the proposed model when extended to higher level.

## 6.2 RECOMMENDATIONS FOR FUTURE WORK

Although we have developed a general state-space model for MMC, MMC still remains a black box in terms of the understanding how this model interacts with the  $\Gamma$  matrix (see Figure5.1). We observed the self balance phenomenon and gave a reasonable math explanation in Chapter 2. Then, we proposed a modulation that could trigger this self balance phenomenon in Chapter 3. After that, we developed a general state-space model for MMC to catch the detailed dynamics in Chapter 4.

After this dissertation, we have a lot of interesting works to do. We need to explain the trajectory of the convergence/divergence by using the model derived from Chapter 4. One

more step, we need to predict the trajectory without the aid of simulation. Once we could predict the trajectory, we could come up with a general guidance for this type of sensor-less operation to evaluate its stability.

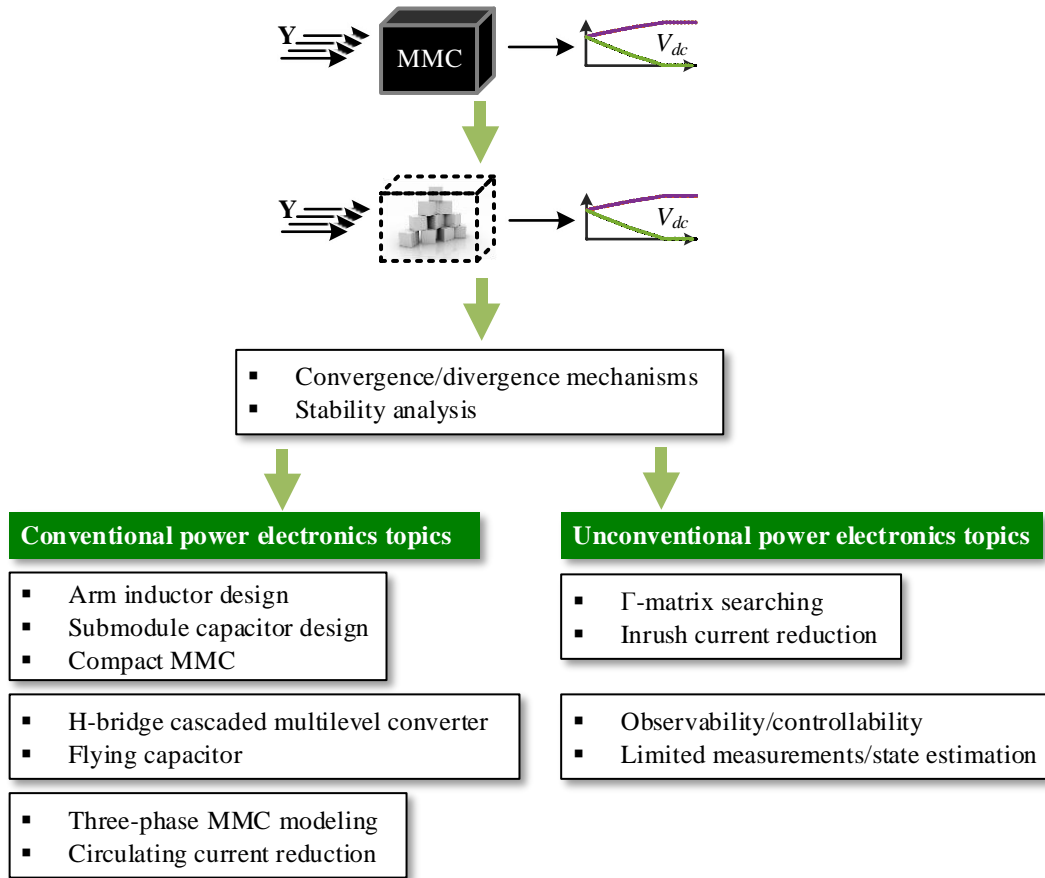


Figure 6.1 Recommendations for future work.

### 6.2.1 STATE-SPACE MODEL OF TWO-LEVEL MMC

Take the two level MMC for example. We have known that there are two continuous state spaces for two-level MMC. The first state space is

$$\begin{bmatrix} \dot{x}_1 \\ \dot{x}_2 \\ \dot{x}_3 \\ \dot{x}_4 \end{bmatrix} = \begin{bmatrix} 0 & 0 & 0 \cdot \left(-\frac{1}{2L}\right) & 1 \cdot \left(-\frac{1}{2L}\right) \\ 0 & 0 & 0 \cdot \left(-\frac{1}{2L}\right) & 1 \cdot \left(-\frac{1}{2L}\right) \\ 0 \cdot \left(\frac{1}{C_1}\right) & 0 & 0 & 0 \\ 0 & 1 \cdot \left(\frac{1}{C_2}\right) & 0 & 0 \end{bmatrix} \begin{bmatrix} x_1 \\ x_2 \\ x_3 \\ x_4 \end{bmatrix} + \begin{bmatrix} \frac{1}{2L} & \frac{1}{2} \\ \frac{1}{2L} & -\frac{1}{2} \\ 0 & 0 \\ 0 & 0 \end{bmatrix} \begin{bmatrix} V_{dc} \\ \frac{di_s}{dt} \end{bmatrix}. \quad (6.1)$$

The system matrices are

$$\mathbf{A}(\boldsymbol{\Gamma}_1^{(2)}) = \begin{bmatrix} 0 & 0 & 0 \cdot \left(-\frac{1}{2L}\right) & 1 \cdot \left(-\frac{1}{2L}\right) \\ 0 & 0 & 0 \cdot \left(-\frac{1}{2L}\right) & 1 \cdot \left(-\frac{1}{2L}\right) \\ 0 \cdot \left(\frac{1}{C_1}\right) & 0 & 0 & 0 \\ 0 & 1 \cdot \left(\frac{1}{C_2}\right) & 0 & 0 \end{bmatrix}, \quad (6.2)$$

$$\mathbf{B} = \begin{bmatrix} \frac{1}{2L} & \frac{1}{2} \\ \frac{1}{2L} & -\frac{1}{2} \\ 0 & 0 \\ 0 & 0 \end{bmatrix}, \quad (6.3)$$

$$\mathbf{U} = \begin{bmatrix} V_{dc} \\ \frac{di_s}{dt} \end{bmatrix}. \quad (6.4)$$

The corresponding switching pattern is

$$\boldsymbol{\Gamma}_1^{(2)} = [0 \quad 1]. \quad (6.5)$$

We denote  $\mathbf{A}(\boldsymbol{\Gamma}_1^{(2)})$  by  $\mathbf{A}_1$ .

State equation (6.1) could be re-written as

$$\dot{\mathbf{X}} = \mathbf{A}_1 \mathbf{X} + \mathbf{B} \mathbf{U}. \quad (6.6)$$

This state space dynamics could be denoted by  $f_1$ ,

$$\dot{\mathbf{X}} = f_1(\mathbf{X}) = \mathbf{A}_1 \mathbf{X} + \mathbf{B} \mathbf{U}. \quad (6.7)$$

The other state space is

$$\begin{bmatrix} \dot{x}_1 \\ \dot{x}_2 \\ \dot{x}_3 \\ \dot{x}_4 \end{bmatrix} = \begin{bmatrix} 0 & 0 & 1 \cdot \left(-\frac{1}{2L}\right) & 0 \cdot \left(-\frac{1}{2L}\right) \\ 0 & 0 & 1 \cdot \left(-\frac{1}{2L}\right) & 0 \cdot \left(-\frac{1}{2L}\right) \\ 1 \cdot \left(\frac{1}{C_1}\right) & 0 & 0 & 0 \\ 0 & 0 \cdot \left(\frac{1}{C_2}\right) & 0 & 0 \end{bmatrix} \begin{bmatrix} x_1 \\ x_2 \\ x_3 \\ x_4 \end{bmatrix} + \begin{bmatrix} \frac{1}{2L} & \frac{1}{2} \\ \frac{1}{2L} & -\frac{1}{2} \\ 0 & 0 \\ 0 & 0 \end{bmatrix} \begin{bmatrix} V_{dc} \\ \frac{di_s}{dt} \end{bmatrix}. \quad (6.8)$$

The corresponding switching pattern is

$$\Gamma_2^{(2)} = [1 \ 0]. \quad (6.9)$$

The system matrices are

$$\mathbf{A}(\Gamma_2^{(2)}) = \begin{bmatrix} 0 & 0 & 1 \cdot \left(-\frac{1}{2L}\right) & 0 \cdot \left(-\frac{1}{2L}\right) \\ 0 & 0 & 1 \cdot \left(-\frac{1}{2L}\right) & 0 \cdot \left(-\frac{1}{2L}\right) \\ 1 \cdot \left(\frac{1}{C_1}\right) & 0 & 0 & 0 \\ 0 & 0 \cdot \left(\frac{1}{C_2}\right) & 0 & 0 \end{bmatrix},$$

$$\mathbf{B} = \begin{bmatrix} \frac{1}{2L} & \frac{1}{2} \\ \frac{1}{2L} & -\frac{1}{2} \\ 0 & 0 \\ 0 & 0 \end{bmatrix},$$

$$\text{and } \mathbf{U} = \begin{bmatrix} V_{dc} \\ \frac{di_s}{dt} \end{bmatrix}. \quad (6.10)$$

We denote  $\mathbf{A}(\mathbf{\Gamma}_2^{(2)})$  by  $\mathbf{A}_2$ .

State equation (6.8) could be re-written as

$$\dot{\mathbf{X}} = \mathbf{A}_2 \mathbf{X} + \mathbf{B} \mathbf{U}. \quad (6.11)$$

This state space dynamics could be denoted by  $f_2$ ,

$$\dot{\mathbf{X}} = f_2(\mathbf{X}) = \mathbf{A}_2 \mathbf{X} + \mathbf{B} \mathbf{U}. \quad (6.12)$$

## 6.2.2 MECHANISMS OF VOLTAGE CONVERGENCE OF TWO-LEVEL MMC

### 6.2.2.1 THE SENSE OF SMELL OF A STATE MACHINE

Before we discuss the MMC behavior, we first introduce the concept of the *sense of smell* of a state machine. For example, a two-level MMC contains two continuous state spaces ( $f_1, f_2$ ). The transition between  $\mathbf{A}_1$  and  $\mathbf{A}_2$  is governed by a state machine  $H$ . In another word,  $H$  determines the moment that MMC should jump out of current continuous state space, and which continuous state space MMC should jump into at that moment.

Let  $i_1^0, i_2^0, V_{C1}^0$  and  $V_{C2}^0$  be the initial value of state variables. Suppose that  $V_{C1}^0 \neq V_{dc}$  and  $V_{C2}^0 \neq V_{dc}$ . The location (coordinates) of initial state variables is denoted by  $p^0$ ,

$$p^0 = [i_1^0 \quad i_2^0 \quad V_{C1}^0 \quad V_{C2}^0]^T \quad (6.13)$$

Similarly, location (coordinates) of balance point is denoted by  $p$ ,

$$p = [* \quad * \quad V_{dc} \quad V_{dc}]^T \quad (6.14)$$

\* denotes no specific definition of *balance value* for certain state variables. The displacement from  $p$  to  $p^0$  is denoted by  $d^0$ ,

$$d^0 = p^0 - p = [i_1^0 - * \quad i_2^0 - * \quad V_{C1}^0 - V_{dc} \quad V_{C2}^0 - V_{dc}]^T \quad (6.15)$$

Since we do not have specific balance value for  $i_1$  and  $i_2$ , the first two entries in  $d^0$  are set to zero to simplify the analysis. Therefore,

$$d^0 = p^0 - p = [0 \quad 0 \quad V_{C1}^0 - V_{dc} \quad V_{C2}^0 - V_{dc}]^T \quad (6.16)$$

**Definition:** Suppose the state machine  $H$  determines the continues dynamics  $f_i$  to be applied at moment  $t^0$ .  $H$  is said to have a *good sense of smell* if the inner product of  $d^0$  and  $f_i$  is no greater than zero. In another word,

$$\langle d^0, f_i \rangle \leq 0 \quad (6.17)$$

This definition is consistent with our intuitions.  $f_i$  represents the dynamics of state variables. For example, suppose  $f_i$  to be

$$f_i = [0 \quad 0 \quad -1 \quad 0]^T. \quad (6.18)$$

This means

$$\frac{dV_{C1}}{dt} = -1. \quad (6.19)$$

This indicates that  $V_{C1}$  has a trend to decrease.

Suppose  $p^0$  to be

$$p^0 = [* \quad * \quad 1001 \quad 1000]^T. \quad (6.20)$$

Suppose the balance point  $p$  to be

$$p = [* \quad * \quad 1000 \quad 1000]^T. \quad (6.21)$$

This indicates that  $V_{C1}$  (1001 V) is greater than the expected balance point voltage (1000 V). Therefore,

$$d^0 = p^0 - p = [0 \quad 0 \quad 1 \quad 0]^T \quad (6.22)$$

And

$$\langle d^0, f_i \rangle = (d^0)^T \cdot f_i = [0 \ 0 \ 1 \ 0] \cdot \begin{bmatrix} 0 \\ 0 \\ -1 \\ 0 \end{bmatrix} = -1 \leq 0 \quad (6.23)$$

Although the initial value of  $V_{C1}$  is greater than the balance value,  $V_{C1}$  has a trend to decrease. We could expect  $V_{C1}$  to come closer to the balance point after a while. This indicates that  $H$  has chosen a good  $f_i$  to kick in at the right moment. We can claim that  $H$  has a good sense of smell.

Otherwise,  $H$  is said to have a *bad sense of smell* if the inner product of  $d^0$  and  $f_i$  is greater than zero. In another word,

$$\langle d^0, f_i \rangle > 0 \quad (6.24)$$

### 6.2.2.2 UNDERSTAND TWO-LEVEL MMC BEHAVIORS

We are going to test the sense of smell for the state machine  $H$  of a two-level MMC. The state machine  $H$  follows the law set up in Chapter 3, which is

- i. Determine the level of  $v_a$ ;
- ii. Assign the level number to the level pointer at every switching cycle;
- iii. Find the  $\Gamma$ -matrix pointer which the level pointer points to;
- iv. Read the row (submodule pattern) which the  $\Gamma$ -matrix pointer points to;
- v. Generate the gating signal for each submodule according to the submodule pattern;
- vi. Reassign the  $\Gamma$ -matrix pointer to the next row and wait for the next call from level pointer.

For the two-level MMC case, this state machine law can be interpreted as follows,

- i. The state machine always chooses the state space from the adjacent levels as the next state space;
- ii. The kick-off time of next state space is arbitrary within one switching cycle.

We should also notice some properties of  $\mathbf{U}$ .

- i. The first entry of  $\mathbf{U}$  is  $V_{dc}$ , which is a constant;
- ii. The second entry of  $\mathbf{U}$  is  $di_s/dt = (v_a - V_s)/L$ . this entry is a bounded number since  $v_a$ ,  $V_s$  and  $L$  are all bounded.

We should always have these conditions in mind when we evaluate the state machine. A single-phase two-level MMC is studied to verify the state machine proposed in Chapter 3. A switching model is built in MATLAB/Simulink. The simulation circuit is shown in Figure 6.2. The key parameters of the system are summarized in Table 19. Ideal switches, inductors, and capacitors with no parasitic parameters as well as ideal voltage sources were used. In the simulation setup, discrete-Tustin/Backward Euler (TBE) with a sample time of  $0.1 \mu\text{s}$  is selected. The initial values of capacitor voltages are 1000V. The initial values of the inductor current are determined by MATLAB/Simulink.

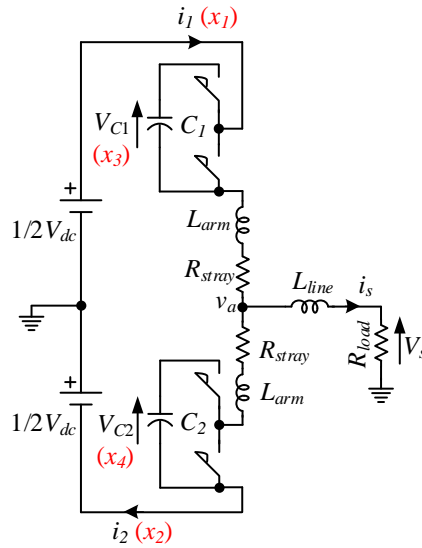


Figure 6.2 Two-level single-phase MMC circuit for state machine study.

Table 19

Two-level MMC simulation key parameters for state machine study.

Fundamental Frequency, $f_0$	60 Hz
Switching Frequency, $f_{sw}$	10 kHz
DC-Bus Voltage, $V_{dc}$	1000 V
Load Resistance, $R_{load}$	6.2 $\Omega$
Line Inductance, $L_{line}$	1 mH
Arm Inductance, $L_{arm}$	0.1 $\mu$ H
Stray Resistance, $R_{stray}$	0.1 $\Omega$
Submodule Capacitance, $C_i$	85 $\mu$ F
Number of Submodules per Arm	1

where  $i = 1, 2$ .

We are going to calculate the  $\langle d^0, f_i \rangle$  along with time.

A time-step of  $\Delta T = 0.1 \mu\text{s}$  was used to match with the simulation. The system matrix  $\mathbf{A}$  is a function of switching patterns. The state machine decision (instantaneous switching patterns) and the input value ( $\mathbf{U}$ ) are extracted from simulation. Then  $\langle d^0, f_i \rangle$  is calculated accordingly. Figure 6.3 shows the  $\langle d^0, f_i \rangle$  results from the state machine proposed in Chapter 3.

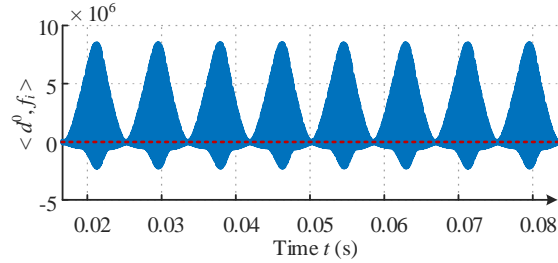
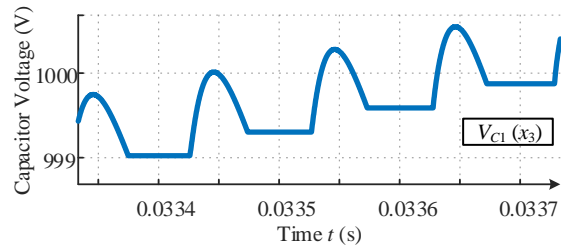
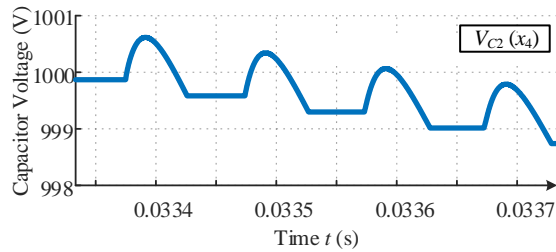


Figure 6.3 The  $\langle d^0, f_i \rangle$  resulting from the state machine proposed in Chapter 3.

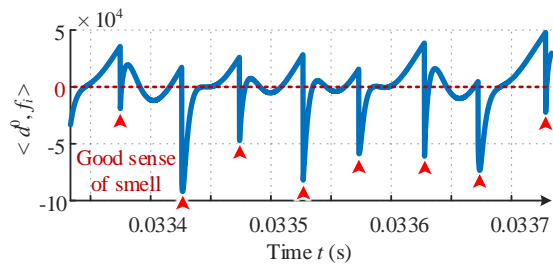
If we zoom in to see the details of the state machine and the dynamics of capacitor voltage, we will find that  $H$  always has a good sense of smell. Figure 6.4 gives an example to show that  $H$  makes eight decisions in five switching cycles.  $\langle d^0, f_i \rangle$  is always negative when  $H$  launches a new decision [see red arrow in Figure 6.4 (c)]. We can conclude that the proposed  $H$  has a good sense of smell.



(a)



(b)



(c)

Figure 6.4 (a) Upper arm capacitor voltage; (b) lower arm capacitor voltage; and (c)

the sense of smell  $\langle d^0, f_i \rangle$ .

### 6.2.3 DISCUSSIONS ON HIGH LEVEL MMC

I hope that the similar analysis could also be applied to higher level MMCs.

We have introduced a concept of *sense of smell* in Chapter 6.2.2. This could be one index to evaluate a state machine. However, when we go to high level MMC, this index might not be strong enough to guarantee the stability of the system. We need to introduce other indices to help assess the state machine.

Once we have a tool to assess the state machine we propose, we can move on to minimize the inrush current on the arm inductor without losing stability. There might be a chance that we need to look for a proper algorithm that can searching in the pool of  $\Gamma$  matrix. I have come up with some interesting topics to work on after finishing the stability analysis. Just list a few here,

- ❖ The inrush current is large in this dissertation. It is possible to look for a better  $\Gamma$  matrix to reduce the inrush current. Due to the massive data in  $\Gamma$  matrix, we might need to rely on some algorithms to search for the optimized  $\Gamma$  matrix.
- ❖ Although there is no sensor in this dissertation, it is possible that we add some sensors to the system and increase the stability. So, checking the controllability and the observability is critical. It is also possible to use state estimation to help us stabilize the system.
- ❖ We have demonstrated that  $\Gamma$ MM based MMC could reduce the dc capacitance. Since the arm current waveform is totally different from convention MMC, the component design needs to be re-considered. There is a chance we can have a compact MMC by using  $\Gamma$ MM.
- ❖ The  $\Gamma$ MM philosophy can also be applied to other type of multilevel converters, for example H-bridge cascaded multilevel converter. But when it comes to H-bridge, the entries in  $\Gamma$  matrix is no longer just 1 and 0. It is going to be 1, 0, and  $-1$ . It is promising to extend the  $\Gamma$ MM philosophy to other type of multilevel converter as well.

- ❖ In this dissertation I only discussed about single-phase model. The circulating current is missed out from this model. We need to have three-phase model in order to evaluate the circulating current.

I apologize that I have to stop here in this dissertation. This is definitely not the end of understanding the nature of MMC. Instead, I believe this is just a beginning. There are many mysterious phenomena hidden in MMC. There will be a day that MMC is no longer a black box. And we will have a thorough understanding of MMC nature at that time. Not now but some day in future.

## **APPENDICES**

## APPENDIX A: PROOF BY INDUCTION AND CONTRADICTION

The conjectures provided in Chapter 2.4.3 summarized two angles to approach to this math problem. We are going to take second conjecture b as example to proof since second conjecture b contains the majority levels compared to the other three items. If second conjecture b is proved, the other three proofs are trivial. The item that under analysis are as follows,

- If the rank of  $\left[\hat{\mathbf{\Gamma}}_k^{(N-1)} \quad \hat{\mathbf{\Gamma}}_{k+1}^{(N-1)}\right]^T$  is  $m$  for an  $(N - 1)$ -level MMC, then the rank of  $\left[\hat{\mathbf{\Gamma}}_k^{(N)} \quad \hat{\mathbf{\Gamma}}_{k+1}^{(N)}\right]^T$  is  $m + 2$  for an  $N$ -level MMC, where  $2 \leq k \leq N - 3$  and

$$\hat{\mathbf{\Gamma}}_k^{(N)} = \begin{bmatrix} \mathbf{0} & \hat{\mathbf{\Gamma}}_k^{(N-1)} & \mathbf{1} \\ 1 & \mathbf{T}_{k-1(a)}^{(N-1)} & 1 \\ 0 & \mathbf{T}_{k-1(b)}^{(N-1)} & 0 \end{bmatrix} \hat{\mathbf{\Gamma}}_{k+1}^{(N)} = \begin{bmatrix} \mathbf{0} & \hat{\mathbf{\Gamma}}_{k+1}^{(N-1)} & \mathbf{1} \\ 1 & \mathbf{T}_{k(a)}^{(N-1)} & 1 \\ 0 & \mathbf{T}_{k(b)}^{(N-1)} & 0 \end{bmatrix};$$

This conjecture can be decomposed as follows,

- Row independent: let  $\hat{\mathbf{\Gamma}}_k^{(N-1)}$  be full rank, where  $rank\left(\hat{\mathbf{\Gamma}}_k^{(N-1)}\right) = 2N - 5$ , then  $\hat{\mathbf{\Gamma}}_k^{(N)}$  is full rank, where  $rank\left(\hat{\mathbf{\Gamma}}_k^{(N)}\right) = 2N - 3$ .
- Column independent: let  $\hat{\mathbf{\Gamma}}_k^{(N)}$  and  $\hat{\mathbf{\Gamma}}_{k+1}^{(N)}$  be row independent, then  $\left[\hat{\mathbf{\Gamma}}_k^{(N-1)} \quad \hat{\mathbf{\Gamma}}_{k+1}^{(N-1)}\right]^T$  is column vector independent.

The reason to decompose the original conjecture into two parts is that the rows of  $\hat{\mathbf{\Gamma}}_k^{(N)}$  should linearly independent if  $\hat{\mathbf{\Gamma}}_k^{(N)}$  is full rank since  $\hat{\mathbf{\Gamma}}_k^{(N)}$  is  $(2N - 3) \times (2N - 2)$ . The columns of  $\left[\hat{\mathbf{\Gamma}}_k^{(N-1)} \quad \hat{\mathbf{\Gamma}}_{k+1}^{(N-1)}\right]^T$  should be linearly independent if  $\left[\hat{\mathbf{\Gamma}}_k^{(N-1)} \quad \hat{\mathbf{\Gamma}}_{k+1}^{(N-1)}\right]^T$  is full rank since  $\left[\hat{\mathbf{\Gamma}}_k^{(N-1)} \quad \hat{\mathbf{\Gamma}}_{k+1}^{(N-1)}\right]^T$  is  $(4N - 6) \times (2N - 2)$ .

We are going to prove the above conjectures by contradiction. A classic proof by contradiction from mathematics is the proof that the square root of 2 is irrational[69]. If it were rational, it could be expressed as a fraction  $a/b$  in lowest terms, where  $a$  and  $b$  are integers, at least one of which is odd. But if  $a/b = \sqrt{2}$ , then  $a^2 = 2b^2$ . Therefore,  $a^2$  must be even. Because the square of an odd number is odd, that in turn implies that  $a$  is even. This means that  $b$  must be odd because  $a/b$  is in lowest terms. On the other hand, if  $a$  is even, then  $a^2$  is a multiple of 4. If  $a^2$  is a multiple of 4 and  $a^2 = 2b^2$ , then  $2b^2$  is a multiple of 4, and therefore  $b^2$  is even, and so is  $b$ . So  $b$  is odd and even, a contradiction. Therefore, the initial assumption—that  $\sqrt{2}$  can be expressed as a fraction—must be false.

### A.1 ROW INDEPENDENT

Let

$$\hat{\mathbf{\Gamma}}_k^{(N)} = \begin{bmatrix} \alpha_1 \\ \alpha_2 \\ \vdots \\ \alpha_{2N-3} \end{bmatrix}_{(2N-3) \times (2N-2)}, \hat{\mathbf{\Gamma}}_k^{(N-1)} = \begin{bmatrix} \beta_1 \\ \beta_2 \\ \vdots \\ \beta_{2N-5} \end{bmatrix}_{(2N-5) \times (2N-4)}, \boldsymbol{\lambda} = \begin{bmatrix} \lambda_1 \\ \lambda_2 \\ \vdots \\ \lambda_{2N-3} \end{bmatrix}_{(2N-3) \times 1} \quad (\text{A.1})$$

Where  $\alpha_i$  is row vector of  $\hat{\mathbf{\Gamma}}_k^{(N)}$ ,  $\beta_i$  is row vector of  $\hat{\mathbf{\Gamma}}_k^{(N-1)}$ ,  $\boldsymbol{\lambda}$  is a column vector.

Let  $\hat{\mathbf{\Gamma}}_k^{(N-1)}$  be full rank, where  $\text{rank}(\hat{\mathbf{\Gamma}}_k^{(N-1)}) = 2N - 5$ . If  $\hat{\mathbf{\Gamma}}_k^{(N)}$  is non full rank,  $\exists \boldsymbol{\lambda} \in \mathbf{R}^{(2N-3) \times 1}$  :

$$-\lambda_i \alpha_i = \lambda_1 \alpha_1 + \lambda_2 \alpha_2 + \dots + \lambda_{i-1} \alpha_{i-1} + \lambda_{i+1} \alpha_{i+1} + \dots + \lambda_{2N-3} \alpha_{2N-3} \Leftrightarrow \boldsymbol{\lambda}^T \hat{\mathbf{\Gamma}}_k^{(N)} = \mathbf{0}.$$

Therefore

$$\begin{aligned}
\boldsymbol{\lambda}^T \hat{\boldsymbol{\Gamma}}_k^{(N)} &= \boldsymbol{\lambda}^T \begin{bmatrix} \mathbf{0} & \hat{\boldsymbol{\Gamma}}_k^{(N-1)} & \mathbf{1} \\ 1 & \mathbf{T}_{k-1(a)}^{(N-1)} & 1 \\ 0 & \mathbf{T}_{k-1(b)}^{(N-1)} & 0 \end{bmatrix} \\
&= (\boldsymbol{\lambda}^T)_{1 \times (2N-3)} \begin{bmatrix} \mathbf{0}_{(2N-5) \times 1} & (\hat{\boldsymbol{\Gamma}}_k^{(N-1)})_{(2N-5) \times (2N-4)} & \mathbf{1}_{(2N-5) \times 1} \\ 1 & (\mathbf{T}_{k-1(a)}^{(N-1)})_{1 \times (2N-4)} & 1 \\ 0 & (\mathbf{T}_{k-1(b)}^{(N-1)})_{1 \times (2N-4)} & 0 \end{bmatrix} = \mathbf{0}
\end{aligned} \tag{A.2}$$

$$\begin{aligned}
& (\boldsymbol{\lambda}^T)_{1 \times (2N-3)} \begin{bmatrix} \mathbf{0}_{(2N-5) \times 1} & (\hat{\boldsymbol{\Gamma}}_k^{(N-1)})_{(2N-5) \times (2N-4)} & \mathbf{1}_{(2N-5) \times 1} \\ 1 & (\mathbf{T}_{k-1(a)}^{(N-1)})_{1 \times (2N-4)} & 1 \\ 0 & (\mathbf{T}_{k-1(b)}^{(N-1)})_{1 \times (2N-4)} & 0 \end{bmatrix} \\
&= \left[ \lambda_{2N-4} \quad \lambda_1 \beta_1 + \lambda_2 \beta_2 + \cdots + \lambda_{2N-5} \beta_{2N-5} + \lambda_{2N-4} \mathbf{T}_{k-1(a)}^{(N-1)} + \lambda_{2N-3} \mathbf{T}_{k-1(b)}^{(N-1)} \quad (\sum \boldsymbol{\lambda}) - \lambda_{2N-3} \right]_{1 \times (2N-2)} \\
&= \mathbf{0}
\end{aligned} \tag{A.3}$$

Therefore,

$$\begin{cases} \lambda_{2N-4} = 0 \\ \lambda_1 \beta_1 + \lambda_2 \beta_2 + \cdots + \lambda_{2N-5} \beta_{2N-5} + \lambda_{2N-4} \mathbf{T}_{k-1(a)}^{(N-1)} + \lambda_{2N-3} \mathbf{T}_{k-1(b)}^{(N-1)} = \mathbf{0} \\ \sum \boldsymbol{\lambda} = \lambda_{2N-3} \end{cases} \tag{A.4}$$

Therefore,

$$\lambda_1 \beta_1 + \lambda_2 \beta_2 + \cdots + \lambda_{2N-5} \beta_{2N-5} + \lambda_{2N-3} \mathbf{T}_{k-1(b)}^{(N-1)} = \mathbf{0} \tag{A.5}$$

$$\begin{aligned}
& \lambda_1 \beta_1 + \lambda_2 \beta_2 + \cdots + \lambda_{2N-5} \beta_{2N-5} + \lambda_{2N-3} \mathbf{T}_{k-1(b)}^{(N-1)} \\
&= \lambda_1 \beta_1 + \lambda_2 \beta_2 + \cdots + \lambda_{2N-5} \beta_{2N-5} + (\lambda_1 + \lambda_2 + \cdots + \lambda_{2N-5} + \lambda_{2N-3}) \mathbf{T}_{k-1(b)}^{(N-1)} \\
&= (\lambda_1 \beta_1 + \lambda_2 \beta_2 + \cdots + \lambda_{2N-5} \beta_{2N-5} + \lambda_{2N-3} \mathbf{T}_{k-1(b)}^{(N-1)}) + (\lambda_1 + \lambda_2 + \cdots + \lambda_{2N-5}) \mathbf{T}_{k-1(b)}^{(N-1)} \\
&= (\lambda_1 + \lambda_2 + \cdots + \lambda_{2N-5}) \mathbf{T}_{k-1(b)}^{(N-1)} \\
&= \mathbf{0}
\end{aligned} \tag{A.6}$$

Note that  $\mathbf{T}_{k-1(b)}^{(N-1)}$  is derived from  $\hat{\mathbf{\Gamma}}_{k-1}^{(N-1)}$  by manipulating the left most “0” in first row of  $\hat{\mathbf{\Gamma}}_{k-1}^{(N-1)}$  to “1”. Therefore,  $\mathbf{T}_{k-1(b)}^{(N-1)}$  contains at least one entry to be one. Therefore,  $\mathbf{T}_{k-1(b)}^{(N-1)} \neq \mathbf{0}$ .

Therefore,

$$\lambda_1 + \lambda_2 + \cdots + \lambda_{2N-5} = 0 \quad (\text{A.7})$$

$$\mathbf{0} = \lambda_1 \beta_1 + \lambda_2 \beta_2 + \cdots + \lambda_{2N-5} \beta_{2N-5} \quad (\text{A.8})$$

A contradiction appears since  $\hat{\mathbf{\Gamma}}_k^{(N-1)}$  is full rank.  $\hat{\mathbf{\Gamma}}_k^{(N-1)}$  is full rank  $\Leftrightarrow \mathbf{0} \neq \lambda_1 \beta_1 + \lambda_2 \beta_2 + \cdots + \lambda_{2N-5} \beta_{2N-5}$ . Therefore, the initial assumption—that  $\hat{\mathbf{\Gamma}}_k^{(N)}$  is non full rank—must be false.

then  $\mathbf{T}_{k-1(b)}^{(N-1)}$  is linearly dependent to  $\hat{\mathbf{\Gamma}}_k^{(N-1)}$ .  $\mathbf{T}_{k-1(b)}^{(N-1)}$  is derived from  $\hat{\mathbf{\Gamma}}_{k-1}^{(N-1)}$  by manipulating the left most “0” in first row of  $\hat{\mathbf{\Gamma}}_{k-1}^{(N-1)}$  to “1”. The definition of  $\mathbf{T}_{k-1(b)}^{(N-1)}$  does not guarantee that  $\mathbf{T}_{k-1(b)}^{(N-1)}$  is linearly independent to  $\hat{\mathbf{\Gamma}}_k^{(N-1)}$ . If the definition of  $\mathbf{T}_{k-1(b)}^{(N-1)}$  guarantees that  $\mathbf{T}_{k-1(b)}^{(N-1)}$  is linearly independent to  $\hat{\mathbf{\Gamma}}_k^{(N-1)}$ , then a contradiction appears. Therefore, the initial assumption—that  $\hat{\mathbf{\Gamma}}_k^{(N)}$  is non full rank—must be false.

## A.2 DISCUSSION

We have two sets of conjectures from Chapter 2.4.3. They are equivalent to each other. We have presented the math analysis regarding the second conjecture. The overall logic of the second conjecture is proof by induction. In fact, it is unnecessary to prove the conjecture by induction. The logic of the first conjecture is direct proof. The matrices presented in Chapter 2 have a property, which is the matrices contains only ones and zeros. These matrices were the subject of intensive study during the late 1950s and early 1960s by H. J. Ryser, D. Ft. Fulkerson, R. M. Haber, and D. Gale, and many remarkable theorems were

proved [70]. The original  $\Gamma$  before submatrix extraction has a property that the row and column sum vectors are fixed. This special matrix is discussed in [70]. Many remarkable theorems were proved in [70].

## APPENDIX B: MATLAB SCRIPT

```
%%%%%%%%%%%%%%%%%%%%%%%%%%%%%%%%%%%%%%%%%%%%%%%%%%%%%%%%%%%%%%%%%%%%%%%%
% - It takes 30s to run this script on my laptop
%   if NN = 100;
% - It takes 12 hours if NN = 433;
% - It takes 36 hours if NN = 533.
% Yunting 6-7-18
%%%%%%%%%%%%%%%%%%%%%%%%%%%%%%%%%%%%%%%%%%%%%%%%%%%%%%%%%%%%%%%%%%%%%%%%
clc; clear all;
% generate the Y matrix
% initiate the Y(N-1) matrix with 3-level MMC
YN_1 = [0 0 1 1;           % first level
        0 1 0 1;           % second level
        1 0 0 1;           % second level
        0 1 1 0;           % second level
        1 1 0 0];          % third level
% initiate the maximum level NN you hope to check
NN = 1000;
% generate the Y matrix of N-level MMC
for N = 1:NN
% generate the kth level Yk matrix
    for k = 1:N
        if k == 1
            Yk = [zeros(1, N-1) ones(1, N-1)]; % fist
level
        else
            if k < N-1
                % extract the kth level matrix from the (N-1)-level MMC Y
matrix
                N_1 = N-1; %
(N-1)-level MMC
                m = 1 + (k-2) * (2*N_1 - 3) + 1; %
starting row
                n = m + (2*N_1 - 3) - 1; %
ending row
                Yk = YN_1(m:n,:);
                % have a zero vector to the left
                zero = zeros(2*N_1 - 3, 1);
                Yk = [zero Yk];
                % have a one vector to the right
                one = ones(2*N_1 - 3, 1);
                Yk = [Yk one];
                % extract Y(k-1)
                if k-1 == 1
                    Yk_1 = YN_1(1,:);
                else

```

```

        m = 1 + (k-3) * (2*N_1 - 3) + 1; %
starting row
        Yk_1 = YN_1(m,:);
end
% generate T(k-1)a
[a, b] = size(Yk_1);
for i = 1:b
    if Yk_1(b-i+1) == 1 % search for the
right most "1"
        Tk_1a = Yk_1;
% convert the right most "1" to "0"
        Tk_1a(b-i+1) = 0;
        break
    end
end
% generate T(k-1)b
for i = 1:b
    if Yk_1(i) == 0 % search for the
left most "0"
        Tk_1b = Yk_1;
% convert the right most "0" to "1"
        Tk_1b(i) = 1;
        break
    end
end
% finalize Yk
Yk = [Yk; 1 Tk_1a 1; 0 Tk_1b 0];
else
    if k == N-1
        % extract the (k-1)th level matrix from the (N-1)-level
        MMC Y matrix
        N_1 = N-1; % (N-1)-
level MMC
        m = 1 + (k-3) * (2*N_1 - 3) + 1; %
starting row
        n = m + (2*N_1 - 3) - 1; %
ending row
        Yk_1 = YN_1(m:n,:);
% have a zero vector to the right
zero = zeros(2*N_1 - 3, 1);
Yk = [Yk_1 zero];
% have a one vector to the left
one = ones(2*N_1 - 3, 1);
Yk = [one Yk];
% extract first row of Y(k-1)
row_Yk_1 = Yk_1(1,:);
% generate T(k-1)a

```

```

        [a, b] = size(row_Yk_1);
        for i = 1:b
            % search for the right most "1"
            if row_Yk_1(b-i+1) == 1
                Tk_1a = row_Yk_1;
            % convert the right most "1" to "0"
                Tk_1a(b-i+1) = 0;
                break
            end
        end
        % generate T(k-1)b
        for i = 1:b
            % search for the left most "0"
            if row_Yk_1(i) == 0
                Tk_1b = row_Yk_1;
            % convert the right most "0" to "1"
                Tk_1b(i) = 1;
                break
            end
        end
        % finalize Yk
        Yk = [Yk; 1 Tk_1a 1; 0 Tk_1b 0];
    else
        Yk = [ones(1, N-1) zeros(1, N-1)]; %
fist level
    end
end
end
if k == 1
    YN = Yk;
else
    YN = [YN; Yk];
end
end
% update Y(N-1). save YN to Y(N-1)
YN_1 = YN;
% check the rank of any two adjacent levels
for k = 1:N-1
    if k == 1
        Y1 = YN(1, :);           % extract the kth
level Y1
        Y2 = YN(2:2*N-2, :);    % extract the next
level Y2
    else
        if k < N-1
            % extract the kth level Y1

```

```

        m = 1 + (k-2) * (2*N - 3) + 1; %
starting row of Y1
        n = m + (2*N - 3) - 1;          % ending
row of Y1
        Y1 = YN(m:n,:); % extract the kth level
Y1
        % extract the kth level Y2
        m2 = n + 1; % starting row of Y2
        n2 = m2 + (2*N - 3) - 1;      % ending
row of Y2
        Y2 = YN(m2:n2,:);
    else
        % extract the kth level Y1
        m = 1 + (k-2) * (2*N - 3) + 1; %
starting row of Y1
        n = m + (2*N - 3) - 1;          % ending
row of Y1
        % extract the kth level Y1
        Y1 = YN(m:n,:);
        % extract the kth level Y2
        Y2 = YN(n+1,:);
    end
end
    Y12 = [Y1;Y2];
% check the rank of any two adjacent levels
    Y12rank = rank(Y12);
    if Y12rank ~= (2*N-2)
        formatSpec = 'The rank of %dth level and %dth
level of a %d-level MMC is %d\n';
        fprintf(formatSpec,k,k+1,N,Y12rank)
        break
    end
end
end
formatSpec = 'All ranks checked!\n';
fprintf(formatSpec)

```

## **BIBLIOGRAPHY**

## BIBLIOGRAPHY

- [1] A. Lesnicar and R. Marquardt, "An innovative modular multilevel converter topology suitable for a wide power range," *2003 IEEE Bol. PowerTech - Conf. Proc.*, vol. 3, pp. 272–277, 2003.
- [2] W. Liu, K. Zhang, X. Chen and J. Xiong, "Simplified model and submodule capacitor voltage balancing of single-phase AC/AC modular multilevel converter for railway traction purpose," in *IET Power Electronics*, vol. 9, no. 5, pp. 951-959, 4 20 2016.
- [3] T. Zhao, G. Wang, S. Bhattacharya, and A. Q. Huang, "Voltage and power balance control for a cascaded h-bridge converter-based solid-state Transformer," *IEEE Trans. Power Electron.*, vol. 28, no. 4, pp. 1523–1532, 2013.
- [4] X. She, A. Q. Huang, T. Zhao, and G. Wang, "Coupling effect reduction of a voltage-balancing controller in single-phase cascaded multilevel converters," *IEEE Trans. Power Electron.*, vol. 27, no. 8, p. 3530, 2012.
- [5] J. Shi, W. Gou, H. Yuan, T. Zhao, and A. Q. Huang, "Research on voltage and power balance control for cascaded modular solid-state transformer," *IEEE Trans. Power Electron.*, vol. 26, no. 4, pp. 1154–1166, 2011.
- [6] Y. Liu, A. Q. Huang, W. Song, S. Bhattacharya, and G. Tan, "Small-signal model-based control strategy for balancing individual DC capacitor voltages in cascade multilevel inverter-based STATCOM," *IEEE Trans. Ind. Electron.*, vol. 56, no. 6, pp. 2259–2269, 2009.
- [7] A. F. Jabbar and M. Mansor, "Voltage Balancing for seven layer multi Level Cascaded Multilevel Inverter," *2013 IEEE Conference on Clean Energy and Technology (CEAT)*, pp. 323–326, 2013.
- [8] Y. Okazaki, H. Matsui, M. M. Muhoro, M. Hagiwara, and H. Akagi, "Capacitor-Voltage Balancing for a Modular Multilevel DSCC Inverter Driving a Medium-Voltage Synchronous Motor," *IEEE Trans. Ind. Appl.*, vol. 52, no. 5, pp. 4074–4083, 2016.
- [9] H. Yang and M. Saeedifard, "A Capacitor Voltage Balancing Strategy With Minimized AC Circulating Current for the DC–DC Modular Multilevel Converter," in *IEEE Transactions on Industrial Electronics*, vol. 64, no. 2, pp. 956-965, Feb. 2017.

- [10] C. Sun, J. Zhang, X. Cai and G. Shi, "Voltage balancing control of isolated modular multilevel dc-dc converter for use in dc grids with zero voltage switching," in *IET Power Electronics*, vol. 9, no. 2, pp. 270-280, 2 10 2016.
- [11] H. Peng, R. Xie, K. Wang, Y. Deng, X. He and R. Zhao, "A Capacitor Voltage Balancing Method With Fundamental Sorting Frequency for Modular Multilevel Converters Under Staircase Modulation," in *IEEE Transactions on Power Electronics*, vol. 31, no. 11, pp. 7809-7822, Nov. 2016.
- [12] A. Dekka, B. Wu and N. R. Zargari, "A Novel Modulation Scheme and Voltage Balancing Algorithm for Modular Multilevel Converter," in *IEEE Transactions on Industry Applications*, vol. 52, no. 1, pp. 432-443, Jan.-Feb. 2016.
- [13] Z. Li *et al.*, "Power Module Capacitor Voltage Balancing Method for a  $\pm 350$ -kV/1000-MW Modular Multilevel Converter," in *IEEE Transactions on Power Electronics*, vol. 31, no. 6, pp. 3977-3984, June 2016.
- [14] F. Deng and Z. Chen, "Voltage-Balancing Method for Modular Multilevel Converters Switched at Grid Frequency," in *IEEE Transactions on Industrial Electronics*, vol. 62, no. 5, pp. 2835-2847, May 2015.
- [15] Y. Li, E. A. Jones and F. Wang, "The Impact of Voltage-Balancing Control on Switching Frequency of the Modular Multilevel Converter," in *IEEE Transactions on Power Electronics*, vol. 31, no. 4, pp. 2829-2839, April 2016.
- [16] R. Darus, J. Pou, G. Konstantinou, S. Ceballos, R. Picas and V. G. Agelidis, "A Modified Voltage Balancing Algorithm for the Modular Multilevel Converter: Evaluation for Staircase and Phase-Disposition PWM," in *IEEE Transactions on Power Electronics*, vol. 30, no. 8, pp. 4119-4127, Aug. 2015.
- [17] P. M. Meshram and V. B. Borghate, "A simplified nearest level control (NLC) voltage balancing method for modular multilevel converter (MMC)," *IEEE Trans. Power Electron.*, vol. 30, no. 1, pp. 450-462, 2015.
- [18] W. Li, L. Grégoire, and J. Bélanger, "A Modular Multilevel Converter Pulse Generation and Capacitor Voltage Balance Method Optimized for FPGA Implementation," *IEEE Trans. Ind.*, vol. 62, no. 5, pp. 2859-2867, 2015.
- [19] A. Dekka, B. Wu, N. R. Zargari, and R. L. Fuentes, "Dynamic Voltage Balancing Algorithm for Modular Multilevel Converter: A Unique Solution," *IEEE Trans. Power Electron.*, vol. 31, no. 2, pp. 952-963, 2016.

- [20] F. Z. Peng, "A generalized multilevel inverter topology with self voltage balancing," *IEEE Trans. Ind. Appl.*, vol. 37, no. 2, pp. 611–618, 2001.
- [21] F. Zhang, S. Yang, F. Z. Peng, and Z. Qian, "A zigzag cascaded multilevel inverter topology with self voltage balancing," *Conf. Proc. - IEEE Appl. Power Electron. Conf. Expo. - APEC*, pp. 1632–1635, 2008.
- [22] S. P. Gautam, L. Kumar, and S. Gupta, "Single-phase multilevel inverter topologies with self-voltage balancing capabilities," *IET Power Electron.*, vol. 11, no. 5, pp. 844–855, 2018.
- [23] C. Gao and J. Lv, "A New Parallel-Connected Diode-Clamped Modular Multilevel Converter With Voltage Self-Balancing," in *IEEE Transactions on Power Delivery*, vol. 32, no. 3, pp. 1616-1625, June 2017.
- [24] X. Liu *et al.*, "A Novel Diode-Clamped Modular Multilevel Converter With Simplified Capacitor Voltage-Balancing Control," in *IEEE Transactions on Industrial Electronics*, vol. 64, no. 11, pp. 8843-8854, Nov. 2017.
- [25] C. Gao, X. Jiang, Y. Li, Z. Chen, and J. Liu, "A DC-link voltage self-balance method for a diode-clamped modular multilevel converter with minimum number of voltage sensors," *IEEE Trans. Power Electron.*, vol. 28, no. 5, pp. 2125–2139, 2013.
- [26] S. K. Chattopadhyay and C. Chakraborty, "A new multilevel inverter topology with self-balancing level doubling network," *IEEE Trans. Ind. Electron.*, vol. 61, no. 9, pp. 4622–4631, 2014.
- [27] S. N. B, L. Umanand, K. Gopakumar, and S. R. B, "A New Two Phase Five-Level Converter for Three Phase Isolated Grid-Tied Systems with Inherent Capacitor Balancing and Reduced Component Count," *IEEE J. Emerg. Sel. Top. Power Electron.*, vol. 6777, no. c, 2018.
- [28] A. Elserougi, M. I. Daoud, A. M. Massoud, A. S. Abdel-Khalik, and S. Ahmed, "Investigation of sensorless capacitor voltage balancing technique for modular multilevel converters," *IECON Proc. Industrial Electron. Conf.*, pp. 1569–1574, 2014.
- [29] A. Ghazanfari and Y. A. R. I. Mohamed, "A Hierarchical Permutation Cyclic Coding Strategy for Sensorless Capacitor Voltage Balancing in Modular Multilevel Converters," *IEEE J. Emerg. Sel. Top. Power Electron.*, vol. 4, no. 2, pp. 576–588, 2016.
- [30] A. A. Elserougi, A. M. Massoud and S. Ahmed, "Modular Multilevel Converter-Based Bipolar High-Voltage Pulse Generator With Sensorless Capacitor Voltage Balancing

Technique," in *IEEE Transactions on Plasma Science*, vol. 44, no. 7, pp. 1187-1194, July 2016.

- [31] G. P. Adam, O. Anaya-Lara, G. M. Burt, D. Telford, B. W. Williams, and J. R. McDonald, "Modular multilevel inverter: pulse width modulation and capacitor balancing technique," *IET Power Electron.*, vol. 3, no. 5, p. 702, 2010.
- [32] Schay Géza, *A Concise Introduction to Linear Algebra*. Boston: Birkhäuser, 2012.
- [33] S. Du, A. Dekka, B. Wu, and N. Zargari, *Modular multilevel converters: analysis, control, and applications*. Hoboken: Wiley-IEEE Press, 2018.
- [34] A. M. Mathai and H. J. Haubold, *Linear algebra: a course for physicists and engineers*. Berlin: De Gruyter, 2017.
- [35] H. J. Knaak, "Modular multilevel converters and HVDC/FACTS: A success story," *Proc. of the 2011 14th European Conf. on Power Electron. and Appl.*, Birmingham, 2011, pp. 1-6.
- [36] K. Sharifabadi, L. Harnefors, H. Nee, S. Norrga, and R. Teodorescu, (2016). *Design, Control and Application of Modular Multilevel Converters for HVDC Transmission Systems*. Newark: Wiley.
- [37] B. Jacobson, P. Karlsson, G. Asplund, L. Harnefors, and T. Jonsson, "VSC-HVDC transmission with cascaded two-level converters," *CIGRE Sess.*, pp. B4–B110, 2010.
- [38] Q. Tu, Z. Xu, H. Huang, and J. Zhang, "Parameter design principle of the arm inductor in modular multilevel converter based HVDC," *2010 Int. Conf. Power Syst. Technol.*, Hangzhou, pp. 1–6, 2010.
- [39] H. Yuan, X. Yuan, and J. Hu, "Modeling of Grid-Connected VSCs for Power System Small-Signal Stability Analysis in DC-Link Voltage Control Timescale," *IEEE Trans. Power Syst.*, vol. 32, no. 5, pp. 3981–3991, 2017.
- [40] J. Hu, J. Zhu, and M. Wan, "Modeling and Analysis of Modular Multilevel Converter in DC Voltage Control Timescale," *IEEE Trans. Ind. Electron.*, vol. PP, no. c, p. 1, 2018.
- [41] J. Lyu, X. Cai and M. Molinas, "Optimal design of controller parameters for improving the stability of MMC-HVDC for wind farm integration," *IEEE Jour. Emer. Sel. Top. Power Electron.*, vol. 6, no. 1, pp. 40-53, Mar. 2018.

- [42] Z. Xu, B. Li, S. Wang, S. Zhang, and D. Xu, "Generalized Single-Phase Harmonic State Space Modeling of the Modular Multilevel Converter with Zero-Sequence Voltage Compensation," *IEEE Trans. Ind. Electron.*, vol. PP, no. c, pp. 1–1, 2018.
- [43] N. M. Wereley, "Analysis and control of linear periodically time varying systems," Ph.D. Dissertation, Massachusetts Institute of Technology, 1991.
- [44] G. Love, "Small signal modelling of power electronic converters, for the study of time-domain waveforms, harmonic domain spectra, and control interactions," Ph.D. Dissertation, University of Canterbury, 2007.
- [45] A. Antonopoulos, L. Ängquist, L. Harnefors, K. Ilves, and H. Nee, "Global Asymptotic Stability of Modular Multilevel Converters," *IEEE Trans. Ind. Electron.*, vol. 61, no. 2, pp. 603–612, 2014.
- [46] L. Ängquist, A. Antonopoulos, D. Siemaszko, K. Ilves, M. Vasiladiotis, and H.-P. Nee, "Open-loop control of modular multilevel converters using estimation of stored energy," *IEEE Trans. Ind. Appl.*, vol. 47, no. 6, pp. 2516–2524, Nov./Dec. 2011.
- [47] L. Harnefors, A. Antonopoulos, S. Norrga, L. Ängquist, and H.-P. Nee, "Dynamic analysis of modular multilevel converters," *IEEE Trans. Ind. Electron.*, vol. 60, no. 7, pp. 2526–2537, Jul. 2013.
- [48] A. A. Taffese and E. De Jong, "Arm Voltage Estimation Method for Compensated Modulation of Modular Multilevel Converters," *2017 IEEE Manchester PowerTech*, pp. 1–6.
- [49] G. Bergna-diaz, J. Freytes, X. Guillaud, S. D. Arco, and J. A. Suul, "Generalized Voltage-Based State-Space Modeling of Modular Multilevel Converters With Constant Equilibrium in Steady State," *IEEE J. Emerg. Sel. Top. Power Electron.*, vol. 6, no. 2, pp. 707–725, 2018.
- [50] H. Yang, Y. Dong, W. Li, and X. He, "Average-Value Model of Modular Multilevel Converters Considering Capacitor Voltage Ripple," *IEEE Trans. Power Deliv.*, vol. 32, no. 2, pp. 723–732, 2017.
- [51] J. Wang, R. Burgos, and D. Boroyevich, "Switching-cycle state-space modeling and control of the modular multilevel converter," *IEEE J. Emerg. Sel. Top. Power Electron.*, vol. 2, no. 4, pp. 1159–1170, 2014.
- [52] M. Vatani, B. Bahrani, M. Saeedifard, and M. Hovd, "Indirect Finite Control Set Model Predictive Control of Modular Multilevel Converters," *IEEE Trans. Smart Grid*, vol. 6, no. 3, pp. 1520–1529, 2015.

- [53] Z. Liu, K.-J. Li, J. Wang, Z. Javid, M. Wang, and K. Sun, "Research on Capacitance Selection for Modular Multilevel Converter," *IEEE Trans. Power Electron.*, vol. PP, no. c, pp. 1–1, 2018.
- [54] S. P. Engel, and R. W. D. Doncker, "Control of the Modular Multi-Level Converter for minimized cell capacitance." in *Proc. 14th Eur. Conf. on Power Electron. & Appl.*, Sept. 2011, pp. 1-10.
- [55] L. M. Cunico, G. Lambert, R. P. Dacol, S. V. G. Oliveira, and Y. R. d. Novaes, "Parameters design for modular multilevel converter (MMC)." in *Proc. Brazilian Power Electron. Conf.*, Oct. 2013, pp. 264-270.
- [56] H. Saad *et al.*, "Modular multilevel converter models for electromagnetic transients," *IEEE Trans. Power Deliv.*, vol. 29, no. 3, pp. 1481–1489, 2014.
- [57] Z. Shen and V. Dinavahi, "Real-Time Device-Level Transient Electrothermal Model for Modular Multilevel Converter on FPGA," *IEEE Trans. Power Electron.*, vol. 31, no. 9, pp. 6155–6168, 2016.
- [58] S. S. Khan and E. Tedeschi, "Modeling of MMC for fast and accurate simulation of electromagnetic transients: A review," *Energies*, vol. 10, no. 7, 2017.
- [59] D. Shu, V. Dinavahi, X. Xie, and Q. Jiang, "Shifted Frequency Modeling of Hybrid Modular Multilevel Converters for Simulation of MTDC Grid," *IEEE Trans. Power Deliv.*, vol. 33, no. 3, pp. 1288–1298, 2018.
- [60] H. Saad *et al.*, "Dynamic averaged and simplified models for MMC-based HVDC transmission systems," *IEEE Trans. Power Deliv.*, vol. 28, no. 3, pp. 1723–1730, 2013.
- [61] U. N. Gnanarathna, A. M. Gole, and R. P. Jayasinghe, "Efficient Modeling of Modular Multilevel HVDC Converters (MMC) on Electromagnetic Transient Simulation Programs," *IEEE Trans. Power Del.*, vol. 26, no. 1, pp. 316–324, 2011.
- [62] M. Senesky, G. Eirea, and T. J. Koo, "Hybrid Modelling and Control of Power Electronics," *Hybrid Sys.: Computation and Control, Lecture Notes in Computer Science*, Springer, 2003, pp.450-465
- [63] A. Dekka, B. Wu, R. L. Fuentes, M. Perez and N. R. Zargari, "Evolution of topologies, modeling, control schemes, and applications of modular multilevel converters," *IEEE Journ. Emerg. Sel. Top. Power Electron.*, vol. 5, no. 4, pp. 1631-1656, Dec. 2017.

- [64] G. Bergna-Diaz, J. A. Suul and S. D'Arco, "Energy-based state-space representation of modular multilevel converters with a constant equilibrium point in steady-state operation," *IEEE Trans. Power Electron.*, vol. 33, no. 6, pp. 4832-4851, Jun. 2018.
- [65] Y. Liu and F. Z. Peng, " A Four-Level Modular Multilevel Converter with Self Voltage Balancing and Extremely Small DC Capacitor," *IEEE Applied Power Electronics Conference and Exposition (APEC)*, Anaheim, CA, USA, 2019.
- [66] Y. Liu and F. Z. Peng, " A Modular Multilevel Converter with Self Voltage Balancing," *IEEE Applied Power Electronics Conference and Exposition (APEC)*, Anaheim, CA, USA, 2019.
- [67] S. Debnath, J. Qin, B. Bahrani, M. Saeedifard, and P. Barbosa, "Operation, Control, and Applications of the Modular Multilevel Converter: A Review," *IEEE Trans. Power Electron.*, vol. 30, no. 1, pp. 37–53, 2014.
- [68] X. Li, C. Mishra, and J. De La Ree. "Frequency Control of Decoupled Synchronous Machine Using Koopman Operator Based Model Predictive." *arXiv preprint arXiv:1901.05341* (2019).
- [69] Online: [https://en.wikipedia.org/wiki/Proof\\_by\\_contradiction](https://en.wikipedia.org/wiki/Proof_by_contradiction).
- [70] A. Brualdi, "Matrices of Zeros and Ones with Fixed Row and Column Sum Vectors," *LINEAR ALGEBRA AND ITS APPLICATIONS* 33: pp. 158-251, 1980.